Martin K. Kneip

Magnetization Dynamics in Diluted Magnetic Semiconductor Heterostructures

Magnetization Dynamics in Diluted Magnetic Semiconductor Heterostructures

Dissertation

presented to the Institute of Physics of the
University of Technology, Dortmund, Germany
in partial fulfilment of the requirements for the degree of
Doktor rer. nat.

presented by

Martin K. Kneip

dipl.-phys. dipl.-kfm.

Dortmund, 26th August 2008

Accepted by the faculty of the Institute of Physics
of the University of Technology, Dortmund, Germany.

Day of the oral exam: 2nd October 2008

Examination board:

Priv.-Doz. Dr. Dmitri Yakovlev

Prof. Dr. Metin Tolan

Prof. Dr. Werner Weber

Dr. Bärbel Siegmann

Contents

List of Figures

List of Tables

List of Listings

Introduction

Already in ancient times the Greek had the knowledge about electrostatic charging of amber, the resin of conifers, which was denoted by the Greek word electron ($\check{\eta}\lambda\varepsilon\kappa\tau\rho\sigma\nu$). The first realization of this effect is accredited to the great Greek philosopher Thales of Milet[1]. Nevertheless, the effect was not used for centuries until beginning of modern times in 18$^{\text{th}}$ century. Since then our life was revolutionized by applications and devices based on the electric charge, so that our contemporary life is unimaginable without this technology.

Especially the rapid development in the last hundred years has its reason in the comprehension of the underlying mechanisms. The cognition of the particle electron is of particular importance in this regard. The name electron for the unit of the electric charge was introduced by George Johnstone Stoney together with Hermann Ludwig Ferdinand von Helmholtz in 1894 [Sto94, Sto95], closely followed by the experimental discovery of the electron by Joseph John Thomson [Tho97] and Emil Wiechert [Wie97] in 1897. Motivated by the discovery of the electron, Thomson developed the famous "Plum pudding model" of the atom [Tho04], which was later proved incorrect by Ernest Rutherford and substituted by the "Rutherford model" [Rut11]. However, this model could not explain origin and principle of the observed spectral lines of different gases like e.g. hydrogen, for which already several empirical correlations had been discovered [Bal85, Lym06, Pas08]. Therefore, Niels Bohr has advanced the "Rutherford model" to the "Bohr model" in 1913 [Boh13]. In the "Bohr model" the electrons have discrete orbits around the nucleus. Although this model achieved success, it could not explain the abnormal Zeeman-effect and the fine structure of atomic spectra.

These phenomena could be explained by an eigen angular momentum of electrons, the so-called spin. The half-integer electron spin was postulated by George Eugene Uhlenbeck and Samuel Abraham Goudsmit in 1925 [Uhl25, Uhl26] because of spectroscopic investigations. They have interpreted the spin as the fourth quantum number, which was proposed by Wolfgang Pauli [Pau25] beside the energy E, the orbital angular momentum $\vec{L}$ and its projection L_z. This concept of an intrinsic angular momentum was very successful and could simultaneously explain earlier experiments by Albert Einstein and Wander Johannes de Haas [Ein15], as well as Otto Stern and Walter Gerlach [Ger22c, Ger22b, Ger22a, Ste88]. Thus, the detected

[1] * ∼624 v. Chr.; † ∼546 v. Chr.

twofold splitting of a silver atom ray in an inhomogeneous magnetic field on the "Stern-Gerlach experiment" in 1922 is regarded as the first direct observation of the electron spin.

Because many fundamental effects in solid state physics, like e.g. ferromagnetism, are spin-related, the discovery of spin had one of the biggest impacts on modern physics. The new degree of freedom, which is offered by the spin, is technologically used in magneto-electronics, which is based on spin-polarized currents in metallic structures [Aki02, Aws02, Wol01, Žut04]. Spin-dependent transport structures based on the famous giant magnetoresistance (GMR) [Bai88, Bin89, Grü86, Pat07, Pri98] or tunneling magnetoresistance (TMR) effect [Jul75, Miy95, Moo96, Moo95], like spin valves or magnetic tunnel junctions (MTJ) [Hir02], are used e.g. in read heads of hard disks [Tsa94], magnetic field sensors [Dau94, Ton98] or magnetic memory modules (magnetoresistive random access memory (MRAM)) [Kat00, Par99, Teh00] and challenge the conventional semiconductor electronics [Dau99, Har00, Hir02, Wol01]. MRAMs for instance have, compared to common semiconductor memory modules, the big advantage, that they do not loose the stored information without being refreshed [Dre04]. Hence, electronic devices (e.g. computers) can be realized, which are immediately operable after switching-on, without loading operationally necessary data from a permanent storage into the random access memory (RAM). Because MRAMs combine the advantages of existing memory technologies (high integration density and low costs of dynamic random access memory (DRAM), high speed of static random access memory (SRAM) and nonvolatility of flash-memory) [Ino02], they have the potential for "universal memory", replacing current memory technology.

Analogue to conventional charge-based electronics, where the contemporary information and communication technology was only enabled by semiconductor electronics, crucial disadvantages of metallic components limit further progress. In metals the carrier density cannot be changed continuously and metals have no band gap, so that they are unsuitable for many electronic and all opto-electronic components. Adding the spin degree of freedom for mainstream charge-based electronic devices has the potential advantages of nonvolatility, increased data processing speed, decreased electric power consumption, and increased integration densities compared with conventional semiconductor devices [Wol01]. Furthermore, the proceeding reduction of structural sizes in electronic components will soon result in a dominance of quantum mechanical effects (especially the spin-dependent exchange interaction among carriers). Compared with the spatial coherence of carriers, the spin is a relatively stable value and, thus, potentially very suitable for future electric components. From these aspects arises the recent big attention for the spin in semiconductor electronics [Ohn98, Wol01]. This new research area is called "spintronics" and may denote the next evolution-step for electronics and can be the begin of the age of spin-electronics [Win04]. It is envisioned that in particular merging photonics with spintronics will lead to a multitude of spin-based multifunctional devices such as spin-light emitting diodes (LED), spin-field-effect transistors (FET), spin-vertical cavity surface emitting

lasers (VCSEL), spin-resonant tunneling devices (RTD), optical switches working at terahertz frequency, modulators, encoders, decoders, and quantum bits for quantum computation and communication [Wol01, Žut04]. Especially in the field of quantum computing [DiV95, Ste98], where the required quantum mechanical two-level-system (the so-called qubit) can be realized by the two possible spin-states of a particle with spin $\frac{1}{2}$ [Ima99, Los98, Sas01], a big impact by means of spintronic devices is expected [Aki06a, Aki02].

Successful incorporation of spins into the existing semiconductor technology inevitably implies experimental possibilities to create spin-polarized electrons and currents respectively (spin-injection), to controllably switch their spin-state (spin manipulation), to transport and store orientation and/or phase of the spin-state (spin-transport, spin memory, spin coherence), and finally to reliably read out the spin-state (spin detection). Good progress is already achieved on spin-injection [Fie99, Oes99, Ohn99b] and spin-transport [Häg98, Kik99]. Spins can be injected[2] in a semiconductor by several methods: Traditionally optical injection [Mei84, Oes02] has been used, where the angular momentum of absorbed circularly polarized photons is transferred to electrons through spin-orbit interaction. As a light source is needed, this method is unfavorable for electronic components. More desirable is electrical spin-injection, where transfer from a magnetic layer to a nonmagnetic semiconductor layer was used at the beginning [Gar99, Ham99, Ham00, Joh98, Sch00b]. To avoid mismatch between the layers, alternatively doping of semiconductors with magnetic impurities was established [Fie99, Jon00, Oes99]. Semiconductors doped with magnetic ions are nowadays the most promising materials for spintronic devices [Die94, Fur88a, Fur88b, Jai92]. Examples are well-known $A^{III}B^{V}$ and $A^{II}B^{VI}$ semiconductors like GaAs, InAs, GaN, CdTe, ZnSe, ZnO etc., which have metal ions in the cation sublattice isoelectronically substituted by magnetic ions, like Mn, Fe, Cr, V etc. This allows growing ternary alloys with a wide range of magnetic ion concentrations up to 100 %. These materials are called diluted magnetic semiconductors (DMS) as opposed to "concentrated" magnetic semiconductors. In the latter the magnetic ion is a part of its regular lattice, whereas in the former the magnetic ions partially substitute the nonmagnetic host atoms [Aki02]. The ternary nature gives good possibility of tuning lattice constant and band parameters by varying the amount of substituted cations. As first investigations were done on macroscopic mono-crystals, predominate thin films [Deb81, Kol84b] and heterostructures [Bic84, Kol84a] since the 80$^{\text{th}}$. Nowadays it is possible to create stoichiometric compositions, which are not stable as volume crystals [Dur89, Kol86b]. This progress in fabrication leads to a rich spectrum of entirely new physical phenomena not accessible by bulk growth [Fur96].

DMS combine optical and transport properties typical to a semiconductor (narrow optical resonances, high electron mobility) with features specific for magnetic materials (antiferromagnetism, ferromagnetism or paramagnetism) [Aki06a]. Most popular as magnetic ions are manganese Mn^{2+}-ions because of several advantages: Mn^{2+}-ions can be incorporated in siz-

[2]Spin-injection usually means creation of nonequilibrium spin population.

able amounts in $A^{II}B^{VI}$ semiconductors without considerably change of the crystallographic quality of the host material, Mn^{2+}-ions are electrically neutral in $A^{II}B^{VI}$ semiconductors and Mn^{2+}-ions possess a relatively large magnetic moment due to the half-filled d-shell [Fur88b]. Comprehensive information about the properties of DMS with Mn-ion is collected in several reviews [Die94, Fur82, Fur86, Fur88a, Fur88b, Fur96, Goe88, Jai92].

If Mn-ions are incorporated in $A^{II}B^{VI}$ semiconductors, like (Cd,Mn)Te and (Zn,Mn)Se, which are investigated in this thesis, a strong paramagnetism appears. Thus, the conduction band electrons can be completely aligned already by weak external magnetic fields. But because of the needed magnetic field and additionally because of the covering of paramagnetism by the thermic motion of the electrons at room temperature, DMS are presently unsuitable for integrated components. Nevertheless $A^{II}B^{VI}$ DMS have also several advantages. On the one hand they have good structural quality, sharp absorption edge formed by excitons, and show strong band edge photoluminescence (PL), which allows one to apply the broad spectrum of optical experimental techniques, in particular in magnetic field [Die94, Fur88b, Fur88a]. By contrast, luminescence is poor in $A^{III}B^{V}$ DMS materials, such as (Ga,Mn)As. On the other hand they have the unique possibility to tailor electronic and magnetic properties independently. Thus, $A^{II}B^{VI}$ DMS are very suitable for testing novel design concepts for spintronics applications and are nowadays widely used in this respect [Aws02, Fre99].

In DMS the carrier spin manipulation arises from the spin-flip exchange scattering of free carriers on the localized magnetic moments of the magnetic ions. Formation of magnetic polarons [Die83, Naw81] and a variety of exceptional strong magneto-optical and magneto-transport effects originate from the strong exchange interaction of the localized Mn^{2+} magnetic moments with spins of the conduction band electrons (s-d-exchange interaction) and/or valence band holes (p-d-exchange interaction). Among the effects are giant Zeeman-splitting of the band states, which may exceed 100 meV at low temperatures, giant Faraday rotation [Gaj78] and Kerr rotation effects [Die94]. The magnetic properties of the Mn-ion system, which depend strongly on the Mn concentration, play a key role in these effects. For example, neighboring Mn-ions interact antiferromagnetically, which leads to the formation of high ordered clusters and spin-glass phases at higher Mn concentration [Fur88a]. An overview about the basic properties of $A^{II}_{1-x}\mathrm{Mn}_x B^{VI}$ DMS, like crystal and band structure and magnetic and optic properties, is presented in the first chapter of this thesis. Comprehensive collection of the data for paramagnetic ions can be found in [Abr70] and references therein, and for conduction electrons and holes in semiconductors in [Mei84].

The prerequisite of spintronic implementations in DMS is detailed knowledge about the coupled systems of magnetic ions, lattice (the phonon system) and free carriers which determine transport, magneto-optical and magnetic properties of DMS. The spin and energy transfer between the coupled systems, where spins are hold by free carriers (electrons and holes) and by Mn-ions, controls the magnetization dynamics in DMS. Present state of knowledge on mag-

netization dynamics in $A^{II}B^{VI}$ semiconductors with Mn^{2+}-ions is given in the second chapter. The focus lies thereby on the description of the coupled systems. Theoretical basis for spin and energy transfer between the systems will be considered, which often can not be separated from each other.

Access to the magnetization dynamics is offered by the impact of the Mn-spin system temperature on the magneto-optical properties. As already mentioned, the giant magneto-optical effects originate from the strong sp-d-exchange interaction between the localized electrons in the $3d$-shell of the Mn-ions and the delocalized s-type electron states in the conduction band and the p-type hole states in the valence band. These effects are based on polarization of the carrier spins interacting with the localized magnetic Mn-ions, which in turn are polarized by an external magnetic field. As a result the magnitudes of the spectroscopic responses are proportional to the magnetization of the Mn-spin system. Besides the strength of external magnetic fields, the magnetization is determined by the temperature of the Mn-spin system, which can differ from the bath temperature (i.e. lattice temperature). Therefore, heating of the Mn-system can strongly influence magneto-optical and magnetotransport properties.

As internal thermometer of the Mn-spin temperature the giant Zeeman-splitting of excitons (band states) is exploited, which is highly sensitive to the magnetic Mn-ions due to the sp-d-exchange interaction. This allows studies in a wide temporal range from picoseconds to hundreds of microseconds. To drive the Mn-spin system out of equilibrium with the lattice, several methods are employed [Yak09]. The experimental approach via heating by means of photogenerated (by pulsed laser excitation) or electrically accelerated carriers, which is used in thesis, and the associated experimental setup for time-resolved measurements are described in chapter three.

Concerning the magnetization dynamics, detailed understanding of dynamical properties of the localized Mn-spins, namely spin dephasing and particularly spin relaxation is one emphasis of current research. As the electric charge is a conserved quantity, which cannot be affected by scattering processes for instance, the spin can loose its information - the direction of the spin-vector, i.e. the spin polarization - in scattering processes [Win04] or due to spin-orbit and hyperfine coupling [Žut04]. While the occupation of electronic spin states in undistorted systems is given by an equilibrium distribution, is the spin polarization a nonequilibrium state. The relaxation of the spin leads therefore to equilibration of spin polarization and, thus, is of great importance for spintronics. The time within the spin polarization gets lost, is the spin relaxation time. Typical values for spin relaxation times vary from less than one picosecond for free carriers to years for some nuclears [Aki06a]. The fact that nonequilibrium electronic spin in semiconductors lives relatively long (typically a nanosecond), allows for spin-encoded information to travel macroscopic distances [Žut04].

First findings on spin relaxation in Mn^{2+}-ions were already achieved in the 60^{th} [Blu62, Lam60], but on materials with very low Mn^{2+} content ($x \ll 0.01$), where magnetic ions may be

considered as isolated. In these materials different mechanisms of spin relaxation are important in comparison to the magnetic semiconductors with much higher Mn content, which are actual for spintronics. In bulk $A^{II}_{1-x}\mathrm{Mn}_x B^{VI}$ DMS spin relaxation of Mn^{2+}-ions was investigated during the last decade [Bin91, Far96, Sca88, Sca96a, Str90, Str92]. A strong dependance of the spin-lattice and spin-spin relaxation times on the Mn content x and lattice temperature T_L was shown.

In this thesis spin dynamics in (Zn,Mn)Se/(Zn,Be)Se and (Cd,Mn)Te/(Cd,Mg)Te DMS quantum well (QW) heterostructures with a type-I band alignment are studied, where the carriers are quantum confined. It is already well-known that the spin relaxation time of free carriers ($\sim 10^{-12}$-10^{-11} s [Cam01, Cro97]) is much faster than for Mn-ions (10^{-8}-10^{-3} s [Far96, Kel01, Kel04, Sca96a, Sch00a]). Thus, spin relaxation of the magnetic ion becomes a bottleneck for fast spin switching in magnetic semiconductors [Aki06a]. Nevertheless, the free carriers cannot be neglected, because the presence of free carriers (their concentration, temperature and spin polarization) modifies strongly the efficiency of energy and spin transfer between the systems of DMS and, thus, is of great importance for static characteristics and dynamical properties of DMS materials. Especially the important role of free carriers in heating of the Mn-system, by its interaction with photoexcited carriers with excess kinetic energy, and in the cooling of the Mn-system in the presence of cold background carriers, provided by modulation doping, is established.

The studies are separated in three chapters. In the fourth chapter of this thesis, new results on energy and spin transfer between free carriers and Mn-ion system are presented. Contributions of direct heating of the Mn-system by photocarriers and indirect heating via nonequilibrium phonons are distinguished and their competition is discussed. In the fifth chapter dynamics of spin-lattice relaxation (SLR) of magnetic Mn-ions in (Zn,Mn)Se/(Zn,Be)Se and (Cd,Mn)Te/(Cd,Mg)Te DMS QW heterostructures is investigated and new experimental studies on (Zn,Mn)Se/(Zn,Be)Se heterostructures are shown. As the manganese SLR is of key importance for the dynamical processes in DMS, a number of studies have already been performed for (Cd,Mn)Te-based heterostructures [Sch00a, Sch01b, Sch01a] with Mn concentrations not exceeding $x = 0.05$.

Crucial for spintronic devices is the ability to tune the spin relaxation time precisely, as the spin relaxation time is important in double respects. On the one hand spin polarization must be conserved over long times and distances, if the spin shall be processed or stored in a region, which is spatial separated from the spin-injector [Wol01]. Especially for the possibility of utilizing spins as quantum bits for quantum information processing, long spin polarization is needed. On the other hand short spin relaxation time is needed for fast switching between different spin-states. For instance semiconductor lasers can be switched off extremely fast by reorientation of spins [Oes02]. This very relevant topic is devoted the sixth chapter, before the thesis is summarized in the last chapter. Especially for one of the biggest drawbacks for

precise tuning, that the magnetization dynamics in DMS cannot be controlled separately from the static magnetization, solutions via electric field control of the magnetization dynamics or via the technological concept of “digital alloying” are presented.

Chapter 1

II-VI diluted magnetic semiconductors

Contents

In this thesis QW heterostructures containing (Cd,Mn)Te and (Zn,Mn)Se are investigated. To facilitate the presentation and understanding of the results, discussed in the following chapters, it is necessary to give an overview about the structural, electronic and magnetic properties of these materials in the first sections of this chapter. The crystal structure is described in section 1.1 on the basis of the binary II-VI semiconductors CdTe and ZnSe, which is due to the close resemblance of the properties between the binary compounds and their ternary DMS derivatives. This applies analogue for (Cd,Mg)Te and (Zn,Be)Se, which are used in some of the investigated heterostructures.

In the second section 1.2 the band structure of wide-band-gap $A^{II}_{1-x}\mathrm{Mn}_x B^{VI}$ bulk alloys[1] is presented, starting in subsection 1.2.1 with the host semiconductors CdTe and ZnSe in absence of an external magnetic field. Also here resembles the band structure of the $A^{II}_{1-x}\mathrm{Mn}_x B^{VI}$ alloys qualitatively that of the nonmagnetic $A^{II}B^{VI}$ "parent" material having the same crystal structure. Because all investigated compounds have the same crystal structure, the band structures are very similar, especially at the Γ-point. Calculation of the electronic states can be done by the envelope-function-approximation [Alt83a], which describes the particular layers of a QW structure by volume bands. The latter are described in the section for CdTe and ZnSe according to the Kohn-Luttinger-theory [Lut56]. Subsection 1.2.2 discusses effects of incorporated manganese ions, especially of the Mn d-electrons, on the electronic states. The impact on the optical properties, due to intra-ion transitions in the half-filled Mn $3d^5$-shells, is considered in particular.

The subsequent section 1.3 outlines the magnetic properties of (Cd,Mn)Te and (Zn,Mn)Se. Firstly an short overview about possible types of magnetic orders in solid states is given, which is needed for the further understanding. In the second subsection 1.3.2 the case of free carriers in the host semiconductor is considered. Pauli paramagnetism as well as Landau diamagnetism occur if an magnetic field is applied. For the remaining section the focus is shifted to the peculiarity of DMS, namely that an amount of the cations in the lattice is exchanged by the magnetic ions. Starting point are the magnetic properties of isolated Mn-ions outlined in subsection 1.3.3.

Because of the insertion of Mn-ions, simultaneously localized spins and magnetic moments are integrated in the crystal. The localized spins of the half-filled d-shell of the Mn-ions incur two types of exchange interactions. The strong Kondo-like sp-d-exchange interaction between the band electron spins and the localized moments of the magnetic ions influences strongly the electronic properties. The Heisenberg inter-ion d-d-exchange interaction is weaker and underlies the static and dynamic magnetic properties of the $A^{II}_{1-x}\mathrm{Mn}_x B^{VI}$ DMS. Both exchange interactions are introduced briefly in subsection 1.3.4. Furthermore, the giant Zeeman-splitting

[1] $A =$ Cd,Zn; $B =$ S,Se,Te

is introduced as consequence of the significant influence of the sp-d-exchange interaction on the band structure.

The approximation of non interacting Mn-spins, made in subsection 1.3.3, is only valid for very strong diluted systems ($x < 0.01$), so that the influence of the d-d-exchange interaction between Mn-spins is introduced in the discussion of the magnetic properties in subsection 1.3.4.3. The magnetic dipole-dipole interaction can continued to be neglected. Furthermore, the magnetic phases in $A^{II}_{1-x}\mathrm{Mn}_x B^{VI}$ DMSs are addressed briefly in this subsection. Big importance arises from precise knowledge about the magnetic properties, because they bear on the optical and electrical properties of a DMS through the sp-d-exchange [Fur88a].

In section 1.4 the peculiarities of DMS QW heterostructures are described. $A^{II}_{1-x}\mathrm{Mn}_x B^{VI}$ alloys are excellent candidates for these structures because of the tunability of their lattice parameters and band gaps, especially with regard to flexibly band structure engineering [Dat85]. In the section the effects of the spatial confinement on the energy bands, the density of states, the spin-orbit splitting and the resulting selection rules are reviewed.

In the last section introduction into excitons in semiconductors is given. Both the free exciton and the situation of excitons in QWs is described. Finally also the situation of quantized motion of excitons in magnetic field will be considered.

1.1 Crystal structure of (Cd,Mn)Te and (Zn,Mn)Se

Solid states in crystalline phase have a spatial symmetry, arising from the continuous arrangement of the atoms in the crystal lattice. The materials, investigated in this thesis, are based on the II-VI binary compound-semiconductors CdTe and ZnSe. The latter have the propensity to crystallize in a variety of polymorphic modifications. In general, structures for II-VI semiconductors are hexagonal wurtzite and cubic zincblende (sphalerite) [Ave67]. CdTe and ZnSe possess under normal conditions the zincblende structure [Yeh92].

In the ternary materials (Zn,Mn)Se, (Zn,Be)Se and (Cd,Mn)Te and (Cd,Mg)Te a small amount of the Zn^{2+}-ions and Cd^{2+}-ions, respectively, is exchanged by likewise bivalent Be^{2+}-, Mg^{2+}- and Mn^{2+}-ions, respectively. Bulk crystals of BeSe exhibit the zincblende structure [Wyc63], of MgTe the wurtzite structure [Kle51, Kuh71, Par71, Zac27], of MnSe the rock-salt (NaCl) structure [Dur89] and of MnTe the hexagonal NiAs structure [Oft27]. Therefore, the crystal structure of the ternary materials is dependant on the exchanged amount of cations. The corresponding composition ranges and the upper limits for successful incorporation of the magnetic Mn-ions are given in table 1.1. It is remarkable that such high values of x for the Mn-ions in ternary alloys can be reached, although the crystal structures of MnSe and MnTe are

[2]Special epitaxial growth (e.g. molecular beam epitaxy (MBE)) enables the zincblende structure for $\mathrm{Cd}_{1-x}\mathrm{Mn}_x\mathrm{Te}$ with $x > 0.77$ up to pure MnTe [Zak95] and for $\mathrm{Zn}_{1-x}\mathrm{Mn}_x\mathrm{Se}$ with $x > 0.3$ up to pure MnSe [Kol86b].

Table 1.1 – Crystal structures and ranges of composition of DMS ternary materials [Fur88a, Fur96]. The upper limit on x is imposed by the fact that neither MnSe nor MnTe crystallize in the zincblende or wurtzite structure.

Compound	**Crystal structure**	**Composition range**[2]
$Cd_{1-x}Mn_xTe$	zincblende	$0 < x < 0.77$
$Zn_{1-x}Mn_xSe$	zincblende	$0 < x < 0.3$
$Zn_{1-x}Mn_xSe$	wurtzite	$0.3 < x < 0.57$

neither zincblende nor wurtzite. For higher concentrations a mixture of wurtzite and rocksalt structure was observed in $Zn_{1-x}Mn_xSe$ [Juz56]. In $Cd_{1-x}Mn_xTe$ even a mixture of zincblende, NiAs and pyrite-typestructure was observed [Paj78]. In this thesis only samples with low Mn concentration in zincblende structure were investigated.

The zincblende structure, which is schematically represented in figure 1.1, is based on the cubic space group T_d^2-F$\bar{4}$3m [Ave67].[3] It has the same arrangement as diamond and consists of two face-centered-cubic (fcc) lattices. Contrary to diamond one lattice is occupied with cations and the other with anions. The two lattices are displaced against each other by a quarter of the space diagonal, so that every ion is tetraedrically surrounded by four ions of the other kind. Each cation has four next neighbors of anions at the corners of a regular tetrahedron at a distance of $\frac{\sqrt{3}}{4}$ and twelve next-nearest neighbors of ions of the same kind at a distance of $\frac{\sqrt{2}}{2}$ of the edge length of the unit cell of one sublattice. The edge length of the unit cell is represented by the lattice constant a_0. In ZnSe the lattice constant constitutes 5.668 Å [Ave67] and in CdTe 6.487 Å [Bot81]. The lattice constant for the ternary materials $a_{0,ternary}$ can be calculated by Vegard's law

$$a_{0,ternary} = (1 - x) \cdot a_{0,binary1} + x \cdot a_{0,binary2} \tag{1.1}$$

as linear interpolation between values of the corresponding binary semiconductors $a_{0,binary1;2}$ [Den91, Fur83, Veg21, Fur96]. For a general characterization it is more convenient to calculate

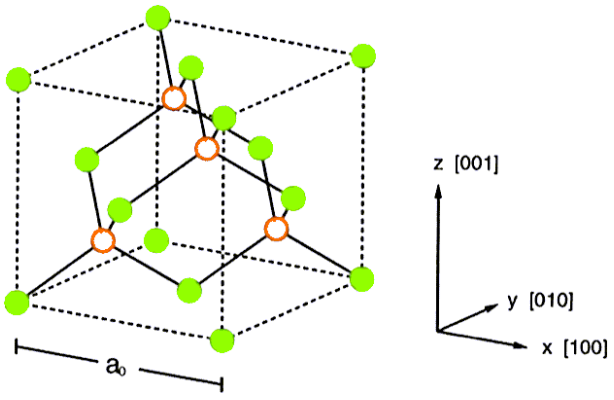

Figure 1.1 – Unit cell of zincblende structure. The open spheres represent the metallic cations and the others the semi-metallic anions. The two sublattices are displaced against each other by a quarter of the space diagonal.

[3] T_d^2 is the Schönflies notation and F$\bar{4}$3m is the crystallographic description according to Hermann-Mauguin.

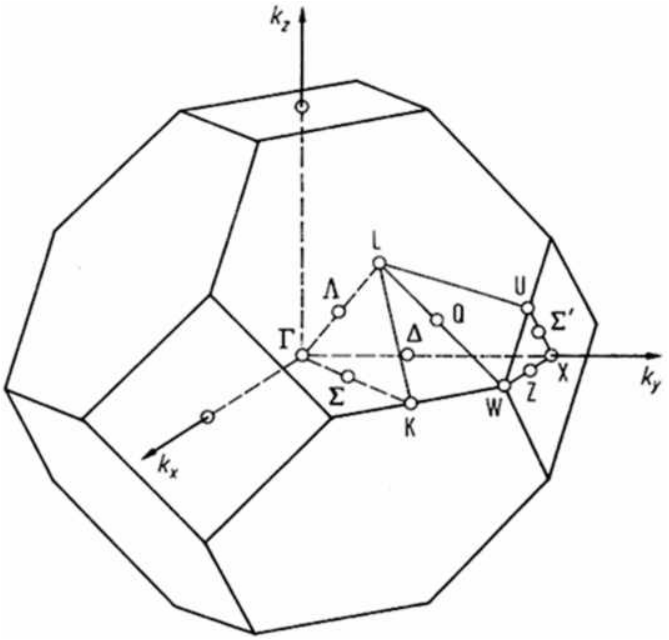

Figure 1.2 – First Brillouin zone of zincblende lattice with points of symmetry. Points of high symmetry are the Γ-, X- and L-point.

the mean cation distance $d = \sqrt{2}a_0$, which is independent on the lattice structure [Fur88a, Fur96]:

$$\mathrm{Cd}_{1-z}\mathrm{Mg}_z\mathrm{Te}: \quad d\left[\text{Å}\right] = 4.587 - 0.030z \quad \text{[Bot81, Cam97]}, \tag{1.2}$$

$$\mathrm{Cd}_{1-x}\mathrm{Mn}_x\mathrm{Te}: \quad d\left[\text{Å}\right] = 4.587 - 0.105x \quad \text{[Bot81, Yod85]}, \tag{1.3}$$

$$\mathrm{Zn}_{1-x}\mathrm{Mn}_x\mathrm{Se}: \quad d\left[\text{Å}\right] = 4.009 + 0.164x \quad \text{[Mad99, Yod85]}, \tag{1.4}$$

$$\mathrm{Zn}_{1-y}\mathrm{Be}_y\mathrm{Se}: \quad d\left[\text{Å}\right] = 4.009 - 0.366y \quad \text{[Mad99, Gal97]}. \tag{1.5}$$

Even the structure transition in $\mathrm{Zn}_{1-x}\mathrm{Mn}_x\mathrm{Se}$ does not affect the linear relation of d [Yod85].

An important aspect for zincblende structures arises from symmetry. The $\mathrm{T_d}$ point group, which is a subgroup of the full spherical group $\mathcal{O}(3)$, contains 24 proper and improper symmetry-conserving rotations. In contrast to monatomic semiconductors in diamond structure, like silicon or germanium, possess zincblende structures no center of symmetry or inversion. Hence, zincblende crystals may have different physical and chemical properties in different directions. As a consequence zincblende crystals are piezoelectric [Ave67].

The inversion as symmetry operation leaves spinors invariant and causes, in combination with the Kramers-degeneration against time reversal, that all states in absence of magnetic field with $\Psi_\uparrow(\vec{k}) = \Psi_\downarrow(\vec{k})$ are at least twofold spin-degenerated [D'y71, Ell54a, Ell54b]. In contrast holds in zincblende the general Kramers-degeneration $\Psi_\uparrow(\vec{k}) = \hat{\tau}\Psi_\uparrow(\vec{k}) = \Psi_\downarrow(-\vec{k})$ with the operator for time reversal $\hat{\tau}$, which leads to loss of the spin-degeneration [LYV96].

On consideration of the reciprocal lattice of zincblende (figure 1.2), the Γ-, X- and L-point can be identified as points with high symmetry of the Brillouin-zone [Bou36].

The chemical bond between the metallic and semi-metallic ion in II-VI semiconductors is a tetrahedral s-p^3-bond based on the two s-valence electrons of the metal and the six p-valence electrons of the semi-metal. The additional Be-, Mg- and Mn-ions, respectively, substitute the group II elements on the cation places. Also these contribute with two s-valence electrons to the bond. Because of the differences in electronegativity of the involved ions, has the bonding of the sp^3-hybridized atomic orbitals partly ionic and partly covalent character, depending on the concrete material system.

Contrary to the lattice constants remain the bondlengths for CdTe, ZnSe, MnTe and MnSe over the hole composition range of $Zn_{1-x}Mn_xSe$ and $Cd_{1-x}Mn_xTe$ constant [Bal84, Bun87b, Bun87a, Pon90]. This can only mean that the real crystal lattice is locally highly distorted [Kos93]. Balzarotti stated that the cation-sublattice is undistorted in first order and the structural necessary alignment takes only place in the anion-sublattice, which abandons fcc symmetry [Bal84]. Contrary to that shows X-ray data that both sublattices are microscopically distorted [Abr85].

1.2 Band structure of (Cd,Mn)Te and (Zn,Mn)Se

1.2.1 Band structure of zincblende semiconductors

The special properties of the band structure of semiconductors become obvious, paying regard to the differences to metals and isolators. In metals the electronic bands are partly filled, so that many electrons can contribute to high conductivity. Isolators have either empty or completely filled bands, so that electrons cannot contribute to the conductivity due to the Pauli principle. Because of the huge energy gaps ($E_g \gtrsim 4\,\mathrm{eV}$) between the lowest empty band (conduction band) and the uppermost filled band (valence band) of isolators, conductivity cannot be achieved by thermal excitation of electrons from the valence band to the conduction band. At $T = 0\,\mathrm{K}$ this situation is similar for semiconductors. But, in contrast to isolators, semiconductors have only small energy gaps in the region of a few eV. Therefore, electrons can be excited from the valence band to the conduction band via thermal energy for $T \neq 0\,\mathrm{K}$ [Kit05].

For many optical properties of semiconductors only the energy dispersion near the fundamental band gap is relevant. This holds also for the optical transitions utilized in the experimental part of this thesis, which occur near $k = 0$ in the middle of the Brillouin-zone at the Γ-point. Therefore, this part of the band structure is specified in this section. For a discussion of the general band structure one can refer e.g. to [Lar88b]. Starting point is the carrier wave function. This has to fulfill the Schrödinger-equation ([Ash76])

$$\hat{H}\Psi_{n\vec{k}}(\vec{r}) = \left[-\frac{\hbar^2}{2m_0}\vec{\nabla}^2 + V_{lattice}(\vec{r})\right]\Psi_{n\vec{k}}(\vec{r}) = E_{n\vec{k}}\Psi_{n\vec{k}}(\vec{r}) \tag{1.6}$$

in the crystalline potential

$$V_{lattice}(\vec{r}+\vec{R}) = V_{lattice}(\vec{r}) \tag{1.7}$$

with the periodicity of the underlaying Bravais lattice for all Bravais lattice vectors $\vec{R}$. Thereby is m_0 the free electron mass and $\Psi_{n\vec{k}}(\vec{r})$ the electron wave function in crystal lattice with index n and wave vector $\vec{k}$. According to Bloch's theorem, the eigenstates can be expressed as modulated plane Bloch-wavefunctions

$$\Psi_{n\vec{k}}(\vec{r}) = \exp^{i\vec{k}\vec{r}} u_{n\vec{k}}(\vec{r}) \tag{1.8}$$

with the lattice-periodic potential $u_{n\vec{k}}$. The eigenvalues are characterized by eigenstates $E_{n\vec{k}}$. Eigenstates for fixed n in solid states are called energy bands with band index n and wave vector $\vec{k}$. The possible energy states $E_{n\vec{k}}$ are filled with electrons according to the Pauli principle. The energetically highest filled energy bands are called valence bands and the proximate band conduction band. The energy difference between the energetically highest valence band and the minimum of the conduction band is denoted as energy gap E_g.

Using the tight-binding-model in absence of spin-orbit splitting, the valence band is p-like with orbital angular momentum of $L = 1$, which leads to a threefold degeneration. The conduction band is s-like with orbital angular momentum $L = 0$ at the Γ-point. Using the, in solid state physics usual, nomenclature for irreducible representations by Koster [Kos69], the valence band has Γ_{15}-symmetry and the conduction band Γ_1-symmetry. The dispersion relation of the band structure is approximately parabolic in the vicinity of the Γ-point. As in zincblende the minimum of conduction band and the maximum of valence band is at the Γ-point in the center of the Brillouin-zone, the investigated materials are direct semiconductors. In materials with an indirect band gap, like silicon or germanium, the maximum and minimum occur at different k values, so that only phonon assisted optical excitations are possible.

Provision for the carrier spins and its coupling with the orbital angular momentum alters the band structure. From the Dirac-equation yields the spin-orbit interaction [Win03]

$$\hat{H}_{SO} = -\frac{\hbar}{4m_0^2c^2}\vec{\sigma}\cdot\vec{p}\times\left(\vec{\nabla}V\right), \tag{1.9}$$

which splits the valence band in states with total angular momentum $J = L + S = {}^3/_2$[4] and $J = {}^1/_2$ at $k = 0$. Thereby, $\vec{\sigma}$ is the spin operator and $\vec{p}$ the electron momentum operator. Via group theory these states can be described by an irreducible representation, corresponding to the symmetry at the Γ-point, as a two-fold degenerated Γ_7-state ($J = {}^1/_2$) and a four-fold degenerated Γ_8-state ($J = {}^3/_2$). The Γ_7-doublet is called spin-off-band (so band) and separated from the Γ_8-quartet by the spin-orbit splitting energy Δ_{so}. The conduction band is a two-

[4] $S = {}^1/_2$ is the electron spin

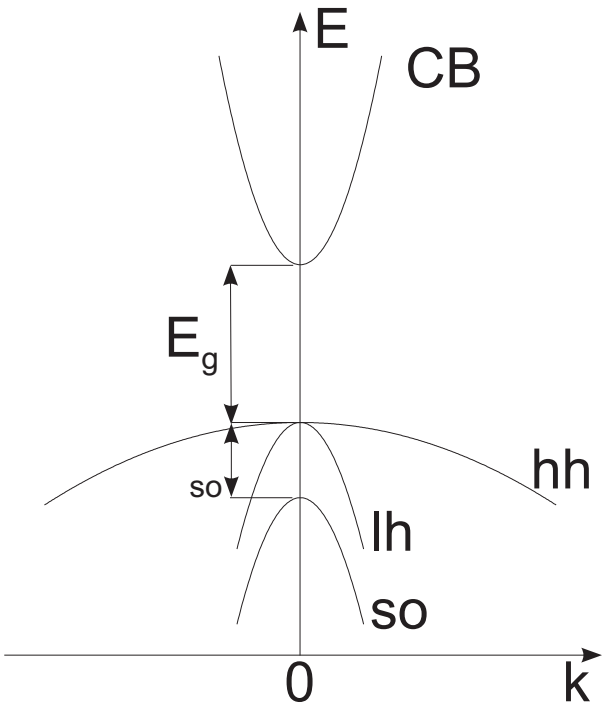

Figure 1.3 – Schematic representation of the band structure of zincblende semiconductors in the vicinity of the Γ-point in parabolic approximation [Rud05].

fold spin-degenerated Γ_6-band. As the conduction band is mainly formed by the s-like wave functions of the atomic orbitals with $L = 0$ and $S = 1/2$, it has total angular momentum $J = 1/2$. The valence band is based on p-like wave functions with $L = 1$ and $S = 1/2$. For $k \neq 0$ the Γ_8 states with $J_z = \pm 3/2$ split into two bands with different bending. Because of their effective masses they are called heavy-hole (hh) band (states with $J_z = \pm 3/2$) and light-hole (lh) band (states with $J_z = \pm 1/2$). The spin-orbit splitting arises due to the interaction of the intrinsic magnetic moment of the electron spin with the magnetic field, generated by electron motion. The magnitude of the spin-orbit splitting is known to affect the location of the lowest hole levels in the valence band. Thus, any change in spin-orbit splitting affects the luminescent properties of semiconductors [Lip98]. As the Γ_7-band lies energetically about 950 meV and 430 meV, respectively, below the Γ_8-band in CdTe and ZnSe, respectively, [Al-03, Wör97], it is nearly always full occupied at low temperature. Therefore, the Γ_7-band has no effect on the optical properties in the region of the fundamental band gap. Because of the weak coupling between conduction and valence band, due to the wide fundamental band gap, the dispersion of the conduction band can be assumed as isotropic and parabolic. It can be described similar to the dispersion of free electrons $E(k) = \frac{\hbar^2 k^2}{2m}$. To take into account the influence of the periodic lattice potential on the carriers, the mass m has to be substituted by an effective mass m_{eff}:

$$E_{cb}(k) = E(k = 0) + \frac{\hbar^2 k^2}{2m_{eff}}. \tag{1.10}$$

In contrast the dispersion of the Γ_8-valence band is not isotropic and mostly described by means of the Kohn-Luttinger-theory [Lut55, Lut56]. The valence band can be described by a 4×4 matrix containing the wave vector $\vec{k}$ in the second power [Kuh95]. By means of a Hamilton-

Operator with the same symmetry, the energy dispersion can be derived from the condition $\det(\hat{H}_{\Gamma_8 vb} - E) = 0$:

$$E(\vec{k}) = -\frac{\hbar^2}{2m_0}\left(\gamma_1 k^2 \pm \sqrt{4\gamma_2^2 k^4 + 12(\gamma_3^1 - \gamma_2^2)(k_x^2 k_y^2 + k_x^2 k_z^2 + k_y^2 k_z^2)}\right), \tag{1.11}$$

with the Kohn-Luttinger-parameters γ_1, γ_2 and γ_3. These parameters are different for CdTe and ZnSe and given in table A.4 in chapter A of the appendix. The different parabolic dispersions of light-hole and heavy-hole band are given by this equation. Using

$$\left(\frac{1}{m_{eff}}\right)_i = \frac{1}{\hbar^2}\frac{\partial^2 E(\vec{k})}{\partial k_i^2}\bigg|_{\vec{k}=0} \qquad i = x, y, z \tag{1.12}$$

results from 1.11 for the effective masses of the valence band states in [100]- and [111]-direction, respectively:

$$\frac{m_0}{m_{eff,hh/lh}} = \gamma_1 \pm 2\gamma_2 \qquad \vec{k} \parallel [100], \tag{1.13}$$

$$\frac{m_0}{m_{eff,hh/lh}} = \gamma_1 \pm 2\gamma_3 \qquad \vec{k} \parallel [111]. \tag{1.14}$$

In direction of the axes results for CdTe $m_{eff,lh} = 0.11m_0$ [5] and $m_{eff,hh} = 0.53m_0$ [6] and for ZnSe $m_{eff,lh} = 0.27m_0$ and $m_{eff,hh} = 0.81m_0$.

As already stressed in the previous section, the zincblende lattice possess no center of inversion because of the two-atomic basis. But spin-degeneration of electron and hole states requires spatial inversion symmetry ($E_\uparrow(\vec{k}) = E_\uparrow(-\vec{k})$) and time reversal symmetry (Kramers-degeneration: $E_\uparrow(\vec{k}) = E_\downarrow(-\vec{k})$) simultaneously:

$$E_\uparrow(\vec{k}) = E_\downarrow(\vec{k}). \tag{1.15}$$

Therefore, this bulk inversion asymmetry (BIA) leads to removal of spin-degeneration, i.e. spin splitting of the bands occurs already for $k \neq 0$ without external magnetic field B. The resulting spin splitting of the Γ_6 valence band can be described in third order in k by the Dresselhaus Hamiltonian [Dre55, D'y84, Kai03]

$$\hat{H}_{Dresselhaus} = \frac{\hbar}{2}\vec{\sigma} \cdot \vec{\Omega}_{BIA}(\vec{k}) \tag{1.16}$$

[5] see [Har89, Law71]

[6] In literature exist several different values for these masses ranging from $m_{eff,lh} = 0.103m_0$ [Ben78] and $m_{eff,hh} = 0.4m_0$ [Cha88] to $m_{eff,lh} = 0.15m_0$ [Woj79] and $m_{eff,hh} = 0.63m_0$ [Woj79].

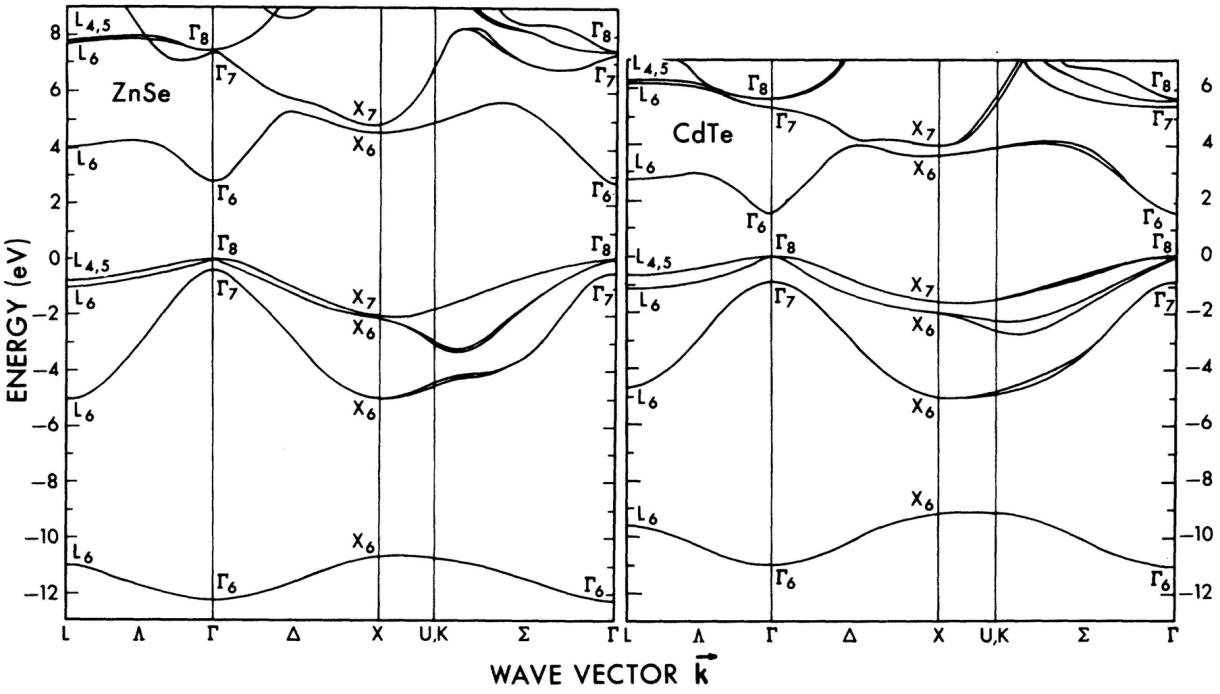

Figure 1.4 – Calculated band structure of ZnSe and CdTe according to Chelikowsky and Cohen [Che76]

with the spin operator $\vec{\sigma}$ and

$$\vec{\Omega}_{BIA}(\vec{k}) = \frac{2\gamma}{\hbar} \begin{pmatrix} k_x \left(k_y^2 - k_z^2\right) \\ k_y \left(k_z^2 - k_x^2\right) \\ k_z \left(k_x^2 - k_y^2\right) \end{pmatrix}, \tag{1.17}$$

where γ is the spin-orbit coefficient. The Dresselhaus Hamiltonian corresponds to a Zeeman Hamiltonian with an effective magnetic field $\vec{\Omega}_{BIA}(\vec{k})$, which depends on material, geometry and wave vector $\vec{k}$. The electron precesses, due to the effective magnetic field, with a frequency proportional to $|\vec{\Omega}_{BIA}(\vec{k})|$ around an axis in direction $\vec{\Omega}_{BIA}(\vec{k})$ [Kna96]. The splitting $\Delta E_{Dresselhaus}$ due to the Dresselhaus term amounts in polar coordinates to

$$\Delta E_{Dresselhaus}(\vec{k}) \propto \gamma k^3 \sin\vartheta \left[1 - \sin^2\vartheta \left(1 + 2\sin^2(2\varphi)\right) + \frac{9}{4}\sin^2(2\varphi)\sin^4\vartheta\right]^{\frac{1}{2}} \tag{1.18}$$

with $k_x = k\sin\vartheta\cos\varphi$, $k_y = k\sin\vartheta\sin\varphi$ and $k_z = k\cos\vartheta$ [Rud05]. For $\vec{k} \parallel [100]$ is $\Delta E_{Dressel}(\vec{k}) = 0$ and for all other directions is $\Delta E_{Dressel} \propto k^3$.

The complete band structure of CdTe and ZnSe according to pseudo-potential calculations by Chelikowsky and Cohen for directions of high symmetry is shown in figure 1.4.

1.2.2 Band structure of zincblende semiconductors containing manganese

The qualitative devolution of the band structure, pictured in figures 1.4 and 1.3, remains unchanged for the ternary compounds (Cd,Mg)Te, (Cd,Mn)Te, (Zn,Be)Se and (Zn,Mn)Se, if only a small amount of cations is exchanged with respect to the binary semiconductors CdTe and ZnSe [Bec88]. Theoretically can the effect of the manganese atom on the band structure of the host semiconductor be described in terms of an average medium theory, such as the virtual crystal approximation, the coherent potential approximation or another appropriate theoretical procedure [Agg87, Gun89, Has83, Has88, Has90, Hui89, Lar85, Lar88b, Mašˇ87, Wei86, Wei87]. In first order the changes of the band structure can be quantified as continuous transition from the band structure of the host $A^{II}B^{VI}$ material to a hypothetic tetrahedrally bonded MnB^{VI} material [Fur96, Liu04, Wei86, Wei87].

Hence, the fundamental band gap at the Γ-point becomes influenced by the concentration of the substituted cations[7]. The variation of the fundamental band gap with the manganese content can be described by a linear dependence in first approximation [Fur88a, Kos93]. The relation between band gap and lattice constant for several ternary II-VI semiconductors is shown in figure 1.5. The small deviation of the linear dependence which can be seen in the figure is known as "bowing" [Bec88, Tho67]. The effect of bowing is rather small in wide-band-gap DMS[8], so that the band gap energy for a given composition can be estimated by the virtual crystal approximation (VCA) [Fur88a]:

$$E_g(x) = (1-x)\cdot E_g(x=0) + x\cdot E_g(x=1) = E_g(x=0) + x\cdot \Delta E_g \tag{1.19}$$

with $\Delta E_g = E_g(x=1) - E_g(x=0)$. Using the energy gaps of the binary compounds for liquid helium temperature ($T = 4.2\,\mathrm{K}$), results for the ternary compounds

$$\mathrm{Cd}_{1-x}\mathrm{Mn}_x\mathrm{Te} : E_g(x) = 1.606 + 1.592x \text{ [eV]} \ (x < 0.77) \ [\text{Bot81, Hei86, Yod85}] \tag{1.20}$$

and

$$\mathrm{Zn}_{1-x}\mathrm{Mn}_x\mathrm{Se} : E_g(x) = 2.82 + 0.48x \text{ [eV]} \quad [\text{Fur88a}]. \tag{1.21}$$

As in the $A^{II}B^{VI}$ "parent" material, the temperature affects the energy gap in DMS by a linear relationship. The energy gap tends to open wider as the temperature decreases [Bec88, Fur96].

[7] This influence can be dramatic at higher concentrations. For example, in (Zn,Be)Se changes the fundamental band gap to an indirect band gap ($\Gamma \rightarrow X$) for Be concentrations over 0.46. This leads to rapid degeneration of the optical properties [Cha00, Slo06].

[8] In (Cd,Mn)Te bowing is even absent [Bec88].

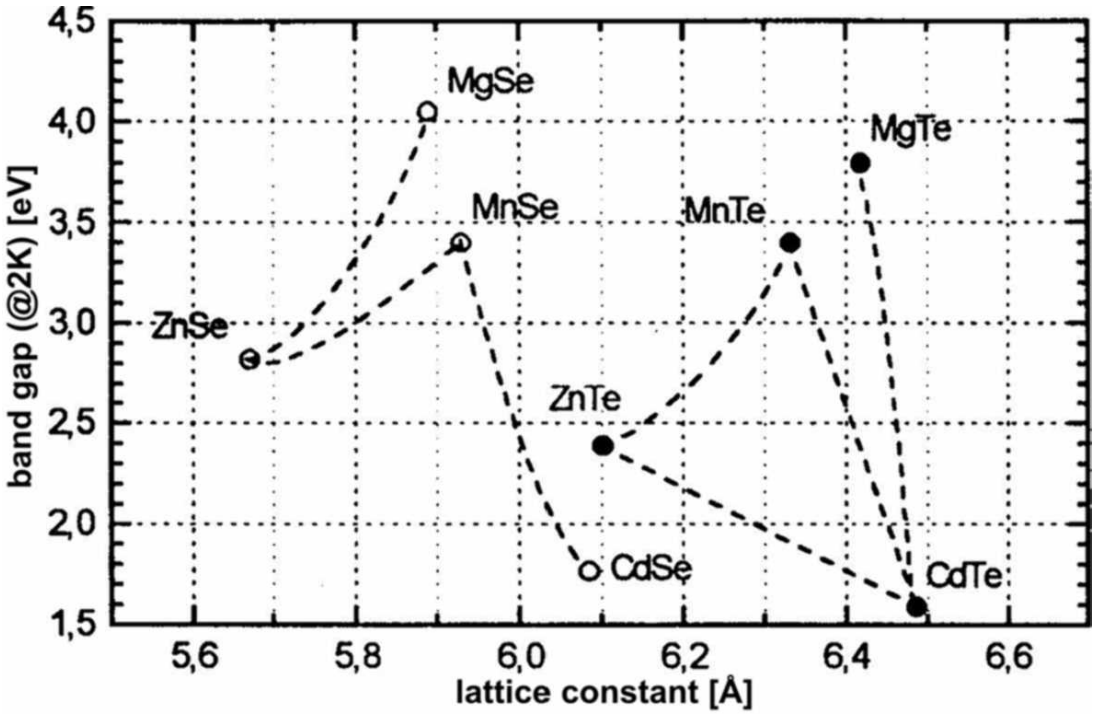

Figure 1.5 – Relation between lattice constant a_0 and fundamental band gap in several II-VI semiconductors [Mac96]. The ternary compounds lie on the dashed lines between the binary compounds.

Apart from the bowing, an additional anomalous temperature dependence of the energy gap at low temperatures can be observed in several $A^{II}_{1-x}\mathrm{Mn}_x B^{VI}$ alloys, especially strong in (Zn,Mn)Se [Byl86, Byl87, Dio85, Gaj87, Ike68, Kol86c, Lee84]. This might be due to second-order corrections to the energy of the band edge states, originating from the p-d- and s-d-exchange interaction with the localized magnetic moments [Byl86]. This correction can be a possible explanation for the peculiar temperature dependence of bowing in DMS [Kos93, Gaj87].

An isolated manganese atom has the electronic configuration (Ar) $4s^2 3d^5$. As already mentioned, the $4s^2$-electrons substitute the s- valence electrons of the cations, if manganese is incorporated in an $A^{II}B^{VI}$ lattice, and contribute therefore to the formation of valence and conduction band. Contrary the electrons of the half filled d-shell cannot contribute to the band structure, but their effects superimpose on the band structure of the host semiconductor. The reason for this is that the energy of the narrow band, originating from the ground state of the $3d^5$ electrons, lies approximately 3.5 eV below the valence band edge (E_{vb}) [Fra85, Oel82, Tan86, Web81]. The ground state $e_d^{+\sigma}$ is an orbital singlet. This cannot be further split by the crystal field of the semiconductor matrix nor by the spin-orbit interaction. Solely the spatial extension of the wave functions increases slightly because of hybridization with the p-bands of the host semiconductor [Lee84, Lee86, Mor82, Ngu83, Tao82]. The position of the ground state is rather insensitive to the host material [Fur96]. The corresponding excited state $e_d^{-\sigma}$ is about 3.5 eV above the top valence band in (Cd,Mn)Te [Wal89]. The reason for this energy difference ($\Delta E_{e_d^\sigma} \approx 7\,\mathrm{eV}$) between the states follows from the required changing of the number of

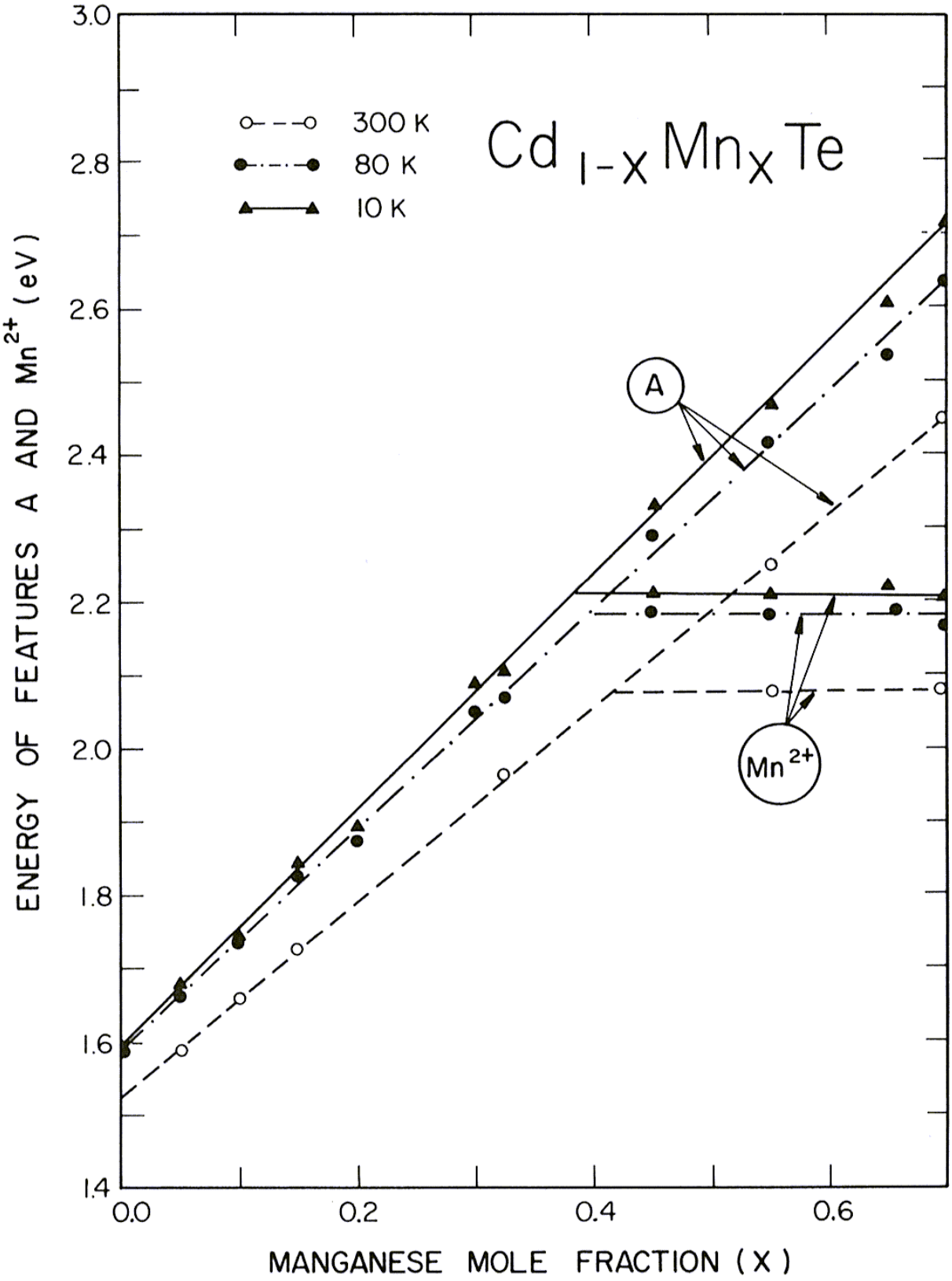

Figure 1.6 – Experimental results for the variation of the energy gap in $Cd_{1-x}Mn_xTe$ with Mn concentration for three temperatures according to [Lee84]. The measured peak (A) corresponds to the free exciton. The concentration independent feature at higher manganese concentrations is related to manganese intra-ion transitions. [Fur88b]

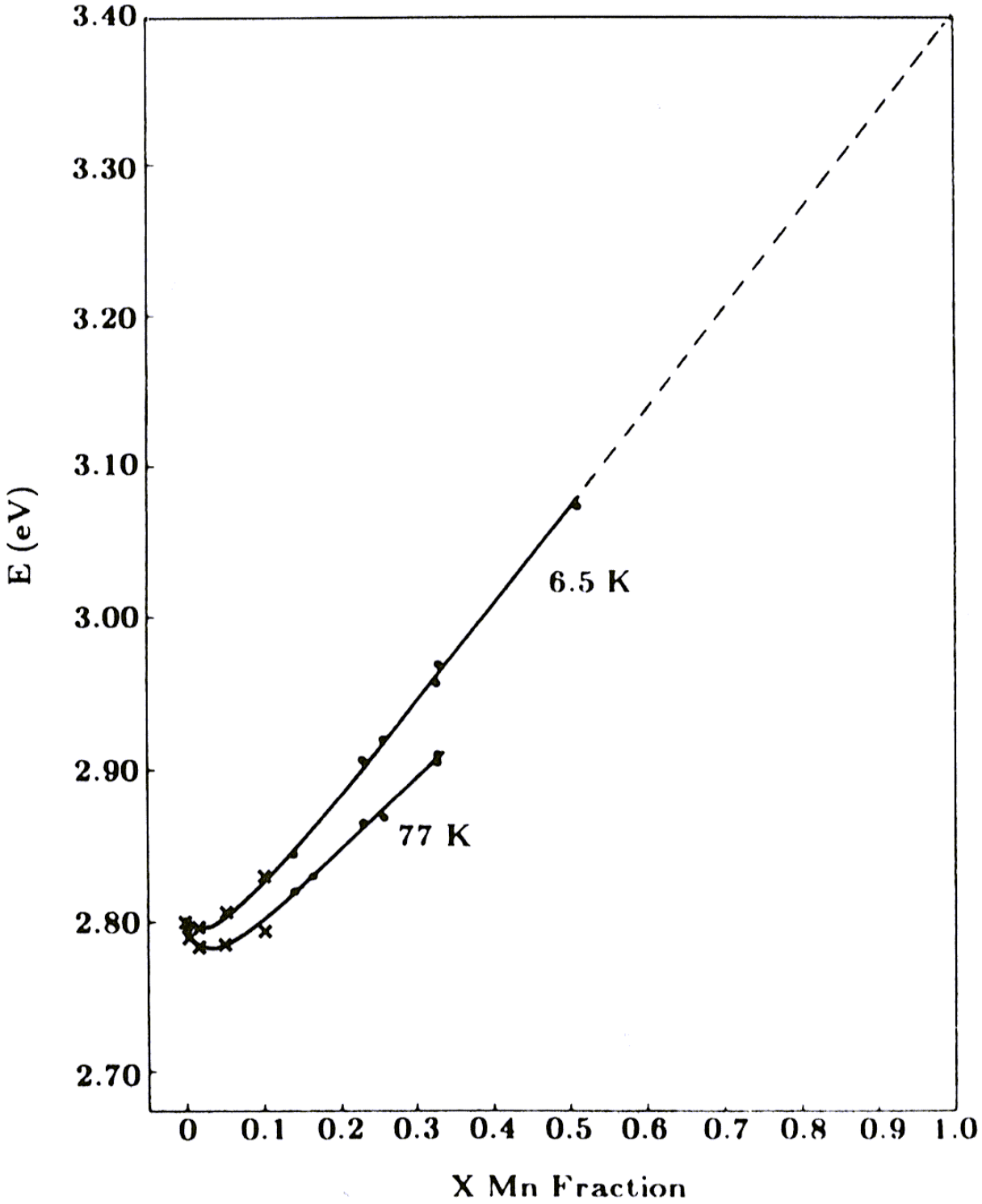

Figure 1.7 – Experimental results for the variation of the energy gap in $Zn_{1-x}Mn_xSe$ with Mn concentration for two temperatures according to [Bec88]. Cross-hatched points originate from [Twa83] and dots from [Kol86c]. At low x appears noticeable bowing. [Fur88b]

electrons in the d-shell for a transition. Because of the parallel alignment of all five spins in the orbital ground state, this would require an exceptional energy-consuming add of an electron with an opposite spin [Has90]. In this respect the $3d^5$ orbit conducts similar to a complete shell. Nevertheless, these states are very important in formulating p-d type hybridization mechanism [Bha83, Has86, Lar85, Lar88b, Lar88a] (see 1.3.4.1, especially equation 1.44).

Dissociated from this transition are spin-flip intra-ion transitions. These do not change the number of electrons occupying the $3d$-shell, but flip the direction of some electron spins. While the excited spin of a Mn-ion relaxes to the ground state, the neighboring spin becomes excited. Such transitions are possible because the $3d$-shell of the Mn-ion is only half-filled, which is a peculiarity of $A^{II}_{1-x}\mathrm{Mn}_x B^{VI}$ compounds compared to binary $A^{II}B^{VI}$ or other II-VI ternary compounds.

According to Hund, the $3d^5$ manganese electrons of a free Mn atom constitute in the ground state a ${}^6S$ multiplet with $L = 0$, $S = 5/2$ and $J = 5/2$. The higher states require flipping of at least one of the d-electron spins. Dominant for optical properties are transitions involving the lowest energy. Such states emanate from the ground state by flipping the spin of one electron ($S = 3/2$). They are labeled ${}^4P$ ($L = 1$), ${}^4D$ ($L = 2$), ${}^4F$ ($L = 3$) and ${}^4G$ ($L = 4$), corresponding to $S = 3/2$ and $L = 1, 2, 3, 4$. According to figure 1.8 the transition ${}^6S \rightarrow {}^4G$ has the lowest energy.

The crystal field of the $A^{II}B^{VI}$ host lattice is mainly induced by the Coulomb field of the four tetrahedrally surrounding next anions. Thus, it is not strong enough to break Hund's rule. The ground state remains the ${}^6S$ state. It is labeled as ${}^6A_1$ in group theoretical notation, as it changes from the spherical symmetry of the free Mn^{2+}-ion to the tetrahedral symmetry of the crystal field.

The ninefold[9] degenerated excited state ${}^4G$ is lifted in a cubic crystal field and splits in four levels: ${}^4T_1$, ${}^4T_2$, ${}^4E$ and ${}^4A_1$ [Abr70, Sug70]. As shown in figure 1.8, the ${}^4T_1$ and ${}^4T_2$ states are lowered by the crystal field while the ${}^4E$ and ${}^4A_1$ states are energetically almost coincident with the ${}^4G$ state and practically unaffected by the crystal field [Gri61, Tan54].

In the free ion case transitions between the ${}^6S$ and any excited state are forbidden by the $\Delta S = 0$ selection rule and the parity selection rule. By placing Mn^{2+}-ions in a zincblende $A^{II}B^{VI}$ semiconductor, the first rule is relaxed due to spin-orbit interaction and the second rule due to the absent inversion symmetry in the zincblende crystal lattice. The transitions become allowed. Energetically favored is the ${}^6A_1 \rightarrow {}^4T_1$ transition, which occurs at energies around 2.2 eV [Fur96]. This transition often governs the optical properties at high values of x. At higher manganese contents also transitions with higher states can be observed due to broadening and overlap of the states [Lan65, Mor84, Mor82, Tao82].

[9]The states of the free atom have a degeneracy of $2L + 1$.

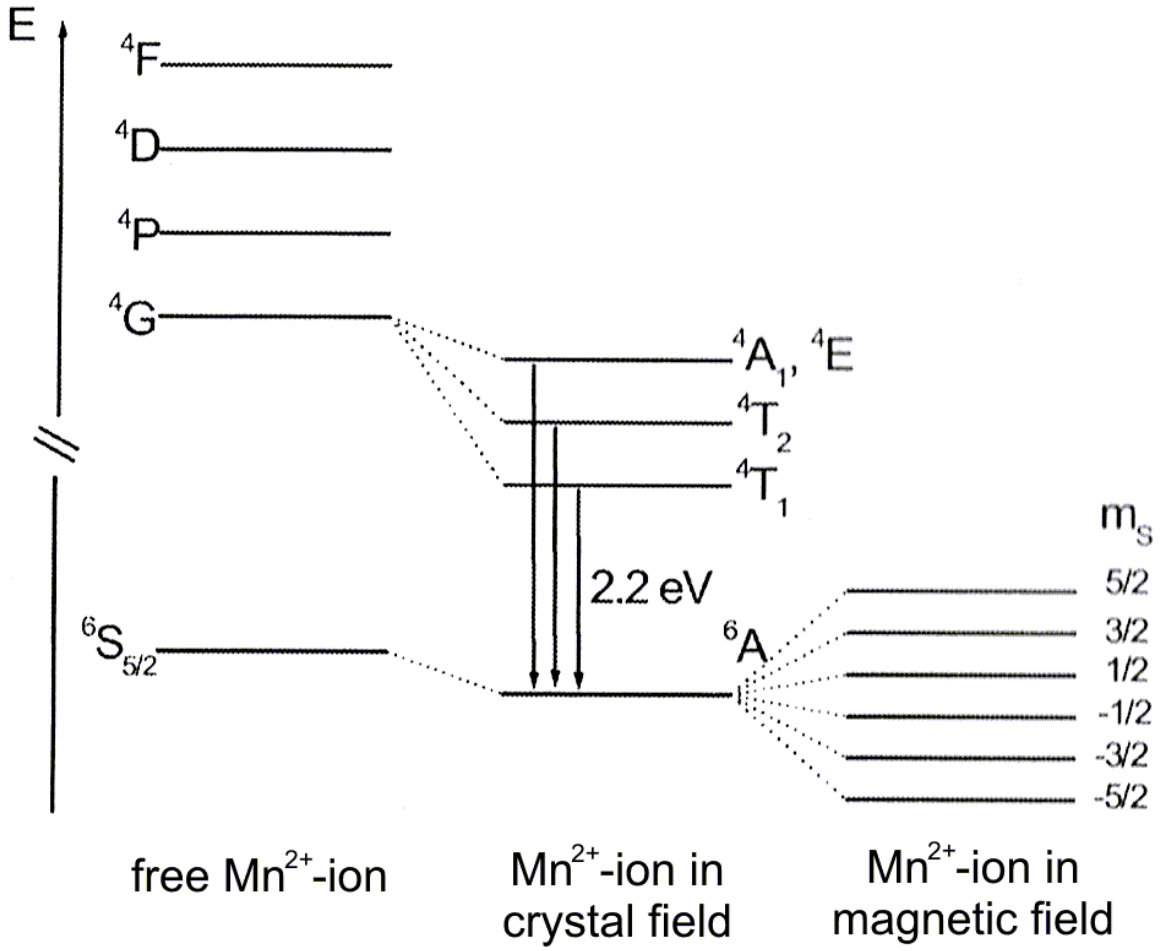

Figure 1.8 – Scheme of the lowest energy states of the Mn $3d$-shell. Shown are three cases: on the left the isolated Mn-ion, in the middle the splitting of the $^4T_1$ level in crystal field and on the right the splitting of the ground state ^6A in external magnetic field. The internal Mn transition ($^6A_1 \rightarrow^4 T_1$) amounts to 2.2 eV. [Kel04]

The temperature dependence of the intra-ion transitions is qualitatively similar to the dependence of the energy gap of the $A^{II}B^{VI}$ host material [Fur96]. More detailed information on these transitions is included in [Abr70, Bal62, Gri61, Sug70].

1.3 Magnetic properties

1.3.1 Basic principles of magnetism

Magnetic properties emerge from the occurrence of a magnetic ordering in a solid state. Magnetic ordering was theoretically postulated by Weiss in 1907 [Wei07] and quantum-mechanically explained by Heisenberg in 1928 [Hei28]. Classically is magnetism not explainable, being a direct consequence of the Bohr-van-Leeuwen theorem. This indicates that magnetic phenomena can only have quantum-mechanical origin, since the magnetism of classical systems vanishes in thermic equilibrium.

Source of the magnetism in matter is the magnetic moment of electrons, which is induced by spin and orbital angular momentum [Kit05]. Although nucleons also have a magnetic moment, it can be neglected due to the large difference in masses between nucleons and electrons. Magnetic ordering is based upon a collective alignment of the magnetic moments of the atoms of a crystal lattice. The moments are either permanent or induced. An alignment can occur either spontaneous or enforced by an external magnetic field. Spontaneous occurrence of long-range ordering arises from the competition of energetically favorable ideal alignment of the spins (minimum of inner energy U) and entropically favorable complete disorder (minimum of entropy S). The relation between both values is given by the free energy $F = U - TS$. While at low temperatures the inner energy dominates (aligned spins), rises with increasing temperature the impact of entropy in form of fluctuations around the ground state. At the so-called ordering temperature prevails the entropy-contribution and a phase transition to an unordered phase occurs.

Several types of magnetic ordering can be distinguished, which can be divided into two groups. The dia- and paramagnetism shows no long-range magnetic ordering in absence of external magnetic fields. In contrast occurs for ferro-, ferri- and antiferromagnetism a spontaneous long-range magnetic ordering, manifesting in a macroscopic magnetization for ferro- and ferrimagnetism. As at zero magnetic field in dia- and paramagnetic systems the magnetic symmetry and the crystal symmetry coincide, causes the spontaneous long-range magnetic ordering a reduction of symmetry. Due to the fact that time-inversion causes spin reversal, the symmetry is broken.

The relation between magnetization $\vec{M}$ and magnetic field strength $\vec{H}$ establishes via the magnetic susceptibility $\hat{\chi}_m$:

$$\vec{M} = \hat{\chi}_m \cdot \vec{H} = (\mu_r - 1) \cdot \vec{H} = \frac{\hat{\chi}_m}{\mu_0} \cdot \vec{B} \tag{1.22}$$

with $\vec{B} = \mu_0 \mu_r \vec{H}$ and the magnetic permeability μ_0. The magnetic susceptibility is defined as the difference of relative permeability of a material μ_r and relative permeability of vacuum ($\mu_r = 1$). The relative permeability is the relation between magnetic flux density B in mater and magnetic flux density B_0 in vacuum at the same magnetic field strength H: $\mu_r = \frac{B}{B_0}$.[10] The five types of magnetic ordering are consecutively described.

1.3.1.1 Larmor Diamagnetism

Although diamagnetism is in all solid states existent, it can be observed only in atoms or ions with complete filled electron shells. Otherwise the weak diamagnetism is obscured by other types of magnetic ordering. In diamagnets a magnetic moment is induced by an ex-

[10] In accordance with modern literature, only B is consecutively used for the magnetic field.

ternal magnetic field. The electrons precess in direction of the field and act against the inducing field according to the Lenz rule. Therefore, the susceptibility is negative and small ($10^{-9} < |\chi_{dia}| < 10^{-5}$) [Ash76, Ash07]. An exclusion are perfect diamagnets (superconducting materials), which have $\chi_{dia} = -1$. Diamagnetism is temperature-independent [Stö04].

1.3.1.2 Paramagnetism

Paramagnetism exists in atoms or ions with partly filled orbitals possessing unpaired electrons, so that uncompensated magnetic moments can occur. In absence of magnetic fields and long-range interactions, the magnetic moments are distributed statistically. Hence, an average macroscopic magnetic moment vanishes. The magnetic moments can be aligned by an external magnetic field. The susceptibility of paramagnetism is positive and in an order of magnitude of $10^{-3} < |\chi_{para}| < 10^{-2}$ [Ash76, Ash07]. Three manifestations of the paramagnetism can be distinguished: the Van Vleck paramagnetism, the Langevin paramagnetism and the Pauli paramagnetism.

The Langevin paramagnetism appears for magnetic moments of atoms or ions in the ground state. The magnetization is given thermodynamically for N ions in a volume V by:

$$M = -\frac{N}{V}\frac{\partial F}{\partial B} = n\frac{\partial F}{\partial B}, \tag{1.23}$$

with the number of magnetic moments per unit volume n. The free energy F is defined by

$$\exp\left(-\frac{F}{k_B T}\right) = \sum_n \exp\left(-\frac{g\mu_B B}{k_B T}\right). \tag{1.24}$$

For low temperatures it is sufficient to provide only for the $n = 2J + 1$ lowest states. Therefore follows for the macroscopic magnetization of free magnetic moments $\mu = -g\mu_B J$ without interaction, i.e. the spins can be regarded as independent from one another, [Ash76, Ash07]:

$$M = -ng\mu_B J\mathcal{B}_J(y) \quad \text{with} \quad y = \frac{g\mu_B JB}{k_B T}. \tag{1.25}$$

In the equation is

$$g = 1 + \frac{J(J+1) + S(S+1) - L(L+1)}{2J(J+1)} \tag{1.26}$$

the Landé g-factor of electrons, μ_B the Bohr magneton and $\mathcal{B}_J(y)$ the Brillouin-function. The latter is described by [Ash76, Ash07]:

$$\mathcal{B}_J(y) = \frac{2J+1}{2J}\coth\left(\frac{2J+1}{2J}y\right) - \frac{1}{2J}\coth\left(\frac{y}{2J}\right). \tag{1.27}$$

For high temperatures and weak magnetic fields the Brillouin-function can be simplified, so that the susceptibility can be described by the classical Curie law

$$\chi_{para}^{Langevin} = \frac{C}{T} \tag{1.28}$$

with the Curie constant C.

In contrast the Van Vleck paramagnetism is temperature independent. It arises from magnetic moments of excited states. In case of non-vanishing orbital angular momentum $J \neq 0$, the Van Vleck paramagnetism is about three orders weaker than the Langevin paramagnetism and, thus, is negligible.

The Pauli paramagnetism finally arises from the magnetic moment of delocalized electrons and, therefore, is important for metals. It will be described further in subsection 1.3.2.

1.3.1.3 Heisenberg model

The long-range interaction of magnetic moments is dominated by the exchange interaction between electron spin and crystal anisotropy, which is based upon the spin-orbit interaction [Kit05, Kru68]. The magnetic dipole-dipole interaction[11] is, except for phase transitions [Aha73], by factor 10^{-3} weaker and can be neglected.

Description of the crystal anisotropy is microscopically carried out by the one-ion-model and the ion-pair-model. For the $3d$-electrons in manganese prevails the one-ion contributions, whose, with reasonable certainty sufficient, lowest order term amounts to

$$\hat{H}_{anisotropy} = -D \sum_i (S_i^z)^2. \tag{1.29}$$

The constant D is named anisotropy constant. In three-dimensional isotropic alignments holds $D = 0$.

The exchange interaction results from Coulomb interaction and Pauli principle [Ash76, Ash07]. Description of the interaction yields the Heisenberg model [Hei28]:

$$\hat{H}_{exchange} = -2 \sum_{i \neq j} \hat{J}_{ij} \vec{S}_i \cdot \vec{S}_j. \tag{1.30}$$

The equation provides the contribution to the Hamiltonian by composition of two spin vectors $\vec{S}_{i,j}$ by a quantum mechanical exchange integral $\hat{J}_{ij}$.

In isolators appears both, the direct exchange and the superexchange, as contributions of the exchange integral. The direct exchange is based on the overlap of electron wave functions of

[11] $\hat{J}_{dipole} = 2\sqrt{2}\frac{g^2\mu_B^2}{a_0^3}$

neighboring ions. For distant ions is the direct exchange negligible. However, by a nonmagnetic ion the exchange can be mediated between the magnetic ions. This case is the superexchange [Rad63].

The distinction of the types of long-range ordering is conducted by the contributions to the exchange integral $\hat{J}_{ij}$.

1.3.1.4 Ferromagnetism

The ferromagnetic ordering is the experimentally first discovered long-range magnetic ordering [Bar19]. The exchange integral is positive, so that the magnetic moments align parallel at each other. The positive susceptibility ($10^2 < |\chi_{ferro}| < 10^6$) follows the Curie-Weiss law

$$\chi^{ferro} = \frac{C}{T - \Theta}, \tag{1.31}$$

where Θ is the, Curie-Weiss temperature called, ordering temperature of the ferromagnetic phase. With rising temperature decreases the ferromagnetism and passes finally into a paramagnetic phase. This second order phase transition occurs at Θ [Nol96]. The order parameter is the magnetization.

In ferromagnetic materials form regions of different magnetization, so-called domains, which can be aligned unitary by an external magnetic field [Bar19, Wei07]. Furthermore, shows the magnetization of ferromagnets hysteresis.

1.3.1.5 Ferrimagnetism

The peculiarity of ferrimagnets are two or more spin-sublattices, whose magnetic moments are not parallel aligned. Different values of magnetization in the sublattices lead, even in the case of two antiparallel aligned sublattices, to a resulting magnetic moment. Exchange contributions within the sublattices (positive exchange integral contribution) as well as between the sublattices (negative exchange integral contribution) have to be taken into account. If the exchange integral for the contributions between the sublattices is bigger than the intra-sublattice exchange integral, the magnetic moments align antiparallel. Ferrimagnetic materials pursue the Curie-Weiss law and form domains.

1.3.1.6 Antiferromagnetism

In the simplest case an antiferromagnetic material has two sublattices, whose equal magnetic moments compensate by antiparallel alignment. This is a special case of ferrimagnetism. The lack of macroscopic magnetic moment makes manipulation and identification of antiferromag-

netic ordering difficult. Antiferromagnetic ordering was postulated in 1953 by Neél and experimental verified for the first time in 1960 by Roth and Slack [Rot60, Sla60].

The exchange integral is negative for antiferromagnetic materials. With respect to the dimensionality of the spin n, that means how many components i, j of the spin vector $\vec{S}_{i,j}$ are incorporated in equation 1.30, exist three possible antiferromagnetic spin structures: the one-dimensional Ising antiferromagnets (magnetic moments parallel or antiparallel to easy-axis), the two-dimensional XY antiferromagnets (magnetic moments aligned in easy-plane) and the three-dimensional Heisenberg antiferromagnets (isotropic alignment of magnetic moments).

The temperature dependence of antiferromagnetic materials is similar to ferromagnets:

$$\chi_{afm} = \frac{C}{T - T_{Neel}}. \tag{1.32}$$

The antiferromagnetic phase evolves from a paramagnetic phase for temperatures below the Neél temperature T_{Neel}. As order parameter is the magnetization unsuitable, as it vanishes due to the compensation of the magnetic moments. Instead, a linear combination of the magnetic moments inside of a unit cell is used, which has to be invariant regarding the symmetry group of the antiferromagnet [Ned65, Pas95, Sa00]. Since the order parameter gets zero approaching T_{Neel}, the phase transition is of second order. Domains in antiferromagnets are discriminated by the different orientations of the order parameter [Bro93].

1.3.2 Magnetic effects of free electrons

Up to now unregarded is the contribution of conduction electrons to the magnetic moment of a metal or semiconductor. Conduction electrons have two peculiarities: They are not spatially localized and they do not respond independently because of the constraints of the Pauli exclusion principle. To solve the conduction electron problem, the classical theory of the free electron gas is not a productive approach. Classically is expected that the spins align parallel to an applied external field with a resulting magnetic moment $\sim N\frac{\mu_e^2 \vec{B}}{k_B T}$ for N atoms [Kit05]. The moment of an electron with spin $\sigma = 1/2$ and g-factor $g_e = 2$ amounts to $\mu_e = \mu_B(g_e\sigma + l)$, where l is the free electron orbital angular momentum. However, this alignment is not allowed for the conduction electrons, as most of the states with parallel spin are already occupied. Only electrons near the Fermi energy E_F can flip, so that the electrons contribute only partly to the magnetization. Due to this consideration, Pauli corrected the classical theory by application of the Fermi-Dirac-distribution [Pau27].

Qualitatively the situation of conduction electrons can be understood according to figure 1.9. In absence of an external magnetic field, the free electrons fill the energy states equal for both orientations of the spin up to the Fermi-energy E_F. This follows from the Pauli principle. The density of states accounts to $D(E) \propto \sqrt{E}$. In magnetic field the orientation parallel to the

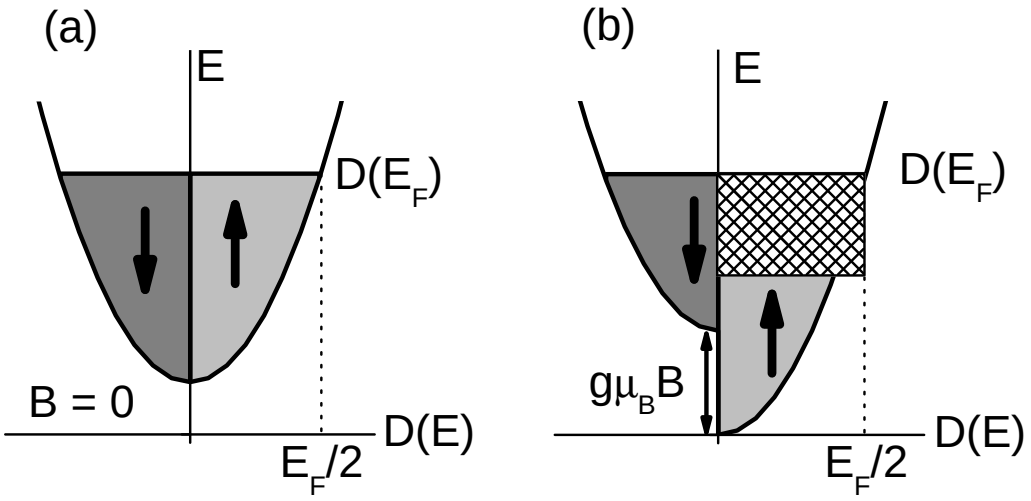

Figure 1.9 – Density of states (a) without magnetic field and (b) with magnetic field. In absence of magnetic field no spin direction is preferred. In magnetic field the spin subband with spins parallel to the magnetic field direction is preferred. Hence, its energy decreases, leading to a majority of electrons with parallel spin alignment. The resulting energy difference is called Zeeman-splitting. [Sän06]

direction of the field is energetically favored. Thus, the electronic levels of the spins parallel or antiparallel to the magnetic field split by the Zeeman energy [Zee97]

$$\Delta E_{Zeeman} = g_e \mu_B B. \tag{1.33}$$

The magnetization is proportional to the number of electrons per unit volume with spin antiparallel or parallel to magnetic field. This can be expressed by the density of states $D(E)$, whose relevant variation occurs on the scale of E_F [Ash76, Ash07].

As already mentioned, only electrons at E_F change their spins, so that the susceptibility depends on the density of states at the Fermi-energy $D(E_F)$ [Ash76, Ash07]

$$\chi_{para}^{Pauli} = \mu_B^2 D(E_F). \tag{1.34}$$

Contrary to the Langevin paramagnetism χ_{para}^{Pauli} is only weakly temperature dependent, and even for $k_B T \ll E_F$ independent on the temperature. From this equation can be deduced that the Pauli paramagnetism is considerable stronger in doped than in undoped semiconductors, because at low temperatures the density of states at the Fermi-energy decreases and vanishes for $T = 0\,\mathrm{K}$.[12]

So far was assumed that the electron movement is not influenced by the external magnetic field. Only the paramagnetic effects arising from the coupling of the electron spin with the magnetic field were considered. But also the orbital motion of the electrons couples with the field, leading to diamagnetic effects. According to Landau, the diamagnetic moment for free

[12]The Fermi-energy lies between the conduction band and valence band at $T = 0\,\mathrm{K}$.

electrons is one third of the paramagnetic moment [Lan30, Mis69, Pei55]. Therefore, the total susceptibility accounts to

$$\chi_{dia}^{Landau} = \frac{1}{3}\frac{m}{m_{eff}}\mu_B^2 D(E_F) = \frac{1}{3}\frac{m}{m_{eff}}\chi_{para}^{Pauli}, \tag{1.35}$$

where additionally the electron mobility is taken into account by the effective mass m_{eff}. It should be mentioned that in doped semiconductors the diamagnetic Landau contribution can be substantially larger than the paramagnetic Pauli contribution [Ash76, Ash07].

In effective mass approximation both contributions can be included to the Hamiltonian by the following term

$$\hat{H}_B = \frac{(\vec{p} - e\vec{A})^2}{2m_{eff}} \cdot + g_e \mu_B \vec{\sigma} \cdot \vec{B}, \tag{1.36}$$

where $\vec{\sigma}$ is the spin operator, $\vec{A}$ the vector potential and $\vec{p}$ the electron momentum operator. The first term corresponds to the Landau diamagnetism and the second term (the "Zeeman term") to the Pauli paramagnetism. The former is responsible for Landau-quantization and spin splitting of Landau-levels.[13]

1.3.3 Magnetic properties of (Cd,Mn)Te and (Zn,Mn)Se without Mn-Mn-interaction

Magnetic properties of matter originate mainly from the magnetic moments of electrons. Although nucleons also have a magnetic moment, this can be neglected due to the large difference in masses between nucleons and electrons. Responsible for the magnetic properties in (Cd,Mn)Te and (Zn,Mn)Se are the parallel aligned, unpaired spins of the half-filled Mn^{2+}-ion d-shell, which generate a magnetic moment due to their spin and angular momentum [Kit05]. In absence of magnetic fields and long-range interactions the magnetic moments are distributed statistically, so that an average macroscopic magnetic moment vanishes.

As the ground state of the Mn-ion ${}^6S$ has no orbital angular momentum ($J = S \neq 0$), the Van Vleck paramagnetism can be neglected compared with the Langevin paramagnetism. Furthermore, the electrons are localized, so that no contribution to the magnetization is given by the Pauli paramagnetism. In this case the macroscopic magnetization for free magnetic moments

[13] The Landau term derives from the Lorentz force, which acts on a particle under a magnetic field $\vec{B} = \vec{\nabla} \times \vec{A}$.

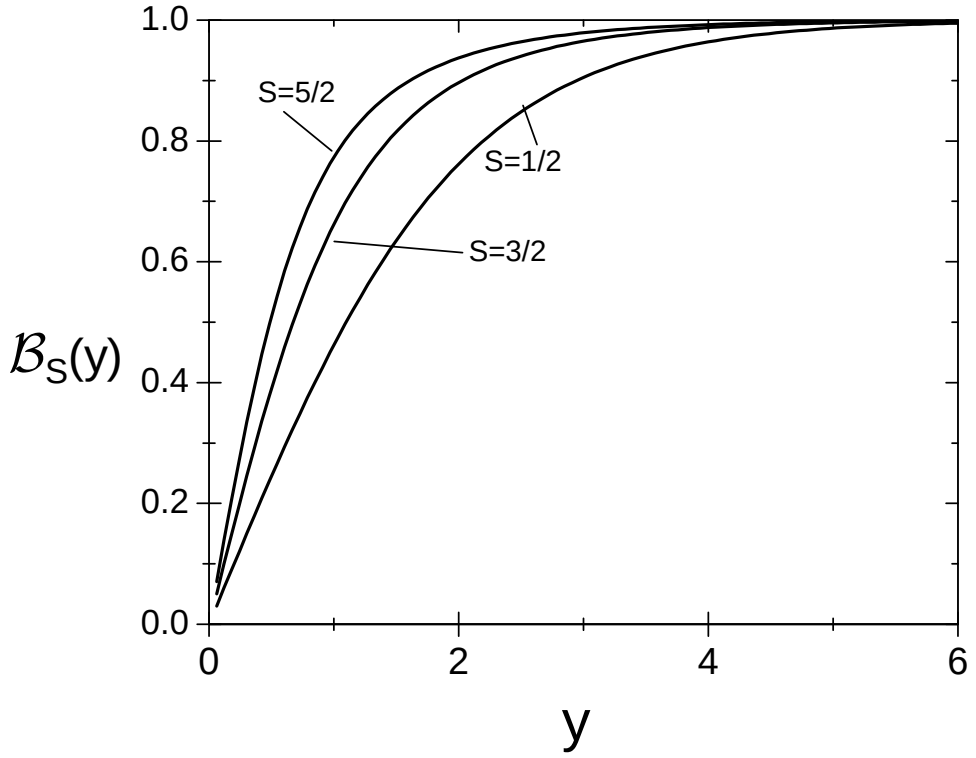

Figure 1.10 – Brillouin function for $S = 1/2, 3/2, 5/2$. [Aki06a]

$\mu = -g_{Mn}\mu_B S$ without interaction, i.e. Mn^{2+}-ion spins can be regarded as independent from one another, results

$$\begin{aligned} M &= -ng_{Mn}\mu_B \langle S_z \rangle \\ &= ng_{Mn}\mu_B S\mathcal{B}_S \left(\frac{g_{Mn}\mu_B SB}{k_B T_{Mn}} \right), \end{aligned} \tag{1.37}$$

with the number of magnetic moments per unit volume $n = xN_0$. Thereby, N_0 is the inverse unit-cell volume. The z-component of the thermal expected value of the spin $\langle S_z \rangle$ is thereby defined by

$$\langle S_z \rangle = -S\mathcal{B}_S \left(\frac{g_{Mn}\mu_B SB}{k_B T_{Mn}} \right), \tag{1.38}$$

with $S = 5/2$ for the Mn^{2+}-ions. T_{Mn} is the manganese spin temperature and equals the lattice temperature in equilibrium condition. The Landé g-factor constitutes for $J = S$ $g_{Mn} = 2$ according to 1.26.

The Brillouin-function is shown in figure 1.10 for $S = 1/2, 3/2, 5/2$. In the limit of small y, corresponding to high T_{Mn}, the dependence on the argument y is linear and, therefore, also linear on T_{Mn}^{-1} and B. Contrary, for large y (low T_{Mn}) the Brillouin-function is only weakly dependent on its argument and constitutes 1 in the limit of $y >> 1$. In the latter case the magnetic ions are fully polarized by external magnetic field [Aki06a].

In the limit of low fields or high temperatures obtains $\frac{g_{Mn}\mu_B SB}{k_B T_{Mn}} \ll 1$, so that M is linear in B:

$$M = \frac{\chi}{\mu_0} B, \tag{1.39}$$

where the static magnetic susceptibility χ is of the Curie form

$$\chi = \frac{C_0 x}{T}, \tag{1.40}$$

with the Curie constant $C_0 = N_0 \left(g_{Mn}\mu_B\right)^2 S(S{+}1) \left(3k_B\right)^{-1}$. At low temperatures the magnetic susceptibility is a nonmonotonic function of x. It has a maximum around $x \sim 0.14$ [Ose80].

Apart from the effect of the manganese ions, the DMS host lattices CdTe and ZnSe are weak diamagnets. Although weak, it has to be regarded in a quantitative analysis of magnetic data [Kos93]. This happens by adding the diamagnetic susceptibility χ_d as summand to the static magnetic susceptibility 1.40 [Ose88]. Especially relevant is the diamagnetic contribution for very low manganese concentrations ($x < 0.001$)[Ose88]. χ_d values for CdTe and ZnSe are given in table A.3 in the appendix.

Assuming an external magnetic field $\vec{B}$ parallel to the z-axis ($\vec{B} = (0, 0, B)$), the ground state of the Mn-ion splits in six $(2S + 1)$ equidistant sublevels,according to the z-component of the total spin. These are given by

$$E = g_{Mn}\mu_B m_S B, \tag{1.41}$$

with $m_S = -5/2, -3/2, -1/2, 1/2, 3/2, 5/2$ as depicted in figure 1.8.

1.3.4 Exchange Interactions

As pointed out in the introduction of this chapter, manganese based DMS have the peculiarity of two types of exchange interactions associated with the presence of the magnetic ions in the lattice. These are the interaction of the Mn^{2+}-ions among each other (d-d-exchange interaction) and the strong magnetic field- and spin-dependent impacts of the electronic band structure due to the interaction between localized d-electrons of the Mn^{2+}-ions and delocalized s- and p-orbitals of the band electrons (sp-d-exchange interaction). The former determine the magnetic and the latter the physical phenomena involving conduction and valence band states (e.g. magneto-transport properties and magneto-optics), impurity levels (e.g. negative magneto-resistance, magnetic-field-induced metal-insulator transition and formation of magnetic polarons) and exciton levels (e.g. giant Faraday rotation). For deeper insight in these effects, which are not described consecutively, can be referred to [Fur88b, Fur96, Kos93]. For the understanding it is

very convenient to distinguish between an electronic system (the semiconductor s- and p-type band states) and a magnetic system (the localized manganese d-electrons).

1.3.4.1 sp-d exchange interaction

Applying an external magnetic field to a nonmagnetic semiconductor leads to splitting of the valence band and conduction band into Landau levels. Theses are further split into two sub-levels with regard to the two possible orientations of the electron spin. If localized magnetic ions are incorporated into the semiconductor, this band structure is significantly influenced due to the sp-d-exchange coupling. Assuming a Hamiltonian $\hat{H}_0$ describing the situation in the non-magnetic semiconductor, the sp-d-exchange contribution to the band structure can be expressed by an additional Kondo-like exchange term [Liu61]

$$\hat{H}_{sp-d} = \sum_{\vec{R}_i} \left[\hat{J}_{sp-d} \left(\vec{r} - \vec{R}_i \right) \right] \vec{S}_i \cdot \sigma \tag{1.42}$$

for the Hamiltonian [Gał80a, Gun85, Myc81], where σ and $\vec{S}_i$ are the spin operators for the band and Mn^{2+} electrons, respectively, with the coordinates $\vec{r}$ and $\vec{R}_i$, respectively. $\hat{J}_{sp-d}$ designates the exchange coupling integral for the sp-d-exchange. The summation is over all lattice sites occupied by Mn^{2+}-ions.

To simplify $\hat{H}_{sp-d}$ two approximations are useful: the molecular field approximation (MFA) and the VCA [Fur96]. Both approximations are possible, as the electron wave function is so strongly extended that the electrons interact with a large number of Mn^{2+}-ions. Thus, averaging over several lattice position in both approximations is allowed. In the MFA the spin operator $\vec{S}_i$ is exchanged by its thermal average $\langle \vec{S} \rangle$ taken over all Mn^{2+}-ions. In the VCA the sum over all Mn positions in the lattice $\sum_{\vec{R}_i} \hat{J}_{sp-d} \left(\vec{r} - \vec{R}_i \right)$ is exchanged by $x \sum_{\vec{R}} \hat{J}_{sp-d} \left(\vec{r} - \vec{R} \right)$, where the summation is carried out over all sites of the fcc cation sublattice denoted by $\vec{R}$, but weighted with the Mn content x. The resulting Hamiltonian

$$\hat{H}_{sp-d} = \langle \vec{S} \rangle \cdot \sigma x \sum_{\vec{R}} \left[\hat{J}_{sp-d} \left(\vec{r} - \vec{R} \right) \right] \tag{1.43}$$

has the periodicity of the lattice and allows, therefore, to use the same wave functions as the crystal lattice Hamiltonian 1.6. Thus, the modifications of the band structure due to the sp-d-exchange interaction is determined by the values of the exchange constant $\hat{J}_{sp-d}$. Thereby, two different interactions have to be distinguished: the interaction between the d-electrons and the s-like Γ_6 electrons ($|S\rangle$), which is denoted by $\alpha = \langle S|J|S \rangle$ at the Γ-point; and the interaction between the d-electrons and the p-like Γ_8 electrons ($|X\rangle$), which is denoted by $\beta = \langle X|J|X \rangle$ at the center of the Brillouin-zone [Gaj79].

The size of the exchange interaction is influenced by two competing effects [Bha83]. Positive contribution is given by parallel (ferromagnetic) alignment of the spins due to direct $1/r$-potential Coulomb exchange between the band electrons and the Mn-$3d$-electrons. Negative contribution is given by the so-called kinetic exchange, originating from the hybridization of the $3d$-electrons with the s- and p-band electrons and leads to an antiferromagnetic alignment of the spins of the Mn-ions and band electrons. Because s-d-hybridization is forbidden at the Γ-point by symmetry [Bha83, Die81], the parameter α for the s-like conduction band is only determined by the direct ferromagnetic potential exchange. On the other hand for the p-like valence band outweighs the negative contribution by the strong p-d-hybridization of the valence band states the direct exchange contribution [Has90, Lar88b]. Compared with α, the parameter β is, therefore, larger and negative. Generally, β can be written in two parts $\beta = \beta_{pot} + \beta_{hyb}$, corresponding to the particular contribution. The value of β_{pot} is approximately equal to α [Bha83]. A parametrization of the p-d type hybridization mechanism can be achieved by the Schrieffer-Wolff expression [Lar88b, Sch66, Sch67] with the band structure parameters introduced in subsection 1.2.2, the hybridization parameter V_{pd} and the density of cations per volume N_0

$$N_0\beta_{hyb} = -32(V_{pd})^2 \left[\left(e_d^{+\sigma} + \Delta E_{e_d^\sigma} - E_{vb} \right)^{-1} + \left(E_{vb} - e_d^{+\sigma} \right)^{-1} \right]. \tag{1.44}$$

Experimentally determined values for α and β in (Cd,Mn)Te and (Zn,Mn)Se, which can be achieved by comparison of magnetization and optical measurements of the Zeeman-splitting, are listed in table A.8 in the appendix. It should be stressed that neither β nor α are sensitive to the Mn concentration x.

In case of an external magnetic field $\vec{B}$ parallel to the z-axis ($\vec{B} = (0, 0, B)$), obtains $\left\langle \vec{S} \right\rangle = \langle S_z \rangle$ ($\left\langle \vec{S_y} \right\rangle = \left\langle \vec{S_x} \right\rangle = 0$) for the thermal expected value of the total spin of the ground state in equation 1.43.

1.3.4.2 d-d exchange interaction

Calculation of the modifications of the magnetization 1.37 due to the interaction of the randomly distributed magnetic ions is a very challenging task. In the Hamiltonian, the d-d-exchange interaction can be taken into account by the following effective spin Hamilton-Operator [Lar89]:

$$\hat{H}_{d-d} = -\sum_{i \neq j} \sum_{\alpha,\beta} \vec{S}_{i,\alpha} \hat{J}^{d-d}_{\alpha,\beta} \left(\vec{R}_{ij} \right) \vec{S}_{j,\beta}. \tag{1.45}$$

Thereby, $\hat{J}_{\alpha,\beta}$ denotes the exchange coupling tensor and $\vec{R}_{ij} = \vec{R}_i - \vec{R}_j$ the distance vector of both spins. $\vec{S}_{i,\alpha}$ and $\vec{S}_{j,\beta}$, respectively, corresponds to the components α and β, respectively, of

the Mn-spin i at $\vec{R}_i$ and j at $\vec{R}_j$, respectively. The exchange coupling tensor can be separated in a sum of three contributions [Kac01]:

$$\hat{J}^{d-d}_{\alpha,\beta} = J^{d-d}\delta_{\alpha\beta} + \frac{1}{2}\left(\hat{J}^{d-d}_{\alpha,\beta} - \hat{J}^{d-d}_{\beta,\alpha}\right) + \left[\frac{1}{2}\left(\hat{J}^{d-d}_{\alpha,\beta} + \hat{J}^{d-d}_{\beta,\alpha}\right) - J^{d-d}\delta_{\alpha\beta}\right], \tag{1.46}$$

with $J^{d-d} = \frac{1}{3}Tr\hat{J}^{d-d}_{\alpha,\beta}$. Usually most important is the first isotropic exchange term, which can be described by a Heisenberg-Hamilton-Operator [Lar89]:

$$\hat{H}_H = -\sum_{i\neq j} J^{d-d}\left(\vec{R}_{ij}\right)\vec{S}_i\vec{S}_j. \tag{1.47}$$

By $J^{d-d}\left(\vec{R}_{ij}\right)$, which is denoted as coupling constant of the isotropic exchange interaction, the overlap of the wave functions of the spins is displayed.

The second, antisymmetric tensor leads to the Dzyaloshinsky-Moriya exchange interaction [Dzy57, Dzy58, Mor60, Ste53] and can be written for two adjacent Mn-ions in the following way [Lar89]:

$$\hat{H}_{DM} = -\sum_{i\neq j}\vec{D}_{ij}\left(\vec{R}_{ij}\right)\left(\vec{S}_i \times \vec{S}_j\right). \tag{1.48}$$

Thereby is the vector $\vec{D}_{ij}$ perpendicular to the plane, which is spanned by two Mn-ions and the in-between lying anion. The pseudo-dipolar (PD) interaction results from the third, traceless symmetric tensor [Kac01]:

$$\hat{H}_{PD} = \hat{H}_{eff} - \hat{H}_H - \hat{H}_{DM}. \tag{1.49}$$

It is important to mention that the repartition of the interactions into three parts does only define the form of the exchange coupling tensor, but not any microscopic model.

In Mn-based II-VI DMS the isotropic part outbalances all others suchlike that the latter can be neglected for most static problems [Lar88b]. The relevance of the anisotropic part arises mainly from the description of dynamic processes, like SLR, which are discussed later in this thesis. As the Hamiltonian is invariant against rotations, it commutates with each coordinate of the total magnetization. Therefore, the magnetization of a system would remain constant in time regime in absence of anisotropic interactions, like the Dzyaloshinsky-Moriya exchange interaction or the magnetic dipole-dipole interaction [Sca96a]. The latter are the domination mechanisms in spin-spin interactions between Mn^{2+}-ions. Conclusions about quantity, prefix and range of the isotropic exchange interaction can be made on basis of thermodynamical values, like magnetization M, magnetic susceptibility χ, specific heat C_m or phase transitions.

Four main mechanisms leading to spin-spin interactions can be distinguished from each other: the Bloembergen-Rowland interaction (i.e. virtual excitation of conduction pairs of holes

and electrons) [Blo55] and the Ruderman-Kittel-Kasuya-Yosida-interaction (RKKY) (i.e. indirect exchange interaction via electrons) [Yos57], which are one-hole-one-electron processes; the double exchange [Zen51], which is based on two-electronprocess; and the superexchange [And50a, And59], which is based on two-hole processes [Kac01]. In Mn-based II-VI DMS the superexchange is dominant. All other mechanisms contribute only by approximately 5 % to the spin-spin interactions [Lar85]. More detailed overview on the different exchange interactions in DMS is given in [Kac01].

The dominant isotropic Heisenberg superexchange relies on coupling of two adjacent Mn-ions by virtual hopping-processes via the $4p$-orbitals of the intermediate anions [Lar85, Lar88b, Lar88a]. It is induced by p-d-hybridization. Thus, it can be considered as being mediated by the sp-d-exchange process[14]. This accounts for the fact that the parameters α and β are considerably larger than the coupling constant J^{d-d} [Fur96]. Therefore, formulation of the superexchange can be made with the same band structure parameters as β_{hyp} [Fur88a, Lar88b]:

$$J^{d-d}\left(\vec{R}_{ij}\right) = -2(V_{pd})^4 \left[\left(e_d^{+\sigma} + \Delta E_{e_d^\sigma} - E_{vb}\right)^{-2}\left(\Delta E_{e_d^\sigma}\right)^{-1} + \left(e_d^{+\sigma} + \Delta E_{e_d^\sigma} - E_{vb}\right)^{-3}\right] f(r). \tag{1.50}$$

The dimensionless function $f(r)$ with $r \equiv \frac{R_{ij}}{a_0}$ accounts for the spatial dependence of the coupling constant $J^{d-d}\left(\vec{R}_{ij}\right)$ and is well described by a Gaussian decay [Kos93]. This is due to the fact that the d-d-exchange interaction is primarily a nearest-neighbor interaction.

Experimental access to the exchange constant of Mn-ions on direct adjacent cation positions J_{NN} is given by measurements of magnetization or optical splitting of the band-edge exciton at low temperatures [Agg85, Sha86, Sha87]. For high magnetic fields ($B > 10\,\mathrm{T}$) shows the magnetization a striking steplike distribution as function of magnetic field [Sha84]. This can be ascribed to prising of the antiferromagnetic coupled spins of adjacent neighbors. It should be stressed in this context that the amplitude of the steps decreases with falling Mn content [Lar86]. This traces back to the fact that the probability for the existence of antiferromagnetically coupled Mn-ion pairs is decreasing with falling Mn concentration.

Description of a pair of two adjacent Mn-ions in magnetic field is given by the Hamilton-Operator [Nag80]

$$\hat{H} = -2J_{NN}\vec{S}_1\vec{S}_2 - g_{Mn}\mu_B\left(S_1^z + S_2^z\right)B. \tag{1.51}$$

[14] It can be regarded as a twofold step of the same hybridization process.

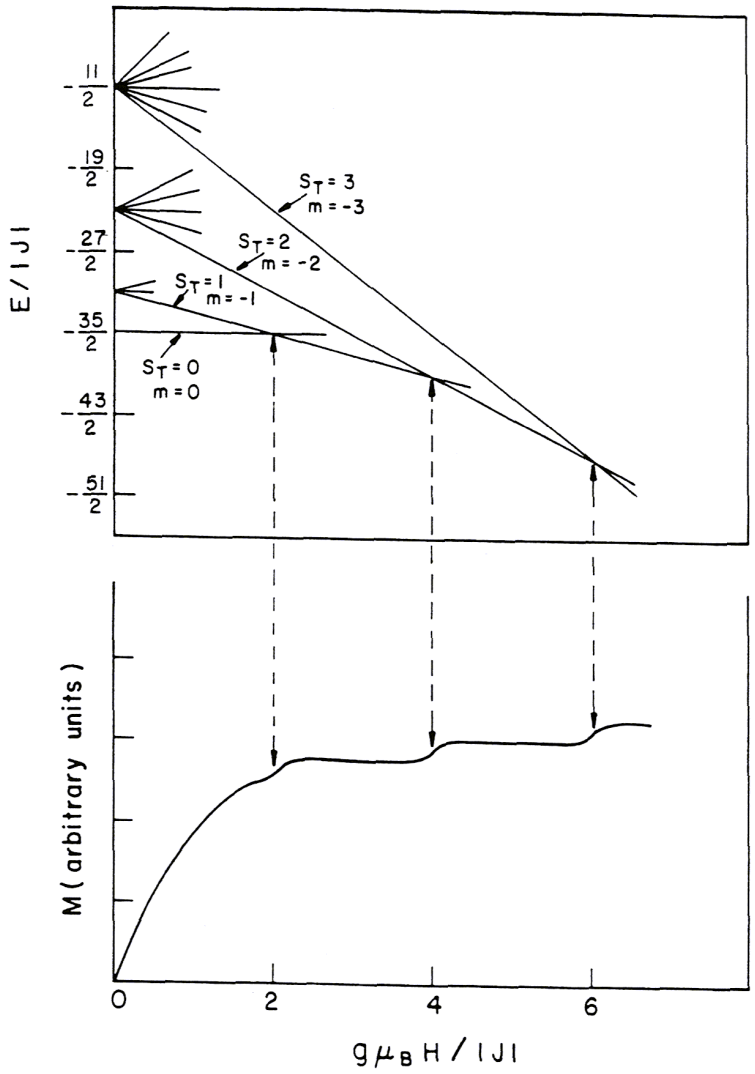

Figure 1.11 – Energy level scheme of an interacting Mn^{2+}-ion pair as functions of magnetic field. Only the ground and three excited states are shown. The parameter S_T is the total spin for a pair. The magnetization steps in high magnetic fields, shown in the lower part of the figure, reflect the crossing of the lowest energy levels. For clarity the relative size of the steps is overdrawn. [Fur87b]

The spin of the Mn-ions couples thereby to the total spin $\vec{S}$ with $0 \leq S \leq 5$, whereas each state is $(2S+1)$-fold degenerated at zero field. Thus, for $S_1 = S_2 = 5/2$ the eigenvalues of the Hamiltonian arise to

$$E = -J_{NN}\left(\left(S\left(S+1\right) - \frac{35}{2}\right) - g_{Mn}\mu_B mB\right), \tag{1.52}$$

where $-S \leq m \leq S$ is the magnetic quantum number. From 1.52 follows that the antiferromagnetic singlet ground state with $S = 0$ has the lowest energy until $g_{Mn}\mu_B mB = 2J_{\mathrm{NN}}S\left(S+1\right)$. As long as this condition is valid, no pairs contribute to the total magnetization. Thereafter the states with $S = 1, 2, 3, 4, 5$ and $m < 0$ have the lowest energetic state. Once one of this states becomes the ground state, immediately all pairs contribute to the magnetization, which leads to the escalating of the magnetization in five steps, shown in figure 1.11. Experimental determination of magnetic field strengths, at which the magnetization steps occur, enables to acquire the exchange constant of nearest-neighbors J_{NN} and also for the coupling constants of the next-to-nearest-neighbors J_{NNN}. The latter are also antiferromagnetic coupled. In (Zn,Mn)Se results $J_{\mathrm{NN}}/k_{\mathrm{B}}$ = -12.6 K [Sha87] and in (Cd,Mn)Me $J_{\mathrm{NN}}/k_{\mathrm{B}}$ = -6.3 K [Agg85, Lar86] and

$^{J_{NNN}}/_{k_B}$ = -1.1 K [Wan90]. The ratio between the next-nearest- and nearest-neighbors is of about one order of magnitude weaker and, therefore, the principal reason for the type-III antiferromagnetic arrangement of the spins [And50b, Kos93], which was clearly observed in neutron diffraction studies [Gie88]. In type-III antiferromagnetism occur antiferromagnetic ordered clusters in the vicinity of several magnetic ions. The clusters grow with decreasing temperature and, finally, fill out the solid state completely [Fur88a].

Another estimate for the coupling constants of the next-to-nearest-neighbors can be obtained from J_{NN} and the effective exchange integral J_1 [15]. According to [Lew88] yields, in good agreement with the precedent values, $^{J_2}/_{k_B}$ = -3.0 K in (Zn,Mn)Se and $^{J_2}/_{k_B}$ = -1.2 K in (Cd,Mn)Te. For the fifth and sixth neighbors a ferromagnetic exchange interaction was determined by perturbation theory calculations [Yu92].

Alternatively to this high field magnetization measurements, by inelastic neutron scattering [Cor86, Gie84, Gie87, Gie90], Raman scattering [Bar87] and low field magnetic susceptibility [Spa86] a variety of further techniques for measuring the exchange constant exists.

1.3.4.3 Magnetic properties of (Cd,Mn)Te and (Zn,Mn)Se with Mn-Mn interactions

The approximation of not interacting Mn-spins, assumed in the previous subsection (1.3.3), is only valid in strong diluted systems ($x < 0.01$), where the Mn-ions can be regarded as isolated. The probability of isolated atoms with no nearest magnetic neighbors decreases, and the number of Mn-ions being member of clusters increases, with rising Mn content[16]. For arbitrary x first of all the d-d-exchange interaction of the Mn-electrons among themselves has to be taken into consideration, so that the magnetization cannot be expressed by the standard Brillouin-function any longer. However, at low magnetic fields the magnetization M remains linear in B, as in the diluted case, so that it is possible to define a static magnetic susceptibility χ. Experimental measurements show a classical Curie-Weiss behavior at high temperatures [Ose82, Spa86][17]

$$\chi = \frac{C_0 x}{T - \Theta(x)} = \frac{C_0 x}{T - \Theta_0 x}, \tag{1.53}$$

with the negative Curie-Weiss temperature $\Theta_0 = -\frac{2}{3k_B} S(S+1) \sum_n z_n J_n$, where z_n denotes the number of the nth neighbors and J_n the corresponding Heisenberg exchange constants [Kos93]. The Curie-Weiss temperature accounts for (Cd,Mn)Te Θ_0 = -470 $\pm$ 34 K [Spa86] and for (Zn,Mn)Se Θ_0 = -956 $\pm$ 50 K [Lew88].

[15] The effective exchange integral J_1 is determined from the Curie-Weiss temperature (see equation 1.53), neglecting terms $n \geq 2$. Therefore it is absolutely larger than the true nearest-neighbor exchange constant J_{NN}. In the case of nearest-neighbors and $S = 5/2$ the Curie-Weiss temperature is reduced to $\Theta(x) = -70x\,^{J_1}/_{k_B}$.

[16] For further information about the probability of the occurrence of clusters and the corresponding spin Hamiltonian can be referred to [Kre65, Nag80].

[17] The last term is only valid in linear approximation, taking into account only nearest-neighbors.

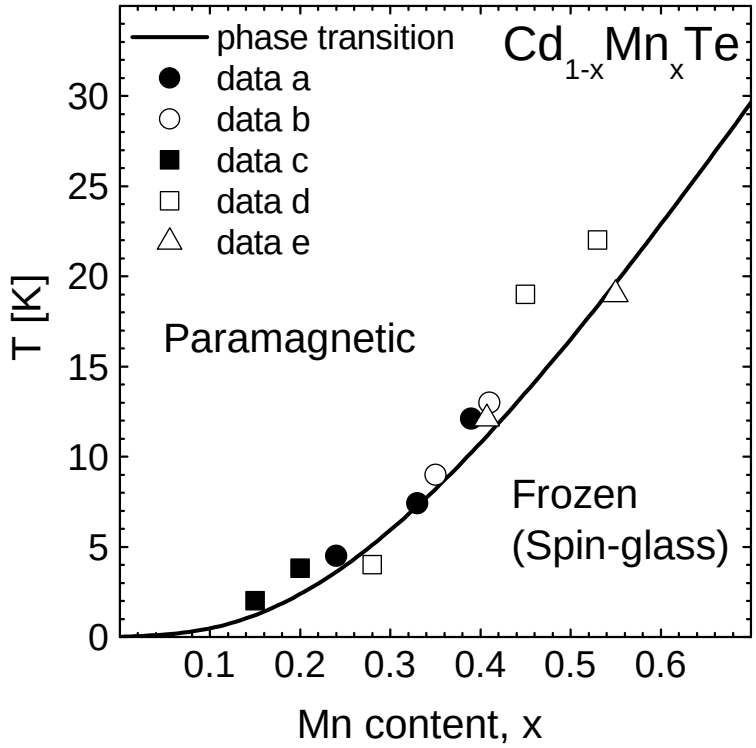

Figure 1.12 – Magnetic phase diagram of $Cd_{1-x}Mn_xTe$. The magnetic phases depend on x and T. The phase boundary is based on the occurrence of a characteristic cusp in the temperature variation of the static magnetic susceptibility. The paramagnetic phase occurs at high temperatures and low Mn concentrations. At low temperatures and high Mn concentrations the frozen spin-glass phase is prevalent. The data points are taken from [Yak98] (data a and b), [Aws87a] (data c), [Saw94] (data d), [Pie95] (data e) and [Nov86] (phase transition).

At low temperatures a departure from this law in form of a characteristic cusp in the temperature variation of the static magnetic susceptibility at a critical temperature T_g was experimentally detected [Esc82, Gał80b, Nag80, Ose80, Ose81, Ose82, Ose85, Son76, Son77b, Spa86]. By this cusp, and additionally by a linear temperature dependence of the specific heat at T_g [Kha81] and remanence effects and irreversible behavior of the magnetization below T_g [Gra80, Ose82], a phase transition from the high-temperature paramagnetic phase to a low-temperature frozen phase is evidenced [Bra84, Jon87, Gał80b, Mau90, Ose82, Twa86]. Although the temperature of the phase transition decreases with decreasing manganese content, the phase transition occurs even in the limit $x \to 0$ [Bra84, Jon87, Nov81, Nov84, Nov85, Nov86, Twa86]. This is an evidence that also next-to-nearest-neighbor and higher interactions are important (summands with $n \geq 2$ in $\sum_n z_n J_n$). From neutron diffraction experiments is known that the low-temperature frozen phase exhibits no long range magnetic ordering [Dol82, Gaj79, Gie82] and is macroscopically disordered. This indicates a spin-glass phase with the possibility of short-range antiferromagnetic clusters. Characteristic for spin-glass is that the magnetization depends on the magnetic history. This means the magnetization is different, depending on whether the DMS was cooled down in vanishing or finite magnetic field [Ket81, Kie84]. The formation of the spin-glass phase is ascribed to the d-d-exchange interaction and the magnetic dipole-dipole interaction [Nov86]. Magnetic phases diagram for $Cd_{1-x}Mn_xTe$ is given in figure 1.12.

Although for the three discussed cases (low x, high x and high T, high x and low T) subsists different characteristics, the behavior of the magnetization versus magnetic field strength is qualitatively similar to the Brillouin-function. Nevertheless, because of the strong interaction

between the Mn^{2+}-ions, the effective spin occurring in the antiferromagnetic clusters, reduces the expected value of the total spin and the alignment of spins by an external magnetic field is hindered (higher saturation field for the magnetization). To include these effects, two empirical parameters S_{eff} and T_0 are introduced to modify equation 1.38 [Gaj79]:

$$\langle S_z \rangle = -S_{eff} \mathcal{B}_S \left(\frac{g_{Mn} \mu_B S B}{k_B (T + T_0)} \right). \tag{1.54}$$

S_{eff} is called effective spin ($S_{eff} < S$) and T_0 antiferromagnetic temperature ($T_0 \geq 0$). The latter is typically substituted by the effective temperature $T_{eff} = T + T_0$. For small x, where the antiferromagnetic coupling between the nearest-neighbors is dominant, these parameters can be physically interpreted. $n \cdot S_{eff}$ is the saturation magnetization for the alignment of the spins of the nearest-neighbor-clusters, which are in the energetically favorable antiferromagnetic configuration without external magnetic field [Sha90]. The value $S = \frac{5}{2}$ for the Mn^{2+}-ion spin is only valid for isolated spins. The antiferromagnetic temperature T_0 regards the long-range interaction, which act against this alignment [Lar86].

From experimental data for (Cd,Mn)Te [Oss93, Yak95] and (Zn,Mn)Se [Yu95, Zeh98], shown in figure 1.13, can be obtained that both parameters depend on the manganese concentration x. The functional dependence for (Zn,Mn)Se is given by

$$S_{eff} = -0.804 + \frac{0.364}{x + 0.109} \tag{1.55}$$

$$T_0 = 47.2x - 281x^2 + 714x^3 \,\text{[K]} \tag{1.56}$$

[Kel01][18] and for (Cd,Mn)Te by

$$S_{eff} = 0.017 + 0.595 \cdot \exp\left(\frac{-x}{0.025}\right) + 1.841 \cdot \exp\left(\frac{-x}{0.185}\right) \tag{1.57}$$

$$T_0 = 43.38x \,\text{[K]} \tag{1.58}$$

[Oss93].

By insertion of 1.54 is the magnetization 1.37 modified to:

$$M = n g_{Mn} \mu_B S_{eff} \mathcal{B}_S \left(\frac{g_{Mn} \mu_B S B}{k_B T_{eff}} \right). \tag{1.59}$$

This equation is only valid up to $B \approx 10\,\text{T}$. The, in 1.3.4.2 mentioned and explained, steplike behavior at very high fields cannot be described by 1.59. Beside the gradual distribution, the Zeeman-splitting shows a linear rise, which can be seen clearly for fields above 20 T. This is due to formation of clusters of multiple (≥ 3) antiferromagnetic coupled Mn-ions and spin-flip transitions within these clusters. Several models are proposed including these effects [Hei87,

[18] In [Kel01] the equation for S_{eff} has a leading-sign error.

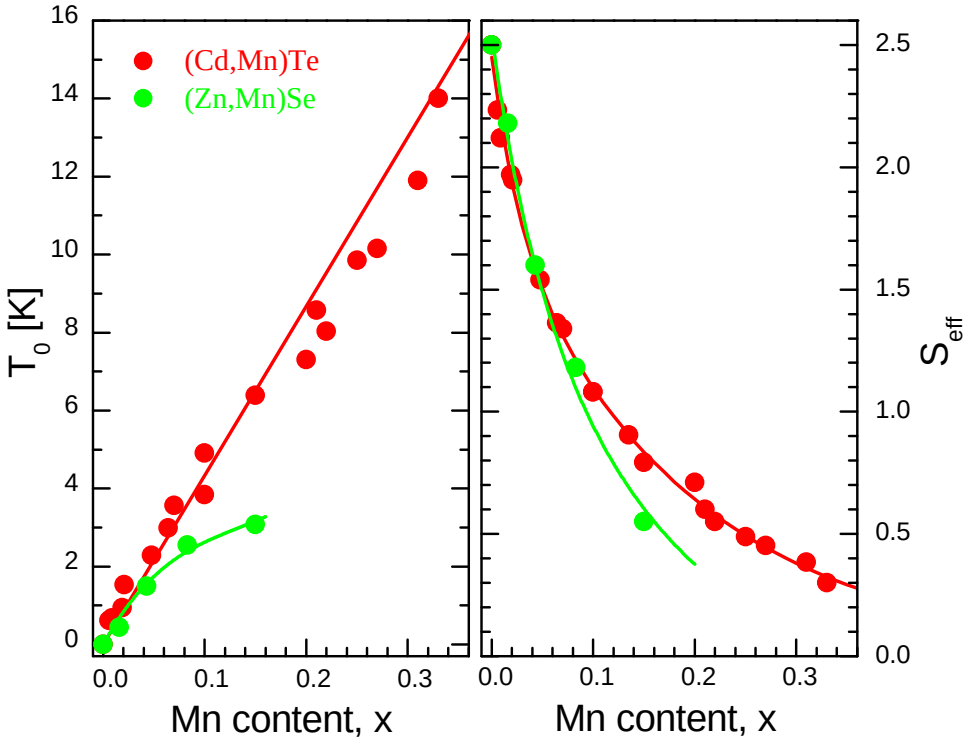

Figure 1.13 – The dependencies of the phenomenological parameters S_{eff} and T_0 on the Mn concentration for (Cd,Mn)Te and (Zn,Mn)Se. The data for (Zn,Mn)Se are taken from [Kel01, Yu95] and for (Cd,Mn)Te from [Aki06a].

Nic95]. As these effects are relevant for fields exceeding the magnetic fields used in this thesis, it is sufficient to use equation 1.59 for further considerations.

1.3.4.4 Giant Zeeman-splitting

The major consequence of the sp-d-exchange is the modification of the band structure in presence of external magnetic fields. Paramagnetic DMS have spin splittings with values being much larger than expected by the regular Zeeman term. This is called giant Zeeman-splitting.

For a general case of a parabolic conduction band, the eigenenergies of the electrons in the lth Landau level can be represented by [Fur88a][19,20]

$$\begin{aligned} E_l\left(m_s\right) &= E_g + E_{Landau}(l) + E_{Zeeman}(m_s) + E_{giantZeeman}(m_s) \\ &= E_g + \hbar\omega_c(l+\frac{1}{2}) + m_s\left(g_e\mu_B B - N_0 x\alpha\left\langle S_z\right\rangle\right), \end{aligned} \tag{1.60}$$

where $l = 0, 1, 2\ldots$ is the Landau quantum number[21], $m_s = \pm\frac{1}{2}$ the z-component of the electron spin, ω_c the cyclotron frequency and g_e^* the g-factor, obtained by solving $\hat{H}_0$ of the

[19]The case of an external magnetic field $\vec{B}$ parallel to the z-axis ($\vec{B} = (0, 0, B)$) is assumed.
[20]The eigenenergies for the sp-d-exchange were achieved in first order perturbation theory from equation 1.43.
[21]Derivation of the Landau energy is given in subsection 1.4.6.

nonmagnetic semiconductor, i.e. without the correction due to sp-d-exchange interaction. More convenient is the definition of an effective g-factor including the sp-d-exchange effect [Fur88a]

$$E_l\left(m_s\right) = E_g + \hbar\omega_c(l+\frac{1}{2}) + m_s g_e^{eff}\mu_B B, \tag{1.61}$$

where the effective g-factor is defined as [Dat85, Fur88a]

$$g_e^{eff} \;=\; g_e - N_0 x\frac{\alpha\left\langle S_z\right\rangle}{\mu_B B}. \tag{1.62}$$

Analogue results for light and heavy hole [Fur96]

$$g_{hh}^{eff} \;=\; g_{hh} - N_0 x\frac{\beta\left\langle S_z\right\rangle}{\mu_B B} \tag{1.63}$$

$$g_{lh}^{eff} \;=\; g_{lh} + \frac{1}{3}N_0 x\frac{\beta\left\langle S_z\right\rangle}{\mu_B B}. \tag{1.64}$$

The g_i^{eff} $(i = e, lh, hh)$ are by two orders of magnitude larger than that in nonmagnetic semiconductors ($g^{eff} \sim 50$) and leads therefore to extremely huge splittings of the order of 100 meV and more [Aki06a].

In wide-band-gap $A_{1-x}^{II}\mathrm{Mn}_x B^{VI}$ compounds the g-factors g_i^{eff} are of the order of unity and the effective masses m_{eff} are large. Therefore, spin splitting predicted by ordinary sp-band theory (Zeeman term $g_e\mu_B m_s B$ in 1.60) and also orbital Landau splitting ($\hbar\omega_c(l+\frac{1}{2})$ in 1.60) are much weaker than the splitting due to $\hat{H}_{sp-d}$, except for very low Mn concentrations. This is shown in figure 1.14 for the splitting of conduction and valence band. In absence of magnetic ions dominates the Landau contribution $E_{Landau} = \hbar\omega_c^e(l_e+\frac{1}{2}) - \hbar\omega_c^h(l_h+\frac{1}{2})$ (figure 1.14(a)). For small Mn-ion concentrations additional significant influence of the giant Zeeman-splitting contribution $E_{giantZeeman} = xN_0\left\langle S_z\right\rangle(m_s\alpha - \frac{1}{3}m_j\beta)$ occurs (figure 1.14(b)). For Mn-ion concentrations above $x = 0.02$, the giant Zeeman-splitting contribution is dominant (figure 1.14(c)). Consequently, the terms involving $\hbar\omega_c$ and g_i can be neglected [Fur88a, Kos93][22]. Hence, the splitting for conduction and valence band can be simplified[23]:

$$\Delta E_{\Gamma_6} \;=\; xN_0\alpha\left\langle S_z\right\rangle m_s \qquad \text{with } m_s = \pm\frac{1}{2}, \tag{1.65}$$

$$\Delta E_{\Gamma_8} \;=\; \tfrac{1}{3}xN_0\beta\left\langle S_z\right\rangle m_j \qquad \text{with } m_j = \pm\frac{1}{2}(\text{lh}), \pm\frac{3}{2}(\text{hh}). \tag{1.66}$$

[22] At high magnetic fields ($B > 10\,\mathrm{T}$) saturates the giant Zeeman-splitting, so that the conventional Zeeman term becomes important. Because of the opposite sign of both effects, the splitting in this region decreases. Nevertheless, the approximation is valid in this thesis, because the magnetic field does not come up to the needed high values.

[23] Due to the exchange interaction, $E(\vec{k})$ is anisotropic [Gaj78]. The equations 1.65 and 1.66 hold only for $\vec{k} \parallel \vec{B}$.

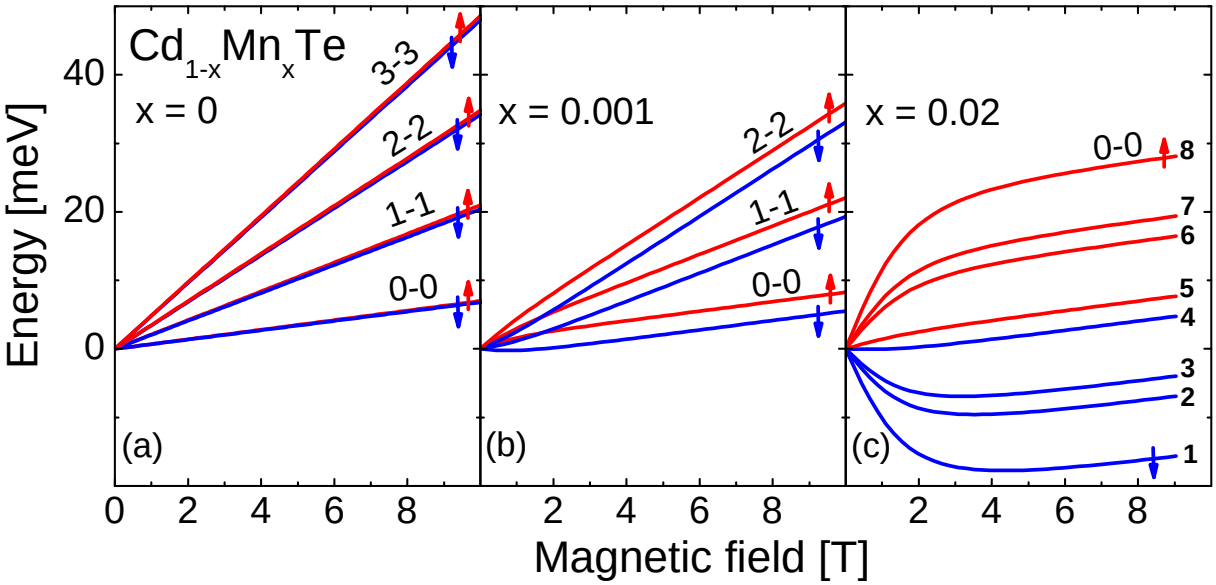

Figure 1.14 – Competition between Landau level energy $E_{Landau} = \hbar\omega_c^e(l_e+\frac{1}{2}) - \hbar\omega_c^h(l_h+\frac{1}{2})$ and giant Zeeman-splitting energy $E_{giantZeeman} = xN_0 \langle S_z \rangle (m_s\alpha - \frac{1}{3}m_j\beta)$ for different Mn concentrations in magnetic field, shown exemplary for the valence band and conduction band contributions in $Cd_{1-x}Mn_xTe$. (a) For $x = 0$ dominates the Landau contribution. (b) For $x = 0.001$ the Landau splitting as well as the giant Zeeman-splitting influence significantly the band structure. (c) For $x = 0.02$ dominates the giant Zeeman-splitting. The saturation of the giant Zeeman-splitting with increasing field can be seen very clearly, while E_{Landau} and $E_{Zeeman} = m_s g_e \mu_B B - \frac{1}{3} g_h m_j \mu_B B$ increase linearly. Direction of the spin is given by the grey arrows. For the calculation the respective values for S_{eff} and T_0 were calculated according to equations 1.57 and 1.58. [Sän06]

The resulting giant Zeeman-splitting of the Γ_6 conduction band in two and the Γ_8 valence band in four spin levels is depicted in figure 1.15. The degeneracy of the bands is totally lifted. This situation is qualitatively similar to spin splitting in nonmagnetic semiconductors, which is due to the fact that the Hamiltonian 1.43 has a form identical to the spin part of $\hat{H}_B$ (1.36). Combined with the cognition that the parameter β is larger and negative compared with α, results from equations 1.65 and 1.66 that the splitting of the heavy-hole is considerably larger and opposite in sign than of the conduction and light-hole band.

The electric-dipole-allowed one-photon transitions for linear polarization parallel to the magnetic field ($\Delta m_j = 0$ (π)) and for the two circular polarizations rotating transverse to the magnetic field ($\Delta m_j = \pm 1$ (σ^+ and σ^-)) are also shown in figure 1.15. The first can be observed in Voigt geometry ($\vec{B} \perp \vec{k}$), the latter in Faraday geometry ($\vec{B} \parallel \vec{k}$). Most important are the heavy-hole transitions between the band-edge states denoted by a and d in the figure, which are significantly stronger than the light-hole transitions c and b. The selection rules, governing the transitions between the levels, remain the same, compared with nonmagnetic semiconductors.

It can be seen that the Zeeman-splitting closely resembles the magnetization of a paramagnet. This can be deduced from the linear relationship between Zeeman-splitting and magnetization in terms of $\langle S_z \rangle$ in the equations 1.65 and 1.66. From the presence of $\langle S_z \rangle$ (compare 1.38) follows, in turn, that the giant Zeeman-splitting is non-linear in B and strongly dependent on

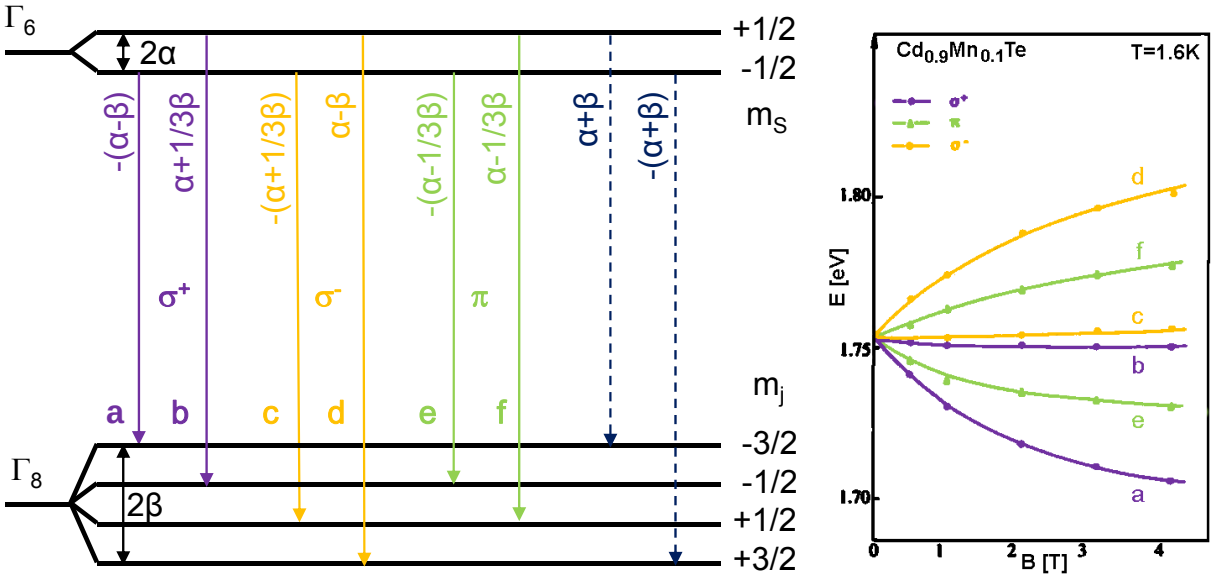

Figure 1.15 – Schematic picture of the giant Zeeman-splitting of the conduction band (Γ_6) and valence band (Γ_8) for a wide-band-gap $A^{II}_{1-x}\mathrm{Mn}_x B^{VI}$ alloy in magnetic field at the center of the Brillouin-zone at the Γ-point. Heavy-holes are indicated by $\pm\frac{3}{2}$ and light-holes by $\pm\frac{1}{2}$. The six electric-dipole-allowed one-photon transitions with $\Delta m_j = 0, \pm 1$ are shown by continuous arrows. The dashed arrows show transitions with $\Delta m_j = \pm 2$, which are forbidden for single-photon processes. The transitions labeled by e and f can be excited in Voigt geometry ($\vec{B} \perp \vec{k}$) with linear polarized light. The four other one-photon transitions occur in Faraday geometry ($\vec{B} \parallel \vec{k}$) for the two circular polarizations rotating transverse to the applied magnetic field. The heavy hole transitions a and d have threefold transition-probability than the light hole transitions b and c.
On the right side experimental results for the giant Zeeman-splitting of the $1s$ exciton in $\mathrm{Cd}_{0.9}\mathrm{Mn}_{0.1}\mathrm{Te}$ in Faraday configuration are shown, according to [Gaj88]. The continuous lines are drawn to guide the eye.

the temperature of the spin system formed by the Mn-ions (see figure 1.16). This is contrary to the case of non-magnetic semiconductors . From this arises that the giant Zeeman-splitting is

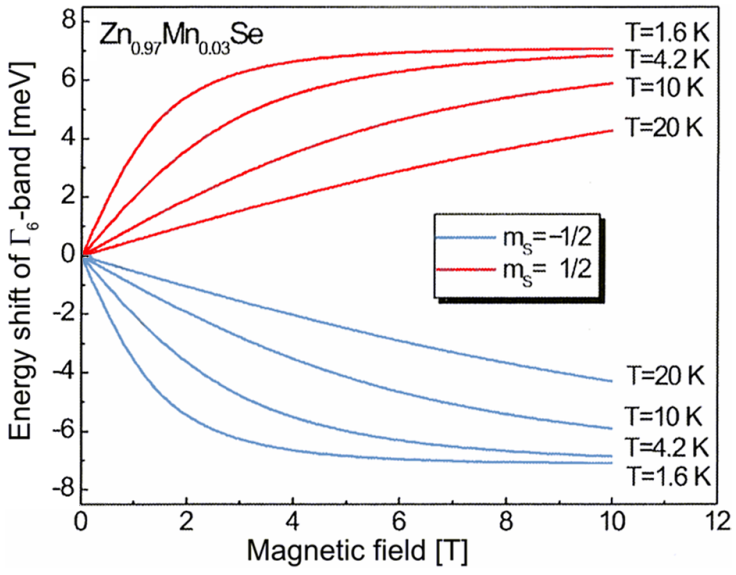

Figure 1.16 – Temperature and magnetic field dependance of the giant Zeeman-splitting according to equation 1.65. Shown are results for the Γ_6 conduction band of $\mathrm{Zn}_{0.97}\mathrm{Mn}_{0.03}\mathrm{Se}$. The splitting increases linearly at low fields and saturates at high field. The branches for different temperatures show a strong dependence of the giant Zeeman-splitting on the temperature of the Mn-spin system, giving suitable access to this temperature. For the calculations $S_{eff} = 1.82$ and $T_0 = 1.18\,\mathrm{K}$ are used, according to equations 1.55 and 1.56. [Kel04]

very suitable for experiments. The relation of the splitting with the exchange term $\hat{H}_{sp-d}$ allows direct access to the parameters α and β, to details of the magnetization M and the temperature of the magnetic system of the Mn^{2+}-ions by optical measurements. As described later in section 3.1, the size of the energy shift for the free-exciton ground-state at a specific magnetic field is directly linked to the Mn-ion temperature. The excitonic Zeeman-splitting behaves equal to the band edge splitting [Fur88a]. Closing should be mentioned that the giant Zeeman-splitting is dependent on the Mn concentration, which can be clearly seen from equations 1.65 and 1.66.

1.4 Quantum well heterostructures

Most of experimental data included in this thesis are measured in DMS heterostructures based on (Cd,Mn)Te and (Zn,Mn)Se. Heterostructures are layered materials, whose properties are substantially determined by the composition of different semiconductor materials. The growth of the different materials occurs via epitaxy. Possible techniques are liquid phase epitaxy (LPE), vapor phase epitaxy (VPE), metal organic chemical vapor deposition (MOCVD) or metal organic vapor phase epitaxy (MOVPE). The samples investigated in this thesis were fabricated by molecular beam epitaxy (MBE) [Bic84, Cho70, Dat85, Gun85, Kol84a], which is the most sophisticated method. It allows the precision of atomic monolayers. Concentration of free carriers in heterostructures can be varied in a wide range by n-type or p-type modulation doping. Static and dynamical properties can be controlled by the growth of heteromagnetic structures with variable concentration of magnetic ions along the growth axis [Sch05] or, as shown later in this thesis, by the digital alloy (DA) approach. Especially MBE enables for the heterostructure concept fabrication of samples with Mn concentrations exceeding the limits of bulk crystals (see table 1.1) [Kol85], flexibly band structure engineering [Dat85], and preparation of $A^{II}_{1-x}\mathrm{Mn}_x B^{VI}$ layers and superlattices of exceptionally high quality [Her84, Pes87, Sun85]. Brief description of the MBE technique is given in section A.1.1 of the appendix.

The sophisticated heterostructure growth techniques allow to realize structures with reduced dimensionality by combination of semiconductors with different band gap sizes like QWs and superlattices [Che93]. The geometry of these structures affects strongly the band structure, e.g. by spatial confinement of carriers or by symmetry degeneration, compared with the bulk material. In QWs the spacial distribution of the carriers is constrained in plane, so that they can move quasi-free parallel to the interfaces. Therefore the carriers form a quasi-two-dimensional electron or hole gas. Is the typical extent of the confined area in region of the de Broglie wavelength $\left(\lambda = 2\pi\sqrt{\frac{\hbar^2}{2mk_BT}}\right)$ of the carriers and smaller than the scattering length of free carriers, the possible energy levels are quantized, i.e. in this direction exist discrete energy levels. This calls for quantummechanical methods to describe QWs and their properties. From the confinement of the particle motion on the length l of a QW follows, due to the Heisenberg uncertainty principle, that the impulse of the electron and hole is uncertain in the size of $\frac{\hbar}{l}$. This

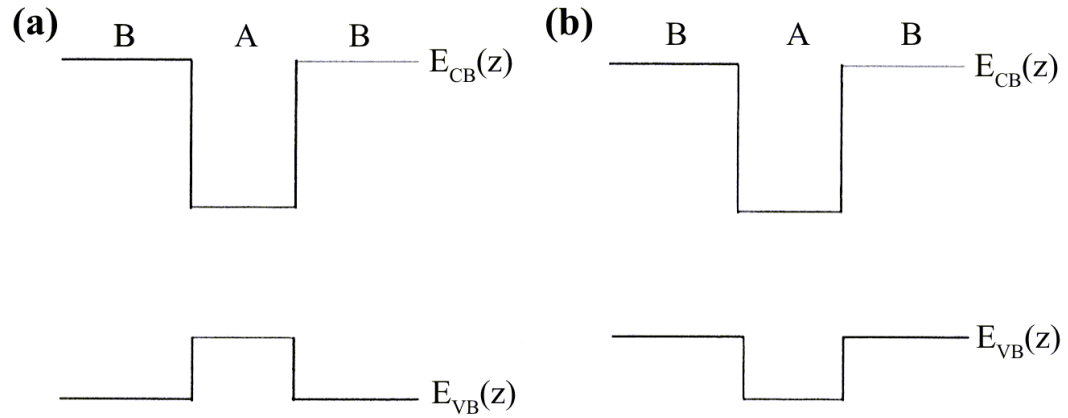

Figure 1.17 – Band edge devolution of (a) type-I and (b) type-II QWs.

leads to an additional energy contribution to the kinetic energy, which is called confinement-energy.

QWs can be created with type-I or type-II band alignment (see figure 1.17). In type-I structures localize electrons and holes in the same semiconductor layer, while in type-II structures he localization takes place in different layers. The band edge for a type-I QW is schematically shown in figure 1.18 for (Zn,Mn)Se. In case of a "straddling" lineup, i.e. the band gap of one layer (A) is embedded within the band gap of the other layer (B) ($E_g^A < E_g^B$), type-I structures can be grown by sandwiching an A-layer between two B-layers [Kla98]. This leads to confinement of free carriers in the conduction and valence band of layer A by the so-called barrier B. Thereby, the barrier layers are much thicker than the penetration length of the confined

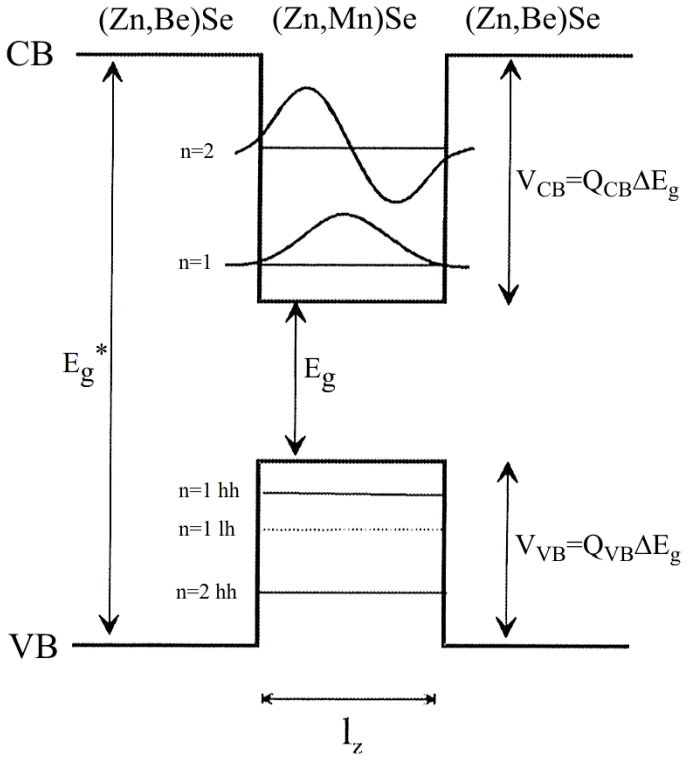

Figure 1.18 – Schematical illustration of a type-I QW with the thickness l_z. The energy gap of the barrier E_g^* is bigger than the energy gap of the QW E_g, so that a confined potential results. The band gap difference ic characterized by the conduction band and valence band offsets Q_{CB} and Q_{VB}, respectively. The envelope-functions for the subband with $n = 1$ and $n = 2$, respectively, are shown schematically. [Kel04]

wave functions. The difference of the band gaps for both materials can be characterized by the valence band offset (VBO)

$$Q_{VB} = \frac{V_{VB}}{\Delta E_g} = 1 - \frac{V_{CB}}{\Delta E_g}. \tag{1.67}$$

Values for the materials, which are investigated in this thesis, are given in table A.7 in the appendix. Methods for determination of the VBO are given e.g. in [Fie97]. The direction perpendicular to the layers is the growth direction, which is defined arbitrarily parallel to the z-axis in this thesis. It is stressed here that the, in the previous sections introduced, parameters $N_0\alpha$ and $N_0\beta$ can decrease significantly in low-dimensional structures [Mer99].

The electronic and magnetic properties of heterostructures are strikingly different from those observed in corresponding bulk materials [Fur88a]. In the following, the effects of spatially confined carriers in QWs on the energy bands and the corresponding density of states are briefly reviewed. Also the quantization of the motion of two-dimensional electrons in a magnetic field is regarded, and the selection rules and the polarization degree of optical transitions are described. DMS QWs and superlattices are detailed reviewed e.g. in the papers of [Cha89, Fur87a, Kol86a, Nur86, Nur89].

1.4.1 Single-particle states in quantum wells

The electrons in a QW can move freely along the x-y-plane, but are restricted in their perpendicular motion along z. The electronic states in QWs ensue from the effective mass approximation, which takes the microscopic crystal structure by introduction of effective parameters into account, by the Hamiltonian

$$\hat{H} = \frac{\hbar^2}{2m_{eff}}\left(\frac{\partial^2}{\partial x^2} + \frac{\partial^2}{\partial y^2}\right) + \frac{\hbar^2}{2m_{eff}}\frac{\partial^2}{\partial z^2} + V_{QW}(z), \tag{1.68}$$

where $V_{QW}(z)$ is the potential in z-direction of the QW and m_{eff} is the isotropic effective mass of the electrons and holes, respectively, in the QW. The energy eigenstates for equation 1.68 are discrete subbands with parabolic dispersion [Coh77]:

$$E_n\left(\vec{k}_{||}\right) = E_n + \frac{\hbar^2 k_{||}^2}{2m_{eff}}, \tag{1.69}$$

where $\vec{k}_{||} = (k_x, k_y)$ corresponds to the wave vector in the QW plane and E_n are the size quantized states. In the case of an infinite and symmetric QW of the width l_z, they are given by [Ter01]

$$E_n = \frac{\hbar^2\pi^2}{2m_{eff}l_z^2}(n+1)^2. \tag{1.70}$$

The calculation of the, in z-direction confined, single-particle states in the conduction band of the QW is enabled by the, so-called, envelope-function-approximation [Bas81, Bas82]. The corresponding volume bands are described in section 1.2.

As basis of the wave function of a particle in the QW, it seems appropriate to use Bloch-wavefunctions. Within the scope of the envelope-function-approximation, the fast oscillating lattice-periodic parts of the Bloch-wavefunctions are modulated by a slow changing envelope-function Υ. Thus the single-particle wave function of a structure with layers A and B can be described by

$$\Phi\left(\vec{r}\right) = \sum_{A,B} \Psi_{\vec{k}}^{A,B}\left(\vec{r}\right) \Upsilon^{A,B}\left(\vec{r}\right), \tag{1.71}$$

where $\Psi_{\vec{k}}$ corresponds to the Bloch-wavefunctions in the layers A and B, respectively. Because of the similarities of the bands in the layers A and B the Bloch-wavefunctions in both materials can be equated approximately. Only the QW potential acts upon the envelope-function [Bas90], which influences only the particle motion along z. Perpendicular to z is the motion, furthermore, determined by the periodic potential of the lattice, so that the wave function can be written as

$$\Phi\left(\vec{r}\right) = \sum_{A,B} \exp\left(i\vec{k}_{||}\vec{r}\right) \Psi_{\vec{k}}^{A,B}\left(\vec{r}\right) \Upsilon^{A,B}\left(z\right). \tag{1.72}$$

The wave function was deduced under two assumptions: The potential step leads only to an energetic shift of the band edge states and not to mixing; and the potential step at the interface of the layers is treated as localized on scale of the change of the envelope-function Υ. At the interface of the layers the wave function and the particle flux density is continuous [Alt83b].

The leakage of the envelope-function into the nonmagnetic barriers (see figure 1.18) causes a decrease of the sp-d-exchange interaction. Its influence on the Zeeman-splitting can be determined by calculation of the envelope-function. Calculation of the first bound state is given in [Kuh95].

In the valence band the calculation of the energy eigenstates is more complicated. In bulk crystals light-hole and heavy-hole bands are degenerated at $k = 0$. The QW potential leads to different masses of heavy and light-holes parallel and perpendicular to the growth direction. This, in turn, lifts the degeneracy at the Brillouin-zone center and leads even to a mixture with anticrossing behavior of both band states at $k \neq 0$ [Wei91, Yu05]. Calculation of the energy levels by means of the Luttinger Hamiltonian is given in [Bas90, Wei91].

In an infinite QW only transitions between conduction and valence band are allowed, which satisfy $\Delta n = 0$. Contrary, in a finite QW also transitions with $\Delta n \neq 0$ are allowed, but those with odd Δn are parity-forbidden [Man00].

1.4.2 Spin-orbit-splitting in quantum wells

The BIA of a bulk semiconductor is described by equation 1.16. In two-dimensional QWs the z-component of $\vec{\sigma}$ and $\vec{\Omega}_{BIA}$ vanishes in 1.16 and the wave vector k_z can be exchanged by its expected value $\langle k_z \rangle$ [D'y86, Pik95]. In this case can be shown easily for QWs with $\vec{k} \parallel [100]$ that the Dresselhaus term is linear in k [Rud05].

Additionally to the lack of inversion symmetry of the bulk material, an additional asymmetry of the structure can occur in terms of an asymmetric QW potential V_{QW}. Also this structure inversion asymmetry (SIA) gives a contribution to the splitting of the Γ_6 conduction band, which is called Rashba-effect [Byc84b, Byc84a, Win03]:

$$\hat{H}_{Rashba} = \varsigma_0 \vec{\sigma} \cdot \vec{k} \times \vec{E}, \tag{1.73}$$

where ς_0 is a material-specific parameter. For a QW grown in z-direction the Rashba Hamiltonian can be written similar to the Dresselhaus Hamiltonian [Kai03, Kai04]:

$$\hat{H}_{Rashba} = \frac{\hbar}{2} \vec{\sigma} \cdot \vec{\Omega}_{SIA}(\vec{k}_{||}), \tag{1.74}$$

with

$$\vec{\Omega}_{SIA}(\vec{k}_{||}) = \frac{2\varsigma}{\hbar} \begin{pmatrix} k_y \\ -k_x \\ 0 \end{pmatrix} \tag{1.75}$$

corresponding to an effective magnetic field lying in the QW-plane. Thereby, the Rashba-parameter $\varsigma \propto \varsigma_0$ depends on the material parameters of the underlying semiconductor bulk material and also on the asymmetry of the QW in growth direction [Kai03, Rud05, Win03].

The resulting spin splitting of the Γ_6-conduction band is, according to 1.75, linear in $\vec{k}_{||} = (k_x, k_y)$ [Rud05]:

$$\Delta E_{Rashba} \left(\vec{k}_{||} \right) = \varsigma k_{||}. \tag{1.76}$$

1.4.3 Heterostructures in magnetic field

The magnetic properties given in the previous section 1.3 can be transferred to heterostructures. As pointed out in the previous explanations of this chapter, one of the unique features of DMS is the presence of a strong sp-d-exchange interaction, which allows the observation of phenomena in DMS that would require considerably higher magnetic fields in non-magnetic semiconductors. Due to this effect the spin splittings of electronic states in DMS (band edge

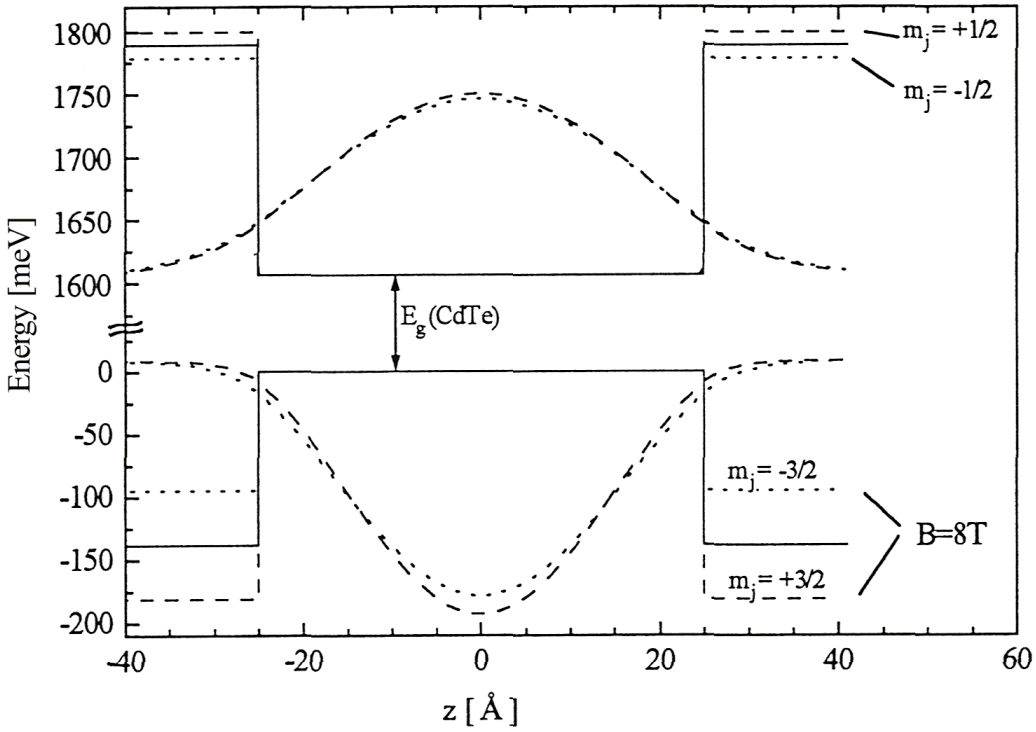

Figure 1.19 – Potential change of a type-I CdTe/$Cd_{0.8}Mn_{0.2}Te$ QW in magnetic field for conduction band and heavy-hole states of valence band in $Cd_{0.8}Mn_{0.2}Te$. The continuous lines show the situation in absence of external magnetic field. By dashed and dotted lines the splittings in an external magnetic field ($B = 8\,\mathrm{T}$), and the corresponding probability density functions are presented. [Fie97]

exciton levels, impurity levels, Landau-levels) can attain values as large as 20 meV at pedestrian magnetic fields [Dat85].

In magnetic field split the Γ_6- and Γ_8-bands of the barriers according to 1.65 and 1.66. In the nonmagnetic layers is the splitting degenerated (regarding m_j), while in the semimagnetic layers the degeneracy is lifted in magnetic field. This leads to changing of the barrier band edges and, therefore, to changing of the height of the QW potential, as depicted in figure 1.19. Due to this, the Zeeman-splitting and the energy subbands have to be calculated for each potential height, belonging to a certain magnetic field. From these levels the energies for the optical transitions in magnetic field can be deduced [Fie97].

Newer results by [Aki93, Gaj93, Gon85, Gon86, Nur85, Pet85, Wu86, Zha85c, Zha85b, Zha85a], showing enhanced Zeeman-splitting than expected from the previous explained calculations, suggest that a direct transfer of the magnetic properties in three dimensions on heterostructures is not possible. Reason for the observed enhanced splitting are trapped excitons at the heterointerfaces. At the interfaces a region with higher paramagnetism is generated by reduction of the antiferromagnetic coupling of the Mn-spins due to missing Mn neighbors in the adjacent QW. An additional rise of the Zeeman-splitting at the interfaces is related to diffusion of manganese from the barrier into the QW. This leads to greater overlap of the excitonic wave function with the Mn-ion-system and therefore to greater Zeeman-splitting [Fie97].

Especially in structures with more than one QW (like multiple quantum wells (MQW) or superlattices) result some particular exchange-induced effects from the different behavior of adjacent DMS and non-DMS layers. Examples are the magnetic freeze-out and boil-off, respectively, of electrons, occurring in magnetic field for structures with donor levels, which are slightly above and below, respectively, the lowest energy state in the QW; tunable resonant tunneling; tunable far-infrared emitters using electrical excitation; quantum oscillations; and "spin superlattices", which consist of confined carriers with opposite spin in adjacent layers [Dat85, Fur87a, Kos93, Ort82]. The effects are related to the particular conditions of the spin splitting of energy levels in layered structures. These are considerably greater splitting in DMS than in adjacent nonmagnetic layers; comparable splitting in DMS layers with the ionization energies of shallow impurities; and noticeable exceedance of the energy difference between consecutive Landau-levels of the same spin by the DMS splitting energy [Kos93]. Especially obvious gets the different splitting by the effective g-factor (see 1.64 and 1.62), which is at low fields in the magnetic barrier layers approximately 100 times higher than the g-factor in the QWs.

Apart from the exchange-induced effects, also strain-induced splitting of heavy- and light-hole bands occurs in superlattices because of the relatively strong lattice variation [Byl87, Cha88, Kos93, Nur85, Zha85b, Zha86].

1.4.4 Density of states in quantum wells

The density of states can be regarded separately for the x-y-plane and along z. In the QW plane, the density of states is constant in parabolic approximation $E = \frac{\hbar^2\left(k_x^2+k_y^2\right)}{2m_{eff}}$:

$$D(E)_{2D} = \frac{m_{eff}}{\pi\hbar^2}. \tag{1.77}$$

Therefore, the density of states at a certain energy E depends only on the amount of allowed QW levels with $E_n \leq E$, which are quantized in z-direction. Contrary, the density of states depends on the energy E in the 3D case [And82].

In an ideal semiconductor the Hamiltonian for an electron in a x-y-plane is perpendicular to the plane B_z under presence of a magnetic field :

$$\hat{H} = \frac{(\vec{p} - e\vec{A})^2}{2m_{eff}} + V_{QW}(z) + \hat{H}_{Zeeman}. \tag{1.78}$$

Within the Landau gauge the Hamiltonian can be divided into electric and magnetic field parts, so that the eigenvalues can be calculated separately:

$$E = E_{Landau} + E_n + E_{Zeeman}, \tag{1.79}$$

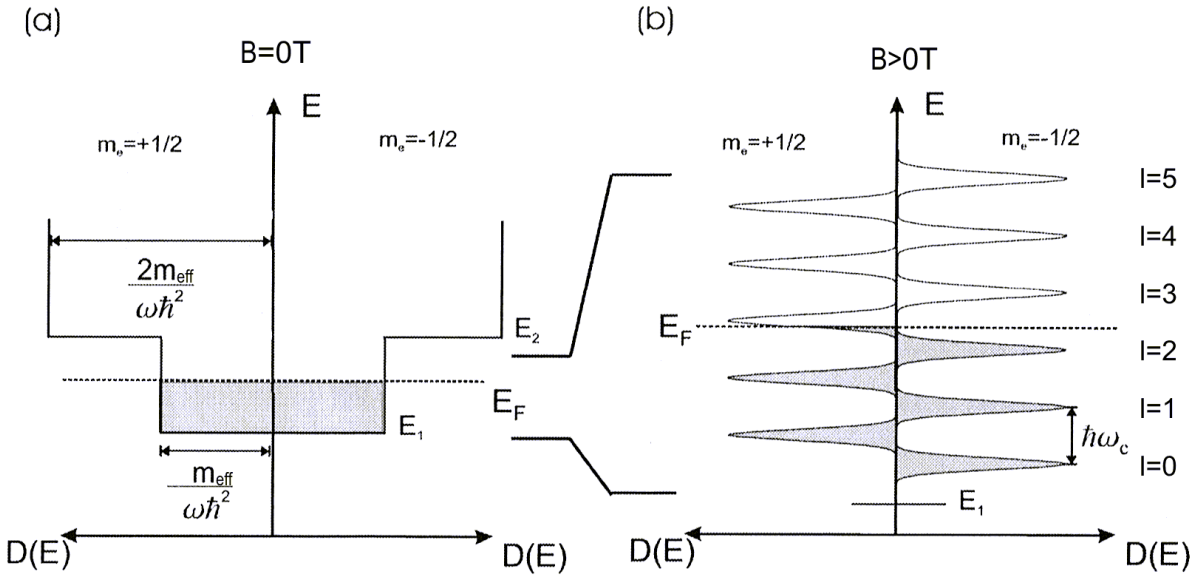

Figure 1.20 – Density of states (a) without or (b) with magnetic field in a QW. The subband energies of the QW levels are labeled by E_i. The distances between the Landau-levels l are the same and increase linear with rising magnetic field. The Landau-levels are broadened by impurities and lattice defects. [Kel04]

with the Zeeman energy E_{Zeeman}, the electric subband position E_n, according to 1.70, and the orbital motion in the x-y-plane

$$E_{Landau} = (l + 1/2)\,\hbar\omega_c, \tag{1.80}$$

where $l = 0, 1, 2, \ldots$ is the quantization index and

$$\hbar\omega_c = \frac{eB_z}{m_{eff}} \tag{1.81}$$

is the cyclotron energy [Ter01].

Whereas in absence of a magnetic field, the motion is only quantized in z-direction due to the QW confinement, in magnetic field also the motion in the x-y-plane is quantized. The case of magnetic field perpendicular and parallel to the growth axis has to be distinguished. Easier to discuss is the, consecutively described, perpendicular alignment, because the movement in z-direction is only determined by the QW potential and not, additionally, by the magnetic field.

With increasing field the dimensionality of the carrier states is continuously tuned from quasi-two to quasi-zero dimensions. From this follows that the zero field density of states for electrons and holes condenses for each electric subband E_n into a series of δ-like bands because of the Landau-quantization. The energetic distance between two succeeding Landau-levels cor-

responds to the cyclotron energy $\hbar\omega_c$ and the amount of allowed states per Landau-level l depends linear on magnetic field:

$$l = \frac{eB_z}{h}, \tag{1.82}$$

assuming that the spin degeneracy is lifted. Due to carrier scattering at impurities and defects, in real QWs the otherwise discrete Landau-levels are broadened. These scattering potentials are shielded by the two-dimensional electron gas (2DEG) in the QW. As this shielding is dependent on the density of states at the Fermi-level, the problem of the Landau-level-broadening has to be solved self consistent [And74, Cai86]:

$$D_l(E) = \frac{1}{\pi^2 l_B^2 \Gamma_l}\sqrt{1-\left(\frac{E-E_l}{\Gamma_l}\right)^2} \qquad \text{if } \Gamma_l^2 \geq (E-E_l)^2\,; \tag{1.83}$$

$$D_l(E) = 0 \qquad \text{if } \Gamma_l^2 \leq (E-E_l)^2\,, \tag{1.84}$$

where $l_B = \sqrt{\frac{\hbar}{eB}}$ is the magnetic length and Γ_l is the broadening of the Landau-level l. The latter can be calculated by a sum over the scattering amplitudes of the single scattering potentials. From experiments by [Gor85] is known that the broadening of the Landau-levels is most suitable approximated with a Gauss-function.

To determine the total energy shift of the QW levels in an external magnetic field, three contributing effects have to be taken into account, analogue to equation 1.43: the Landau-quantization, the intrinsic Zeeman-effect and the sp-d-exchange interaction:

$$\Delta E_e = \left(g_e\mu_B B + \delta_e x N_0 \alpha \langle S_z\rangle\right) m_s + \left(l_e + \tfrac{1}{2}\right)\hbar\omega_c^e \qquad \text{for } m_s = \pm\frac{1}{2}, \tag{1.85}$$

$$\Delta E_{hh} = \tfrac{1}{3}\left(g_{hh}\mu_B B + \delta_{hh} x N_0 \beta \langle S_z\rangle\right) m_j + \left(l_{hh} + \tfrac{1}{2}\right)\hbar\omega_c^{hh} \qquad \text{for } m_j = \pm\frac{3}{2}. \tag{1.86}$$

In the equations corresponds $\omega_c^\alpha = \frac{eB}{m_{eff}^\alpha}$ to the cyclotron frequency, g_α to the intrinsic g-factor of the electrons and heavy-holes, respectively, and l_α to the Landau-quantum number ($l_\alpha = 0, 1, 2, \ldots$). The $\delta_{e,hh} \leq 1$ are introduced to account the leakage of the electron and heavy hole wave functions into the non-magnetic barrier layers. The corresponding one-particle Hamilton-Operators are given in [Kuh95].

As already mentioned in subsection 1.3.4.4, the sp-d-exchange interaction outweighs the intrinsic Zeeman-splitting and the orbital Landau-splitting at low magnetic fields. Thus these can be neglected. The resulting splitting of the conduction band and valence band in magnetic field is given in figure 1.15. For strong magnetic fields, the selection rule $\Delta l = 0$, for transition between electron and hole Landau-levels with quantum numbers l_e and l_h, respectively, has to be taken into account.

1.4.5 Selection rules and polarization degree in quantum wells

The selection rules determine possible optical transitions between conduction and valence band. Zincblende semiconductors possess a Γ_6-conduction band and a Γ_8-valence band. For optical transitions between those, the total angular momentum has to be conserved, i.e. the angular momentum has to fulfill $J_e + J_h = J_p$, with the angular momenta for electron J_e, hole J_h, and photon J_p, respectively. As already mentioned in subsection 1.3.4.4, $J_p = \pm 1$ yields for circular polarized light, so that for inter band transitions, the orbital angular momentum is changed by ± 1. The electron spin remains unchanged for inter band transitions.

The possible transitions with circular polarized light are given by the letters a, b, c, d in figure 1.15 on page 45. The intensity of a transition can be calculated by the ratio of its dipole matrix elements [Rud05]. Heavy-hole transitions are three times more probable than light-hole transitions [Rud05].

Because of the selection rules of the optical transitions, excitation with circular polarized light can achieve a spin polarization

$$P_{spin,cb} = \frac{n^{\sigma^+} - n^{\sigma^-}}{n^{\sigma^+} + n^{\sigma^-}}, \tag{1.87}$$

of the electrons in the conduction band, where n^{σ^+} and n^{σ^-} are the electron densities in the conduction band Landau-levels for the two possible electron spins. As the occupation of the Landau-levels changes with magnetic field, the spin polarization will change as well. Applying the filling factor $\nu = \frac{hn_e}{eB_z}$[24], which corresponds to the number of occupied Landau-levels, holds for even filling factors ($n^{\sigma^+} = n^{\sigma^-}$) $P_{spin,cb} = 0$ and for odd filling factors results a non zero spin polarization.

In QWs the energetic degeneration of light-hole and heavy-hole band is lifted due to the symmetry reduction. Therefore, only one transition can be excited resonantly, which makes spin polarizations up to 100 % possible.

Because the selection rules obtain also for the emission, the circular polarization degree P_c of the respective light-hole and heavy-hole transition is defined by [D'y84]:

$$P_c = \frac{I^{\sigma^+} - I^{\sigma^-}}{I^{\sigma^+} + I^{\sigma^-}}, \tag{1.88}$$

with I^{σ^+} and I^{σ^-}, respectively, corresponding to the PL intensity of the transition under σ^+- and σ^--detection, respectively [Kel04, Rud05]. Thereby is assumed that the holes, participating in the recombination, are unpolarized due to very fast spin relaxation [Bay95, Dam91].

[24] n_e is the carrier density.

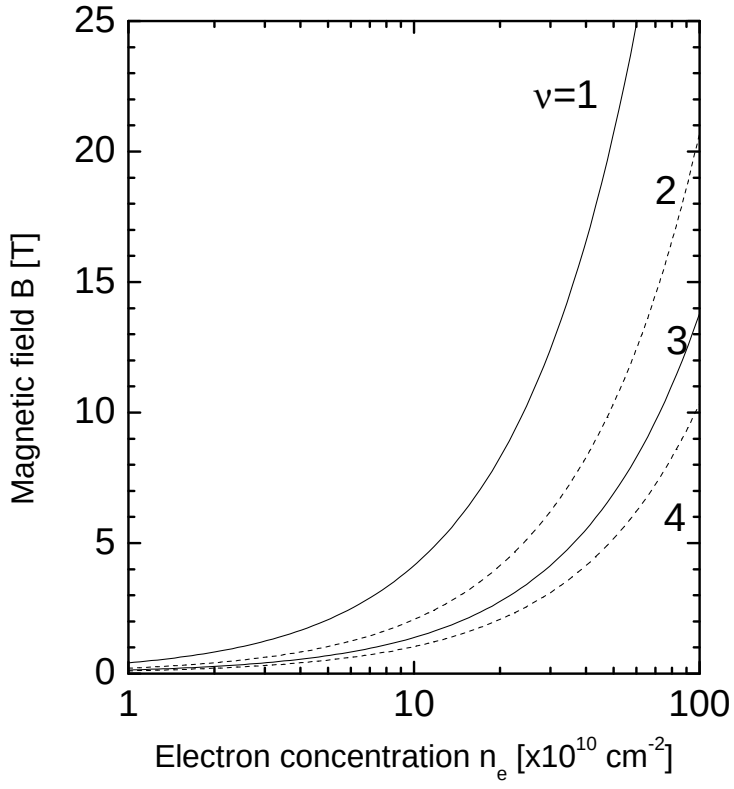

Figure 1.21 – Filling factors of Landau-levels. The filling factor is equal to the number of Landau-levels filled. As the magnetic field is increased the filling factor will decrease since more particles can be put in each Landau-level.

Neglecting magnetic fluctuations and assuming unpolarized excitation, results for the a polarization degree [Zeh98]:

$$P_c = \frac{\tau}{\tau_{spin} + \tau} \tanh\left(\frac{\Delta E_{giantZeeman}\left(T, B\right)}{2k_B T}\right), \tag{1.89}$$

with the life time τ and the spin relaxation time τ_{spin}. It is very important to point out that the equation depends on the giant Zeeman-splitting of the transitions between Γ_6 and Γ_8: $\Delta E_{giantZeeman} = \Delta E_{\Gamma_6} + \Delta E_{\Gamma_8}$, and, therefore, is strongly dependent on the temperature of the manganese spin-system.

1.4.6 Parabolic and half-parabolic quantum wells

Beside rectangular QWs, also parabolic and half-parabolic systems were investigated in this thesis. In such systems, the Mn concentration decreases continuous between the barrier and the QW center, to generate a parabolic profile of the potential. In magnetic field the devolution of the bands can differ from the parabolic shape. From equations 1.65 and 1.66 is known that the giant Zeeman-splitting depends on the Mn concentration. In the investigated CdMnTe systems the Γ_8 valence band splitting for the heavy-hole is four times stronger than for the Γ_6 conduction band (compare table A.8), leading to noticeable different band edge devolution. In the center of the QW the Mn concentration is zero, so that the band energy remains unchanged in magnetic field. With rising Mn concentration also the symmetric splitting of the band edges

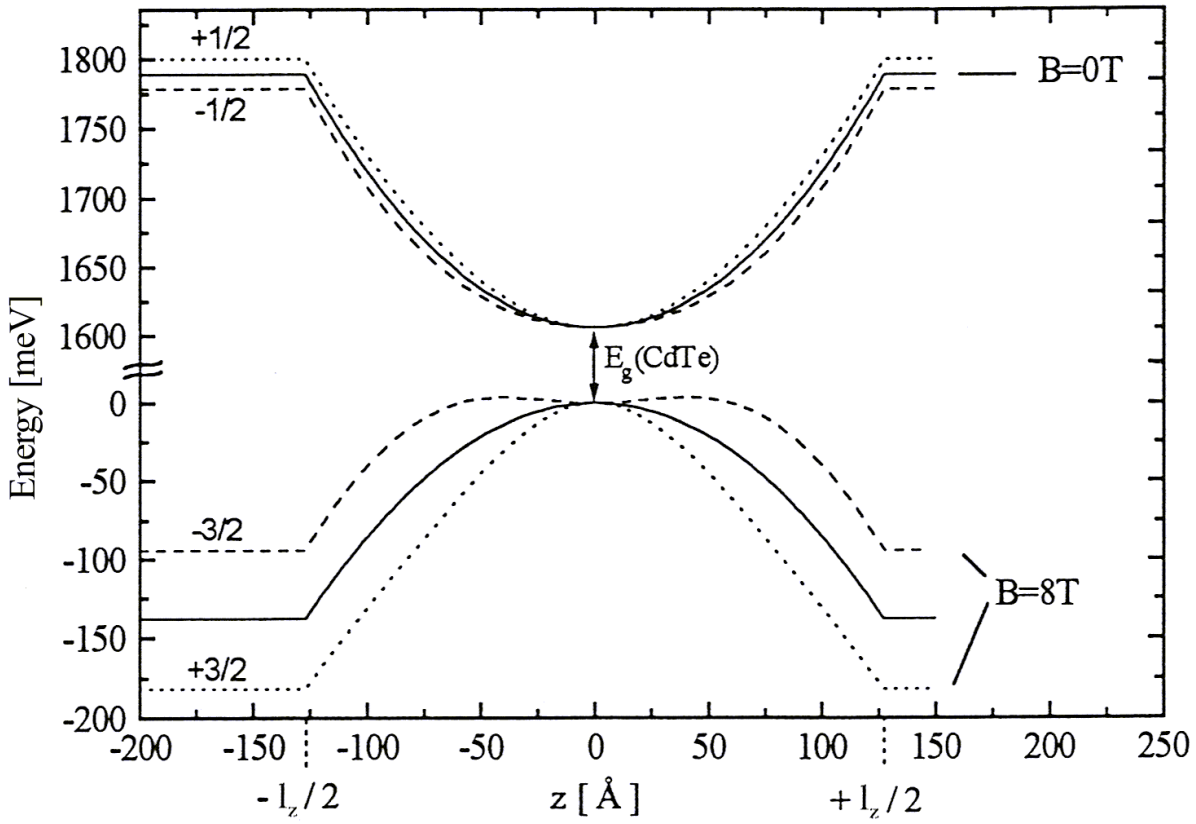

Figure 1.22 – Potential of the conduction and valence band of a parabolic QW using the example of a $Cd_{0.8}Mn_{0.2}Te$ QW with $l_z = 254$ Å. For the valence band only the heavy-hole states are shown. The dotted and dashed depict the potential change in a magnetic field of $B = 8$ T. [Fie97]

increases. For samples with a Mn concentration in the barrier exceeding $x = 0.15$, the splitting reaches a maximum at this concentration and the band edge splitting decreases up to the barrier concentration with rising Mn concentration [Fie97]. This situation is shown exemplary in figure 1.22 for an barrier concentration of $x = 0.2$.

The single-particle states can be calculated by the equidistant energy levels of the harmonic oscillator at $B = 0$ T [Mil84a, Mil84b]. In a parabolic potential $V(z) = \frac{1}{2}Kz^2 \equiv \frac{1}{2}m\omega^2 z^2$ the harmonic oscillator is

$$\hat{H} = -\frac{\hbar^2}{2m}\vec{\nabla}^2 + \frac{Kz^2}{2}, \tag{1.90}$$

where $K = m\omega^2$ determines the bending of the parabola. The corresponding Schrödinger-equation is solved by the wave functions

$$\Psi_n(z) = A_n \exp -\frac{m\omega z^2}{2\hbar} H_n(z), \tag{1.91}$$

with

$$A_n^2 = \frac{1}{2^n n!}\sqrt{\frac{m\omega}{\pi\hbar}} \tag{1.92}$$

and the Hermite polynomial

$$H_n(z) = (-1)^n \exp z^2 \frac{d^n \exp -z^2}{dx^n}, \tag{1.93}$$

with $n = 0, 1, 2, \ldots$. The corresponding energy eigenvalues are [Sch93]

$$E_n = \hbar\omega \left(n + \frac{1}{2} \right). \tag{1.94}$$

In a parabolic quantum well (PQW) the restoring force constant K is defined by

$$K_{VB,CB} = 8 \frac{V_{VB,CB}}{l_z^2}, \tag{1.95}$$

where the conduction band potential V_{CB} and the valence band potential V_{VB} are defined analogue to the rectangular QW depicted in figure 1.18. Using 1.95 and 1.67 with equation 1.94, results for the energy levels in the conduction band and valence band, respectively:

$$E_n^{CB} = \frac{2\hbar}{l_z} \sqrt{\frac{2\left(1 - Q_{VB}\right)\Delta E_g}{m_{eff} m_0}} \left(n + \frac{1}{2} \right) \tag{1.96}$$

$$E_n^{VB} = \frac{2\hbar}{l_z} \sqrt{\frac{2 Q_{VB} \Delta E_g}{m_{eff,hh} m_0}} \left(n + \frac{1}{2} \right), \tag{1.97}$$

with the effective masses $m_{eff,hh}$ and m_{eff}, introduced in subsection 1.2.1. Because of strain and excitonic effects, these values differ slightly for observed transition energies [Fie97].

An exact analytic solution of finite PQWs is given in [Yue93]. It is based on the time-independent Schrödinger-equation (1.90) inside a PQW potential, which is described by confluent hypergeometric functions [Abr65]. Comparison of this solution with the quantization by the harmonic oscillator by [Fie97] shows a good concordance of the results for heavy-hole subbands at arbitrary Mn concentration, and for low electron subbands ($n < 6$) at higher Mn concentrations ($x \geq 0.5$). For lower Mn concentrations the changing of the subband structure by the finite QW has to be additionally incorporated [Fie97].

According to [Mil85] also for the theoretical description of half-parabolic quantum wells (HPQW) the harmonic oscillator approximation can be used. Compared with the PQW, the energy level with even subband index n are the solutions of the HPQW, because whose wavefunctions vanish at the half-parabolic barrier. As shown in figure 1.23, the penetration of the wavefunctions into the half-parabolic barrier leads to distinct decrease of the energy levels $\tilde{n}$ compared with the energy levels n of the parabolic system.

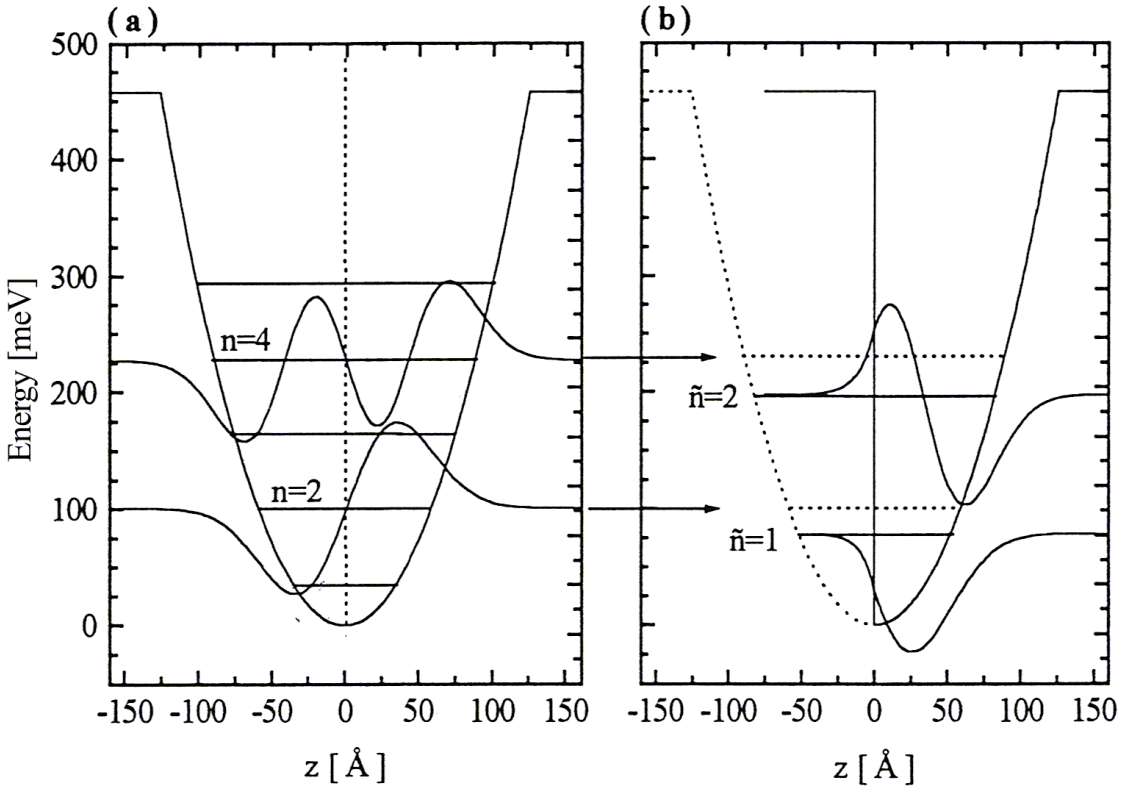

Figure 1.23 – Devolution of the conduction band edge, wavefunctions and energy levels for (a) parabolic and (b) half-parabolic QWs. Shown are the lowest subband levels ($\tilde{n} = 1, 2$) for a HPQW and the corresponding subband levels with $n = 2, 4$ for a PQW. Penetration of the wavefunctions in the barrier leads to a distinct decrease of the energy levels compared with the levels of the parabolic system. [Fie97]

In magnetic field the conventional perturbation theory approach for rectangular QWs [Oss93, War85] cannot be used for PQWs, because the devolution of the potential is not longer approximately parabolic. As demonstrated in [Fie97], for each magnetic field the changing of the band edge has to be calculated numerically for the different spin states. From this the Zeeman-splitting for optical transitions for $B \neq 0\,\mathrm{T}$ can be deduced. In figure 1.24 the Zeeman-splitting for σ^- polarized optical transitions against external magnetic field is shown. The increasing Zeeman-splitting with rising n can be explained perturbation-theoretically by a greater overlap of the wavefunctions with the Mn-system [Fie97]. For half-parabolic systems the calculation of the Zeeman-splitting can be performed analogue. The results are qualitatively the same.

Advantages of PQWs are that the interface and diffusion effects, described in subsection 1.4.3, have less influence on the Zeeman-splitting. On the one hand the continuous change of the Mn concentration reduces the probability for trapped excitons. One the other hand diffusion leads even to an advancement of the QW structure. The latter can be understood on examination of the growth procedure (compare section A.1). So results, primarily by diffusion, balancing of the Mn concentration in the alternating magnetic and nonmagnetic layers, so that the medial band devolution is not altered [Fie97].

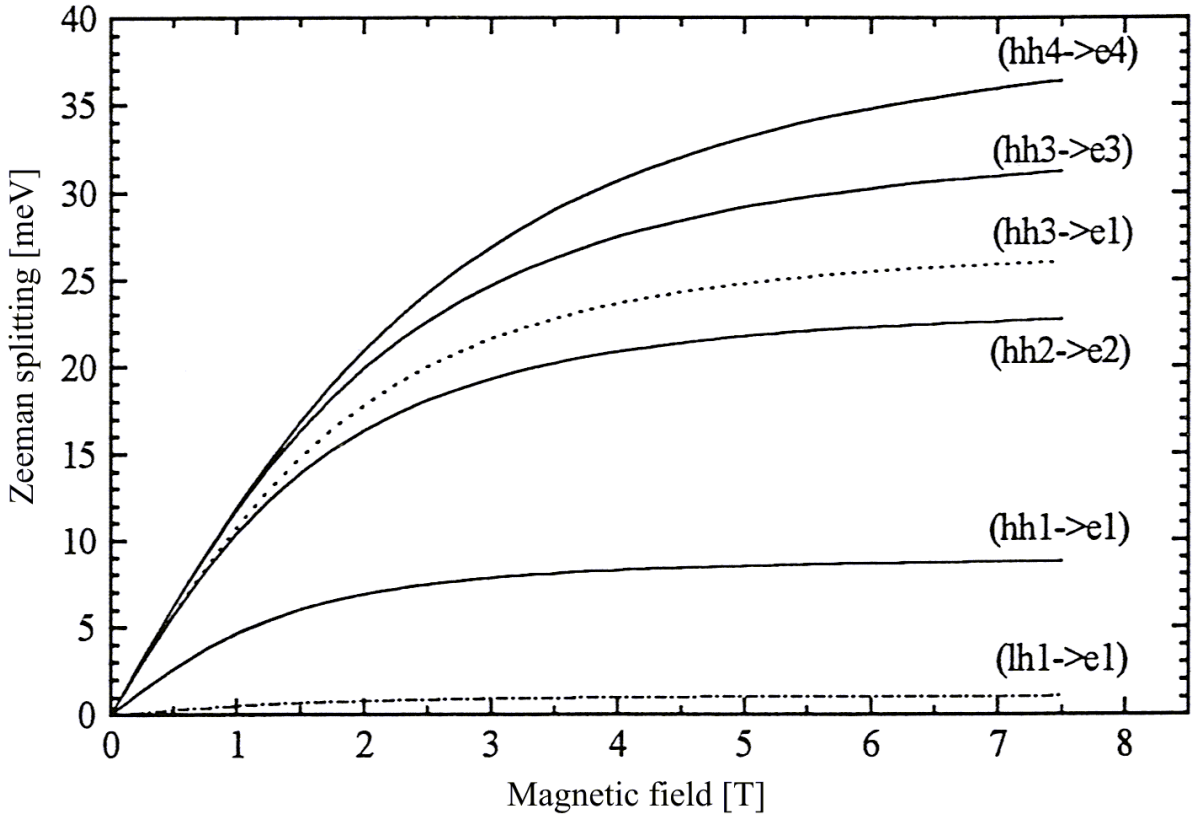

Figure 1.24 – Theoretical Zeeman-splitting of a PQW for different σ^- polarized optical transitions in magnetic field. [Fie97]

1.5 Excitons

In the previous explanations, the Coulomb interaction between electrons and holes was neglected, and solely optical transitions concerning single-particle states were regarded. Optical excitation can lift electrons from the valence band in the empty conduction band of a semiconductor by absorption of photons with energy $\hbar\omega$ and wave vector $\vec{k}_{opt}$. Thereby, energy and impulse conservation count. Absorption is only possible for photons with $E_{photon} > E_g$. By this excitation of an electron from the valence band to the conduction band an electron-hole pair is created, which can form a bound state due to the Coulomb interaction. This quasi-particle is labeled exciton. Its binding energy depends strongly on the material and ranges from 1 meV up to 1 eV. Consequence of exciton formation is considerable changing of the absorption properties near the energy gap [Ell57].

Two types of exciton can be distinguished. Frenkel excitons have large exciton binding energies and an electron-hole distance in order of the lattice constant a_0. Mott-Wannier excitons have low exciton binding energies and electron-hole distances considerably exceeding a_0. Each allowed transition between bound states in the valence and conduction band has a series of excitons. Excitons can propagate within crystal.

1.5.1 Free exciton

The two-particle problem of the exciton is described in effective mass approximation by following Schrödinger-equation [Kno63]:

$$\left[\frac{\vec{p}_e^{\,2}}{2m_{eff,e}} + \frac{\vec{p}_h^{\,2}}{2m_{eff,h}} - \frac{e^2}{4\pi\varepsilon_r\varepsilon_0|\vec{r}_e - \vec{r}_h|}\right]\Psi\left(\vec{r}_e, \vec{r}_h\right) = \left(E - E_0\right)\Psi\left(\vec{r}_e, \vec{r}_h\right). \tag{1.98}$$

The indices e and h stand for the respective values of electrons and holes and ε_r is the static dielectric constant[25] and ε_0 the static electric field constant, taking into account the shielding of the Coulomb interaction by the polarizability of the lattice. The Hamilton operator in equation 1.98 consists of three summands. The first and second term are the Hamilton operators for the conduction band electron and valence band hole, respectively, and the third term regards the Coulomb interaction between electron and hole.

The solution of the Schrödinger-equation can be achieved analogue to the hydrogen problem by using an approach with separation in relative $\vec{r}$ and barycenter coordinates $\vec{R}$:

$$\Psi\left(\vec{r}, \vec{R}\right) = \frac{1}{\sqrt{V_{crystal}}}\exp\left(i\vec{K}\vec{R}\right)\Phi_{nlm}\left(\vec{r}\right), \tag{1.99}$$

with the eigenvalue for the barycenter impulse $\vec{K}$ and crystal volume $V_{crystal}$. Φ_{nlm} are the well-known eigenfunctions of the hydrogen atom, with the main quantum number $n = 1, 2, 3, \ldots$, the orbital quantum number $l = 0, 1, 2, \ldots, (n-1)$, and the magnetic quantum number $m = -l, -(l-1), \ldots, 0, \ldots, (l-1), l$. To take into account the reduced mass of the exciton

$$\mu = \frac{(m_{eff,e}m_{eff,h})}{(m_{eff,e} + m_{eff,h})} \tag{1.100}$$

and the shielded Coulomb interaction, the Bohr-radius a_B can be substituted by an effective Bohr-radius

$$a_{B,3D} = \frac{(4\pi\varepsilon_r\varepsilon_0\hbar^2)}{(\mu e^2)} \tag{1.101}$$

and the Rydberg constant ($Ryd = 13.6\,\text{eV}$) by an effective Rydberg constant

$$Ryd_{eff} = \frac{\mu e^4}{32\left(\pi\varepsilon_r\varepsilon_0\right)^2\hbar^2} = \left(\frac{\mu}{m_0\varepsilon_r^2}\right)\cdot Ryd. \tag{1.102}$$

Thus, the binding energy of the exciton results analog to the hydrogen problem:

$$E_b(n) = \frac{Ryd_{eff}}{n^2}. \tag{1.103}$$

[25] Generally, the dielectric function $\epsilon(\omega)$ is used in the equation. In case of exciton binding energies smaller than typical optical phonon energies it can be replaced with ε_r.

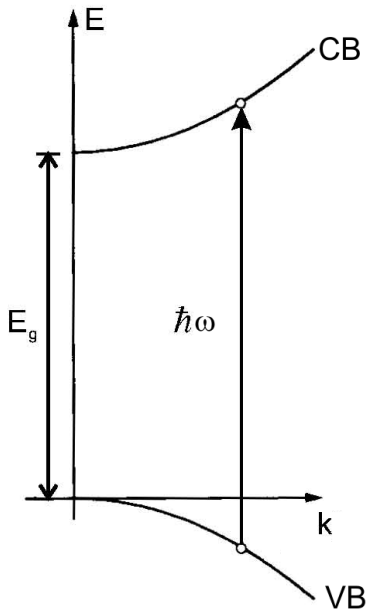

Figure 1.25 – Schematical picture of exciton creation. Lifting of an electron with $\vec{k}_e$ by photon excitation with energy $\hbar\omega$ corresponds to creation of hole with wave vector $\vec{k}_h = \vec{k}_e$. Because of $|\vec{k}_{opt}| \approx 0$, the transition is nearly vertical in the E-k-diagram. [Kli06]

In neglect of the energy of the barycenter $\frac{(\hbar\vec{K})^2}{2\left(m_{eff,e}+m_{eff,h}\right)}$[26], for the total energy of a free exciton results:

$$E(n) = E_0 + \frac{Ryd_{eff}}{n^2}. \tag{1.104}$$

The approximation is possible, because only excitons with $\vec{K} = 0$ (direct transition) can be observed in optical spectra. This results from the impulse conservation law for creation and recombination of excitons, as the photon impulse is negligible compared to the barycenter impulse. For indirect transitions with $\vec{K} \neq 0$, phonons are needed.

Direct exciton absorption is only possible for electrons and holes being at the same position. At finite probability density for $\vec{r} = 0$ have only s-type excitons without angular momentum $(l = 0)$, which is known from calculations of the excitonic contribution to the optical susceptibility and the corresponding absorption coefficient by [Ell57]. The interaction between electron and hole leads to a series (1S, 2S, 3S,...) of sharp exciton lines in the absorption spectrum below the fundamental band edge. The binding energies for the free exciton (1S) in CdTe and ZnSe are given in table A.4 in the appendix. Especially for ZnSe-based semiconductors the optical properties are significantly determined by excitons, because of the high exciton binding energy, resulting from the strong Coulomb interaction.

The creation of an exciton is given schematically in figure 1.25. Thereby must be taken into account that the excitonic energy eigenvalues cannot be mixed with the calculated band structure energies. This follows from the usage of a one-particle approximation for the exciton in the band structure calculation.

[26]The kinetic energy of the barycenter occurs because the system can move quasi-freely in the crystal.

Free excitons can lower their energy by localization. Possibilities are binding on impurities due to Van-der-Waals-interaction or creation of magnetic polarons [Mac96].

1.5.2 Interaction of excitons with Mn^{2+}-ions

Excitons in Mn-based DMS interact with the localized Mn-spins. Responsible for the interaction between the s-type conduction band electrons, p-type valence band holes and Mn $3d^5$-electrons is the sp-d-exchange interaction. The, so far made, considerations concerning the sp-d-exchange interaction hold also for excitons. Therefore, the total Zeeman-splitting of an exciton for a magnetic field in Faraday geometry is

$$\begin{aligned} \Delta E_{totalZeeman,X} &= E_{Zeeman,X} + E_{giantZeeman,X} \\ &= E_{Zeeman,X} + N_0(\alpha-\beta)xS_{eff}\mathcal{B}_{5/2}\left(\frac{5g_{Mn}\mu_B B}{2k_B T_{eff}}\right), \end{aligned} \tag{1.105}$$

where $E_{Zeeman,X}$ is the Zeeman-splitting for an exciton of the host semiconductor. Referring to 1.3.4.4, the exciton ground state splits in six components with the corresponding electric-dipole-allowed transitions.

1.5.3 Quasi-two-dimensional excitons in quantum wells

In QWs particles are confined along z by the QW potential and perpendicular to this direction by the Coulomb potential. If the overlap of the electron and hole wave functions is modified, the excitonic properties are altered compared with the bulk material. For QW widths $l_z \gg a_{B,3D}$ the confinement is only weak. The binding energy of excitons in bulk material is much higher than the confinement energy, so that the interference due to the QW is weak. Only the motion of the barycenter is quantized. Contrary, electron and hole are independently quantized for $l_z \lesssim a_{B,3D}$. This situation with strong confinement results in distortion of the exciton wavefunction and, therefore, to increase of the exciton binding energy [Man00].

The binding energy of the confined excitons with infinite barrier height and $l_z \to 0$ results from the solution of the two-dimensional Schrödinger-equation to [Shi66]:

$$E_b(n) = \frac{Ryd_{eff}}{\left(n-\frac{1}{2}\right)^2}. \tag{1.106}$$

The binding energy is for the two-dimensional 1S exciton four times stronger than for the three-dimensional 1S exciton.[27] This leads to an increase of the oscillator strength. Contrary, from the stronger decrease of the overlap of electron and hole at $r = 0$ for excited states ($n > 1$)

[27] In real QWs with finite barriers and l_z, the exciton binding energy does not exceed the double or triple value of the bulk material.

in the two-dimensional case follows that the oscillator strength decreases for excited excitons [Kel04]. Therefore, it is difficult to observe excitons with ($n > 1$). Calculated binding energies for real quasi-two-dimensional QWs are given for ZnSe-based semiconductors in [Ast02] and for (Cd,Mn)Te in [Del90]. Treatment of the two-particle problem of the exciton in QW in approximation of parabolic bands is given in [Kuh95] and references therein. The effective Bohr-radius is $a_{B,2D} = \frac{\sqrt{3}}{8} \cdot a_{B,3D}$ in the two-dimensional case [Wei91].

From symmetry considerations can be deduced that for light, which is polarized perpendicular to the growth direction, light- and heavy-hole exciton with $n = 1$ are electric-dipole-allowed. Contrary is for light, which is polarized parallel to the growth direction, only the corresponding light-hole exciton is electric-dipole-allowed [And95].

1.5.4 Quasi-two-dimensional excitons in magnetic field

The confinement in QW structures removes the degeneracy of the light- and heavy-hole valence bands at $k = 0$. Thus, one exciton associated with the light-hole and one with the heavy-hole can be observed. In DMS QWs show these excitons a strong splitting even in small magnetic fields[28], because the splitting is greatly enhanced by the presence of the magnetic Mn^{2+}-ions in the barriers, which effectively amplifies the magnetic field on the excitons [Rya81, War85]. Thus, the exciton splitting provides attention for the penetration of the carriers into the barrier layers. It should be stressed that here QWs are regarded, where only the barriers are made of DMS. The QW itself consists of nonmagnetic CdTe or ZnSe. From experimental measurements of the saturation value of the spin splitting can be deduced that, depending on the QW width, parts of the excitonic wave function are in the QW and the rest is in the barrier layer [War85]. Inside the penetration area, the Mn-spins interact with the exciton by the sp-d-exchange. For a quantitative consideration, the probability density for an exciton is weighted with the spin splitting of the barrier. The probability densities (compare figure 1.19) for different spin states are approximately equal in magnetic field. Hence, it is sufficient to use the probability densities without magnetic field for a description of the Zeeman-splitting in a perturbative approach [Oss93, War85]. As already discussed, this simple picture has to be modified by interface effects, as described in subsection 1.4.3.

Binding energies of excitons in real quasi-two-dimensional QWs have been calculated in parabolic approximation by [Ast02] for ZnSe-based structures. The electron-hole Hamilton-Operator for a QW in magnetic field $\vec{B} = (0, 0, B_z)$ is composed of the terms for the conduction band electron $\hat{H}_e$; for the valence band hole $\hat{H}_{hh}$; for the Coulomb interaction between electron

[28] At higher fields even a strong mixing of the states results from the spin splitting. Related effects are consecutively neglected.

and hole $V_{Coulomb}$ (see equation 1.98); for the two-dimensional movement of particles in a magnetic field $\hat{H}_{2D}$; and for the QW potentials $V_{QW,e}$ and $V_{QW,hh}$:

$$\begin{aligned}\hat{H} &= \hat{H}_{hh} + V_{QW,hh} + \hat{H}_e + V_{QW,e} + \hat{H}_{2D} + V_{Coulomb} \qquad (1.107)\\ &= -\frac{\hbar^2}{2m^z_{eff,hh}}\frac{\partial^2}{\partial z^2_{hh}} + V_{hh}\left(z_{hh}\right) - \frac{\hbar^2}{2m^z_{eff}}\frac{\partial^2}{\partial z^2_e} + V_e\left(z_e\right)\\ &\quad + \left(\frac{\left(-i\hbar\vec{\nabla}\vec{\rho}_e + e\vec{A}_e\right)^2}{2m^{xy}_{eff}} + \frac{\left(-i\hbar\vec{\nabla}\vec{\rho}_{hh} + e\vec{A}_{hh}\right)^2}{2m^{xy}_{eff,hh}}\right)\\ &\quad - \frac{e^2}{4\pi\varepsilon_r\varepsilon_0\sqrt{\rho^2 + (z_e - z_{hh})^2}}. \qquad (1.108)\end{aligned}$$

Thereby, m^z_{eff} and $m^z_{eff,hh}$ are the effective electron mass and effective heavy-hole mass, respectively, in growth direction and m^{xy}_{eff} and $m^{xy}_{eff,hh}$ the corresponding effective masses perpendicular to this direction. The slight anisotropy of the electron mass is neglected $\left(m^z_{eff} = m^{xy}_{eff}\right)$. $\vec{A} = \frac{1}{2}\vec{B}\rho_{e,hh}$ is the vector potential in symmetric calibration, which describes the orbital movement of the particles due to the magnetic field. Herefrom results the Landau quantization in the one-particle picture. $\vec{\rho}_e$ and $\vec{\rho}_{hh}$ are the coordinates of electron and heavy-hole, respectively, in the plane of the QW with the potential $V_{e,hh}$ of valence and conduction band, respectively. ρ is the relative coordinate of the exciton with the reduced mass μ. Because of the radial symmetry of the problem, cylindrical coordinates (ρ, Φ) are used.

Evolution of the wave function is possible as product of the solutions of the one-dimensional Schrödinger-equation in growth direction for valence and conduction band and the one-dimensional radial Schrödinger-equation of the Coulomb potential [Kel04]. Diagonalization of the Hamilton-Operator on the basis of such a wave function produces QW binding energies, which are between $l_z = 100$ and 200 Å. This is in good agreement with experimental results [Ast02]. By means of this approach, the solution is only valid for weak magnetic fields ($B \leq 10\,\mathrm{T}$) [Kuh95].

The linear Zeeman effect occurs only for exciton states with a non-vanishing magnetic moment at $B = 0\,\mathrm{T}$, which can be aligned in magnetic field. Always present is the diamagnetic shift, which increases quadratically with the magnetic field. In this case the influence of the magnetic field is described by the diamagnetic operator [Kuh95]

$$\hat{H}_{dia} = \frac{e^2 B_z^2 \rho^2}{8\mu}, \qquad (1.109)$$

which can be included in $\hat{H}_{2D}$ (1.108), beside the relative movement of an exciton in a QW. Therefore, for s-type excitons results an additional exciton energy shift:

$$\Delta E_{dia} \propto \frac{B_z^2}{\mu}\langle r\rangle^2. \qquad (1.110)$$

Here $\langle r \rangle$ is the median distance of electron and hole.

The diamagnetic shift arises from the deformation of the relative motion of electron and hole by Lorentz forces, which is described by a weak admixture of other states in perturbation theory, e.g. p-like states mix into the s-like excitonic ground state. From this admixture arises an angular momentum, which is proportional to B. According to Lenz' rule this momentum is oriented antiparallel to B. Taking into account that the energy of a magnetic dipole also increases linearly with B, results the quadratic dependency of the diamagnetic shift [Kli06].

1.5.5 Trions

Trions are charged excitons, which are created by binding an additional electron (X^-) or hole (X^+) to the exciton. Although they were already predicted in 1958 by [Lam58] in analogy to the charged hydrogen states, first experimental detections were achieved not until 1993 for CdTe QWs [Khe93] and 1995 for GaAs QWs [Fin95, Shi66], respectively. Review of charged excitons in ZnSe-based QWs is given in [Ast02].

Generation of trions in DMS needs presence of low density electron gas ($n_e \approx 10^9$ up to $10^{10}\,\mathrm{cm}^{-2}$), which can be created by slight modulation doping or optical excitation with laser energies higher than the barrier [Kel99]. Hence, in undoped samples for low excitation densities the trion is completely suppressed [Kel01].

In case of negative charged excitons, possible states can be distinguished according to the symmetry of the spin-related part of the electron wave function $|S, S_z\rangle$. The electron spins in the negative charged exciton couple, thereby, to total spin S with the z-component S_z. At zero magnetic field the antisymmetric singlet state $|0, 0\rangle$ is the ground state. This state consists of an electron pair with antiparallel spins and an additional heavy-hole. The Zeeman-splitting of the singlet trion is only determined by the heavy-hole due to $S = 0$. With increasing magnetic field strength also the symmetric triplet states $|1, (0, \pm 1)\rangle$ get stable against dissociation and become the ground state. For the triplet state, the electron spins are aligned parallel to each other. The triplet ground state is a dark state due to translation and rotation invariance resulting from symmetry considerations, which can not be observed in luminescence measurements [Dzy00]. By Landau-level mixing or impurities, the invariance can be lifted [Wój00], making the state optically active. Also bound excited triplet states can be observed [Riv01, Wój00].

Chapter 2

Magnetization dynamics

Contents

Beside the wide investigations of the static magnetic properties of DMS [Fur88a], big interest towards the dynamic magnetic properties has arisen, essentially motivated by the problem of magnetic polaron formation [Aws87c, Aws91, Spa85, Zay87]. Similar to the static magnetic properties described in the previous chapter, also the dynamical properties of the localized Mn-spins, namely spin dephasing and spin-lattice relaxation (SLR) rates, are controlled by concentration dependent exchange interactions between the Mn-ions [Die95].

Basis of spin dynamics in DMS is the interplay between Mn-spin system, free carriers and lattice, which is described in section 2.1. After an overview about the coupled systems, theoretical formulation of spin and energy transfer between them is given along the lines of the explanations in [Yak09]. The model for transfer between the systems traces back to [Kön00a, Kön00b].

Especially the case of presence of carriers with excess kinetic energy is detailed reviewed, because of its strong influence on the magnetic properties. The additional kinetic energy can be transferred to the Mn-ion system, leading to decrease of the magnetization and, therefore, to loss of the giant Zeeman-splitting.

After short description of mechanisms responsible for spin equilibration in nonmagnetic electronic systems in section 2.2, SLR and the mechanisms, which govern SLR, are described more detailed in section 2.3. SLR is the relaxation of the magnetic ion spin by phonon interaction (i.e. with the lattice), which is characterized by the SLR time τ_{SLR}.

Instead of spin relaxation, a Mn-ion can also transfer its spin to another Mn-ion. This so-called spin diffusion is briefly introduced in section 2.4 of this chapter.

2.1 Spin and energy transfer

2.1.1 Coupled systems in diluted magnetic semiconductors

Spin dynamics in DMS is controlled by the energy and spin transfer between its coupled subsystems: the Mn-spin system, the free carriers and the lattice (phonons). These interacting systems are shown schematically in 2.1, where the channels of energy and spin transfer are given by arrows. The systems can be characterized by their temperatures T_i and heat capacities C_i. The strength of the coupling between the systems is given by times τ_i for energy relaxation between the systems. In equilibrium situation the temperatures and spin temperatures of the carriers, Mn-spin system and lattice are equal and, therefore, spin and energy exchange between these systems is absent.

The carrier system includes photogenerated or electrically injected carriers, and resident electrons or holes, provided by n-type or p-type doping, respectively. For simplification, electrons are considered as typical representatives of the carriers in the succeeding explanations. More information about the effects with holes are given e.g. in [Aki06b, Mer09, Yak09] and references therein. Generation of photocarriers occurs via light absorption. The lifetime of photocarriers is limited by various recombination processes, which fall in the subnanosecond range for the exciton recombination in wide-band-gap semiconductors [Yak09].

Quasi-equilibrium distribution of electrons is characterized by the electron temperature T_e. This distribution is achieved by electron-electron collisions in a time, which is inversely proportional to the electron concentration (n_e), and linearly proportional to ${E_e}^{3/2}$, with the kinetic energy of the electrons E_e. This time can be much faster than the time required for sharing excess kinetic energy in the carrier system with the phonon system and Mn-system via the channels shown in figure 2.1.

The phonon system has the largest heat capacity and, therefore, serves as bath. By means of heat pulses also this system can be driven to nonequilibrium situation, which is reviewed in [Aki06a]. Establishing equilibrium in the phonon system requires times in the range of microseconds [Yak09]. The temperature of the phonon system is characterized by the lattice temperature T_L.

The Mn-spin system plays the key role in spin dynamics. Its static and dynamic magnetization depends strongly on the Mn concentration due to antiferromagnetic coupling of adjacent Mn-spins because of the d-d-exchange interaction. It originates from the fact that isolated Mn^{2+}-ions have zero orbital moment and do not interact directly with the phonon system in first order perturbation theory [Yak09]. In strained superlattices splitting of the Mn^{2+}-ion d-shell was observed [Qaz95], which makes phonon interaction possible in second order. The magnetization of the Mn-system in external magnetic field is characterized by the Mn-spin temperature T_{Mn}.

The exchange interaction between the Mn-ions controls the dynamical properties of the localized Mn-spins, which are SLR and spin dephasing. A definition of spin relaxation and spin dephasing can be given phenomenologically in the framework of the Bloch-Torrey equations

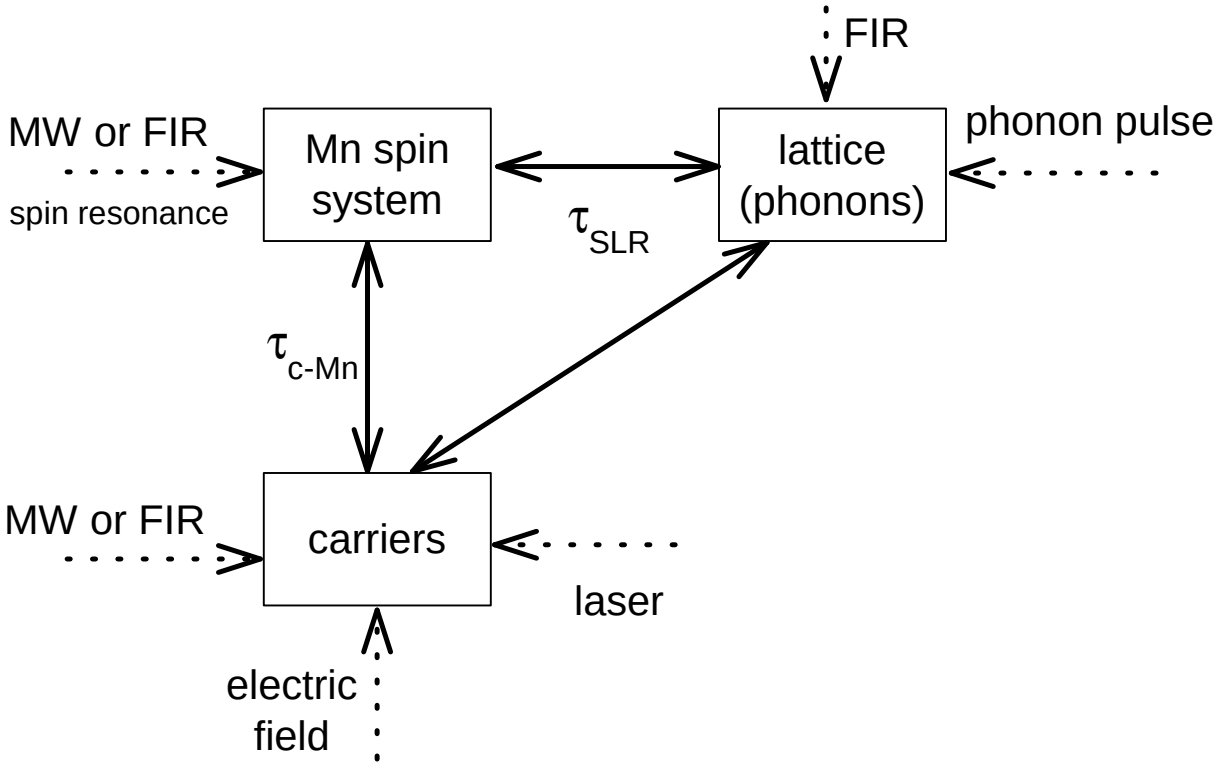

Figure 2.1 – Interacting systems of DMS. Each system can be characterized by its temperature T_i and heat capacity C_i. Channels for energy and spin transfer are shown by solid arrows. The dotted line arrows represent different external impacts, providing heating of the systems.

[Blo46, Tor56] via equations for the spin precession, decay, and diffusion of electronic magnetization $\vec{M}$ in an applied magnetic field $\vec{B}$ [1] [Kap59, Tor56]:

$$\frac{\partial M_x}{\partial t} = \gamma\left(\vec{M}\times\vec{B}\right)_x - \frac{M_x}{t_2} + D\vec{\nabla}^2 M_x, \tag{2.1}$$

$$\frac{\partial M_y}{\partial t} = \gamma\left(\vec{M}\times\vec{B}\right)_y - \frac{M_y}{t_2} + D\vec{\nabla}^2 M_y, \tag{2.2}$$

$$\frac{\partial M_z}{\partial t} = \gamma\left(\vec{M}\times\vec{B}\right)_z - \frac{M_z - M_z^0}{t_1} + D\vec{\nabla}^2 M_z. \tag{2.3}$$

Hereby, D is the diffusion coefficient[2] and $\gamma = \frac{\mu_B g}{\hbar}$ is the electron gyromagnetic ratio. By $M_z^0 = \chi B_0$ the thermal equilibrium magnetization of the system is denoted. While SLR is related to the longitudinal component of the magnetization, spin dephasing is related to the transverse component. The discrimination of both components is essential because of the symmetry reduction in external magnetic fields.

The dephasing of the coherent precession of Mn-spins about the longitudinal magnetic field is caused by anisotropic spin-spin interactions. The phase of the precession gets lost due to spatial and temporal fluctuations of the precessing frequencies. The dephasing time $t_2 = 10^{-12}$ - 10^{-9} s [Die95], which also called decoherence time, indicates the duration of the magneto-dipole and exchange interactions for establishing the spin temperature T_{Mn} inside the Mn-system. This process has only weak influence on the energy of the Mn-spins, since the energy relaxation is determined by the SLR process. The duration for establishing equilibrium between lattice and Mn-spin system, usually via phonon interaction, is given by the time $t_1 = 10^{-8}$ - 10^{-4} s [Die95], which is often called SLR time or energy relaxation time. This time is equivalently the time it takes for the longitudinal magnetization to reach equilibrium. These two phenomenological times constants t_1 and t_2 for the spin components longitudinal and transverse to B allow description of the Mn-spins after optical orientation [Abr70]. While Faraday configuration enables study of t_1, Voigt configuration allows examination of t_2.

In isotropic and cubic solids, the difference between t_1 and t_2 is only significant, if the external magnetic field exceeds the local exchange field by d-d-exchange interaction of neighboring Mn-ions. The equality between relaxation and dephasing times was noticed first in the context of nuclear magnetic resonance (NMR) [Blo46, Wan53] and later extended to electronic spin systems [And58, Pin55]. For comparing experiment and theory this equality is very convenient, as measurements usually yield t_2. Theoretically it is often more convenient to calculate t_1 [Žut04]. In contrast, the equality $t_1 = t_2$ does not apply in anisotropic systems, like e.g. two-dimensional semiconductor heterostructures.

[1] Thereby, the magnetic field is composed of a static longitudinal component along z and an oscillation transverse component perpendicular to z.

[2] For cubic crystal symmetry is D a scalar.

A qualitative reason for $t_1 = t_2$ is that, if the phase acquires a random contribution during a short time interval, the energy uncertainty of the spin levels determining the longitudinal spin is greater than the Zeeman-splitting $\hbar\gamma B_0$ of the levels. In this case the splitting does not play a role in dephasing, and the dephasing field will act equally on longitudinal and transverse spins. In classical terms, a spin, which is oriented along the direction of the magnetic field, can precess a full period about the perpendicular fluctuating field, feeling the same dephasing fields as the transverse components. As the external field increases, the precession angle of the longitudinal component is reduced, inhibiting dephasing [Žut04]. At zero field limit the equilibrium polarization of the Mn-spin system vanishes and both spin components relax with t_2. Nevertheless, the energy relaxation is still determined by the considerably longer SLR time t_1. Both times depend strongly on the concentration of the Mn-ions [Die95].

The experimental results, presented in this thesis, are measured in magnetic fields, which are so strong that the magnetization dynamics is controlled by t_1.

The Mn-spin system receives energy, i.e. is heated in respect to the bath temperature of the phonon system T_L, by means of interaction with free carriers with excess kinetic energy. Diagram 3.4 illustrates the particular case, when the carriers photogenerated by pulsed laser light $I_L(t)$ are used to heat the Mn-spin system. Mn heating under laser excitation has been reported in [Agu96, Fre92, Rya82, Wol95] and studied in more detail in [Bau94, Far96, Hun05a, Hun05b, Kel01, Kel02, Kou03, Kön00b, Kre85b, Kre89, Kul96, Kur02, Tya97, Yak04]. Heating by electrical current was observed for (Cd,Mn)Te/(Cd,Mg)Te QWs [Kön00a] and for (Hg,Mn)Te/(Hg,Cd)Te QWs [Gui04]. It has been shown that, depending on excitation conditions, the Mn temperature can be increased from a few Kelvins up to a hundred Kelvins above the bath temperature.

The localization of the carriers in two or three dimensions occurring in heterostructures, like e.g. digital alloys, leads to spatially inhomogeneous conditions for temperature exchange with the Mn-spin system. Therefore, spin diffusion inside the Mn-spin system between regions with and without carrier interaction has to be taken into account for evaluation of T_{Mn}.

2.1.2 Theoretical formulation of spin and energy transfer

To analyze spin and energy flux between the systems, if the carrier or Mn-system is driven out of equilibrium, the main thermodynamical parameters of the coupled systems in DMS have to be identified and analyzed under electron photogeneration. These are the three system temperatures T_{Mn}, T_e and T_L of the respective systems introduced in the previous subsection.

A model for heat exchange between two systems is given by the Fourier law [Fou22]

$$\frac{\partial Q}{\partial t} = -\kappa \oint_S \vec{\nabla} T \cdot d\vec{S}, \tag{2.4}$$

where $\frac{\partial Q}{\partial t}$ is the amount of heat transferred per unit time, κ the conductivity of the material and S the surface through which the heat is flowing. For a simple linear situation, where uniform temperature across equally sized end surfaces and perfectly insulated sides exists, the heat flux is given as

$$\frac{\partial Q}{\partial t} = -\kappa A \frac{\Delta T}{\Delta x}, \tag{2.5}$$

where A is the cross-sectional surface area, ΔT the temperature difference between the end surfaces and Δx the distance between the end surfaces.

The Fourier law can be used to describe thermal fluxes between the Mn-ion system and the lattice in the case of weak deviations of the temperatures from the equilibrium values ($|T_{Mn} - T_L| << |T_{Mn,L}|$):

$$C_{Mn}\frac{\partial T_{Mn}}{\partial t} = -C_L \frac{\partial T_L}{\partial t} = -q\left(T_{Mn} - T_L\right), \tag{2.6}$$

with the heat capacities C_{Mn} and C_L and the thermal conductivity of the boundary separating the systems $q = \kappa \frac{A}{\Delta x}$.

The linear approximation with the Fourier law is only sufficient for a general qualitative understanding, because typical experimental conditions involve high excitation regime [Kön00a]. From [Sha74] is known that at liquid helium temperature even an excitation density of about $1\ \mathrm{W/cm^2}$ is sufficient to increase the temperature of the carrier system by several times.

Description of the energy transfer between Mn-spin system and carriers is more complicated, because the energy transfer is accompanied by spin transfer. The exchange of energy and spin is provided by flip-flop transitions of electron spin and Mn-spin [Aws87b, Kre85b, Kre89]. This process is based upon the s-d-exchange interaction and conserves the total spin

$$|\sigma_z, S_z > \rightarrow |\sigma_z \pm 1, S_z \mp 1> . \tag{2.7}$$

Here σ_z is the z-component of the electron spin and S_z the z-component of the Mn-ion total spin in the ${}^6A$ ground state. The energy mismatch between the Zeeman-splitting of electrons and Mn-ions is compensated by additional kinetic energy of the electron (see figure 2.2). This energetic difference arises from the fact that the Mn-ions just split in external magnetic field, while the electrons experience the giant Zeeman-splitting of the conduction band in the exchange field of magnetic ions. The coupling of electron system and Mn-ion spin system with the reservoir of electron kinetic energy is possible because of the δ-like scattering potential of localized Mn-spin for carriers. This permits with equal probability any momentum value of the difference between initial and scattered electron state [Yak09]. Recent results on magnetization dynamics for $Zn_{1-x}Mn_xSe$ QWs cannot be explained by the flip-flop mechanism, so that a model based on mixing of heavy-hole and light-hole states is proposed. Thereby, the energy

and spin transfer from hole to Mn-ion is governed by the hole relaxation within one Zeeman heavy-hole subband [Yak07]. The electron system is usually additionally characterized by the nonequilibrium spin $\langle \vec{s}_{NE} \rangle$ at times shorter than the electron spin relaxation time, but exceeding electron-phonon interaction time $\tau_{e-phonon}$. This condition is fulfilled in nonmagnetic $A^{II}B^{VI}$ QWs (see e.g. [Zhu06] for CdTe/(Cd,Mg)Te). Although magnetic ions significantly accelerate the electron spin relaxation time, still transfer of energy and spin during spin exchange between magnetic ions and electrons occurs.

Analogue to the Fourier law a linear dependence of the flux, here spin flux, on the parameter, which describes the system, here $\langle \vec{s}_{NE} \rangle$, exists for weak deviations [Yak09]:

$$\left. \frac{\partial \vec{I}_{\text{Mn}}}{\partial t} \right|_{ex} \frac{n_{Mn}}{n_e} \approx \lambda_{JS} \langle \vec{s}_{NE} \rangle . \tag{2.8}$$

Thereby, the nonequilibrium spin is defined as the difference of the electron spin mean value $\langle \vec{s} \rangle$ and the equilibrium value at T_e $\langle \vec{s}_{T_e} \rangle$:

$$\langle \vec{s}_{NE} \rangle = \langle \vec{s} \rangle - \langle \vec{s}_{T_e} \rangle . \tag{2.9}$$

λ_{JS} is the rate of electron spin relaxation on magnetic ions, n_{Mn} and n_e are the Mn-ions concentration and the electrons concentrations, respectively, and $\vec{I}_{\text{Mn}}$ is the mean value of the Mn-spin, which is changed by the electron exchange scattering.

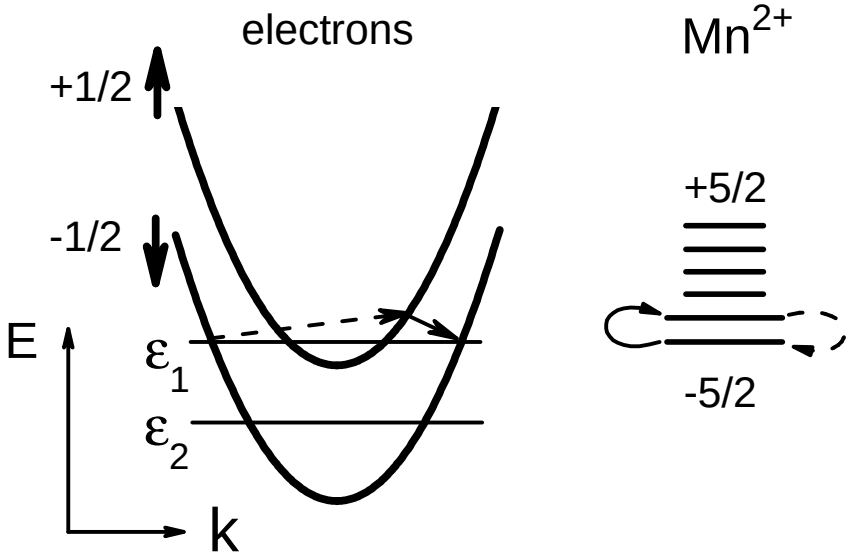

Figure 2.2 – Energy diagram of electron exchange scattering on Mn^{2+}-ion in external magnetic field. Electron scattering from spin up to spin down subband is shown by solid arrows. This process causes Mn-spin heating. The reversed process is denoted by dashed arrows. The efficiency for spin and energy transfer depends on the Fermi-level for a degenerate 2DEG. If the Fermi-level is above the upper spin subband, as indicated by ε_1, the transfer efficiency is independent of giant Zeeman-splitting. If the Fermi-level falls below the bottom of this subband (ε_2) decreases the transfer efficiency exponentially. [Yak09]

Using 2.4 and 2.8, for the spin and energy transfer between electron and Mn-system results in an external magnetic field $\vec{B}$:

$$\left.\frac{\partial E_{Mn}}{\partial t}\right|_{ex} = C_{Mn}\left.\frac{\partial T_{Mn}}{\partial t}\right|_{ex} = q\left(T_e - T_{Mn}\right) + \mu_B g_{Mn}\lambda_{JS} n_e\left(\vec{B}\cdot\langle\vec{s}_{NE}\rangle\right). \tag{2.10}$$

Contrary to the situation in equation 2.6, an energy flux subsists also for $\Delta T = |T_e - T_{Mn}| = 0$, if nonequilibrium electron polarization exists. Consequence of this generation of energy flux by nonequilibrium electron polarization is, in compliance with the Onsager relation [Lan80], that also an energy flux due to $\Delta T \neq 0$ generates nonequilibrium electron polarization. This can be described by equation

$$\frac{d\langle\vec{s}_{NE}\rangle}{dt} = -\lambda_{JS}\langle\vec{s}_{NE}\rangle + \vec{\Lambda}_{ST}\left(T_e - T_{Mn}\right), \tag{2.11}$$

where the vector $\vec{\Lambda}_{ST}$ is strongly related to the magnetic field $\vec{B}$ and vanishes in absence of external magnetic field. Together with equation 2.10 describes equation 2.11 the spin and energy transfer between electron and Mn-system. For phenomenological coefficients of these equations can be referred to [Kön00b]. From this relation follows that the system of electrons can be driven out of equilibrium by increasing the kinetic energy due to a heat impact (see figure 2.1) or by generating nonequilibrium polarization using e.g. optical orientation technique [Mei84]. The latter uses circular polarized light to generate spin oriented carriers.

Because including all possible energy transfer channels leads to a complicated system of equations [Kön00a], here only the effect of the nonequilibrium electron polarization on the energy transfer is regarded for simplicity. In this case, from the balance equation of the nonequilibrium electron polarization caused by the heat exchange between electron and Mn-ion system

$$\frac{d\langle\vec{s}_{NE}\rangle}{dt} = -\lambda_{JS}\langle\vec{s}_{NE}\rangle + \vec{\Lambda}_{ST}\left(T_e - T_{Mn}\right) - \frac{\langle\vec{s}_{NE}\rangle}{\tau_{spin}}. \tag{2.12}$$

follows for the stationary condition of the nonequilibrium electron polarization

$$\langle\vec{s}_{NE}\rangle = \frac{\vec{\Lambda}_{ST}\tau_{spin}\left(T_e - T_{Mn}\right)}{\left(\lambda_{JS}\tau_{spin} + 1\right)}. \tag{2.13}$$

This can be used to renormalize the transfer equation 2.10 by substituting $\langle\vec{s}_{NE}\rangle$:

$$C_{Mn}\left.\frac{\partial T_{Mn}}{\partial t}\right|_{ex} = \left[q + \frac{\mu_B g_{Mn}\lambda_{JS}\tau_{spin} n_e}{\lambda_{JS}\tau_{spin} + 1}\left(\vec{B}\cdot\vec{\Lambda}_{ST}\right)\right]\left(T_e - T_{Mn}\right) = \tilde{q}\left(T_e - T_{Mn}\right). \tag{2.14}$$

According to [Yak09] obtains

$$\vec{\Lambda}_{ST} = -\frac{\vec{B}q}{\mu_B g_{Mn} B^2 n_e} \tag{2.15}$$

and $\left(\vec{B}\vec{\Lambda}_{ST}\right) < 0$, so that the thermal conductivity of the border between electrons and magnetic ions is decreased due to the effect of the nonequilibrium electron polarization:

$$\tilde{q} = \left[1 - \frac{\lambda_{JS}\tau_{spin}}{\lambda_{JS}\tau_{spin}+1}\right] q. \tag{2.16}$$

This means that the energy transfer from electrons to Mn-spin system is suppressed. It can be easily seen from 2.16 that the decrease only occurs for slow relaxation of electron spins $\lambda_{JS}\tau_{spin} \gg 1$, where $\tilde{q} \approx \frac{q}{\lambda_{JS}\tau_{spin}} \ll q$. For fast electron spin relaxation the nonequilibrium electron polarization has practically no influence on the energy transfer.

2.1.3 Manganese spin temperature in stationary condition

Complete formulation of the energy exchange between the three energy reservoirs in DMS is given in [Kön00b, Kön00a] by the following system of equations:

$$\frac{dE_{Mn}}{dt} = -\frac{C_{Mn}}{\xi\tau_{Mn-e}}\left[\xi\left(\Delta\beta_{Mn}-\Delta\beta_e\right)+\Delta E_F\beta_L\right] - C_{Mn}\frac{\Delta\beta_{Mn}}{\tau_{Mn-L}} + G_{Mn} \tag{2.17}$$

$$\frac{dE_e}{dt} = -\frac{C_e}{\xi\tau_{e-Mn}}\left[\xi\left(\Delta\beta_{Mn}-\Delta\beta_e\right)+\Delta E_F\beta_L\right] - C_e\frac{\Delta\beta_e}{\tau_{e-L}} + G_e \tag{2.18}$$

$$\begin{aligned}\frac{d\Delta E_F}{dt} = &-\left(\frac{\partial E_{F,+\frac{1}{2}}}{\partial n_{e,+\frac{1}{2}}}+\frac{\partial E_{F,-\frac{1}{2}}}{\partial n_{e,-\frac{1}{2}}}\right)\\ &\times\left(\frac{n_{Mn}}{\tau_{Mn-e}}[\xi(\Delta\beta_{Mn}-\Delta\beta_e)+\Delta E_F\beta_L]+G_s\right)-\frac{\Delta E_F}{\tau_{nes}},\end{aligned} \tag{2.19}$$

with the characteristic times $\tau_{e-Mn} = \tau_{Mn-e}\frac{C_e}{C_{Mn}}$, τ_{Mn-L} and τ_{e-L} for equalizing the temperatures between the specific systems. The time τ_{nes} is the relaxation time for nonequilibrium carrier spin, which takes into account all nonmagnetic spin relaxation processes, like the Bir-Aronov-Pikus, the Elliott-Yafet, the D'yakonov-Perel and the hyperfine-interaction mechanism. These are described more detailed in section 2.2. In [Kön00b] τ_{nes} was evaluated: $\tau_{nes} = 10^{-10}$ s. By deduction of this model, energy exchange with external sources is only included by the flux parameters G_e, G_{Mn} and G_s for the respective systems. Possibilities for external influences were already given in figure 2.1. At the optical experiments performed in this thesis, G_e is changed by generation of hot photocarriers, and G_s by generation of spin-oriented carriers with circularly polarized light.

In the equations $\beta_i = (k_B T_i)^{-1}$ are the inverted temperatures of the respective systems, $\Delta\beta_{Mn} = \beta_{Mn} - \beta_L$ and $\Delta\beta_e = \beta_e - \beta_L$ correspond to the deviations of the inverted temperatures of the systems and $\xi = \mu_B g_{Mn} B$ is the energy difference between two levels of the Mn-ion with spin S_z and $(S_z - 1)$, i.e. the spin splitting of Mn-ions. The velocities for altering the Fermi-levels with changing electron density in the corresponding spin subband are denoted by $\frac{\partial E_{F,\pm\frac{1}{2}}}{\partial n_{e,\pm\frac{1}{2}}}$.

The concentration of Mn-ions is given by n_{Mn}, and of electrons with spins along and against field direction, respectively, by $n_{e,\pm 1/2}$.

If the amount of photocarriers is no longer negligible in comparison to the number of electrons in the electron gas, one additional equation has to be added, which is responsible for the variation of carrier density with increasing excitation density. For doped QWs, where the density of background carriers exceeds strongly the density of photocarriers, this is not actual.

In equilibrium conditions ($\beta_e = \beta_{Mn}$ and $\Delta E_F = 0$) the term $[\xi(\Delta\beta_{Mn} - \Delta\beta_e) + \Delta E_F \beta_L]$ is equal to zero. Deviations of this value from zero characterize the deviation of the system from the nonequilibrium state. If the Fermi-energy is equal for both spin directions, one gets

$$\frac{\tau_{SLR}}{\tau_{e-Mn}} (\beta_e - \beta_{Mn}) = \beta_{Mn} - \beta_L \tag{2.20}$$

for weak deviations from the thermal equilibrium ($T_e \approx T_{Mn} \approx T_L$). In case of $\tau_{SLR} \gg \tau_{e-Mn}$, the Mn-spin temperature equals the electron system temperature. The influence of the electron temperature on the temperature of the Mn-system vanishes for a completely polarized electron gas.

2.2 Mechanisms for spin relaxation

In semiconductors four nonmagnetic mechanisms for spin relaxation of conduction electrons are relevant: the D'yakonov-Perel, Elliott-Yafet, Bir-Aronov-Pikus and hyperfine-interaction mechanism. Magnetic scattering due to exchange interaction between the electrons and magnetic impurities is not considered here. Also processes concerning hole spins are not regarded. The spin relaxation rates for holes are usually several magnitudes higher than for electrons due to the much stronger spin-orbit interaction in the valence band compared with the conduction band.

Consecutively, the four mechanisms are only briefly described. More information about spin relaxation is included in [Fab99] or [Žut04]. For spin relaxation in $A^{II}_{1-x}\mathrm{Mn}_x B^{VI}$ QWs can be referred to [Cro97] and [Cam01] or more theoretically to [Pul03] and [Sha93]. In QWs the intersubband-relaxation [Döh04] can be important, too, which is based on spin-flip exchange scattering of electrons between different charge subbands.

Which of the described spin relaxation mechanism is dominant, depends on the properties of the particular material, like e.g. band gap, doping or amount of impurities. For small-band-gap semiconductors and such with large spin-orbit coupling, the Elliott-Yafet mechanism is dominant. Also hole spins relax due to the Elliott-Yafet mechanism. For middle-band-gap semiconductors and at high temperatures the D'yakonov-Perel mechanism is relevant. At low temperatures in heavily p-doped semiconductors dominates the Bir-Aronov-Pikus mechanism. The hyperfine-interaction is only relevant for bound electrons.

2.2.1 D'yakonov-Perel mechanism

The very efficient D'yakonov-Perel mechanism was firstly presented by D'yakonov and Perel in 1971 [D'y72]. It describes spin dephasing in systems lacking inversion symmetry, like II-VI semiconductors with zincblende or wurtzite structure, where the inversion symmetry is broken by the presence if two distinct atoms in the Bravais lattice. According to subsection 1.2.1 (especially equation 1.16) causes the lack of inversion symmetry the appearance of an effective magnetic field $\vec{\Omega}(\vec{k})$ due to spin-orbit coupling (equation 1.9). About this field precesses the electron spin with the Larmor frequency $\vec{\Omega}(\vec{k})$.

If the electron wave vector $\vec{k}$ is changed during a spin-conversing scattering process, also the effective magnetic field changes due to its dependency on the electron wave vector. Therefore, the electron spin precesses during several scattering events about an effective magnetic field, which changes in random directions and strengths, each time the electron scatters to a different momentum state (compare figure 2.3). This leads to spin relaxation of the electron spin.

The spin relaxation time in bulk zincblende semiconductors due to the D'yakonov-Perel mechanism amounts to [Pik84]:

$$\frac{1}{\tau_{s,ij}} \propto \tau_p \left[\left(\overline{\Omega^2} - \overline{\Omega_i^2} \right) \delta_{ij} - \overline{\Omega_i \Omega_j} \left(1 - \delta_{ij} \right) \right], \tag{2.21}$$

where the bar denotes averaging over directions of $\vec{k}$, and τ_p is the momentum relaxation time. Beside the BIA (Dresselhaus term), also the inversion asymmetry in low dimensional structures (Rashba-effect (SIA) equation 1.74) or at heterointerfaces [Hal03, Ole01] can contribute to the effective magnetic field. In two-dimensional structures the D'yakonov-Perel mechanism

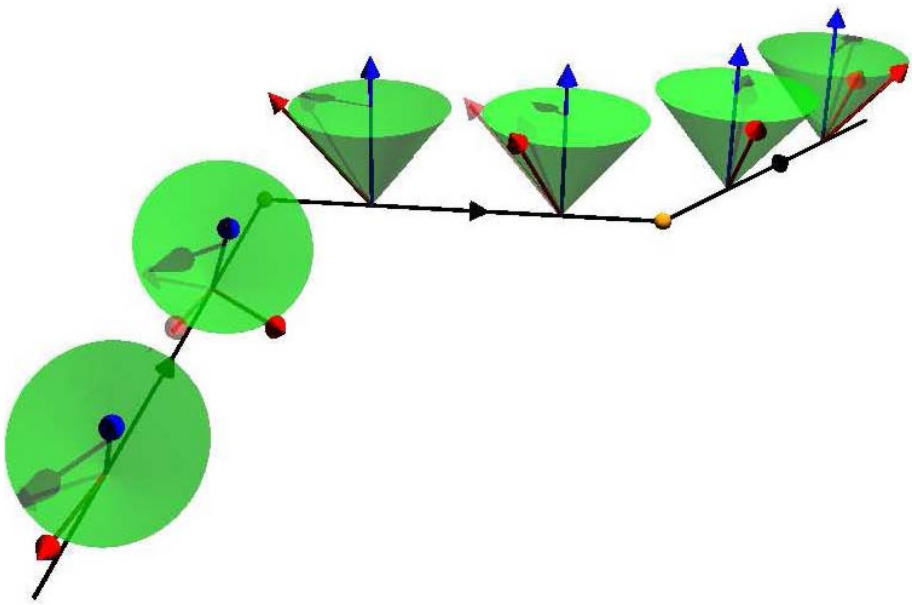

Figure 2.3 – Scheme of D'yakonov-Perel mechanism: The electron precesses around an effective magnetic field, which depends on the electron wave vector. [Rud05]

depends on the orientation of the QW. While the D'yakonov-Perel mechanism is absent for spins aligned along growth direction in (100) oriented QWs [Döh04, D'y86, Ohn99a], the spin relaxation time in (001) QWs is [Ter99]

$$\tau_{spin} = \frac{\hbar^4}{2\gamma^2 E_1^2 k_B T \tau_p (2m_{eff})^3}. \tag{2.22}$$

Thereby, E_1 is the energy of the first charge subband in the QW.

With increasing temperature rises the effectiveness of the D'yakonov-Perel mechanism, because the occupation of higher k-values is accompanied by a higher effective magnetic field [Rud05].

2.2.2 Elliott-Yafet mechanism

Contrary to the D'yakonov-Perel mechanism, the Elliott-Yafet mechanism exists also in systems with inversion symmetry. Basis of this mechanism is coupling of electronic states with opposite spin, which is a direct consequence of the spin-orbit interaction induced by the lattice ions [Ell54b]. Because of the admixture of the opposite spin states to the wavefunctions, those are not longer spin eigenstates. The amplitude of the admixture depends on the strength of the spin-orbit coupling. Thus, the Elliott-Yafet mechanism is especially important in semiconductors with small band gaps [Fab99]. Modification of the amplitudes of the spin-up $|\uparrow\rangle$ and spin-down $|\downarrow\rangle$ parts of the wave functions leads to relaxation of the electron spin [Yaf63]. The modification is caused by momentum scattering (such as by phonons or impurities), which is usually spin-conversing.

The dependence on the momentum relaxation time τ_p for the Elliott-Yafet mechanism is inverted compared with the D'yakonov-Perel mechanism. Intuitively explained, spin relaxation by the Elliott-Yafet mechanism takes place during scattering events and by the D'yakonov-Perel mechanism between scattering events [Rud05].

2.2.3 Bir-Aronov-Pikus mechanism

In p-doped semiconductors spin relaxation can also occur via hole scattering accompanied by spin exchange. This, Bir-Aronov-Pikus mechanism called, mechanism was proposed by Bir, Aronov and Pikus in 1975 [Bir75]. It is based upon electron-hole exchange interaction

$$\hat{H} = A\vec{S} \cdot \vec{J}\delta\left(\vec{r}\right), \tag{2.23}$$

where A is proportional to the exchange integral between conduction and valence states, $\vec{S}$ is the electron-spin operator, $\vec{J}$ the angular momentum operator and $\vec{r}$ the relative position of holes and electrons [Žut04]. Descriptive explained, the electron spin precesses about an effective

magnetic field generated by the hole spin [Fab99]. The fluctuation of this field leads to electron spin flipping. The probability of this spin-flip exchange scattering depends on the state of the holes (degenerate or nondegenerate, free or bound on acceptors) [Žut04].

As the electron-hole exchange interaction decreases with rising temperature, also the efficiency of the Bir-Aronov-Pikus mechanism is reduced. In p-doped materials lacking inversion symmetry, a coexistence of Elliott-Yafet, D'yakonov-Perel and Bir-Aronov-Pikus mechanism exists. Discrimination is given by their particular unique density and temperature dependencies [Žut04].

2.2.4 Hyperfine-interaction mechanism

Hyperfine-interaction mechanism occurs in heterostructures based on semiconductors with a nuclear magnetic moment. It is based upon coupling of the magnetic moments of nuclei and electrons. The spin dephasing takes place via temporal or spatial fluctuations of the magnetic field of the nuclei [Žut04].

The hyperfine-interaction mechanism dominates spin dephasing of localized or confined electron spins (bound on donors or confined in QWs or quantum dots (QD)) [D'y74], but is negligible for free electrons because of strong dynamical narrowing by the itinerant nature of electrons [Ove53][3].

The effective Hamiltonian for this interaction is the Fermi contact potential energy [Sli89]

$$\hat{H} = \frac{2}{3}\mu_B g \sum_j \hbar\gamma_j \vec{S} \cdot \vec{N}_j \delta\left(\vec{r} - \vec{R}_j\right), \tag{2.24}$$

with the gyromagnetic ratio γ_j and spin operators for electron $\vec{S}$ and nuclei $\vec{N}_j$. Thereby, the index j denotes the nucleus at position $\vec{R}_j$.

2.2.5 Spin relaxation in excitons

The heavy-hole exciton in zincblende semiconductors can have four different spin-states with the total spin $| \pm 1, \pm 2 >$. The occupation of the spin states is balanced by spin relaxation. Thereby, two possibilities for spin relaxation between the optically allowed $| \pm 1 >$ states exist. The indirect relaxation proceeds with an intermediate state in terms of a dark exciton. Electron and hole flip their spin independently by means of one of the spin relaxation mechanisms described previously in the current section 2.2. In contrast, direct relaxation enables spin relaxation in one step via electron-hole exchange interaction (equation 2.23). This process is

[3]This effect is called motional narrowing-effect. It is an inhibition of the change of the spin phase by random fluctuations [Sli89]. While the root-mean-square phase changes, the average spin phase remains constant.

dominated by the long-range part of the electron-hole exchange interaction [Pik71], which determines the splitting of excitons, which are linear polarized in the QW plane. Thereby, the elements of the second diagonal of the Hamiltonian for the long-range exchange interaction act descriptively like an effective magnetic field in the QW plane. This field depends on the exciton barycenter impulse, which changes due to scattering events. Analogue to the D'yakonov-Perel mechanism, this spin precession about a randomly fluctuating effective magnetic field leads to spin relaxation. More information about spin relaxation can be gathered from the comprehensive review by Maialle *et al.* [Mai93].

2.3 Spin lattice relaxation

As the SLR is based upon spin-phonon interaction, the SLR time τ_{SLR} depends on the probabilities of phonon induced transitions between the Zeeman sublevels. In DMS this interaction is based on modulation of the exchange field, being induced by lattice vibrations, which acts on the magnetic ions. This microscopic mechanism is explained more detailed later in section 5.1 of this thesis.

Three most important types of macroscopic processes of spin-phonon transitions can be classified, which govern the mechanism of interaction between magnetic ions and phonons: direct, Raman and Orbach transition [Gil75]. For the simple case of a two-level system with spin $S = 1/2$, they are shown in figure 2.4 and described consecutively.

The direct spin-phonon transition can happen among spontaneous or stimulated emission or absorption of resonant phonons with the energy quantum $\hbar\omega = \mu_B g B$. This energy is in the region of acoustic phonons, not exceeding 1 meV, for moderate magnetic fields. The direct transition is an one-phonon process. According to [Abr70], the SLR time for direct transitions is defined as

$$\frac{1}{\tau_{SLR}} = A \cdot B^{\gamma} \coth\left(\frac{\mu_B g B}{k_B T_L}\right), \tag{2.25}$$

with the system coefficient A and the parameter γ, which lies in the region 3 - 5, depending on the concrete microscopic mechanism of spin-phonon interaction (see [Abr70]).

Contrary to the direct transition, the Orbach-process is a two-phonon process [Orb61]: First the Mn-ion passes into a real upper excited state by absorption of one phonon with energy $\hbar\omega_1$. Then it relaxes by emission of a second phonon $\hbar\omega_2 = \Delta - \mu_B g B$ to a different Zeeman-level of the ground state. Therefore, the SLR time for Orbach-processes depends on Δ, the energy distance between ground and excited states

$$\frac{1}{\tau_{SLR}} \sim \left[\exp\left(\frac{\Delta}{k_B T_L}\right) - 1\right]^{-1}. \tag{2.26}$$

The Orbach-process was firstly experimentally recognized by Finn *et al.* [Fin61].

If there is no real excited state, also resonant scattering with a virtual interstate within the Raman-process can occur[4]. Because of this, a wide phonon spectrum can take part in the scattering. Raman-processes have a very strong temperature dependence of the SLR time

$$\frac{1}{\tau_{SLR}} \sim T_L^{\beta}, \tag{2.27}$$

where β is between 5 and 9, depending on the type of magnetic ion [Abr70]. In semimagnetic semiconductors no attention has to be paid to the Phonon-Raman-process. Reason for this is the inhomogeneous broadening of the states, so that the virtual interstates loose their coherence and the scattering occurs by means of the Orbach-process with a real interstate [Sca96a]. This has been proven experimentally by Scherbakov *et al.* by measurement of the temperature dependence, which is much less than $\beta = 5$ [Sch00a].

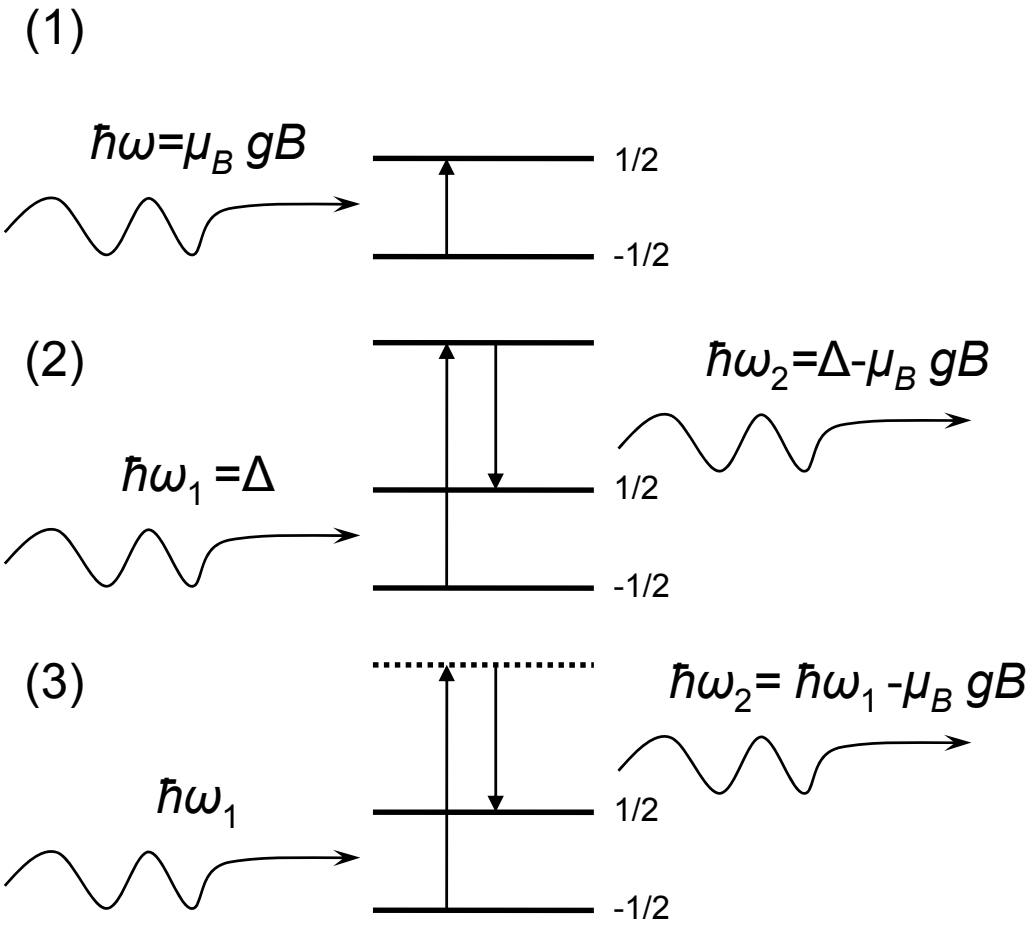

Figure 2.4 – Schematical picture of the three possible spin-phonon transition mechanisms with phonon absorption: (1) direct, (2) Orbach, (3) Raman. For transitions with phonon emission, the shown processes must be reversed. Solid lines correspond to real states and dotted lines to virtual ones. [Aki06a]

[4]This process is the equivalent of Raman scattering.

From equations 2.25 and 2.26 can be concluded that the direct spin-phonon transitions are predominant at liquid helium temperature, while Orbach-processes becomes actual at elevated temperatures [Gil75]. This is confirmed by experimental results at low temperatures [Aki06a].

While the fast exchange scattering of the carriers on the magnetic ions provides efficient energy transfer into the Mn-system, Mn cooling down to the bath temperature is slowed down by relatively long SLR times, characteristic for low Mn concentrations of few percents [Sca96a, Sch00a, Yak04]. In case of long SLR times, the temperature of the Mn-system can be considerably higher than the lattice temperature. This situation is called overheating of the Mn-system.

Furthermore, it has been shown that the SLR rate decreases weakly in magnetic fields B below 12 T [Bin91, Far96, Sca88, Sch00a], but increases rapidly $\left({\tau_{SLR}}^{-1} \propto B^5\right)$ for $B > 17$ T [Str92]. Several peculiarities in the dependence of the SLR rate on the magnetic field were observed. These could be very recently related to crossing of the states of pair and triple clusters of nearest-neighboring and next-neighboring Mn-ions [Deb08]. The important role of clusters in the SLR process will be addressed again later in this thesis.

In DMS heterostructures the SLR rate can be accelerated by realization of the concept of heteromagnetic nanostructures with varying Mn concentrations across the sample [Sch05]. Other concepts to modify the SLR rate will be presented later in this thesis.

2.4 Spin diffusion

Especially in semiconductor nanostructures, the time for SLR is strongly modified by spin diffusion. Microscopically, spin diffusion is based on magneto-dipole spin-spin interaction between magnetic ions [Abr70]. Thereby, the spin jumps from one Mn-ion to another, i.e. diffuses spatially. The time for spin-spin interaction τ_{ss} equals, therefore, the time for a spin-flip transition between two Mn-ions [Aki06a]. Dependence of τ_{ss} on the Mn content is given in figure 2.5. For the spatial escape of spin from a nanostructure element with the size d the diffusion time τ_D can be estimated [Aki06a, Sch04]:

$$\tau_D \sim \frac{d^2}{K_{diff}} = \frac{3d^2\tau_{ss}}{l^2}, \tag{2.28}$$

with the diffusion coefficient $K_{diff} = \frac{l^2}{3\tau_{ss}}$ and the mean distance between neighboring Mn-ions $l = r_0 x^{-1/3}$. For typical nanostructures with 1 nm $\leq d \leq$ 1 nm and values of Mn content x and τ_{ss} according to figure 2.5, one gets diffusion times in $Cd_{1-x}Mn_xTe$[5], which are in the same order of magnitude or even smaller than τ_{SLR}. Scherbakov *et al.* describes experiments in heterostructures and magnetic QDs[6], respectively, where the influence of spin diffusion on the

[5] In $Cd_{1-x}Mn_xTe$ is $r_0 = 0.46$ nm.

[6] The QDs were grown on thin magnetic wetting layers.

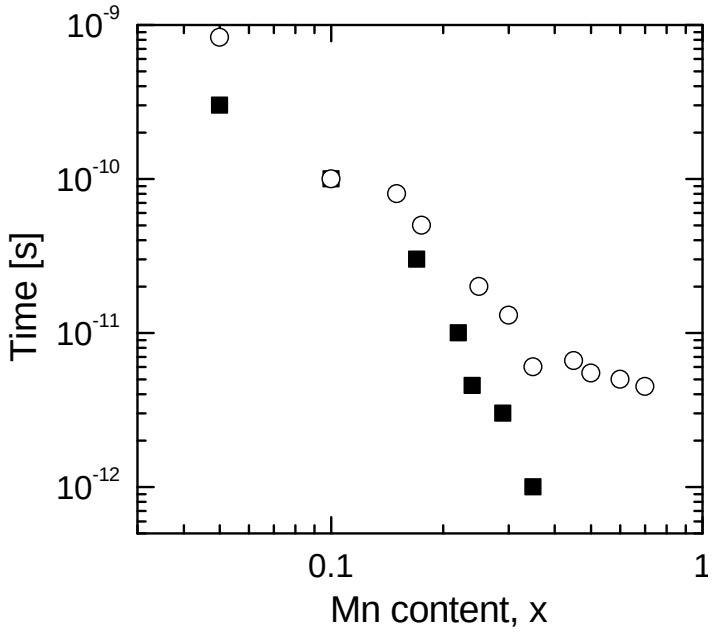

Figure 2.5 – Times for spin-spin interaction in $Cd_{1-x}Mn_xTe$ depending on Mn content at $T_L = 6\,K$. Open cycles correspond to electron spin resonance (ESR) measurements [Say85] and filled squares to electron paramagnetic resonance (EPR) measurements [Kre85a].

SLR was well observed [Sch04, Sch05]. It will be tried to extend these results for heteromagnetic nanostructures to digitally alloyed structures in the framework of this thesis. Hence, on heteromagnetic structures will be dwelled consecutively.

Initial point for the introduction of the concept of heteromagnetic semiconductor structures is the following fact: An increase of the Mn content above $x \sim 0.01$ in the active layer of a spintronic structure results in carrier scattering and nonradiative recombination channels, because of alloy fluctuations and associated defects. Thus, the optical and transport properties are strongly compromised.

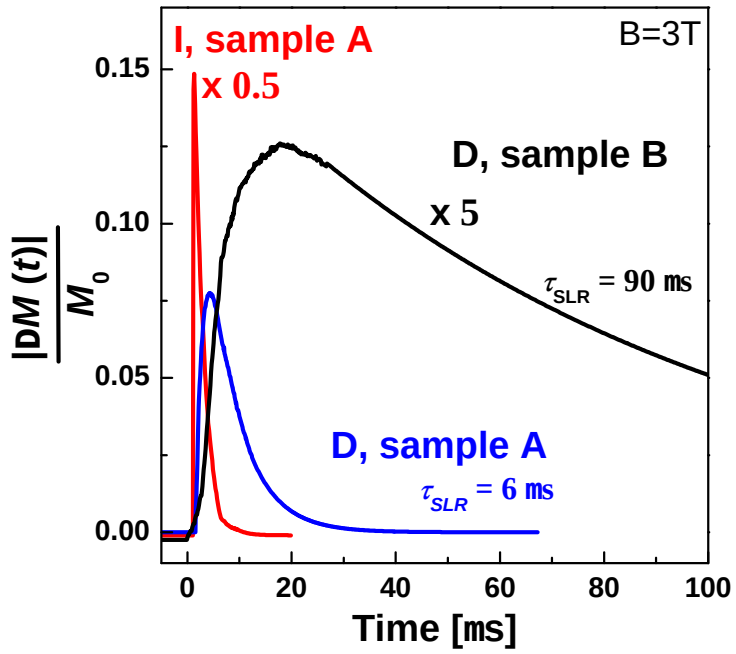

Figure 2.6 – Time evolution of the relative changes in magnetization, $\frac{\Delta M(t)}{M_0}$, measured by monitoring the direct (D) and indirect (I) luminescence of a $Zn_{1-x}Mn_xSe/Be_{1-y}Mn_yTe$ type-II heterostructure (A) and a $Zn_{1-x}Mn_xSe/BeTe$ structure (B) according to [Sch05]. The equilibrium magnetization M_0 was measured at $B = 3\,T$ and $T = 1.6\,K$. For better comparison the results for sample B were multiplied by factor 5 and the results for indirect luminescence by factor 0.5.

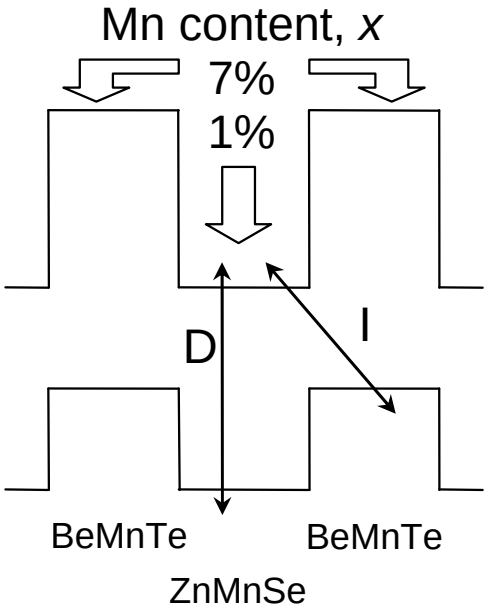

Figure 2.7 – Band scheme of a heteromagnetic nanostructure $Zn_{0.99}Mn_{0.01}Se/Be_{0.93}Mn_{0.07}Te$ with type-II band alignment according to [Sch05].

Heteromagnetic semiconductors have an active layer with a specific required Mn content in contact with another layer ("spin dump"), where the Mn content is high. From measurements on $Zn_{1-x}Mn_xSe/Be_{1-y}Mn_yTe$ heterostructure with a type-II band alignment is known that the additional layer reduces significantly the SLR time by more than one order of magnitude, but does not influence the carrier properties in the active layer [Sch05]. Comparative studies were performed with a $Zn_{1-x}Mn_xSe/BeTe$ structure (see figure 2.6). Advantage of the type-II structure is that two optical transitions can be observed, belonging to spatially direct (D) and indirect (I), respectively, optical transitions, so that the magnetization dynamics in each layer can be monitored separately (see figure 2.7) [Yak01, Yak02]. This concept can be considered as the magnetic counterpart of modulation-doped heterostructures, where the dopant layer is separated from the active layer with free carriers [Sch05]. In modulation-doped heterostructures the carrier density shall be increased to gain better transport properties. Also in this case, doping of the active layer would lead to higher carrier scattering.

Basis of the observed effect is diffusion of Mn-spins between magnetic layers with different Mn content. As will be shown detailed in section 5.1, increasing Mn concentration significantly accelerates the SLR. Over small distances not exceeding 10 nm, spin diffusion can occur much faster than SLR in those layers with low Mn content [Sch04]. Thus, the spin will diffuse from the layers with low x to layers with high x, where it can relax with considerably shorter SLR times. This diffusion process is shown schematically in figure 2.8 for absorption and emission of phonons, i.e. heating and cooling of the Mn-spin system. In homogeneous structures and structures with only one magnetic layer, spin-phonon transitions occur in the magnetic layer (case (a) in figure 2.8). If a spin dump layer with higher Mn content is added in a heteromagnetic structure, the spin-phonon transitions will occur in this layer, because of the higher transition probability. Afterwards diffuses the spin in the active layer, as indicated by hashed arrows in

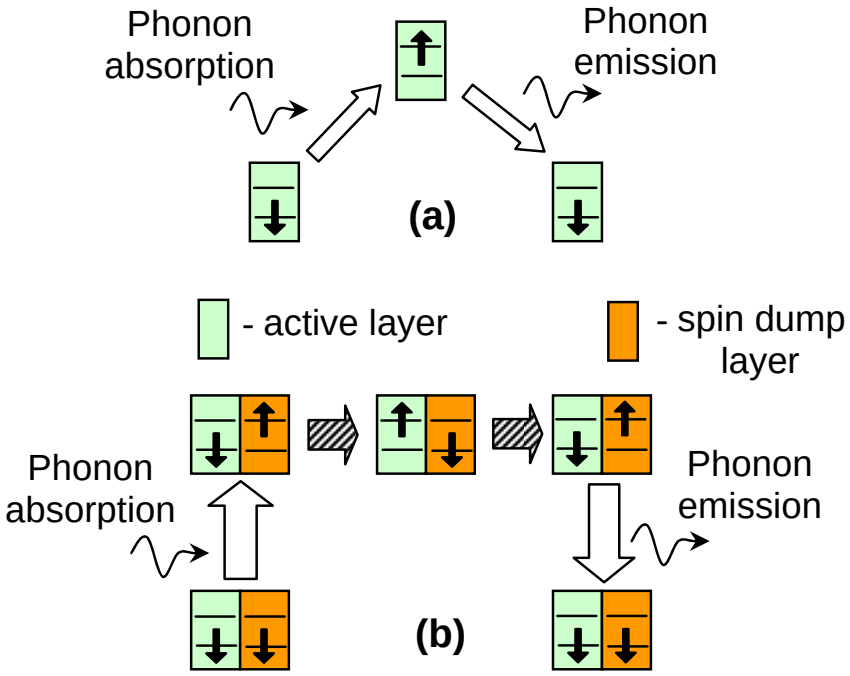

Figure 2.8 – Schematical diagram demonstrating phonon absorption and emission processes in (a) homogeneous magnetic structure and (b) heteromagnetic nanostructure. Diffusion of spin between spin dump and active layer is indicated by hatched arrows. Spin-phonon transitions are denoted by big white arrows. The figure is taken from [Sch05].

figure 2.8(b). Hence, presence of a layer with high x accelerates the overall relaxation of spin polarization.

Chapter 3

Experimental technique

Contents

Generally, experiments detecting spin dephasing and spin relaxation can be divided into those, measuring spectral characteristics of magnetization depolarization, and those measuring time or space correlations of magnetization [Žut04]. Examples for the first group are conduction-electron spin resonance (CESR) [Feh55] and optical spin orientation [Mei84] in combination with the Hanle effect [Bre33, Han24]. By time-resolved photoluminescence (PL), a technique belonging to the second group is used in this thesis. Other examples for experiments in time or space domain are the Johnson-Silsbee spin injection [Joh85] and time-resolved Faraday and Kerr rotation.

The time-resolved PL technique is based on investigation of the evolution of the exciton recombination light, while the coupled systems in DMS relax, after they had been driven out of equilibrium by an external impact. Thereby, the sensitivity of the giant Zeeman-splitting on the spin temperature of Mn-ions T_{Mn} is exploited. The Mn-spin temperature in equilibrium is equal to the lattice temperature $T_{Mn} = T_L$, but may exceed it significantly under external perturbations. Optical detection of the Mn-spin temperature is described in the first section 3.1 of this chapter. The enhancement to time-resolved investigation of the Mn-spin temperature is given in section 3.3. It should be mentioned that time-resolved PL allows not only detection

of spin relaxation, but also study of the different spin and energy transfer channels between the coupled system in DMS.

The various methods for injecting energy into the systems of DMS, which were shown by dotted arrows in figure 2.1, are briefly described in the second section of this chapter (3.2). Especially generation of photocarriers by laser light was used for the investigations in this thesis. Finally, in the last section of this chapter, the experimental setup, which fulfills the requirements of the time-resolved PL technique, is presented.

3.1 Optical detection of Mn spin temperature

To access the dynamical response of the magnetization on external impacts, the internal Mn-spin thermometer is exploited, which is provided by the high sensitivity of the giant Zeeman-splitting of excitons (band states) to the polarization of the magnetic ions. The reason for the strong relationship between giant Zeeman-splitting and magnetization in terms of the average spin of the Mn-ions was already stressed in section 1.3.4.4. According to equations 1.85 and 1.86 the giant Zeeman-splitting, arising from the sp-d-exchange interaction, is in QWs:

$$\Delta E_{giantZeeman} = (\delta_e \alpha - \delta_{hh} \beta)\, x N_0 \langle S_z \rangle , \tag{3.1}$$

with the known parameters for the exchange constants $N_0\alpha$ and $N_0\beta$, the Mn mole fraction x, and the mean thermal value of the Mn-spin z-component $\langle S_z \rangle$ (along the magnetic field $B = B_z$), according to equation 1.54 with the total spin $S = 5/2$ for the Mn^{2+}-ions. For the studied structures the parameters δ_e and δ_{hh} for the wave function leakage into the nonmagnetic barriers are very close to unity, as the carrier wave functions are well localized in the DMS QWs. Together with equation 1.54 can be clearly seen from 3.1 that the splitting is proportional to magnetization, which in turn is a function of external magnetic field and temperature:

$$\Delta E_{giantZeeman}(B, T_{Mn}) = \frac{\alpha - \beta}{\mu_B g_{Mn}} M(B, T_{Mn}) , \tag{3.2}$$

$$M(B, T_{Mn}) = \mu_B g_{Mn} x N_0 S_{eff}(x) \mathcal{B}_{5/2}\left(\frac{5 g_{Mn} \mu_B B}{2 k_B (T_{Mn} + T_0(x))} \right) . \tag{3.3}$$

The splitting $\Delta E_{giantZeeman}$ decreases rapidly with increasing Mn temperature. Physical reason for this is the thermal occupation of higher Zeeman sublevels of Mn-ions, so that the orientation of the Mn-spins decreases in external field.

The giant Zeeman-splitting can be measured by optical spectroscopy. Possible optical transitions in the vicinity of the band gap are given in figure 1.15. In this thesis the heavy-hole transitions with circular polarization (a,d in figure 1.15) are exploited. To observe the giant Zeeman-splitting, a finite equilibrium magnetization has to be induced by application of an external

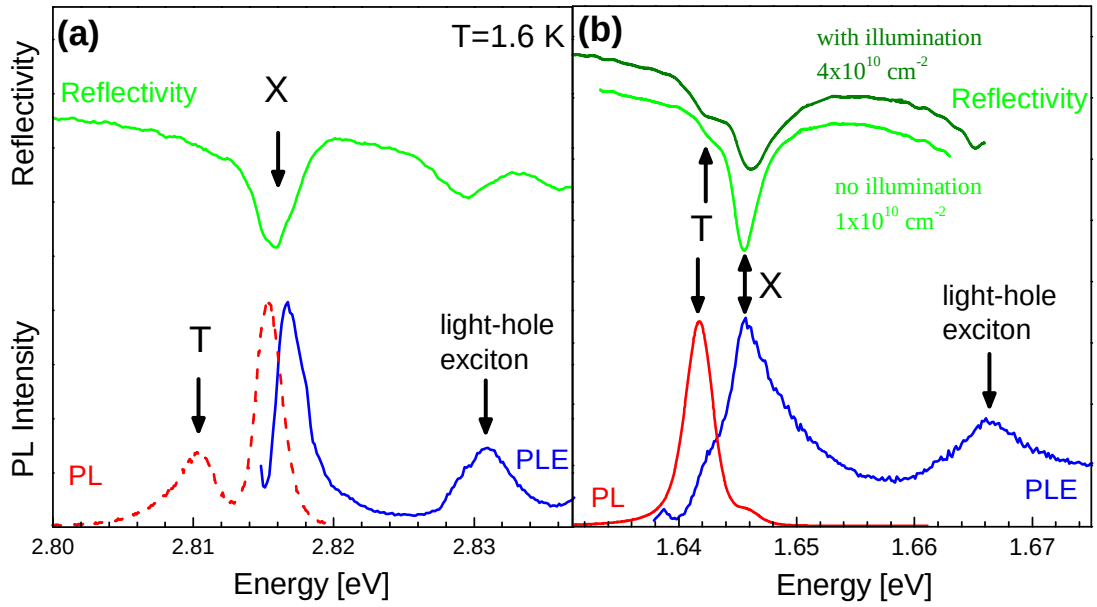

Figure 3.1 – PL, PLE and reflectivity spectra of (a) a 100 Å $Zn_{0.988}Mn_{0.012}Se/Zn_{0.94}Be_{0.06}Se$ QW and (b) a 80 Å $Cd_{0.99}Mn_{0.01}Te/Cd_{0.76}Mg_{0.24}Te$ QW in absence of magnetic field. Trion (T), light-hole (X,1s-lh) and heavy-hole (X,1s-hh) exciton can be distinguished.

magnetic field. The splitting is displayed as red shift of the exciton PL line ($\Delta E_{giantZeeman}$). The spectral position of the excitonic emission line measured in external magnetic fields can be traced by different optical techniques: PL, photoluminescence excitation (PLE) spectroscopy and reflection, as shown in figure 3.1.

In PL spectroscopy, which is used in this thesis, laser radiation transfers photon energy $\hbar\omega > E_g$ into the electronic system of DMS. Thereby, electrons are lifted from the valence band to higher free states in the conduction band and electron-hole-pairs are generated. These pairs relax via emission of acoustical and optical phonons to the band edge on a timescale of few picoseconds. During this relaxation excitons can form, which pass into their ground state. The free electron-hole-pairs localize on defects (bound excitons, predominant in binary semiconductors), on alloy fluctuations (predominant in ternary semiconductors) or potential fluctuations (localized excitons, predominant in QWs). Furthermore, formation of magnetic polarons may occur. Some of the electron-hole-pairs recombine radiative. This luminescence is characteristic for the type of localization as well as for the investigated structure. While PL spectroscopy allows only examination of bound and localized excitons, PLE allows examination of free exciton states.

To prevent thermal ionization of the excitons and broadening of the PL lines due to phonons, PL measurements should be performed at liquid helium temperature.

Typical DMS spectrum measured with PL spectroscopy consists of two lines. While the high energy line corresponds to recombination of heavy-hole exciton, the low energy line belongs to the trion. The trion line is shifted with respect to the exciton line by the additional binding energy of the second electron.

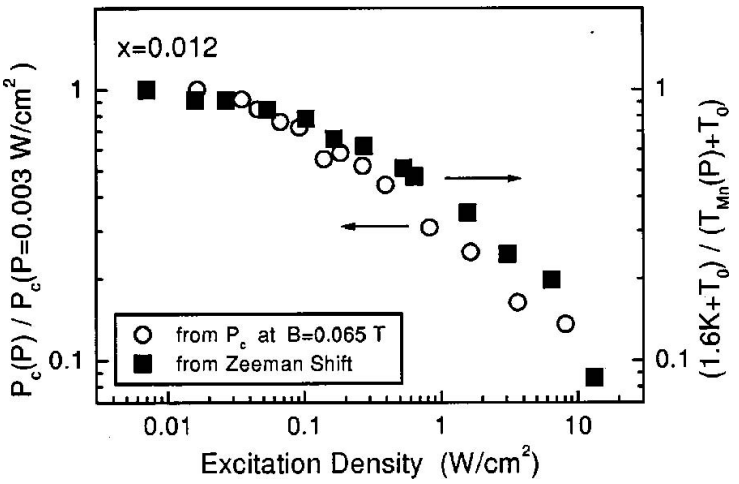

Figure 3.2 – Comparison of circular polarization degree P_C (circles) and giant Zeeman shift of excitonic PL line (squares): The results of both parameters fit exactly each other for all measured photoexcitation densities. Normalization of the parameters to their values at the lowest excitation density was performed. [Kel01]

The relative changes of the giant Zeeman-splitting can be conveniently detected via giant Faraday rotation and Kerr rotation effects and via circular polarization degree of PL [Yak09]. In general, only the lowest energy branch of the giant Zeeman-splitting (see figure 1.15) can be observed in PL spectroscopy at low temperatures. In this case the thermal energy (< 1 meV at $T < 2$ K) is considerably smaller than the giant Zeeman-splitting, so that only the lower branches are filled. As one electron remains in the conduction band after trion recombination, the energy shift in magnetic field is similar for trion and exciton. For magnetic fields $B > 1$ T exceeds the giant Zeeman-splitting of electronic states the trion binding energy of about 5 meV and the exciton gets the lowest state. The measurements in this thesis were usually performed at low excitation densities at $B = 3$ T, so that the trion line was suppressed or rather weak.

To obtain information about the temperature of the Mn-spin system, two characteristics of the magneto-optical spectra can be used, which are related to the giant Zeeman-splitting. Both are effect of the conduction and valence band states. The first characteristic is the energy shift of the exciton emission line due to the increase of the Mn-spin temperature by photoexcitation. This effect can be clearly seen in figure 3.3 for a ZnSe-based QW. Even rather low excitation density of 13 $\mathrm{W/cm^2}$ leads to a drastic increase of T_{Mn} to 23 K. The fits to calculate the Mn temperature in figure 3.3 were achieved independently of the magnetic field. Contrary, the presence of a two-dimensional electron gas in doped QWs leads to an additional variation of the Mn-spin system temperature with the magnetic field [Kön00a]. It is convenient to use the giant Zeeman shift in relatively strong magnetic fields (exceeding 0.5 – 1 T), where its variation can be clearly detected. For measurements in weak magnetic fields (below 0.5 T) the other characteristic, the circular polarization degree of emission, shall be analyzed. It has been shown by Keller *et al.* [Kel01] that both characteristics provide the same information about the temperature of the Mn-system (see figure 3.2).

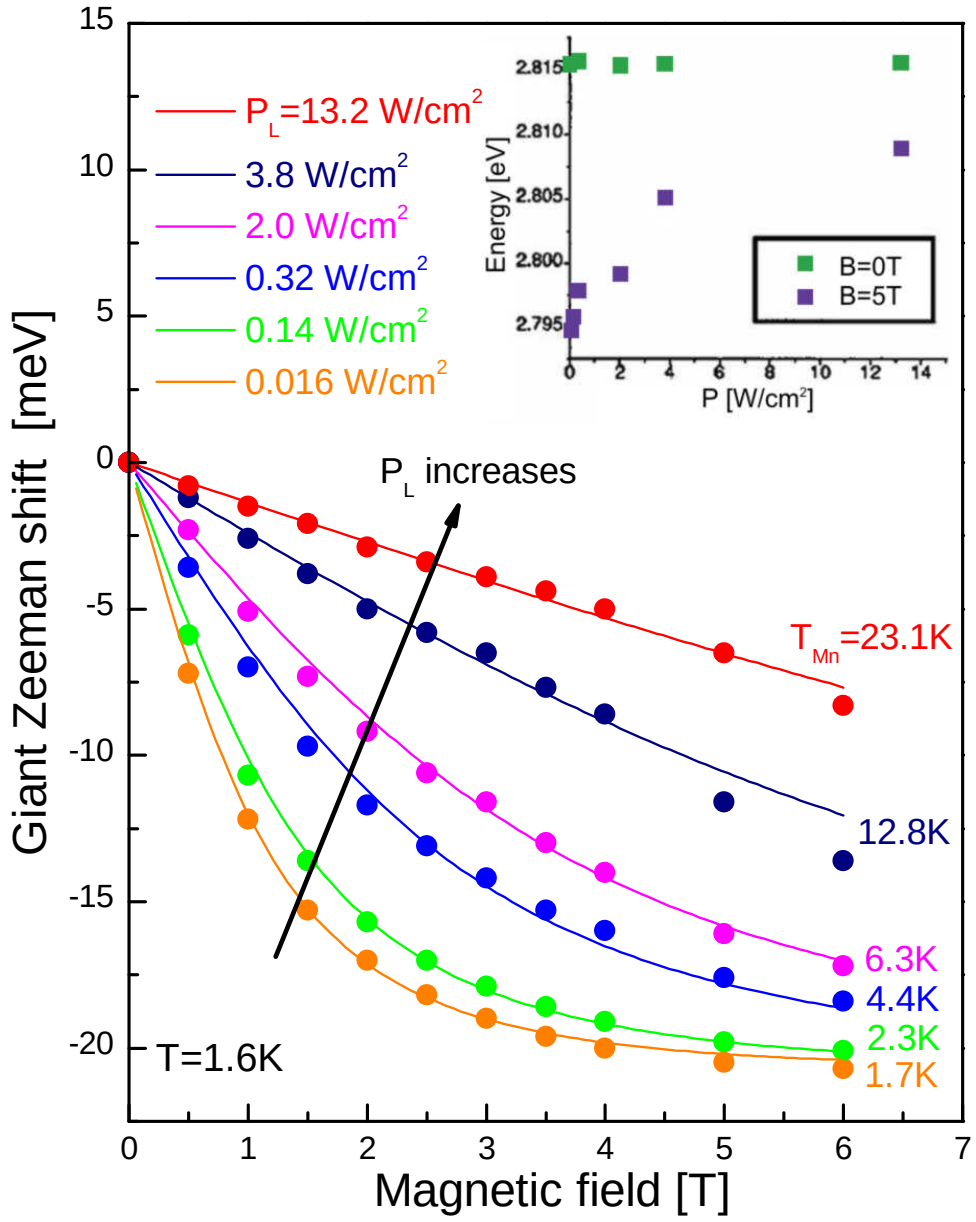

Figure 3.3 – Giant Zeeman shift of excitons for different excitation densities evaluated from PL spectra for a $Zn_{0.988}Mn_{0.012}Se/Zn_{0.94}Be_{0.06}Se$ QW. The lines represent Brillouin fits to calculate the Mn-spin temperature T_{Mn}, which is given in the figure for each excitation density P_L. In the inset is shown that the exciton energy is independent from the excitation density in absence of external magnetic field. [Kel01]

In cases when the giant Zeeman-splitting value $\Delta E_{giantZeeman}$ is measured from the energy shift of exciton transitions in reflectivity, absorption or PLE spectra, the equations 3.1 and 1.54 allow direct access to T_{Mn} value. However, if it is measured from the shift of PL line, a possible contribution of magnetic polaron formation should be taken into account [Mac94, Yak96]. For that, the magnetic field B in equation 1.54 can be substituted by sum of an external magnetic field and exchange field in the magnetic polaron. For the samples reported in this thesis ($x < 0.1$), the magnetic polaron contribution to the giant Zeeman shift of PL line is very small and can be neglected [Yak96, Yak97].

3.2 Heating of the Mn spin system

According to figure 2.1, several methods exists to heat the Mn-system with respect to the bath lattice temperature:

- electric current
- laser light
- phonon pulse
- direct heating of the lattice (the phonon modes are exploited, which are present in the lattice at elevated T_L)
- microwave (MW) or far-infrared (FIR) radiation resonant with the splitting of spin sublevels, $\hbar\omega_{mw,fir} = \mu_B g_{Mn} B$.

Depending on the particular experimental conditions, the methods inject spin and energy in the different systems of DMS. The first three methods heat the Mn-spin system indirectly. They are consecutively described in few words. The direct methods were not exploited for the investigations in this thesis. Examples on investigations of DMS with these heating techniques are given for direct lattice heating e.g. in [Far96, Str92], for MW radiation e.g. in [Hu98, Iva07, Iva08, Kom77, Mal83, Mal85, Sad03, Gis93] and for FIR radiation e.g. in [Ger08, Str90, Str92], respectively. Both use ESR of free carriers and Mn^{2+}-ions.

3.2.1 Heating by laser light

Laser light that is absorbed in a DMS structure generates photocarriers (electrons and holes) with excess kinetic energy. This energy can be transferred to the Mn-spin system, causing an increase of the Mn-spin temperature via two channels shown schematically in figure 3.4. The first channel is a direct one. It is provided by fast spin-flip exchange scattering of free carriers on localized spins of Mn-ions. The efficiency of this channel is characterized by very short transfer times τ_{c-Mn}, faster than 10 ps [Die95]. The exchange scattering provides simultaneous energy and spin transfer and, therefore, is sensitive to the carrier spin polarization [Kön00b, Rya82]. Also excitation of the internal Mn^{2+}-ion transition $^6A_1 \rightarrow {}^4T_1$ by energy transfer from excitonic states may contribute to this direct way [Fal03, Lei97, Som93].

The second channel is indirect and mediated by phonons. On the first stage, free carriers with excess kinetic energy generate nonequilibrium phonons during carrier energy relaxation, and on the second stage these phonons heat the Mn-spin system. Carriers are efficiently coupled with the lattice. Typical times for electron energy relaxation by means of acoustical phonons $\tau_{e-phonon}$ is about 100 ps [Sha74]. Therefore, the indirect mechanism is controlled by SLR of Mn-ions, which couples phonons with the Mn-spin system.

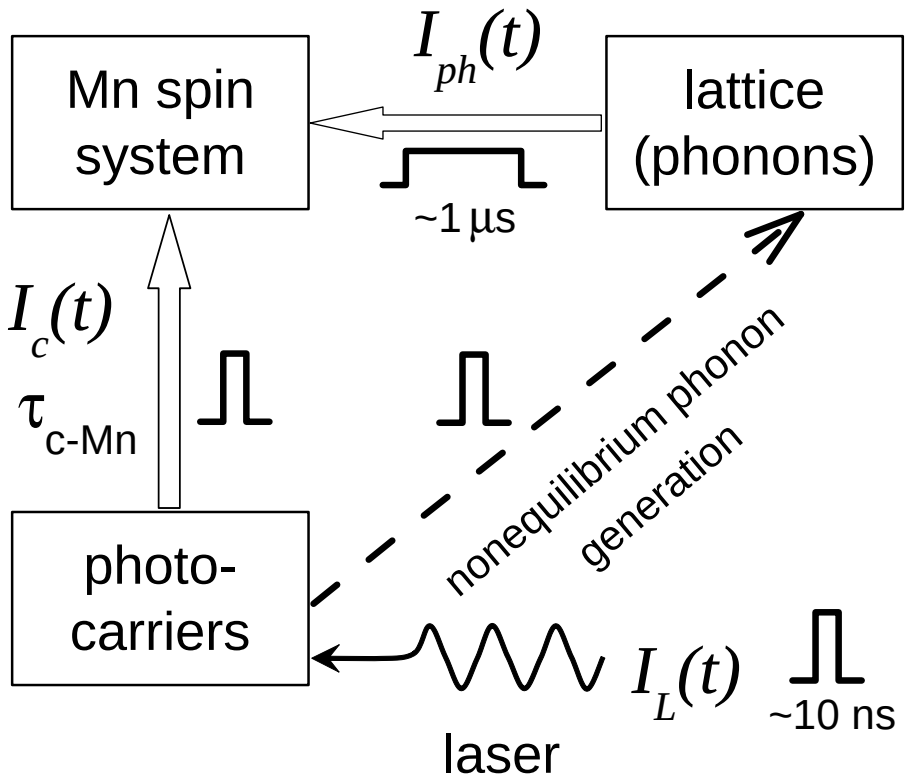

Figure 3.4 – Interacting systems of undoped DMS under heating by laser light $I_L(t)$ with duration of 10 ns. The dashed-line arrow corresponds to phonon generation due to energy relaxation of carriers. Laser light heats the Mn system by carrier $I_c(t)$ and phonon $I_{ph}(t)$ impacts.

Summing up, laser pulses have a two-fold dynamic impact in heating the Mn-system. These two impacts differ in temporal duration, time profile and heating efficiency. While the carrier impact is limited by the laser pulse duration, the phonon impact is given by the typical lifetimes of nonequilibrium phonons of about 1 µs.

The efficiency of heating involving carriers depends strongly on the Mn concentration. From figure 3.5 can be deduced that the heating becomes considerably less efficient for higher Mn concentrations. That this suppression is related to the dependence of the SLR time on the Mn content, will be shown later in this thesis.

The relative contributions of direct and indirect transfers are still under debate [Aki06b, Far96, Hun05a, Kel01, Kne06a, Kön00b, Kou03, Kul96, Sca96a, Tya97, Tya99, Yak04, Yak05]. On one hand it has been shown that the direct transfer is dominant in (Zn,Mn)Se QWs [Kel01, Yak04], in n-type doped (Cd,Mn)Te QWs [Kön00b], and in undoped (Cd,Mn)Te QWs under high excitation density [Kul96, Tya97]. On the other hand, the indirect transfer has been suggested as the leading mechanism in bulk (Cd,Mn)Te [Far96], in (Cd,Mn)Te QWs [Kou03], and in (Cd,Mn)Se QDs [Hun05a, Hun05b]. It is clear now that the relative contribution can be related to the DMS material, to the heterostructure design and to the excitation conditions, i.e., power and duration of laser pulses. However, a comprehensive picture of the energy transfer accounting for all these factors is far from being developed and additional experimental data is

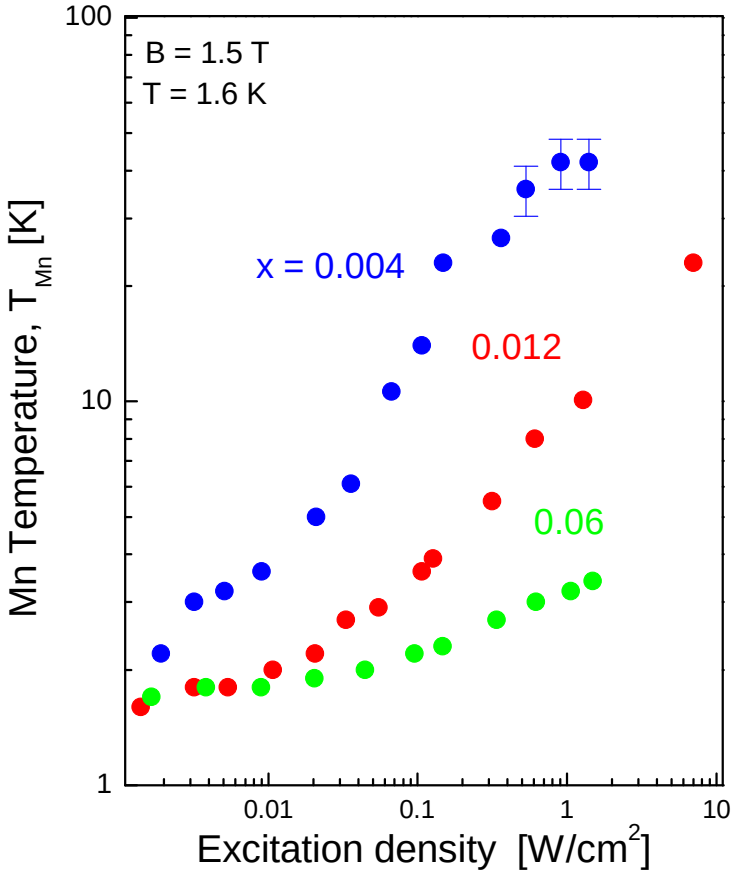

Figure 3.5 – Mn spin temperature dependency on excitation density for different Mn concentrations x. The measurements were performed on $Zn_{1-x}Mn_xSe$/ $Zn_{1-y}Be_ySe$ structures at a magnetic field of $B = 1.5$ T and a bath temperature of $T = 1.6$ K. Above-barrier photoexcitation at $\hbar\omega = 3.4$ eV was used. [Kel01]

required here. An experimental difficulty in collecting established data is caused by the problem of separating contributions from direct and indirect transfer when the laser pulse duration exceeds phonon lifetimes of about 1 µs.

3.2.2 Heating by electric current

Heating by electric current is similar to heating by laser light. Also by this method carriers pass their excess kinetic energy into the Mn-spin system, resulting in increase of T_{Mn}. Contrary to the laser light method, the carriers are not generated, but existing free carriers are accelerated by the applied electric field. Therefore, electric current heating is only reasonable in doped DMS. The efficiency of this technique is demonstrated e.g. in [Kön00a].

Mn heating by electric current is stronger for trions than for excitons. This can be explained by the spatially inhomogeneous density of diluted 2DEGs with a Fermi-energy comparable with localizing potential of the well width fluctuations. The trions are formed in sites containing 2DEG, where the Mn heating should be stronger. The excitons are photogenerated in sites free of background electrons, where weaker heating effect is expected. In the later case, the heating can be provided by energy diffusion inside the Mn-spin system from hot to cold regions [Yak09].

3.2.3 Heating by phonons

By the heat pulse technique, nonequilibrium phonons were generated directly in the lattice. Thereby, the phonons can be injected either by laser radiation or by means of a phonon generator. A phonon generator is a thin metal film evaporated on the sample. This film can be excited either by electrical current or by laser pulses [Aki97, Aki06a, Sch99]. The phonons propagate through the substrate[1] and reach the DMS QW layer. Here nonequilibrium phonons with energy $\hbar\omega = \mu_B g_{Mn} B$ may induce resonant spin-phonon transitions, as the Zeeman sublevels are separated by $\mu_B g_{Mn} B$ in an external magnetic field B [Sch99]. Hence, the population of the upper Zeeman sublevels increases, i.e. the Mn-spin system is heated.

For direct phonon generation by laser light, the lower energy gap of the GaAs buffer layer, compared with the energy gaps of the DMS materials, is exploited. This is shown schematically for a (Zn,Mn)Se/(Zn,Be)Se QW in figure 3.6. Laser light, which is only absorbed in the GaAs buffer layer, generates a phonon flux, which heats the Mn-spin system.

Scherbakov *et al.* have already used combination of phonon impact and laser impact for heating the Mn-system to investigate SLR in (Cd,Mn)Te/(Cd,Mg)Te QWs [Sch00a]. This method is modified in this thesis by the use of laser pulses as sources of the phonon impact, instead of the phonon generator. A comprehensive overview on phonon heating in DMS is given in [Aki06a].

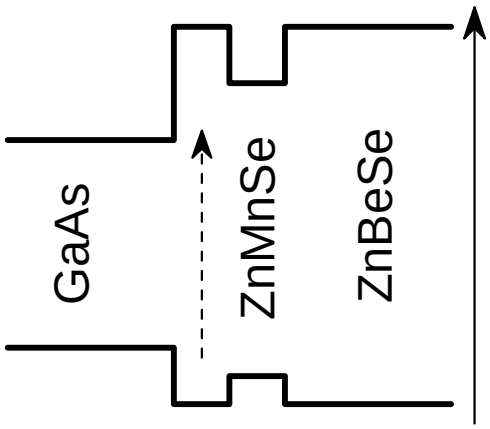

Figure 3.6 – Energy scheme for photoexcitation with different photons. Photons with energies exceeding the energy gap in (Zn,Mn)Se and (Zn,Be)Se (straight trough line) can generate carriers in those. This situation corresponds to heating by laser light described in 3.2.1. Photons with energies below the energy gaps in (Zn,Mn)Se and (Zn,Be)Se, but exceeding the energy gap in the GaAs buffer, (dashed line) are absorbed in the buffer layer. In this case only indirect heating of the Mn-system by phonons takes place.

3.3 Time-resolved measurements

Direct measurements of the temporal evolution of the magnetization by means of a time-domain magnetic spectrometer based on a pick-up electromagnetic coil were already performed [Str90, Str92]. However, this technique is not suited for measurements on thin magnetic layers and

[1] Low-energy phonons with $\hbar\omega < 1$ meV can travel ballistically distances of few mm. High-energy phonons $\hbar\omega >> 1$ meV travel diffusive, as they are strongly scattered by impurities and isotopes [Bro85, Eis86, Ram92].

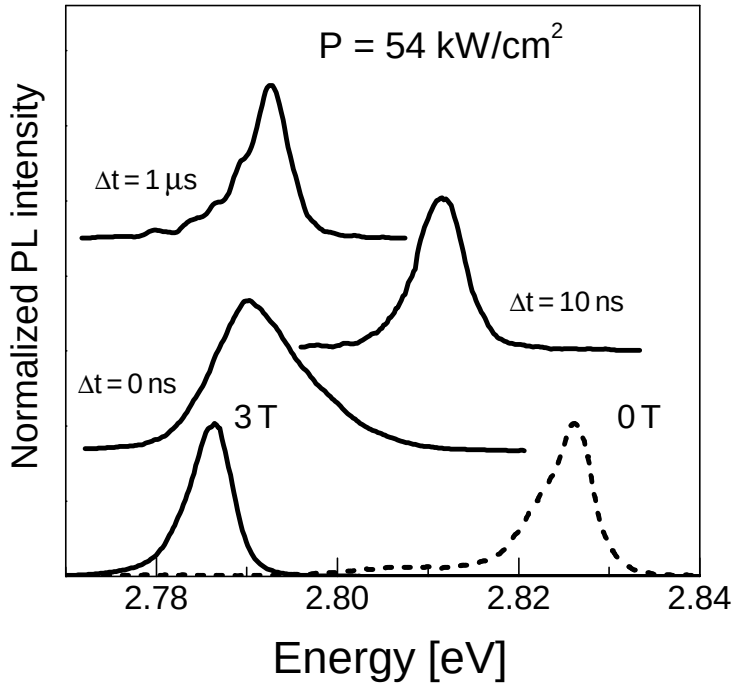

Figure 3.7 – PL spectra of a $Zn_{0.89}Mn_{0.11}Se/Zn_{0.89}Be_{0.11}Se$ QW. The two bottom spectra are taken under very low cw-laser excitation, the others are recorded at different time delays Δt with respect to the laser pulse maximum: $\Delta t \approx 0$ ns (corresponds to the pulse maximum), 10 ns (just after the pulse), and 1 µs later. The excitation density amounts to $P \approx 54\,\mathrm{kW/cm^2}$, the magnetic field to $B = 3$ T (solid lines) and $B = 0$ T (dashed line), respectively, and the bath temperature to $T = 1.6$ K.

nanostructures, because the net changes of magnetization in the whole sample are too small for the sensitivity of the technique.

More advanced is the optical detection technique presented here. The magnetization dynamics of the Mn-spin system is analyzed from the temporal evolution of the giant Zeeman shift, induced by an external heat impact, provided by laser pulses. The Mn-spin system is driven out of equilibrium with the lattice temperature during the laser pulses and is cooled down between the pulses back to lattice temperature. Due to the heating of the Mn-spin system, the upper Zeeman sublevels become occupied and the magnetization decreases. Thus, the corresponding changes in the Mn temperature can be followed via the energy shift of the PL maxima $\Delta E_{PL}^{\max}$ relative to its equilibrium position at a fixed magnetic field. To monitor the PL after a certain time Δt after a laser pulse, the signal is detected by means of a gated charge-couple-device (GCCD) camera with nanosecond time resolution. This technique allows big improvement of the time resolution, compared with time-resolved experiments with pulsed generation of nonequilibrium phonons. In the latter the temporal resolution is limited by the characteristic decay time of acoustical phonons of about 1 µs. The time resolution is a very crucial parameter, as it determines the shortest accessible SLR time.

Typical PL spectra of a $Zn_{0.89}Mn_{0.11}Se/Zn_{0.89}Be_{0.11}Se$ QW structure are given in figure 3.7. The two bottom spectra were detected under continuous wave (cw) laser illumination with very low excitation density, to avoid heating of the Mn-system above the bath temperature. The giant Zeeman shift of the emission line amounts to about 40 meV at $B = 3$ T. The three upper spectra show the emission line at different delays with respect to the impact laser pulse of 7 ns duration. Just after the pulse ($\Delta t \approx 10$ ns) the giant Zeeman shift is reduced to ~ 14 meV, which

corresponds to a heating of the Mn-system up to $T_{Mn} = 17\,\mathrm{K}$. After one microsecond the line is shifted back to lower energies, reflecting the cooling of the Mn-system.

The characteristic exciton recombination time in the studied structures does not exceed 100 ps, which is typical for ZnSe-based QWs [Yak00]. This is much shorter than the duration of the laser pulses. In order to get information about relaxation processes exceeding the laser pulse duration additional illumination of the sample with a cw laser has been provided.

Figure 3.8 shows the time evolution of both, giant Zeeman shift and polarization degree, induced by laser pulse excitation. Fast heating of the Mn-ions occurs during action of the laser pulse and is reflected by a high-energy shift of the PL maximum by 23 meV and a decrease of the polarization degree from 0.9 to 0.2. After the laser pulse, the Mn-system temperature relaxes towards equilibrium with a relaxation time constant of ∼23 ns. However, it saturates at a level, which exceeds the bath temperature. It will be shown later in this thesis that this level is controlled by nonequilibrium phonons. To reach the equilibrium temperature of 1.6 K takes a much longer time of a few µs. The Mn-spin dynamics in the full time range will be given in figure 4.4. Also the temporal behavior of the giant Zeeman shift and the polarization degree is very similar. Thus, both of them are well suited for optical detection of the spin-lattice dynamics.

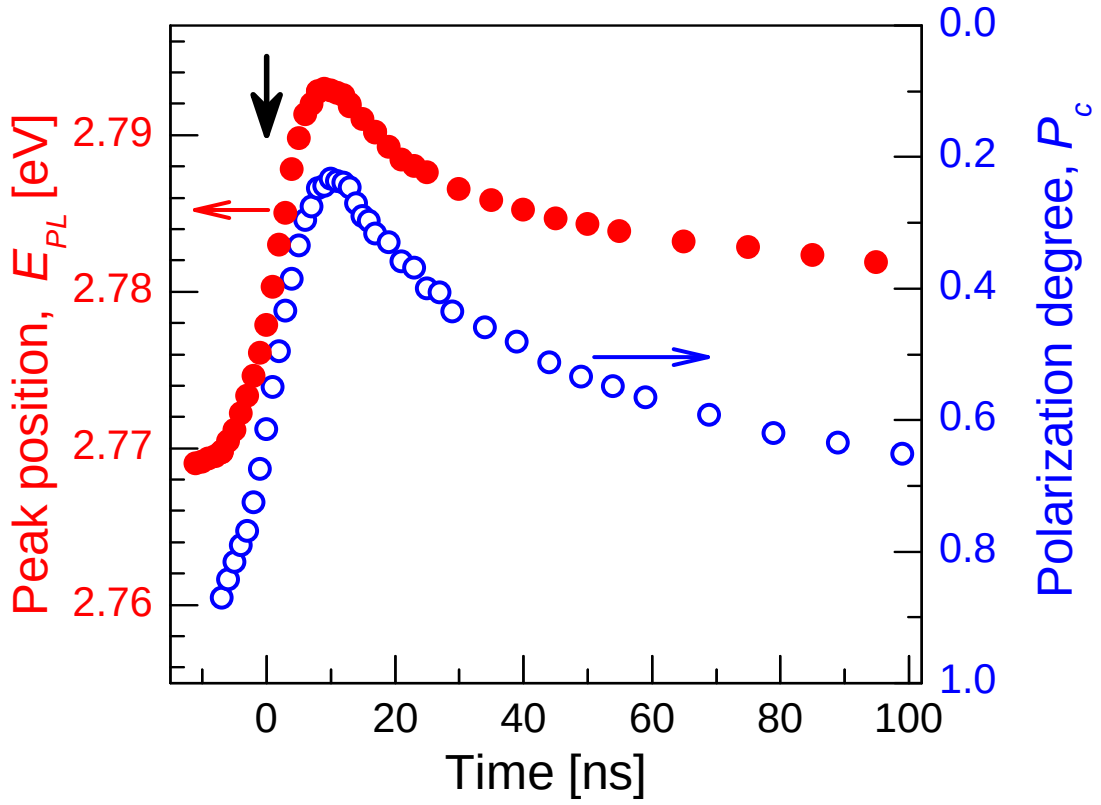

Figure 3.8 – Temporal variation of the PL spectral line position E_{PL} at a magnetic field $B = 3\,\mathrm{T}$ (closed circles) and of the circular polarization degree P_c at $B = 0.12\,\mathrm{T}$ (open circles) in a $Zn_{0.89}Mn_{0.11}Se/Zn_{0.89}Be_{0.11}Se$ QW structure. Excitation density was $P \approx 12\,\mathrm{kW/cm^2}$ and bath temperature $T = 1.6\,\mathrm{K}$. The laser pulse maximum position is indicated by the vertical arrow.

3.4 Experimental setup

The studies of the dynamical shift of the PL line due to relaxation the heated Mn-spin system were performed with the, in figure 3.9 pictured, experimental setup. To heat the Mn-system, a pulsed Nd:yttrium aluminum garnet (YAG) laser (Laser 2000, LCS-DTL-374QT) operating at emission wavelengths of either third harmonic (355 nm) or second harmonic (532 nm) was used. Laser pulse duration was about 7 ns and maximum peak power up to approximately 1 kW at a repetition rate between 1 kHz and 10 kHz. For most of the measurements a repetition rate of 3 kHz was used. The laser power exposed to the sample could be weaken by variable attenuators. The pulsed laser was focused by a lens on the sample, being inside of a superconducting split-coil magnet (Oxford or Cryogenic). Thereby, the sample was immersed in superfluid helium at a bath temperature of 1.6 K. This very low temperature is needed to improve the resolution of the results, because the amount of the giant Zeeman-splitting decreases drastically with growing temperature, as shown in figure 1.16. Magnetic fields up to 10 T were applied parallel to the structure growth axis and to the direction of collected light (Faraday geometry). Measurements without magnetic field were also performed with a helium flow cryostat with high numerical aperture.

The needed additional illumination for electron-hole relaxation processes exceeding the laser pulse duration, which was stressed in the previous section, is provided by a cw HeCd laser (Kimmon, IK Series) at 325 nm or 442 nm. The experimental situation is similar to conventional pump-probe technique. To minimize the heating of the Mn-system, the cw laser was defocused (excitation spots were usually larger than 1 mm in diameter) to reach an excitation density below $0.1\ {}^{\mathrm{W}}/_{\mathrm{cm}^2}$.

In later experiments this heating was further reduced by application of a modulated semiconductor laser (Coherent Cube), which was used instead of the cw laser. To synchronize both pulsed laser, also this laser worked at 3 kHz repetition rate. The pulse length was 250 ns. The laser's emission wavelength was 375 nm at a power density of $72.5\ {}^{\mathrm{mW}}/_{\mathrm{cm}^2}$. The Cube laser requires good collimation of its laser beam, as the radiation is strongly divergent because of the small resonator of the laser. The pulsed operation mode of this laser allows drastic reduction of the contribution of this laser's illumination to the unwanted background heating of the Mn-system by two or three orders of magnitude. Background heating is considerable for low Mn concentration.

The PL generated by the laser radiation was projected on the entrance slit of a 0.5 m spectrometer (Acton 500i) by a so-called four-f-imaging, consisting of four lenses ($f = 19$ cm). Because excitonic PL lies in the UV-region, quartz lenses have to be used. The in-between-image after the second lens was projected on a variable cross-slit. By this slit only small central parts ($< 100\ \mu$m in diameter) of the laser spots could be chosen, to avoid uncertainties caused by spatially inhomogeneous excitation. Directly after the slit it was possible to inspect the PL

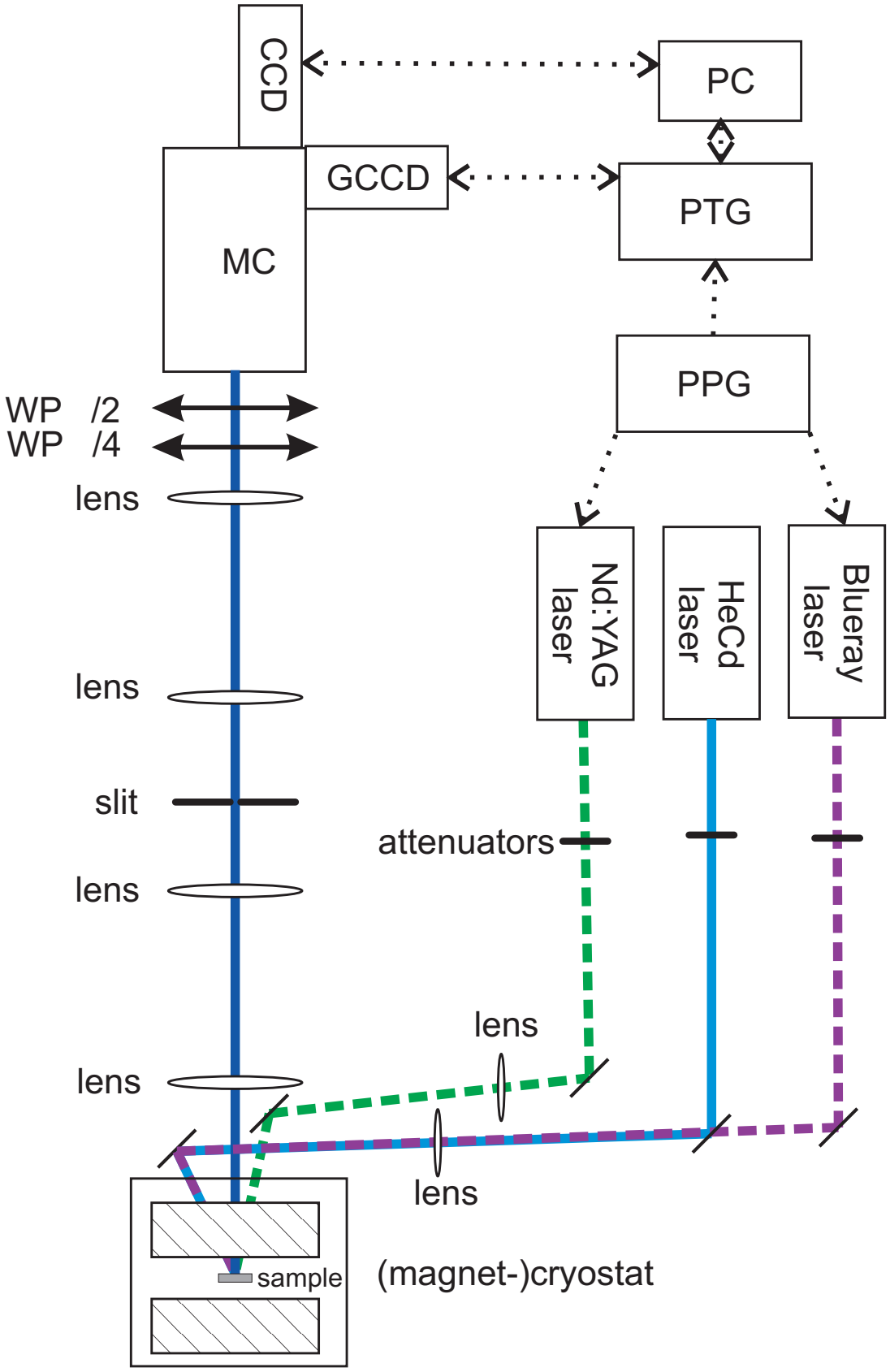

Figure 3.9 – Experimental setup: MC = monochromator, CCD = charge-couple-device camera, GCCD = gated charge-couple-device camera, PPG = programmable pulse generator, PTG = programmable timing generator.

and sample[2], respectively, on a monitor by a microscope and video camera. This construction was needed to make the careful adjustment of the laser spots, which should be exactly upon each other on the sample surface. By means of λ-half and λ-quarter waveplates right-hand σ^+ or left-hand σ^- circular polarization could be chosen for analysis of the sample emission.

To detect PL signal without time resolution, a nitrogen-cooled charge-couple-device (CCD) camera (Princeton Instruments with Silicon photodiode) was used. Time-resolved PL spectra were recorded by means of a gated charge-couple-device (GCCD) camera synchronized with the pulsed laser. Two different GCCD camera models from Princeton Instruments were employed, which were both Peltier-cooled: the older OSMA-system equipped with a IRY-700G/RB Silicon detector and the newer PI-Max system. The older system has the disadvantage that it can be only used with an older version of the measurement software Winspec, not allowing automatic computer-controlled changes of delay and size of the window of the camera gate (see section B.2). Thus, for each measurement all parameters have to be set by hand. The gate signal, which could be delayed with respect to the laser pulses by combination of programmable pulse generator (PPG) (Stanford Research DG535) and programmable timing generator (PTG) (Princeton Instruments PG-200 or ST-133A, respectively), provides a temporal resolution better than 5 ns and 2 ns for the newer system, respectively. More detailed description of the synchronization and measurement-procedure with the GCCD camera is given in section B.2 in the appendix.

A GCCD camera is a modified intensified charge-couple-device (ICCD) camera. An ICCD camera is a CCD camera with a forward-spaced image intensifier. Typical assembly of an intensifier tube is shown schematically in figure 3.10. Incoming light strikes a photocathode and generates electrons. These are multiplied by a microchannel plate (MCP) and impinge a fluorescent screen. The intensifier tube is coupled via a fiber optic taper or a face plate to a CCD chip. In contrast to conventional ICCD cameras, in a GCCD camera a short voltage pulse is applied to the MCP. This allows exposure times less than 2 ns, which exceeds dramatically usual CCD cameras. The duration and interval of the voltage pulses can be controlled variable by a PTG.

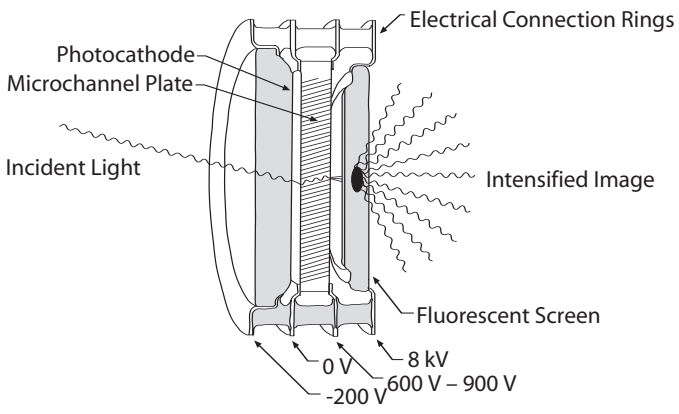

Figure 3.10 – Schematical assembly of the intensifier of an ICCD camera. [Pri08]

[2]By use of simple white lamp for illumination.

Chapter 4

Interaction between carriers and Mn-spin system

Contents

In this chapter experiments concerning energy and spin transfer between carriers and Mn-spin system are presented and discussed. The focus of the studies lies in the distinction of indirect and direct energy transfer between carriers and Mn-spin system. The experiments were performed with nominally undoped samples, so that the carrier system contains only photoexcited carriers generated by laser excitation (compare figure 3.4).

Starting point in the first section 4.1 is the twofold dynamic impact caused by the laser excitation for heating of the Mn-spin system and the resultant response of the Mn-system under different experimental conditions. In the subsequent sections 4.2, 4.3 and 4.4 experimental results for direct and indirect transfer are given and interpreted. The chapter is closed with a comparison of different experimental conditions to distinguish the two transfer channels.

4.1 Twofold dynamic impact for Mn heating

According to section 3.2.1, laser light generates photocarriers with excess kinetic energy, which heat the Mn-spin system via two channels (see especially figure 3.4): the direct way via interaction between carriers and Mn-ions, and the indirect way involving the phonon system. This two-fold impact is subsequent considered with regard to the experimental conditions, given by the used experimental setup.

The temporal profile of the laser pulse $I_L(t)$ is shown in figure 4.1 by the solid line. It can be well described by a Gaussian profile with a half width at half maximum of $\sim$7 ns. Its asymmetry does not exceed 10 %. If photocarriers are generated in the (Zn,Be)Se barriers, they are captured in the (Zn,Mn)Se QWs and recombine there through exciton states. During the lifetime of the photocarriers direct heating can occur. Taking into account our time resolution, and that the carrier lifetimes in the studied structures do not exceed 100 ps, the temporal profile of the carrier impact $I_c(t)$ should coincide with the laser pulse $I_L(t)$. This means that direct heating of the Mn-system by carriers takes place only during the laser pulse action. This is experimentally confirmed as no distinct difference between the laser excitation dynamics and the dynamics of the excitonic emission is observed. Exemplarily results on a (Zn,Mn)Se sample ($x = 0.11$) are shown by dots in figure 4.1.

However, the temporal evolution of the phonon impact $I_{ph}(t)$ differs from the laser pulse. Nonequilibrium phonons are generated by dissipation of the kinetic energy of the photocarriers. While the leading edge of $I_{ph}(t)$ does not exceed $\sim$10 ns (i.e. the integral of the laser pulse), the trailing edge is determined by the characteristic lifetime of acoustic phonons in crystals at low temperatures, which is in the order of 1 µs [Sch99, Sha74]. Summing up, the Mn-system is exposed to a short carrier impact and a long phonon impact. Their temporal profiles are given schematically in figure 4.2.

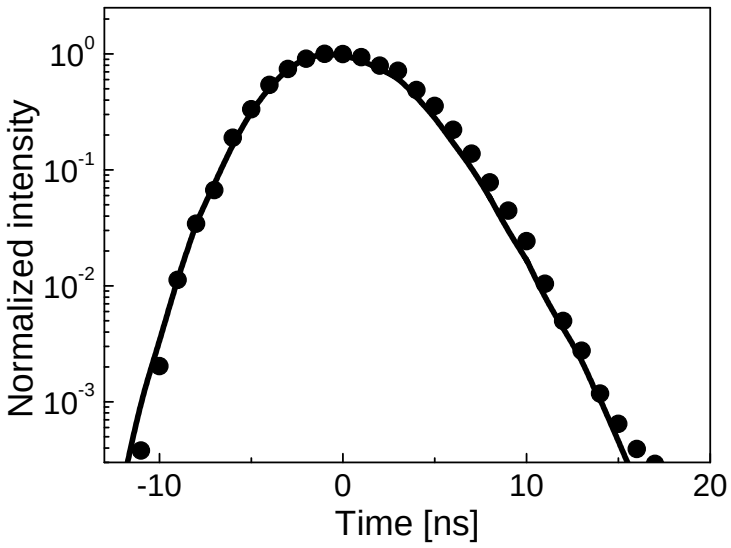

Figure 4.1 – Temporal evolution of a Nd:YAG laser pulse (solid line) and of the PL signal of a $Zn_{0.89}Mn_{0.22}Se/Zn_{0.89}Be_{0.11}Se$ QW sample (dots).

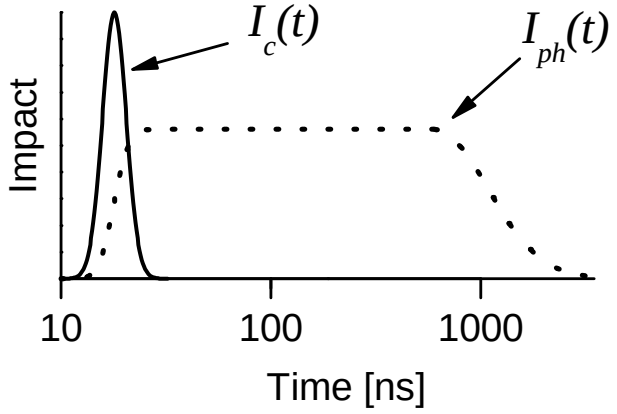

Figure 4.2 – Schematical picture of the two impacts for Mn heating. $I_c(t)$ is the carrier impact due to direct energy transfer from carriers to the magnetic ions, and $I_{ph}(t)$ is the phonon impact due to indirect energy transfer mediated by nonequilibrium phonons.

The dynamical response of the Mn temperature $T_{Mn}(t)$ on an impact will differ for $I_c(t)$ and $I_{ph}(t)$, as it is determined by the difference in characteristic times during which energy can be transferred from the carriers to the Mn-ions (τ_{c-Mn}), from the phonons to the Mn-ions (τ_{SLR}) and from the Mn-ions back to the lattice (τ_{SLR}). Therefore, the response allows to measure these times experimentally. However, the different impact contributions need to be distinguished from the magnetization relaxation, which is not always trivial. The investigations in this chapter are concentrated on the SLR dynamics in (Zn,Mn)Se. Detailed consideration of the interplay of the different energy transfer scenarios determining $T_{Mn}(t)$ for double dynamic impact situation is out of the frame of this thesis. Here only regimes are considered, which have been realized in the experimental conditions, presented in section 3.4.

When τ_{SLR} exceeds the durations of the impact pulses, Δt_c for the carrier impact and Δt_{ph} for the phonon impact, the SLR time can be measured from the decay of $T_{Mn}(t)$. This regime has been realized experimentally by injection of nonequilibrium phonons, enabling the measurement of τ_{SLR} in (Cd,Mn)Te QWs with $x < 0.035$ [Sch00a]. Results for this regime, achieved for laser heating, are presented in the figures 4.4 and 5.1 for (Zn,Mn)Se QWs with $x < 0.035$.

The situation becomes more complicated when the SLR dynamics is faster than the phonon impact. In figure 4.3 the case $\Delta t_c < \tau_{SLR} < \Delta t_{ph}$ is analyzed for different relative contributions of carriers and phonons. The impact profiles are shown by solid lines, and the expected $T_{Mn}(t)$ are given by dashed lines. Cases (a) and (b) are for single impact conditions, when one of the contributions strongly dominates the other. For carrier impact only [case (a)], $\Delta t_c < \tau_{SLR}$ and τ_{SLR} determines the decrease of $T_{Mn}(t)$ toward the lattice temperature. In case (b) yields $\tau_{SLR} < \Delta t_{ph}$ and the SLR time can be measured from the rise of $T_{Mn}(t)$. This is possible due to the sharp rise of the phonon impact $I_{ph}(t)$, which is $\sim \Delta t_c$. The decrease of $T_{Mn}(t)$ follows the slow decay of the phonon impact. The double impact case (c) is realized for the condition $\Theta_c > \Theta_{ph}$, where Θ_c and Θ_{ph} are the maximum T_{Mn} that are obtained under carrier and phonon impacts, respectively. Θ_c and Θ_{ph} can be used to compare the efficiencies of the Mn-system heating by the different impacts. In case (c), the decrease of $T_{Mn}(t)$ has fast and slow components, corresponding to SLR and phonon impact, respectively.

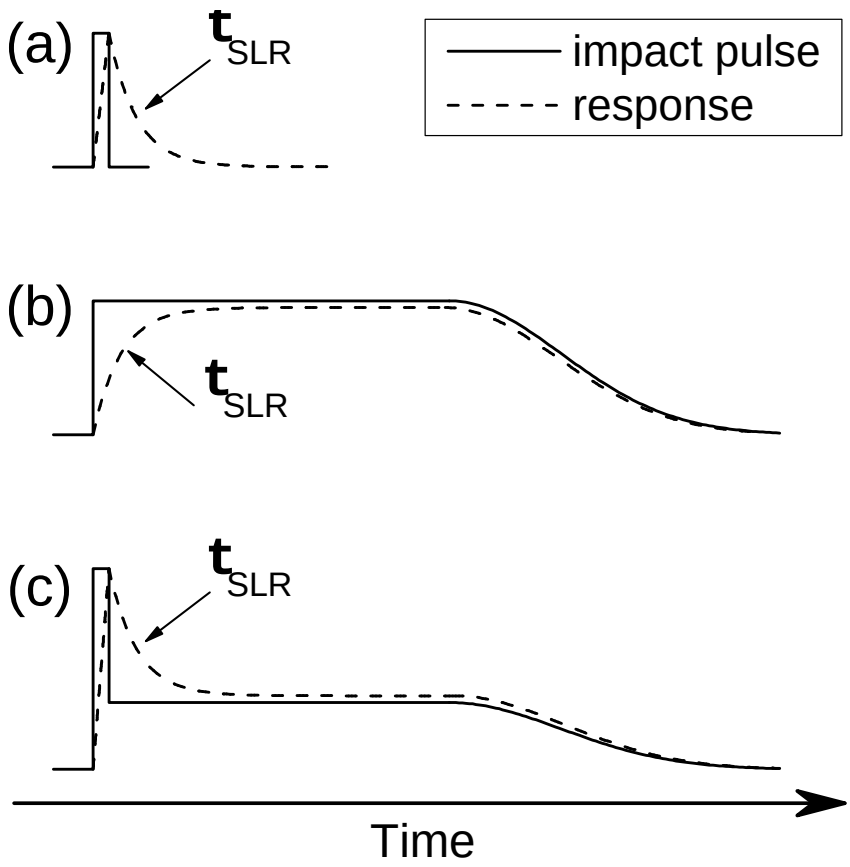

Figure 4.3 – Schematic presentation of the dynamical response of the Mn-system on the impact pulses under various experimental conditions: (a) carrier impact only, with a duration shorter than τ_{SLR}; (b) phonon impact only, with duration longer than τ_{SLR}; (c) double impact of carriers and phonons with $\Delta t_c < \tau_{SLR} < \Delta t_{ph}$ and $\Theta_c > \Theta_{ph}$.

4.2 Direct energy and spin transfer

Energy shifts of emission lines induced by third harmonic (355 nm) Nd:YAG laser pulses at a magnetic field $B = 3\,\mathrm{T}$ are shown in figure 4.4 for $Zn_{1-x}Mn_xSe/Zn_{1-y}Be_ySe$ QWs with Mn concentrations varied from 0.004 up to 0.11. For the sake of convenient comparison the data are normalized by the maximum shift achieved in each structure $\Delta E_{PL}^{\max}$. For the given experimental conditions, $\Delta E_{PL}^{\max}$ varies from 5 meV for $x = 0.004$ up to 26 meV for $x = 0.11$, and the Mn-spin temperature was up to 15 K higher than the bath ($T = 1.6\,\mathrm{K}$). Logarithmic scale for the time delay was chosen to highlight the huge dynamic range of SLR times from 20 ns up to 1 ms covered by the energy shift, which reflects the cooling of the Mn-spin system (see chapter 5). It is, however, remarkable that the heating of the Mn-spin system (the rise of the signal) is very fast and identical for all samples.

The rising part is given in more detail in figure 4.5. One can see the fast heating of the Mn-ions during the action of the laser pulse, which is reflected by the high-energy shift of the PL maxima. The profile of the laser pulse is traced by the dashed line. The solid curve gives the integral of the laser pulse and corresponds to the expected carrier impact on direct

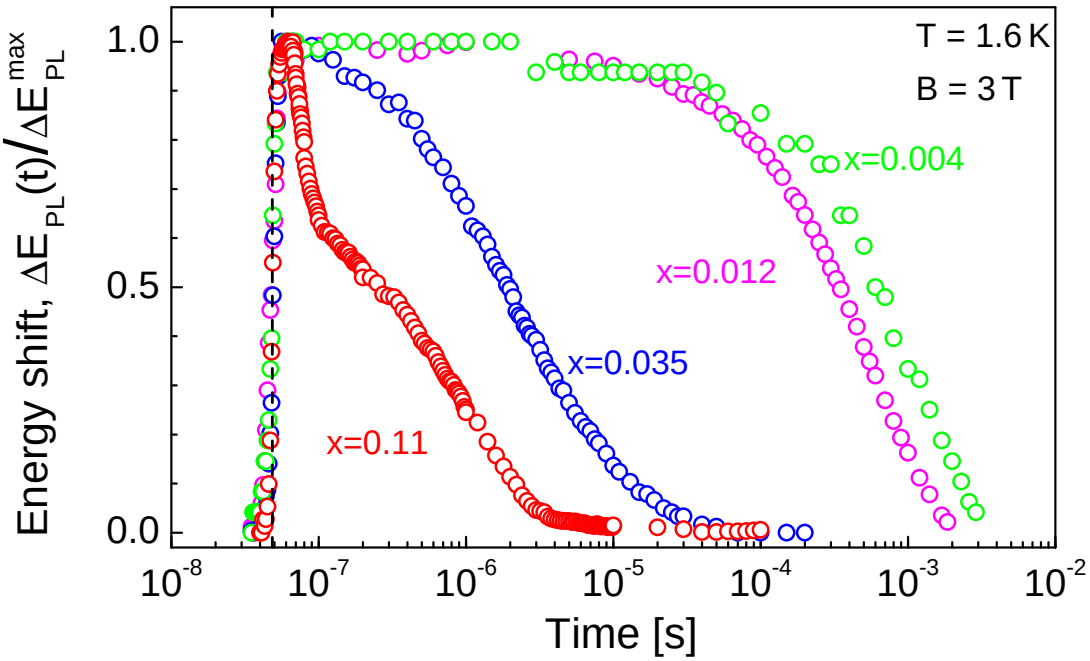

Figure 4.4 – Normalized energy shifts ΔE_{PL} of PL lines induced by 7 ns third harmonic Nd:YAG laser pluses at a magnetic field $B = 3$ T in $Zn_{1-x}Mn_xSe/Zn_{1-y}Be_ySe$ QWs with different Mn content (see table A.2). The maximum shifts $\Delta E_{PL}^{\max}$ are 5, 12, 23, and 26 meV for samples no. 1, 5, 8, and 11, respectively. The temporal position of the maximum of laser pulse is shown by the dashed line. For convenient comparison of the different samples, the data have been plotted on a logarithmic time scale. The measurements were performed at $T = 1.6$ K.

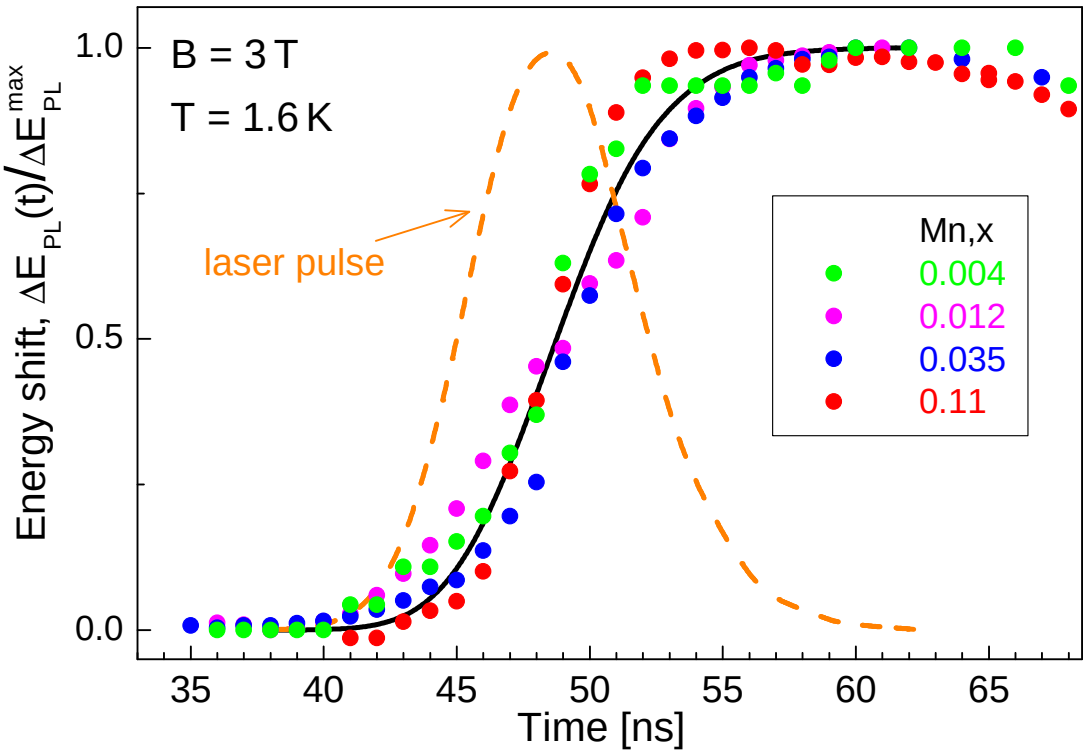

Figure 4.5 – Closeup of the initial parts of dynamic data in figure 4.4 to illustrate only the rise in energy in (Zn,Mn)Se-based QWs with different Mn concentrations (the symbols) in comparison with the laser pulse integral (solid line). The dashed line shows the excitation laser pulse profile. The time scale is linear. The measurements were performed at $T = 1.6$ K and $B = 3$ T.

Mn heating, because of the exciton lifetimes on picosecond scale. The experimental data for all concentrations are grouped closely around this curve, i.e. the rise of the Mn temperature follows closely the integral energy of the laser pulse. As for indirect heating involving nonequilibrium phonons considerably longer heating times are expected, the results allow to conclude that in (Zn,Mn)Se QWs the direct energy transfer dominates over the indirect one. This is in good agreement with the results obtained earlier for cw laser excitation [Kel01].

4.3 Competition between direct and indirect energy and spin transfer

As discussed in section 4.1, the double impact nature of laser excitation leads to a complicated dynamical response of the magnetic ion system under conditions when the SLR time is shorter than the phonon impact time. This regime ($\Delta t_c < \tau_{SLR} < \Delta t_{ph}$) corresponds to the situation sketched in (figure 4.3(c)) and is experimentally realized for the $Zn_{0.89}Mn_{0.11}Se/Zn_{0.89}Be_{0.11}Se$ structure. In this sample with high Mn content ($x = 0.11$) the SLR time $\tau_{SLR} = 20 - 70$ ns is considerably shorter than the phonon lifetimes of about 1 µs, so that also phonon contribution can be investigated.

To highlight the dynamical response of the Mn-system to the phonon impact only, the spectral selectivity of the optical spectroscopy technique is used. For that, 532 nm wavelength laser pulses with a photon energy of 2.33 eV, being smaller than the band gap of (Zn,Mn)Se and (Zn,Be)Se, were utilized. These photons are not absorbed by the (Zn,Mn)Se QW and also not by the (Zn,Be)Se barriers, and, therefore, do not generate carriers in the QWs. This is shown schematically in figure 4.6. However, they are absorbed in the GaAs buffer layer, and the Mn-system in the (Zn,Mn)Se QW is heated by a phonon impact only. These phonons are generated by photocreated carriers in GaAs at distances of less than 1 µm from the (Zn,Mn)Se QW. Thus, the delay of phonon impact (i.e. the time, phonons need for propagation to reach the (Zn,Mn)Se QW) is less than ∼1 ns, which is negligible for this particular experimental situation.

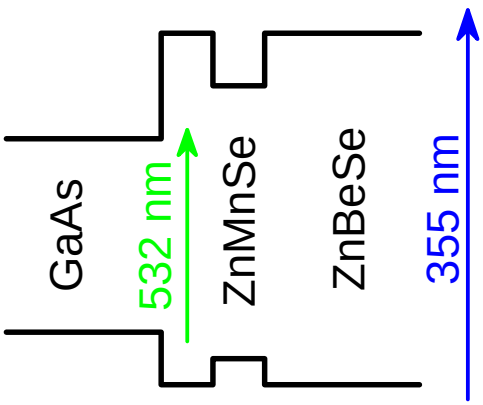

Figure 4.6 – Energy scheme for photoexcitation with different photons. 355 nm photons with energy of 3.49 eV generate carriers in (Zn,Mn)Se and (Zn,Be)Se, but 532 nm excitation with photon energy of 2.33 eV is absorbed only in the GaAs buffer layer. In the latter case only indirect Mn heating by phonons is expected.

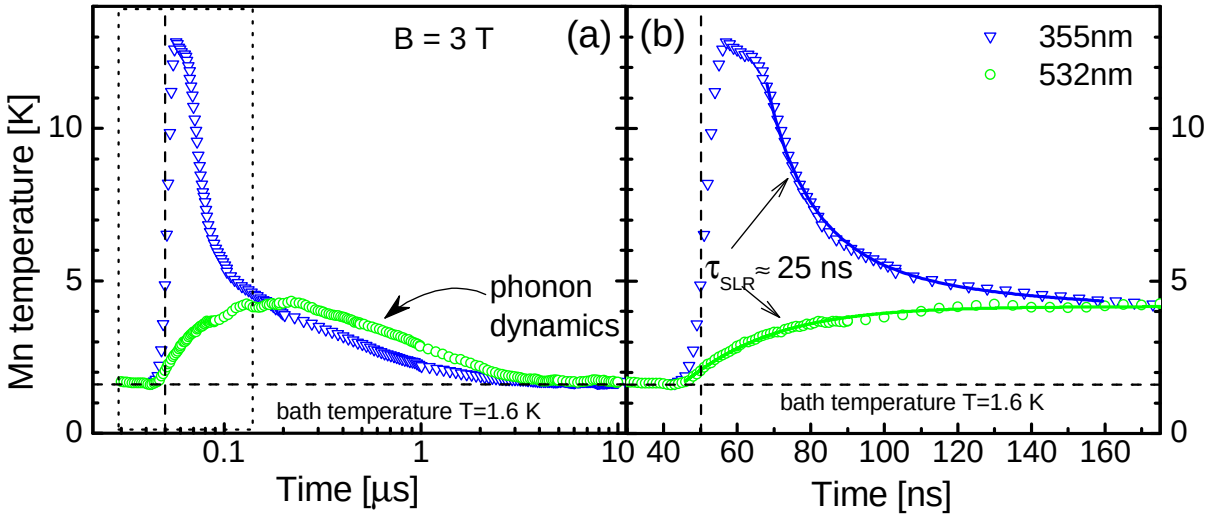

Figure 4.7 – Dynamics of the Mn temperature for two different laser excitation energies: Triangles correspond to 355 nm ($P \approx 9$ kW/cm^2, double impact by carriers and phonons) and circles to 532 nm ($P \approx 15$ kW/cm^2, single impact by phonons only) laser excitations in $Zn_{0.89}Mn_{0.11}Se/Zn_{0.89}Be_{0.11}Se$ QWs. The solid lines show fits of the SLR dynamics with $\tau_{SLR} = 25$ ns. The bath temperature of 1.6 K is indicated by the horizontal dashed line. The vertical dashed line indicates the maximum of laser pulse at 50 ns. On the right side (panel (b)) the region with the different heating dynamics (dotted area) is magnified shown on a linear time scale.

The Mn temperatures obtained from the spectroscopic data at $B = 3$ T are shown in figure 4.7 for the two different laser excitation wavelengths, which were used in these studies.

The rise of the $T_{Mn}(t)$ signal for 532 nm excitation is controlled by τ_{SLR} (case (b) in figure 4.3). The dynamics is given by circles in figure 4.7. $\tau_{SLR} \approx 25$ ns has been extracted from a fit to the data, shown by the solid line. The decay of this signal with a time constant of about 0.6 µs is due to the nonequilibrium phonon dynamics during their cooling to the bath temperature.

355 nm wavelength excitation (photon energy 3.49 eV) leads to absorption in the immediate region of the II-VI heterostructure and should cause a double impact. The dynamics of the Mn-system shown by triangles in the figure 4.7 follows the scenario of case (c) in figure 4.3. The carrier impact drives the Mn temperature up to $\Theta_c \approx 13$ K during the 10 ns of laser pulse action. Afterwards, the Mn-system relaxes on a time scale of $\tau_{SLR} \approx 25$ ns to $\Theta_{ph} \approx 4.2$ K, which is controlled by the phonon impact. At delay times longer than ~100 ns, $T_{Mn}(t)$ follows the phonon impact $I_{ph}(t)$, as can be seen from figure 4.7.

Hence, two processes are clearly seen from the decay. The fast decay is caused by the SLR of Mn-ions. The longer dynamics with a characteristic time of about 1 µs occurs in all samples with SLR times faster than 1 µs, independent of their specific Mn concentration. This part is related to nonequilibrium phonons, which are generated by cooling of photocarriers. Not only the Mn-system, but also the lattice is heated by the laser pulses. Hence, the Mn-system cools down in the first process only to the elevated lattice temperature. The lattice itself cools down to

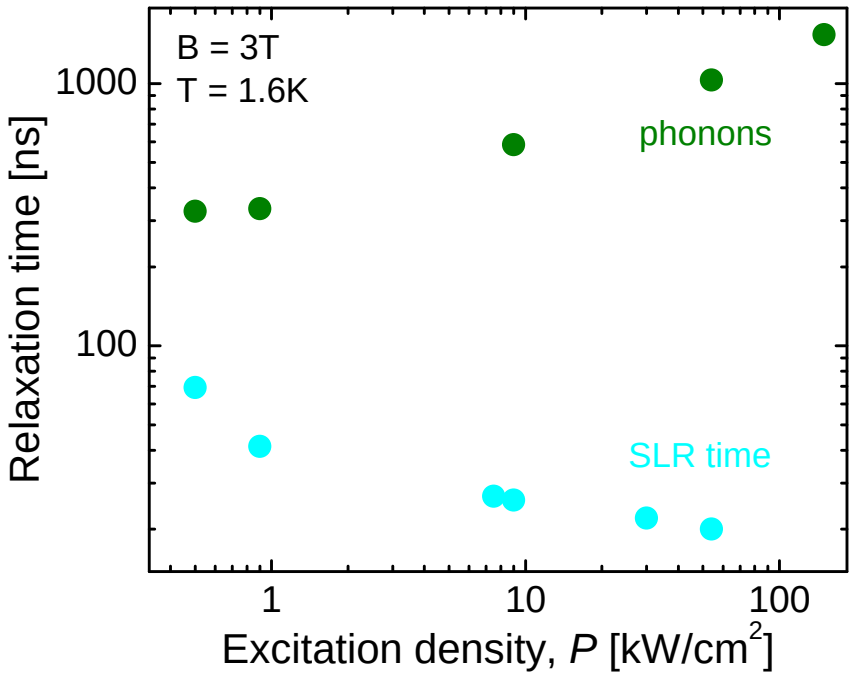

Figure 4.8 – Spin-lattice and nonequilibrium phonon relaxation times measured for different powers of 355 nm laser excitation. The measurements were performed at $B = 3\,\mathrm{T}$ and $T = 1.6\,\mathrm{K}$ with the $Zn_{0.89}Mn_{0.11}Se$ sample.

helium bath temperature on a typical timescale of few microseconds[1], and simultaneously also the Mn-system can transfer its remaining energy via the lattice to the bath to achieve thermal equilibrium.

Summing up, 355 nm and 532 nm laser pulse illumination enables separation of the contributions of the direct and indirect energy transfer mechanisms in time domain. For the given conditions the direct transfer induces $\Delta E_{PL}^{\max} \approx 26\,\mathrm{meV}$, which corresponds to $\Theta_c \approx 17\,\mathrm{K}$, and the phonon contribution does not exceed 14 meV with $\Theta_{ph} \approx 6\,\mathrm{K}$.

An independent confirmation to our assignment of the dynamical ranges is derived from the power dependence of SLR and phonon dynamics in figure 4.8. The SLR time decreases from 70 ns down to 20 ns with increasing power. This is in accord with the known trend of the shorter SLR times at higher lattice temperatures [Far96, Sch00a]. Simultaneously, the time characterizing the phonon dynamics increases from 350 ns to 1200 ns, which is due to a strong decrease of the mean free path of nonequilibrium phonons with increase of their average frequency [Mak85]. Thus, under higher optical excitation, the propagation of phonons is hindered and becomes slower [Kaz89, Mak85], resulting in longer lifetimes of nonequilibrium phonons inside the sample [Sha74].

Examination of a sample with Mn content of only $x = 0.035$ leads to different situation with a SLR time $\tau_{SLR} = 11\,\mu\mathrm{s}$, exceeding considerably the phonon lifetimes. The temporal behavior of the PL energy in this case is shown in figure 4.9. As a result, the rise of the Mn response

[1]The characteristic lifetimes for nonequilibrium phonons in DMS were known from [Sch00a].

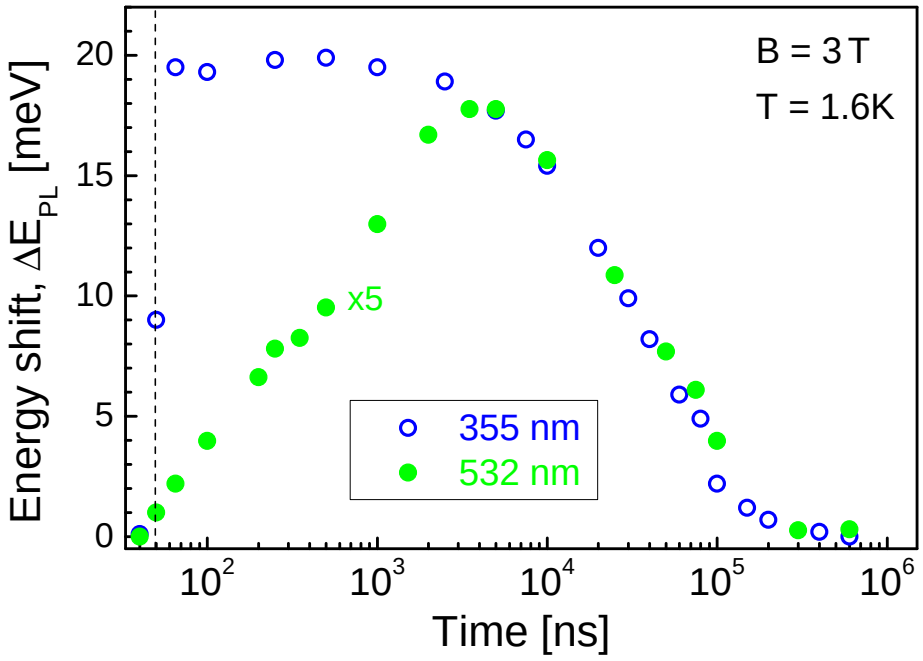

Figure 4.9 – Dynamics of the Mn temperature for a $Zn_{0.965}Mn_{0.035}Se$ QW under excitation with 355 nm (open circles) and 532 nm (closed circles) laser pulses with excitation density $P \approx 50\,\mathrm{kW/cm^2}$. Shown is the temporal behavior of the PL peak energy shift ΔE_{PL} at $T = 1.6\,\mathrm{K}$ and $B = 3\,\mathrm{T}$. The vertical dashed line indicates the maximum of laser pulse at 50 ns. The total energy shift under 532 nm laser excitation was approximately five times less than under 355 nm laser excitation.

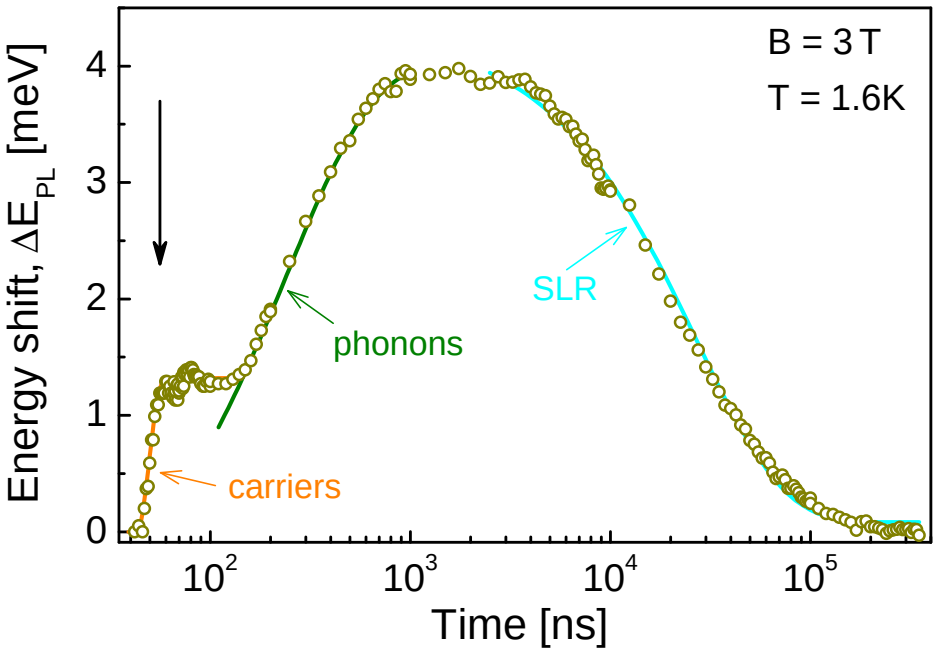

Figure 4.10 – Temporal behavior of the PL line energy shift ΔE_{PL} in a $Cd_{0.985}Mn_{0.015}Te/Cd_{0.6}Mg_{0.4}Te$ MQW. The indirect (phonon) heating is stronger in this sample than the direct heating through carriers. The dynamics of Mn heating allows for distinguishing contributions from carriers and nonequilibrium phonons. The solid lines represent at early times the integral of laser pulse (carriers), then the exponential growth with time constant ~0.3 µs due to phonons, and finally the monoexponential decay with a SLR time of 28 µs. The vertical arrow shows the laser pulse maximum position. The measurements were performed at $T = 1.6\,\mathrm{K}$ and $B = 3\,\mathrm{T}$.

under 532 nm excitation corresponds to the integral over the phonon pulse of about 3 µs. The decay of the Mn response follows the SLR with $\tau_{SLR} = 11$ µs and is identical for 532 nm and 355 nm excitation.

In (Cd,Mn)Te QWs the situation can differ qualitatively from that in (Zn,Mn)Se QWs, where the direct energy transfer from carriers dominates for the Mn-system heating. As one can see in figure 4.10, in a $Cd_{0.985}Mn_{0.015}Te/Cd_{0.6}Mg_{0.4}Te$ sample the direct heating is still prominent, but additional indirect heating can be observed due to the two distinct parts of the rise of the signal. The fast but smaller in amplitude one is due to the direct energy transfer from photocarriers, and the slow one is contributed by the indirect transfer involving nonequilibrium phonons.

Comparison of the heating amplitudes shows even that the indirect heating is more efficient than the direct one. While the phonons heat the Mn-system by $\Theta_{ph} \approx 4.8$ K, only a temperature increase by $\Theta_c \approx 2.8$ K can be assigned to the carrier heating. Figure 4.10 demonstrates clearly that the chosen experimental conditions, namely the short excitation pulses and the nanosecond time resolution, allow for isolating the direct carrier contribution even for the cases when $\Theta_c < \Theta_{ph}$. It can be clearly seen that the direct heating of the Mn-system by carriers takes place only during the laser pulse action, but the indirect phonon heating lasts considerably longer. The decay of the signal exceeds the phonon lifetimes and, therefore, is associated to SLR with $\tau_{SLR} = 28$ µs.

4.4 Influence of excitation density

Varying excitation conditions might change considerably the relative efficiency of direct and indirect energy transfer from photocarriers to Mn-spin system. For deeper insight on the experimental conditions, measurements on the $Zn_{0.89}Mn_{0.11}Se$ QW for excitation densities varied from 0.5 kW/cm² up to 54 kW/cm² were performed. The results for the energy shift $\Delta E_{PL}(t)$ were converted into values of T_{Mn} and are collected in figure 4.11. A pronounced peak at short delays, caused by the direct transfer, loses its dominance upon decreasing excitation density.

To quantify this behavior, the maximal T_{Mn} achieved by direct and indirect transfers as function of excitation density is plotted in figure 4.12. Θ_c was measured at a delay of 10 ns, i.e., just after the laser pulse, and Θ_{ph} was taken at delays of about 200 ns, which exceeds $\tau_{SLR} = 11$ ns for this sample (see table A.2). It is seen that the carrier impact to the Mn heating increases rapidly with the excitation power increase. As for the phonon impact Θ_{ph}, its behavior can be fitted by the well-known dependence of the phonon system temperature T_L under pulsed laser excitation $P \propto (T_L^4 - T^4)$ [Sch99, Sha74]. This result is a consequence of the phonon contribution to the specific heat, which is proportional to T^3 at low temperatures. It should be noted that in the $Zn_{0.89}Mn_{0.11}Se$ sample yields $\Theta_c \geq \Theta_{ph}$ for the whole range of excitation densities studied.

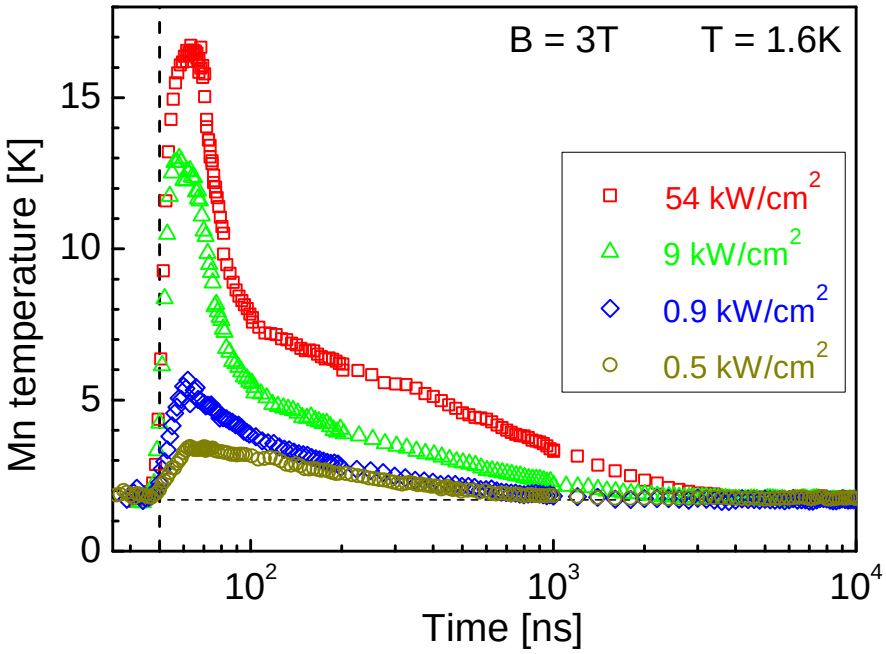

Figure 4.11 – Energy shift of the PL line converted into Mn-spin temperature versus time, measured at different excitation densities of 355 nm laser pulses for $Zn_{0.89}Mn_{0.11}Se/Zn_{0.89}Be_{0.11}Se$ QW. The fast shift of the Mn temperature during the first 10 ns is due to Mn heating by means of photoexcited carriers. The following cooling of the Mn-system shows two stages: the fast one is due to SLR and the slow one is determined by the nonequilibrium phonons kinetics. The vertical dashed line indicates the laser pulse maximum. Experimental conditions were $B = 3\,\mathrm{T}$ and $T = 1.6\,\mathrm{K}$.

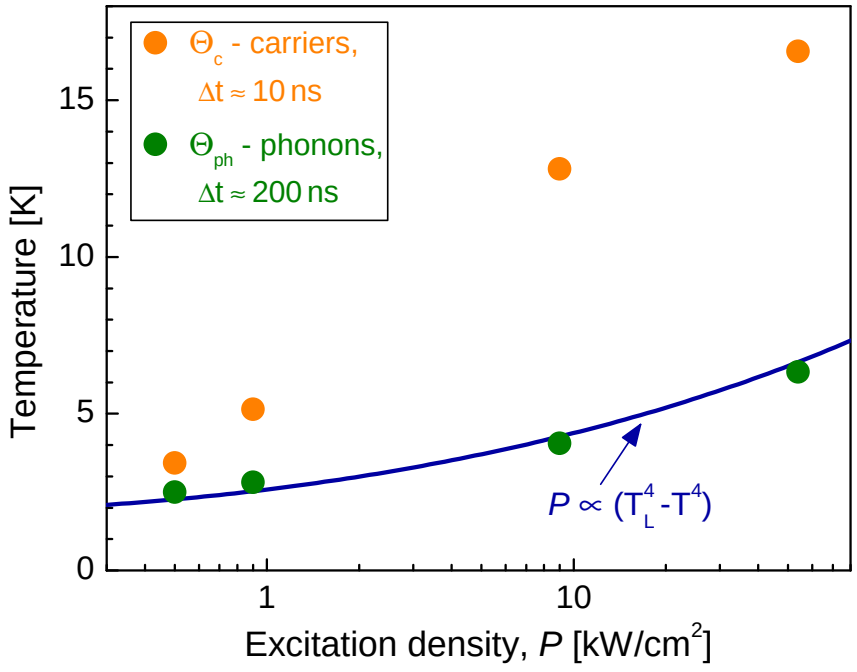

Figure 4.12 – Maximal Mn-spin temperatures achieved by direct carrier heating Θ_c, measured at $\Delta t \approx 10\,\mathrm{ns}$, (closed circles) and by nonequilibrium phonons ($\Theta_{ph} = T_L$), measured at $\Delta t \approx 200\,\mathrm{ns}$, (open circles) as function of excitation density in a $Zn_{0.89}Mn_{0.11}Se/Zn_{0.89}Be_{0.11}Se$ QW. The solid line describes a $P \propto \left(T_L^4 - T^4\right)$ dependence. Experimental conditions were $B = 3\,\mathrm{T}$ and $T = 1.6\,\mathrm{K}$.

4.5 Distinction between direct and indirect heating of the Mn system

In most experimental situations, the distinction between direct and indirect mechanisms of Mn heating by hot photocarriers is not a trivial task. It requires extended sets of experimental data (i.e., for different Mn concentrations, excitation densities, temperatures, and magnetic fields) and careful interpretation. The most severe problem is to achieve a time resolution considerably shorter than the phonon lifetimes of about 1 µs. Here three typical possibilities of experimental situations are discussed.

4.5.1 Steady-state optical excitation

Steady-state optical excitation does not give direct access to the characteristic times and the magnitude of the heating effect, i.e., the Mn-spin temperature is the main parameter for consideration. Very different T_{Mn} have been found in (Zn,Mn)Se QWs under the same excitation conditions [Kel01]. At excitation density of about 10 W/cm² a sample with $x = 0.06$ shows $T_{Mn} = 3$ K, which gives a conservative estimate for the highest temperature of the phonon system. For the same conditions in a $x = 0.004$ sample, $T_{Mn} = 42$ K due to direct heating of the Mn-system by hot photocarriers has been found. For n-type doped (Cd,Mn)Te QWs efficient direct energy transfer has been concluded from the characteristic dependence of T_{Mn} on external magnetic field, which is not expected for the phonon contribution [Kön00b]. However, for undoped (Cd,Mn)Te QWs with x varied from 0.01 to 0.07, the importance of the indirect energy transfer via the phonons has been worked out [Kou03].

4.5.2 Long pulses with low and moderate excitation densities

Usually external modulation of cw lasers is used for experiments with long pulses with low and moderate excitation densities (typically 1 – 100 W/cm²), which allows for easy adaptation of the pulse length for strongly varying SLR times in structures with different Mn concentrations. In such experiments, performed for bulk (Cd,Mn)Te ([Far96, Sca96b]) and (Cd,Mn)Se QDs [Hun05a, Hun05b], the heating times, after switching on the laser pulse, were shorter, but on the order of cooling times of the Mn-system after the end of the pulse. It was also shown that the heating time depends on the excitation density and shortens by an order of magnitude with its increase [Sca96b]. The heating times were associated with the SLR times. On this basis the conclusion of a dominating role of indirect energy transfer involving phonons has been drawn. However, this conclusion might not always be valid. Subsequent will be shown that a long heating time alone, even when it becomes comparable with SLR times, is not sufficient to conclude the dominant role of the indirect energy transfer.

To illustrate this, this situation is analyzed on the basis of the equations in section 2.1.3. Thereby, the situation is simplified to the energy balance for interacting systems of carriers and magnetic ions:

$$\frac{dE_{Mn}}{dt} = C_{Mn}\left(-\frac{\Delta T_{Mn}}{\tau_{SLR}} + \frac{\Delta T_e - \Delta T_{Mn}}{\tau_{Mn-e}}\right), \tag{4.1}$$

$$\frac{dE_e}{dt} = C_e\left(-\frac{\Delta T_e}{\tau_{e-L}} - \frac{\Delta T_e - \Delta T_{Mn}}{\tau_{e-Mn}}\right) + G_e. \tag{4.2}$$

The heating of the lattice itself under low and moderate photoexcitation densities is not taken into account. For the Mn-system (equation 4.1) the energy flux from photocarriers to Mn-system is taken into account by the second term and the energy relaxation to the lattice by the first term. The equation for the carrier system (4.2) consists of the term for the nonequilibrium phonon generation, the term for the energy flux due to the phonon impact, and the energy flux from external sources into the carrier system (G_e), i.e. due to generation of hot photocarriers by laser light. In the equations correspond ΔT_{Mn} and ΔT_e to the deviations of the Mn-ions and carriers, respectively, temperatures from the lattice temperature, C_{Mn} and C_e are the particular specific heats and $\tau_{e-Mn} = \tau_{Mn-e}\frac{C_e}{C_{Mn}}$, $\tau_{SLR}$and τ_{e-L} are the characteristic times for equalizing the temperatures of carriers and magnetic ions, magnetic ions and lattice, and carriers and lattice, respectively. It should be noted that typical values of τ_{e-Mn} and τ_{e-L} are on the order of 1 – 100 ps. As $\tau_{SLR} > 10$ ns for the typical DMS samples, it is always valid that $\tau_{e-Mn}, \tau_{e-L} \ll \tau_{SLR}$. The ratio between τ_{e-Mn} and τ_{e-L} determines the relative contribution of the direct and indirect paths for Mn heating, which was discussed above. The other small parameter in the equations, which is the ratio $\frac{C_e}{C_{Mn}} \ll 1$, is due to the fact that for typical experimental conditions the concentration of photoexcited carriers is always much smaller than the concentration of Mn-ions in DMS samples with $x \geq 0.001$.

With these assumptions, it can be easily shown that the characteristic time for heating of the Mn-system after switching on the photogeneration (which corresponds to the rise time of the signal in experiment) is described by

$$\tau_{in} = \left(\frac{1}{\tau_{SLR}} + \frac{C_e}{C_{Mn}} \cdot \frac{1}{\tau_{e-Mn} + \tau_{e-L}}\right)^{-1} = \left(\frac{1}{\tau_{SLR}} + \frac{1}{\tau^*}\right)^{-1}. \tag{4.3}$$

One can see from 4.3 that the rise time τ_{in} is controlled by the shorter of the two times τ_{SLR} and τ^*.

Two important consequences can be drawn from this simplified model:

(i) First, the rise time τ_{in} should be always much longer than the τ_{e-Mn} and τ_{e-L} times, giving the energy flux rates from carriers to the Mn-spin system and to the phonon system (lattice), respectively. Indeed, if $\tau_{SLR} \ll \tau^*$, then $\tau_{in} \approx \tau_{SLR}$. On the other hand for

$\tau_{SLR} \gg \tau^*$, the following relation holds: $\tau_{in} \approx \tau^* = (\tau_{e-Mn} + \tau_{e-L})\,\frac{C_{Mn}}{C_e}$, and the factor $\frac{C_{Mn}}{C_e} \gg 1$ becomes important.

(ii) To have $\tau_{in} \approx \tau_{SLR}$ the second term in 4.3 should be much smaller than the first one, i.e., $\tau_{SLR} \ll \tau^*$. It is remarkable, that this criterion provides no restriction for the relative ratio of the τ_{e-Mn} and τ_{e-L} times. Therefore, $\tau_{in} \approx \tau_{SLR}$ can occur even in a situation with dominating direct energy transfer (see figure 3.4), when the energy flux from carriers to the Mn-system is much faster than to the lattice $\tau_{e-Mn} \ll \tau_{e-L}$. This means that the experimental observation of Mn heating with the spin relaxation time is not sufficient to conclude a dominant role of the indirect heating process [Far96, Hun05a, Sca96b].

4.5.3 Short pulses with high excitation densities

Short-pulse high-density excitation is realized by means of pulsed lasers. Experiments for generating a dense electron-hole plasma in (Cd,Mn)Te/(Cd,Mg)Te QWs have been reported in [Kul96, Tya97, Tya99]. Very fast heating during 0.5 ns and very high peak temperatures of the Mn-spin system (up to 300 K) are strong arguments for a dominating contribution of the direct energy transfer in these experiments. These conditions lead to strong inhomogeneity of the coupled system of Mn-ions and carriers, and to formation of spatial domains, having very different Mn-spin temperatures.

The moderate excitation density regime, but with high time resolution down to 2 ns, was reported in this chapter. As shown, direct and indirect contributions can be distinguished in time domain with high accuracy by time-resolved spectroscopy. The main advantage of this technique is that the time resolution is on nanosecond scale, which drastically under-runs the typical phonon lifetimes. The direct transfer dominates in (Zn,Mn)Se structures for all studied Mn contents from 0.004 to 0.11. The indirect energy transfer is more efficient in $Cd_{0.985}Mn_{0.015}Te$ QWs.

Chapter 5

Spin-lattice relaxation

Contents

In this chapter the focus is shifted to the magnetization dynamics related to the Mn-spin system. The SLR of Mn-ions is discussed regarding its dependence on the Mn concentration and host material in section 5.1, and on the density of the free carriers (2DEG) in section 5.2. The acceleration of SLR dynamics by increase of the lattice temperature [Sca96a, Sch00a] or in external magnetic fields [Sch00a, Str92] has already been well established.

5.1 Dependence of the spin-lattice relaxation on the Mn content

For low Mn concentrations, where the SLR dynamics takes considerably longer than the characteristic time of the phonon impact of $\sim$1 µs, the SLR times can be extracted from the decay of the dynamical response (as sketched in figure 4.3(a) for Δt_c,$\Delta t_{ph} < \tau_{SLR}$). In figure 5.1 the spectral shift of PL line ΔE_{PL}, induced by the laser impact, is plotted as a function of time for samples with different Mn content. The SLR dynamics was measured by the time-resolved technique described in chapter 3. Once more should be emphasized that the measured values for ΔE_{PL} are proportional to the changes in magnetization, i.e. to changes in the average spin of the Mn-ions. For suitable comparison of the different samples, the data have been normalized to the maximum shift $\Delta E_{PL}^{\max}$ and have been plotted on a logarithmic scale. As seen from the linear dependence on this scale, the spin relaxation can be well described by a single exponential behavior. This holds for all samples with Mn contents ranging from 0.004 up to 0.035.

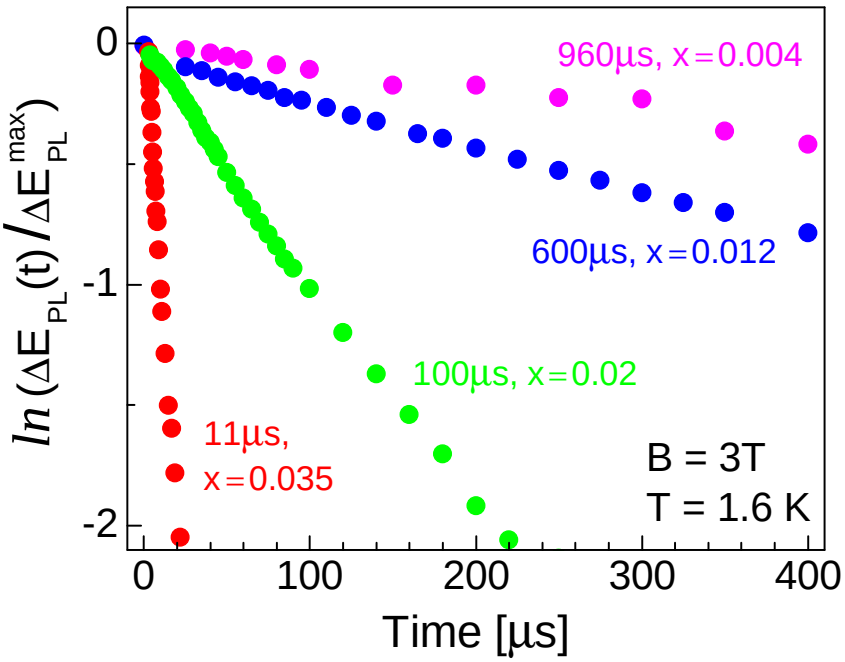

Figure 5.1 – Temporal evolution of PL spectral line shift ΔE_{PL}, which is proportional to the change ΔM of the Mn magnetization in $Zn_{1-x}Mn_xSe/Zn_{0.94}Be_{0.06}Se$ QWs with different Mn content x. The SLR time τ_{SLR} decreases from 960 µs to 11 µs with increasing x from 0.004 to 0.035. The measurements were performed at $B = 3$ T and $T = 1.6$ K.

For $x > 0.04$ the SLR dynamics approaches the duration of the phonon impact. The modifications of the dynamical response in this case were already considered in section 4.3. Complete picture of the results for the SLR time as function of Mn content is plotted in figure 5.2. As the SLR time depends on the magnetic field strength, all measurements were performed at $B = 3$ T. From the plot can be seen that the SLR times of Mn-ions in (Zn,Mn)Se cover the dynamical range of five orders of magnitude from 10^{-3} down to 10^{-8} seconds, when the Mn concentration varies from $x = 0.004$ up to $x = 0.11$. Such behavior was reported previously for bulk materials [Sca88, Bin91, Str90, Str92, Far96]. The difference of the SLR times for bulk DMS to the values reported here, is likely due to the absence of the phonon bottleneck effect in QWs.

The values of τ_{SLR}, obtained for the sample with $x = 0.11$ at the lowest and highest power densities (according to figure 4.8), are shown by two data points. It should be noted that τ_{SLR} for the sample with $x = 0.1$ Mn content was measured under high excitation density of $P \approx 100\,\mathrm{kW/cm^2}$, and, thus, corresponds to a SLR time at a temperature higher than the bath temperature. A shift of its expected value to the regime of low excitation density is shown by the arrow.

The full circles in figure 5.2 show the experimental data for (Zn,Mn)Se-based structures, while the open symbols give the literature data for (Cd,Mn)Te. The literature data for (Cd,Mn)Te follow closely the dependence for (Zn,Mn)Se.

To discuss the results, comprehensive understanding of spin-phonon interaction is needed. Waller suggested a microscopically mechanism [Wal32], which is due to modulation of the spin-

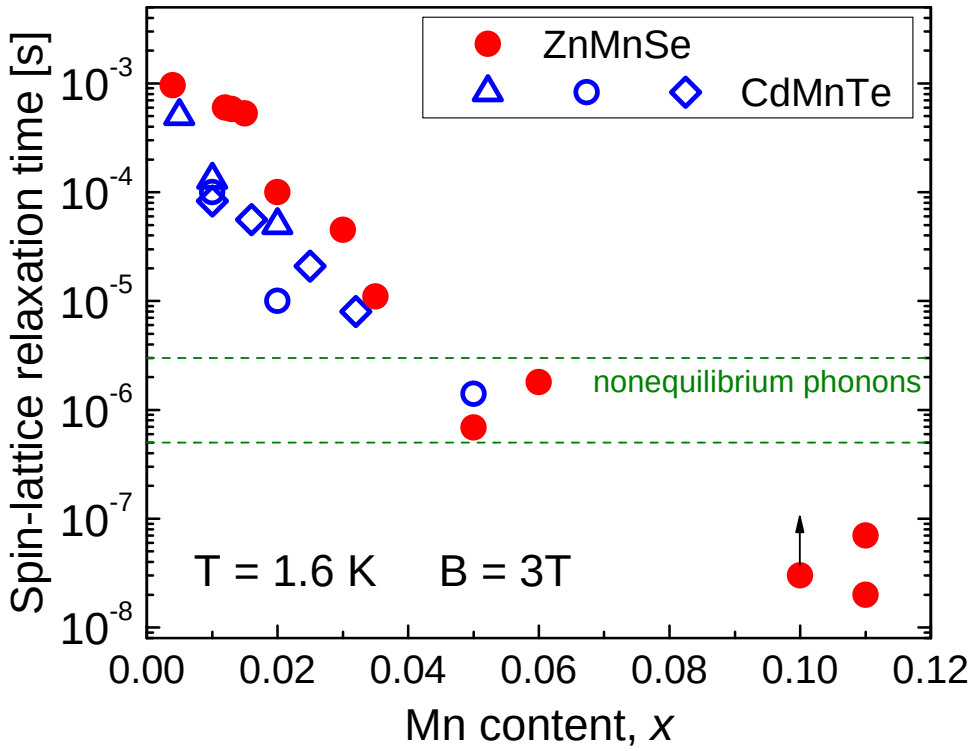

Figure 5.2 – Spin-lattice relaxation time as function of Mn content for nominally undoped $Zn_{1-x}Mn_xSe/Zn_{1-y}Be_ySe$ structures (closed circles). The values are listed in table A.2. Open symbols represent literature data for $Cd_{1-x}Mn_xTe$ bulk samples (triangles and circles) [Far96, Sca96a] and $Cd_{1-x}Mn_xTe$-based heterostructures (diamonds) [Sch00a]. The dashed line indicates typical lifetimes of nonequilibrium phonons.

spin interaction (magnetic dipole-dipole interaction) between neighboring Mn-ions by phonons. This effect is based on changes of the distance between two ions under the action of lattice vibrations. This fluctuation of the distance leads to changing of the local magnetic field, which exists at one ion, because of the magnetic dipole on a neighboring ion. It is obvious that the so-called Waller mechanism depends strongly on the magnetic ion concentration. From calculations in [Abr70] is known, that SLR based on the Waller mechanism occurs on a time scale, which is by several orders insufficiently rapid to explain the experimentally measured dynamical range in the nanosecond and microsecond region. The slow SLR times originate in the small phonon energy density at the resonance frequency for direct processes.

Heitler and Teller [Hei36] have proposed a mechanism, on whose basis relaxation times in the right order were obtained [Vle40]. This mechanism is known as Van Vleck mechanism. Also the Van Vleck mechanism is based upon modulations, which are induced by the motion of the electrically charged ions due to lattice vibrations. Instead of modulation of the internal dipolar field, this mechanism consists of modulation of crystal electric field or ligand field. Theory of this mechanism is given in [Kro39]. Obviously this interaction couples not directly to the electron spin, but the modulated field interacts with the orbital moment of the ion and splits its orbital states. The orbital moment in turn interacts with the spins via the spin-orbit coupling. However, this orbit-lattice interaction is not possible for an isolated Mn^{2+}-ion in a

perfect II-VI semiconductor crystal. Usually the gradient of the ligand field couples with the quadrupolar orbital angular momentum of the ions. But this quadrupolar momentum is zero ($L = 0$) due to the half-filled d-shell in Mn^{2+}-ions. Due to this lack of coupling with the lattice, the electric field of the phonons do not act on the magnetic moments. Hence, the magnetic field induced by temporal variation of the electric field is relativistically small. Interaction of gradients of the electric field with the spin via the quadrupolar moment of the magnetic Mn-ion is not possible. Nonzero matrix elements of the orbit-lattice interaction can only be obtained by admixture of excited states to the ground state via spin-orbit coupling. But, according to [Blu62], this effect is rather small, because the spin-orbit coupling will only mix states with different total spin values into the ground state. Furthermore, the Van Vleck mechanism has no intrinsic dependence on the concentration of magnetic ions [Gil75], which is in contrast to the achieved experimental results.

Hence, the dominating microscopic mechanism for spin-phonon interactions in Mn-based DMS remains the Waller mechanism. To explain the measured fast SLR times the hitherto assumption of isolated Mn^{2+}-ions must be abandoned. In this case Mn-ions tend to form clusters with increasing Mn content. Due to spin-spin superexchange interaction various spin levels are formed in clusters. Transitions between these levels mediated by phonons are allowed ($\Delta S = \pm 1$; $\Delta M = 0, \pm 1$) and governed by the Dzyaloshinsky-Moriya mechanism [Sca96a, Wan92, Wit95]. Example for a possible transition in a manganese pair cluster is given in figure 5.3. As clusters possess a lot of excited states inside the phonon continuum, spins have the opportunity to relax via the more efficient Orbach-process than via the direct process [Sca96a]. Thus, SLR is strongly accelerated in clusters. The amount of clusters or isolated Mn-ions, respectively, depends on the Mn concentration. Assuming a statistical distribution of Mn-ions in the crystal lattice, the probability to find an isolated Mn-ion, which has no neighboring Mn-ion, decreases by $(1 - x)^{12}$ [Kel04]. For a Mn concentration of $x = 0.004$ are more than 95 % of the Mn-ions isolated, but for $x = 0.11$ only less than 25 %.

Determination of the concrete types of clusters (pair, triads), which contribute to the SLR process, requires further experiments. In magnetic semiconductors a variety of clusters with different values of B_1 exist [Kre65]. For the present experimental conditions clusters with

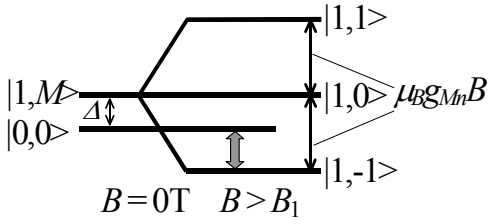

Figure 5.3 – Energy scheme for a manganese pair cluster taken from [Sch00a]. Shown are the singlet $|0,0\rangle$ and the triplet states $|1,M\rangle$. The latter splits in magnetic field according to M, and the $|1,-1\rangle$ triplet state crosses the singlet state at $B = B_1 = \frac{\Delta}{\mu_B g_{Mn}}$ and gets the ground state. At a magnetic field $B > B_1$, the magnetization, i.e. the temperature of the Mn-spin system, can be increased by emission ($|0,0\rangle \rightarrow |1,-1\rangle$ transition) or decreased by absorption ($|1,-1\rangle \rightarrow |0,0\rangle$) of resonant phonons.

$B_1 > 3\,\mathrm{T}$, like nearest-neighbor pairs and triads, cannot contribute, but next-nearest-neighbor clusters have sufficiently low values of B_1 [Fur88a, Str92, Wan92, Wit95].

Further effect on the SLR is given by spin diffusion. Mn-spins from isolated Mn-ions can diffuse via relaxation towards Mn-ions included in clusters [Sca96a]. This cross-relaxation conserves energy and total spin [Kel04]. Transitions, which change the total magnetization in clusters, are only possible because of the exchange interaction modulation by lattice vibrations, when states with different spin are coupled by anisotropic interactions. Three anisotropic interactions can be considered, which couple neighboring Mn-spins antiferromagnetically in clusters [Far96, Sca96a, Wan92]: the exchange interaction, the Dzyaloshinsky-Moriya exchange interaction [Dzy58, Mor60] and the magneto-dipole interaction. All of them are short-range interactions, but the magneto-dipole interaction has the weakest decay with the increasing distance between the Mn-ions and, therefore, the longest range. This mechanism plays the dominant role for SLR dynamics in the limit of very small Mn contents, while the two other become important at higher Mn contents, when Mn clusters are formed. In the latter case the Dzyaloshinsky-Moriya exchange interaction is dominant.

Scalbert [Sca95, Sca96a] has calculated for the Dzyaloshinsky-Moriya exchange interaction the analytical dependency of the SLR rate on temperature and Mn content for Mn pairs:

$$\frac{1}{\tau_{SLR}} \approx \left(\frac{a_B}{a}\right)^2 6x\,(1-x)^6 \left(\frac{3}{\exp\left(\frac{24.4}{T}\right)+3}\right)\left(\frac{9}{\exp\left(\frac{24.4}{T}\right)-1}\right) 10^8\ \mathrm{s^{-1}} \tag{5.1}$$

and Mn triads:

$$\frac{1}{\tau_{SLR}} \approx \left(\frac{a_B}{a}\right)^2 42x^2\,(1-x)^1\,1 \left(\frac{2.1}{\exp\left(\frac{30}{T}\right)-1}+\frac{6}{\exp\left(\frac{43}{T}\right)-1}\right) 10^8\ \mathrm{s^{-1}}. \tag{5.2}$$

The fitting parameter $a = \frac{J}{\frac{\partial J}{\partial R}}$[1] describes the changing of the lattice constants by lattice deformations and achieves the best agreement with experimental results for $a = 0.35\,\text{Å}$, which is in good agreement with the expected value for superexchange interaction [Sca96a]. For low Mn concentrations ($x < 0.02$) follows from equations 5.1 and 5.1 that the SLR is considerably more determined by the amount of clusters with three Mn-ions than Mn-ion pairs. As already for $x = 0.15$ more than half of the Mn-spins belongs to bigger clusters [Kre66], also these have to be taken into account for concentrations higher than $x = 0.1$. However, the calculation of analytical dependencies gets increasingly more complex.

The number of Mn-spins coupled in clusters and the typical cluster size increase progressively for growing Mn concentration [Lar86]. This is the reason for the strong dependence of the SLR time on the Mn concentration. It can be shown in the framework of a simple model, which is accounted for the spin diffusion from Mn-ions to Mn clusters, where the spin has effi-

[1] Thereby is J the nearest-neighbors exchange constant and R the Mn-anion bond length.

cient relaxation, that the SLR rate ${\tau_{SLR}}^{-1}$ has a strong dependence on Mn content with a power law between x^3 and x^4 [Yak09]. This is in good qualitative agreement with experimental results from figure 5.2, which is thus a strong evidence of the dependence of SLR on the Mn content and for the anisotropic Mn-Mn exchange interactions as dominating SLR mechanism.

As confirmed by the experimental data, the property of the host II-VI semiconductor is not of major importance and should not change the strong trend of SLR time dependence on the Mn concentration. But some quantitative variations in τ_{SLR} can be expected. Strength of Mn-Mn interaction depends on the lattice constant, type of crystallographic lattice and the anion atom, which orbitals are involved in the indirect exchange interaction between magnetic ions [Die94]. Also clustering depends on the number of neighbors in the first, second and third coordination spheres in the cation sublattice, which is controlled by the lattice type. (Zn,Mn)Se and (Cd,Mn)Te have the zincblende lattice structure. The lattice constant 5.67 Å in (Zn,Mn)Se is smaller than 6.50 Å in (Cd,Mn)Te, the respective distances between the nearest-neighbor magnetic ions are 4.0 Å and 4.6 Å. The coupling constant of the Heisenberg interaction between nearest-neighboring magnetic ions in (Zn,Mn)Se is larger than in (Cd,Mn)Te, the respective values are -12.3 K (wurtzite lattice) and -6.3 K (zincblende) [Die94]. The larger coupling constant in (Zn,Mn)Se may suggest faster SLR dynamics, which, however, is not confirmed by the results from figure 5.2. Obviously, further experimental and theoretical efforts are required to clarify the influence of the host material on SLR rate of Mn^{2+}-ions.

In (Zn,Mn)Se, contrary to (Cd,Mn)Te with $x < 0.3$, an internal Mn^{2+} ($3d^5$-shell) transition ${}^6A_1 \rightarrow {}^4T_1$ can be excited by energy transfer from excitonic states [Fal03, Lei97, Som93]. The total spin of the excited state is 3/2 instead of the 5/2 of the ground state of the Mn^{2+}-ion, and, therefore, an additional mechanism for the optically induced reduction of the magnetization could be taken into consideration. However, this mechanism does not contribute to the experimental results on the SLR times reported in this thesis, probably due to small amount of excited Mn^{2+}-ions. This belief is corroborated by the hitherto results: (i) Similar SLR times received for the two material systems from figure 5.2; (ii) The results coincide well with the SLR time in (Zn,Mn)Se measured by injection of nonequilibrium phonons. This technique excludes internal excitation of the Mn^{2+}-ion [Kel01, Sch05]; (iii) The same relaxation times for the samples from figure 5.1 have been measured under 532 nm photoexcitation, which does not generate excitons in (Zn,Mn)Se layers.

It is important to note that the studied samples have thicknesses of DMS layers not exceeding 100 – 200 Å. As a result, the SLR dynamics of Mn-ions is free of the phonon bottleneck effect, which might strongly slow down spin dynamics in bulk DMS (see [Aki06a, Sch00a] and references therein). Generally, phonon bottleneck occurs, if the heat capacity of the phonon system is less than the heat capacity of the magnetic system. On the other hand these layers are thick enough to neglect quantum confinement effects for the Mn-ions.

5.2 Effect of free carriers in doped structures

That the dynamics of SLR can be modified significantly by the presence of free carriers, is already known from metals with magnetic impurities [Bar81] and bulk narrow-gap DMS with high concentration of free carriers [Sto96]. Examples of effects caused by such interaction are the Korringa effect and the Knight shift.

Also in the wide-band-gap DMS (Cd,Mn)Te an acceleration of SLR was experimentally found [Sch01b, Sch01a], if free carriers (electrons or holes) are implemented by modulation doping of the barrier layers by donors or acceptors. Thereby, heating by electric current gave qualitatively similar results to the heating by photocarriers. However, the value of the giant Zeeman-splitting suppression, which was a measure for the Mn-ion heating, was about three times larger for the charged exciton transition than for the exciton. This is due to the spatially inhomogeneous heating of the Mn-system. The stronger heating was in the microscopic regions, where the free carriers have higher concentration, as these regions were most efficiently heated by electric current [Yak04].

In contrast to QWs, which are directly doped in the well layer, in modulation doped QWs the carriers are spatially separated from the donators. Thus, impurity potentials, which were created by insertion of donators, are outside of the QW, leading to a very high carrier mobility in the QW. As the Fermi-energy E_F is constant in growth direction, the donors ionize and electrons are transferred in the QW. From this separation results an electric field in growth direction, which leads to parabolic band bending in the QW [Plo83]. The total potential, which acts on the carriers, is described, within the scope of the Kohn-Sham-potential [Koh65], by the sum of the band offset between QW and barrier V, the Hartree-potential of the electric field V_H and the so-called exchange-correlation potential V_{XC}, which describes the residual many-body effects [Sch89]:

$$V_{KS}(z) = V(z) + V_H(z) + V_{XC}(z). \tag{5.3}$$

The contribution by V_{XC} lowers the band gap with increasing electron density, which is known as band gap renormalization.

In order to study this effect in modulation-doped (Zn,Mn)Se QWs, a set of samples with $x = 0.004$ and electron densities varying from $10^{10}\,\mathrm{cm}^{-2}$ up to $5.5\times10^{11}\,\mathrm{cm}^{-2}$ is examined.[2] Samples with electron densities below $10^{10}\,\mathrm{cm}^{-2}$ are nominally undoped, as this electron concentration is only provided by residual impurities. Again the well-established method to heat the Mn-system via photocarriers is used. In doped structures the number of optically generated carriers is negligible compared to the carriers, which exist due to the doping. For the spin-flip exchange scattering between Mn-ions and carriers, the origin of the carriers is irrelevant. Thus,

[2] Samples CB1542, CB2033, CB2034, CB2037 in table A.2.

the effect of the photocarriers is well described by an elevation of the 2DEG temperature due to electron-electron scattering. As already mentioned in section 2.1.3, the Mn-spin temperature equals the electron system temperature in case of a SLR time τ_{SLR} exceeding the time for energy transfer between electron and Mn-system τ_{e-Mn}. This leads to overheating of the Mn-system, if the temperature of the 2DEG is increased due to the electron-electron scattering with the photocarriers.

For the measurement of the excitonic PL line has to be taken into account that the formation of excitons (and trions) is suppressed in the presence of a 2DEG. This results mainly from the so-called phase space filling. The states, which are occupied by the 2DEG, cannot be used for creation of the excitonic wave function due to the Pauli principle. Screening of Coulomb interaction between electron and hole by the 2DEG, which occurs additionally in bulk semiconductors, is not possible in QWs [Bru84], and, hence, plays no role. Calculation of the decrease of the oscillator strength of the $1s$-exciton can be gleaned from [Sch85].

The SLR times, which were achieved by tracing the excitonic PL are depicted in figure 5.4. A decrease from 960 µs down to 70 µs is observed. This means that in the doped samples τ_{SLR} is up to 14 times shorter than in the undoped case. This result was approved by measurements of a set of two modulation-doped $Zn_{0.035}Mn_{0.965}Se$ QWs with electron densities of 3×10^{10} cm^{-2} and 3×10^{11} cm^{-2} (see figure 5.5). All results coincide well with the results for n-doped and p-doped (Cd,Mn)Te-based QWs. Comparison of all results is given in figure 5.5. The enhancement of the SLR rate for magnetic ions is stronger for the presence of free holes [Sch01b]. This is intuitively expected, due to the larger carrier mass, which leads to a larger density of states and

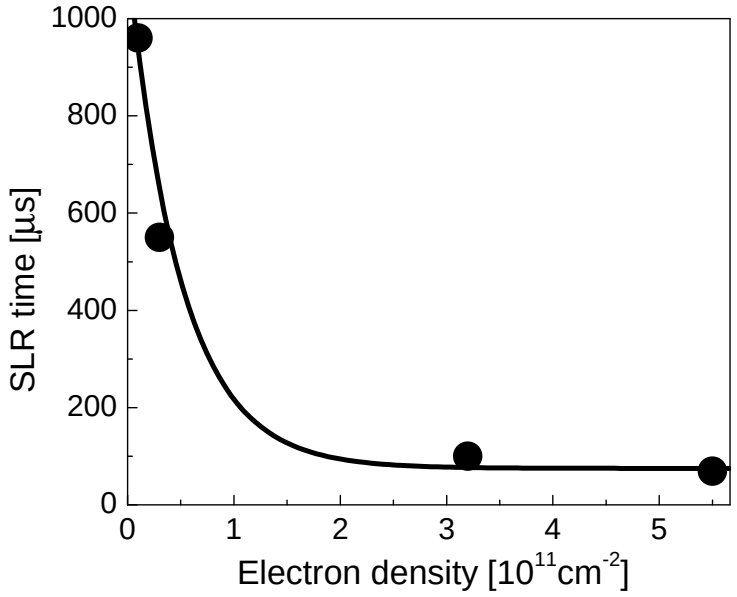

Figure 5.4 – Dependence of the SLR time τ_{SLR} on the concentration of free electrons n_e in $Zn_{0.996}Mn_{0.004}Se/Zn_{0.94}Be_{0.06}Se$ QWs. The solid line is a guide to the eye. The measurement were performed at $T = 1.6$ K and $B = 3$ T.

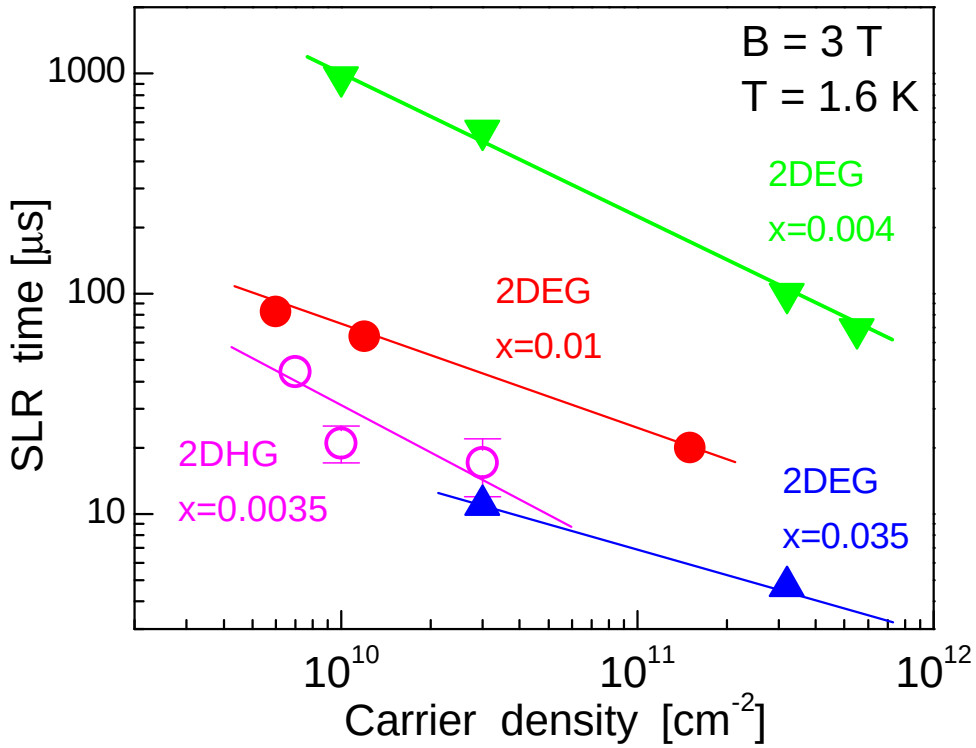

Figure 5.5 – SLR time as function of the carrier density in modulation doped DMS QWs. Triangles correspond to the measured data for (Zn,Mn)Se-based QWs, while circles show data for (Cd,Mn)Te-based QWs taken from [Sch01b, Sch01a]. Closed symbols represent data for structures with 2DEG and open circles for a structure with a two-dimensional hole gas (2DHG). The lines are just guides for the eye.

a stronger p-d-exchange interaction with magnetic ions (about four-five times stronger than the s-d-exchange interaction for electrons).

From the results presented in section 5.1 is known that in undoped $Zn_{1-x}Mn_xSe$ with low Mn content the SLR process due to direct coupling of the Mn-system to the lattice is slow. In contrast, free carriers (electrons and holes) are strongly coupled with both, the magnetic ions and the phonons (see figure 5.6). As mentioned, the carrier interaction with magnetic ions is based on the fast spin-flip exchange scattering. Also electron-phonon coupling is very efficient

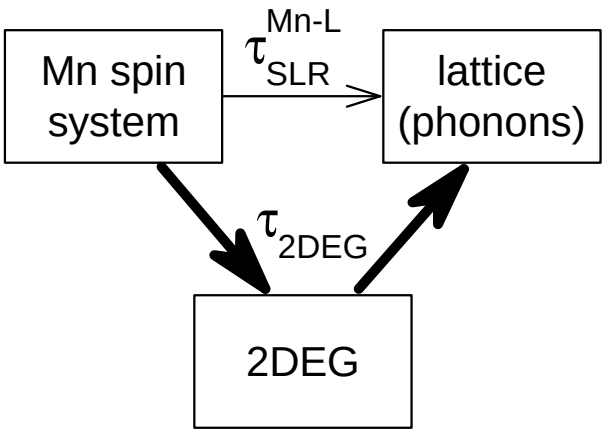

Figure 5.6 – Illustration of the bypass channel for energy transfer from the Mn-system to the lattice through the 2DEG.

with characteristic times of less than 0.1 µs. Therefore, the free carriers in doped structures serve as fast and efficient bypass channel for the slow direct SLR. The efficiency of this channel is controlled by the carrier density and can be characterized by a relaxation time τ_{2DEG}. The experimentally measured SLR time τ_{SLR} can be described in the following way:

$$\frac{1}{\tau_{SLR}} = \frac{1}{\tau_{SLR}^{Mn-L}} + \frac{1}{\tau_{2DEG}}, \tag{5.4}$$

where τ_{SLR}^{Mn-L} is the time characteristic for the process provided by direct interaction of the Mn-ions with the phonon system. Obviously is $\tau_{SLR}^{Mn-L} = \tau_{SLR}$ in undoped samples. The τ_{SLR}^{Mn-L} value can be obtained from measurements on nominally undoped samples. τ_{2DEG} was calculated by Scherbakov *et al.* [Sch01b] from the temporal variation of the inverse temperature of the Mn-ion system β_{Mn}

$$\left.\frac{d\beta_{Mn}}{dt}\right|_{e-Mn} = -\frac{1}{|C_\beta(B)|}\left.\frac{\partial E}{\partial t}\right|_{e-Mn} = \frac{1}{\tau_{2DEG}}\left(\beta_{Mn} - \beta_e\right), \tag{5.5}$$

using a formalism developed in [Kön00b]:

$$\tau_{2DEG} = \frac{|C_\beta(B)|}{|C_\beta(0)|}\left[t_{e-Mn}\left(B, E_F, \beta_e, \beta_{Mn}\right) + t_{SR}\left(E_F, \beta_e, \tau_{spin}\right)\right]. \tag{5.6}$$

C_β is the heat capacity of magnetic ions in the presence of a magnetic field and t_{e-Mn} and t_{SR} are characteristic relaxation times, which can be calculated by means of equations (14) and (25) in [Kön00b]. The other variables in equations 5.5 and 5.6 were already introduced in section 2.1.3.

From equation 5.6 can be deduced that the SLR does not only depend on the carrier density, but also on the magnetic field strength. This yields for the τ_{SLR}^{Mn-L}-channel, too, and was well studied by Scherbakov *et al.* [Sch01b]. Model calculations of the magnetic field dependencies of the three times in equation 5.4 according to [Sch01b] are given in figure 5.7. The dependence of τ_{SLR}^{Mn-L} in the nominally undoped sample is evaluated as interpolation of experimental data. Its devolution is nonmonotonic with a maximum at $B \sim 1$ T. For higher magnetic fields, τ_{SLR}^{Mn-L} decreases steadily [Sch01b, Str92]. The calculated times τ_{2DEG} (according to equation 5.6) for the interaction between 2DEG and Mn-ions show more complicated behavior. For low carrier densities ($n_e \lesssim 5{\times}10^{10}\,\mathrm{cm}^{-2}$) a strong exponential increase of the relaxation time with the magnetic field can be observed. The Zeeman-splitting of the conduction band yields for low electron densities to a strong polarization of the 2DEG already at low magnetic fields. Therewith, the probability of spin-flip exchange scattering decreases, as mentioned above. Hence, the relaxation time gets slower. But with increasing n_e the increase of the relaxation time is postponed for stronger fields. At very high densities ($n_e \gtrsim 8{\times}10^{10}\,\mathrm{cm}^{-2}$) even a decrease with growing magnetic field is observed. This is due to an increase of the amount of electrons near

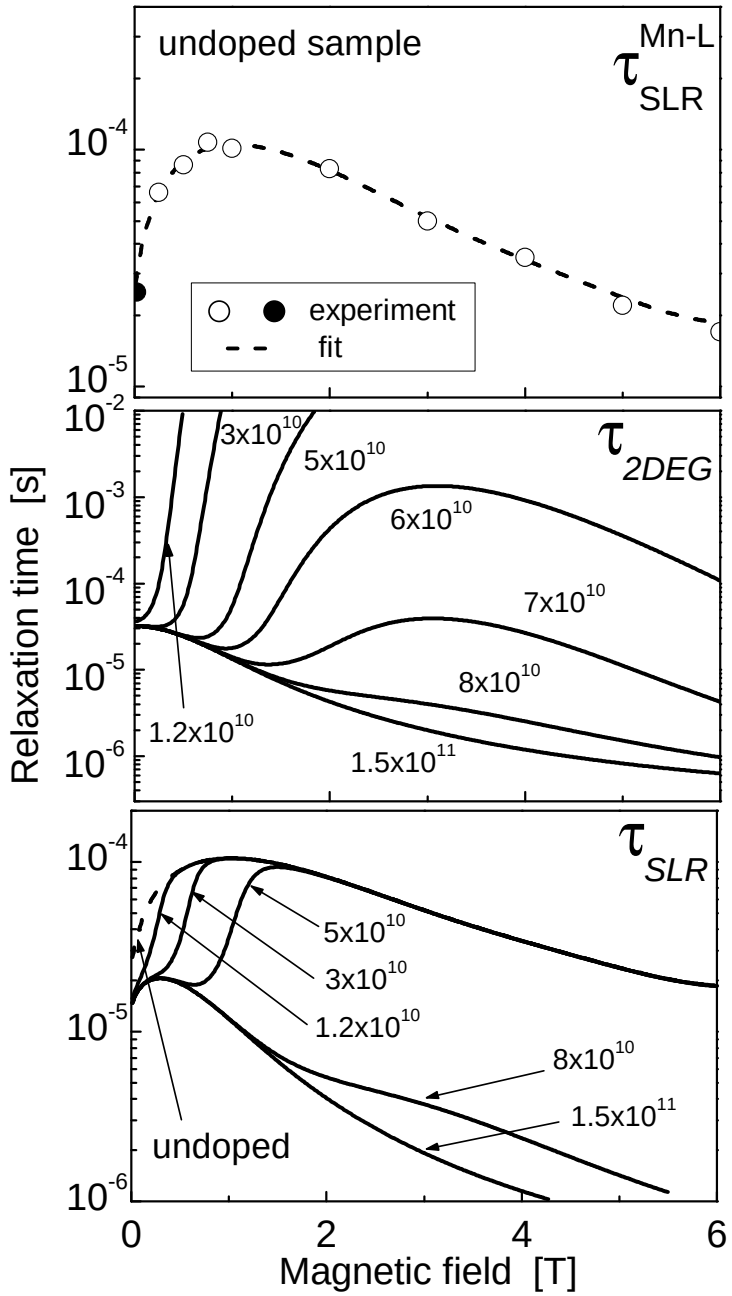

Figure 5.7 – Model calculations of the SLR time as function of the magnetic field; taken from [Sch01b]. The dependence for the SLR time in undoped material, τ_{SLR}^{Mn-L} shown in the top panel, is based upon experimental data ($Cd_{0.99}Mn_{0.01}Te$ QW). The calculations for τ_{2DEG} in a $Cd_{0.99}Mn_{0.01}Te$ QW with an electron gas of different densities, which are presented in the middle panel, were performed using the approach in [Kön00b]. From both dependencies the SLR time τ_{SLR} in doped materials can be achieved according to equation 5.4. Results are shown in the bottom panel. The 2DEG densities are given in cm^{-2}.

the Fermi-energy, which can participate in the spin-flip exchange interaction with increasing giant Zeeman-splitting of the Mn-ions with growing magnetic field.

The spin dynamics in doped QWs, which can be deduced according to equation 5.4 from the results of τ_{SLR}^{Mn-L} and τ_{2DEG}, is shown in the bottom panel of figure 5.7. For low carrier densities ($n_e < 7\times10^{10}\,cm^{-2}$) the SLR time is determined by τ_{2DEG} at magnetic fields below 1 – 2 T, but at higher fields by τ_{SLR}^{Mn-L}. Contrary, τ_{SLR}^{Mn-L} has nearly no influence on the τ_{SLR} behavior for high carrier densities ($n_e \geq 7\times10^{10}\,cm^{-2}$). These results can be directly compared with the experimental results for the doped (Zn,Mn)Se-based samples. At a magnetic field of $B = 3$ T, τ_{SLR} is for low carrier densities ($n_e \lesssim 6\times10^{10}\,cm^{-2}$) determined by τ_{SLR}^{Mn-L}, but for high carrier densities by τ_{2DEG}. As τ_{2DEG} is faster than τ_{SLR}^{Mn-L}, this coincides well with the observed

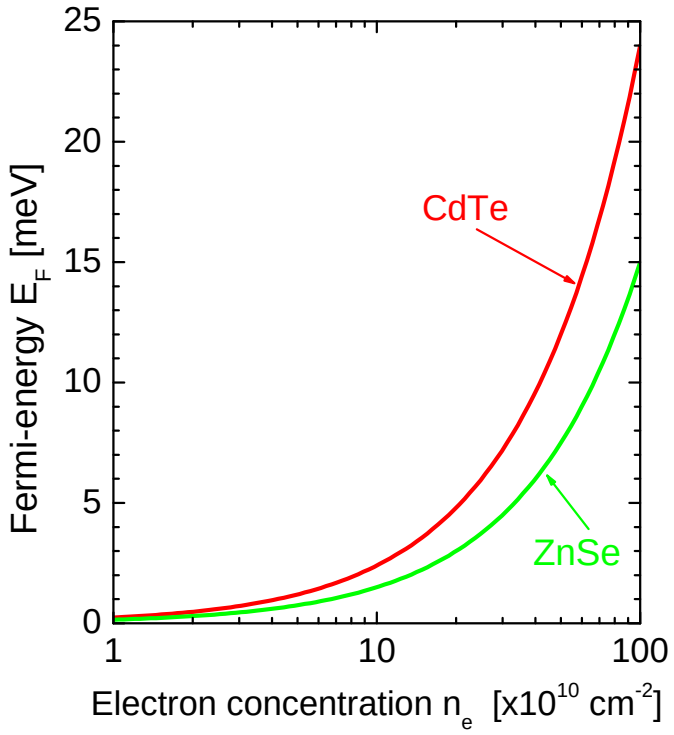

Figure 5.8 – Fermi-energy E_F of the 2DEG in CdTe and ZnSe for different electron concentrations.

increase of τ_{SLR} in nominally doped samples. Comprehensive experimental verification of the calculations was already given in [Sch01b].

For a qualitative explanation of the τ_{SLR} devolution in figure 5.7 it has to be taken into account, that the 2DEG becomes degenerated at low temperatures, if the electron density gets so large that the thermal energy became smaller than the Fermi-energy ($k_BT \ll E_F$). From this can be deduced two effects, which are both related to the fact that in external magnetic field flip-flop process of Mn-electron exchange should conserve not only spin but also the energy of the whole system. This was already briefly stressed in section 2.1.2 (especially figure 2.2).

On the one hand electrons in a degenerated electron gas are described by the Fermi statistic. This means that only electrons, which are separated by k_BT from the Fermi-energy, can participate in interactions. For electrons which take part in flip-flop processes with Mn-ions has to be further fulfilled that the Zeeman-splitting between the spin sublevels of Mn^{2+}-ions lies in this energetic region. The Zeeman-splitting is given by $\Delta E_{Zeeman}\,[\mathrm{meV}] = \mu_B g_{Mn} B = 0.116 \cdot B\,[\mathrm{T}]$. The other electrons in the depth of the 2DEG forbids the Pauli principle participation in electron-Mn interaction. For those no free final states exist, which the electrons can assume after the scattering. Hence, the SLR rate saturates with increasing carrier density for $E_F > k_BT$,ΔE_{Zeeman} and gets independent on n_e.

The second effect is based upon the relation between the Zeeman-splitting and Fermi-energy E_F. For small electron concentrations the Fermi-energy is rather small (e.g. $E_F = 0.3\,\mathrm{meV}$ for $n_e = 1.2{\times}10^{10}\,\mathrm{cm}^{-2}$; see figure 5.8). The Zeeman-splitting $\Delta E_{Zeeman} = \mu_B g_{eff} B$ exceeds already in small magnetic fields E_F due to the large effective g-factor in magnetic semiconductors. Thus, only the lower spin $S_z = -1/2$ subband is filled, if the nonmagnetic spin-relaxation

mechanisms (see section 2.2) are neglected, and one half of the Zeeman-splitting of the conduction band exceeds the Fermi-energy. The 2DEG becomes fully spin polarized. The subband with opposite spin ($S_z = +1/2$) lies above the Fermi-energy and, thus, cannot be occupied. This situation is represented by the energy ε_2 in figure 2.2 on page 73. Hence, for $\Delta E_{Zeeman} > E_F$ energy transfer from Mn-ions to 2DEG by spin-flip exchange scattering becomes impossible for higher magnetic fields. As the Zeeman-splitting increases with increasing magnetic field, this effect should reduce strongly the efficiency of the carrier bypass channel with growing magnetic fields and the τ_{SLR}^{Mn-L}-channel gets dominant.

As already discussed in [Kel04, Kön00a], also heating of the Mn-spin system is significantly modified by the presence of free carriers.

Summing up, the dynamic magnetic properties of DMS heterostructures are significantly modified by the presence of free carriers. The effect reaches one order of magnitude. This provides a new channel to control spin dynamics (spin-lattice or spin-spin relaxation rates) by tuning the density of the free carriers and opens the possibility to design structures with predefined SLR times. This very important possibility for spintronic applications will be scrutinized in the next chapter. It is obvious that the acceleration by the 2DEG vanishes for high Mn concentrations, where the direct SLR via phonons is faster than the flip-flop scattering with the electrons of the 2DEG.

Chapter 6

Control of spin-lattice relaxation

Contents

The huge recent process in application of modern semiconductor structures is linked to the flexibility in designing various parameters of these structures, for example the ability to design separately the static and dynamical properties. Especially control of the SLR time τ_{SLR} becomes obvious because it can turn out as a bottleneck for the speed of applications. Problematical is that in II-VI DMS both, the static properties and the dynamic properties, as seen from the investigations on the SLR dynamics in the previous chapter, depend strongly on the Mn concentration. This means that by designing a specific value for the giant Zeeman-splitting of carriers, which is proportional to the static magnetization, thereof the SLR time for the Mn-system, which corresponds to the chosen Mn content, is also determined. This correlation between the static and dynamic magnetization via the Mn content limits drastically the possibility of designing DMS structures.

In this chapter two approaches are presented to overcome this limitation and to control SLR in DMS heterostructures. The first approach is based upon the strong influence of the density of the free carriers (2DEG) in DMS on the SLR time, as shown in section 5.2. By applying an electric field to a DMS sample the density of free carriers can be changed, resulting in control of the SLR time. Contrary, the static magnetization in DMS QWs is rather independent of the presence of free carriers. The successful application of this technique is presented in section 6.1.

The second approach exploits that the limitation given by the correlation of static and dynamic magnetic properties is not a principal one. The underlying mechanisms for both are dif-

ferent, which makes it possible to decouple them. Neighboring and next-neighboring Mn-spins interact antiferromagnetically and form clusters. With increasing Mn content, more and more spins become coupled in the clusters and the typical cluster size increases [Lar86]. The static magnetization is mainly determined by paramagnetic Mn-spins not bound to clusters. Contrary to that, the magnetization dynamics is dominated by anisotropic Mn-Mn exchange interactions in antiferromagnetic clusters [Die95].

This strong sensitivity of the magnetization dynamics to clustering of the Mn-ions is exploited by the technological concept of "digital alloying" offered by MBE. In section 6.2 results on digital alloy (DA) samples are shown, whose SLR dynamics of magnetic Mn-ions has been accelerated by an order of magnitude compared to common "disordered alloys" with the same Mn concentration. Disordered alloys have a random distribution of magnetic ions in the cation sublattice. Remarkably no noticeable change in the giant Zeeman-spin splitting of excitonic states (i.e. no effect on the static magnetization) is observed in the studies. These results are extended towards DAs with parabolic shape of QW confining potential in section 6.3.

In the last section of this chapter the important influence of spin diffusion in acceleration of spin dynamics is discussed in structures with a nonuniform concentration of the magnetic Mn-ions.

6.1 Electric field control of 2DEG

As presented in section 5.2, the presence of free electrons in a $Zn_{0.996}Mn_{0.004}Se$ QW reduces τ_{SLR} by an order of magnitude. This is in line with the reported data for $Cd_{1-x}Mn_xTe$-based QWs, where the SLR has been accelerated by the presence of either electrons [Sch01b] or holes [Sch01a] provided by modulation doping. These free carriers, being efficiently coupled with both, the Mn-spins and the phonon system, provide an additional channel for spin and energy transfer from the Mn-spin system into the lattice. That opens the possibility to tune the SLR time by adjusting the carrier density. While Scherbakov *et al.* tuned the carrier concentration by laser illumination, here control of the carrier density by application of a gate voltage along the structure growth axis is presented.

Two $Zn_{0.985}Mn_{0.015}Se/Zn_{0.94}Be_{0.06}Se$ samples with semitransparent gold contacts, to apply a gate voltage, were fabricated as described in section A.1.3. The 2DEG density n_e in the unbiased structure was about 1.5×10^{11} cm^{-2} and was varied by the applied voltage from about 5×10^{10} cm^{-2} up to 3.1×10^{11} cm^{-2}. Thereby, the voltage was changed from $U = 0.7$ V to -1.5 V. The electron density is estimated from the linewidth of the emission line. This method is reliable when the Fermi-energy exceeds the inhomogeneous broadening due to alloy fluctuations, which is about 4 meV in the studied samples. It allows us to make direct evaluations for $n_e \geq 1.4\times10^{11}$ cm^{-2}, while only extrapolations were possible below this value.

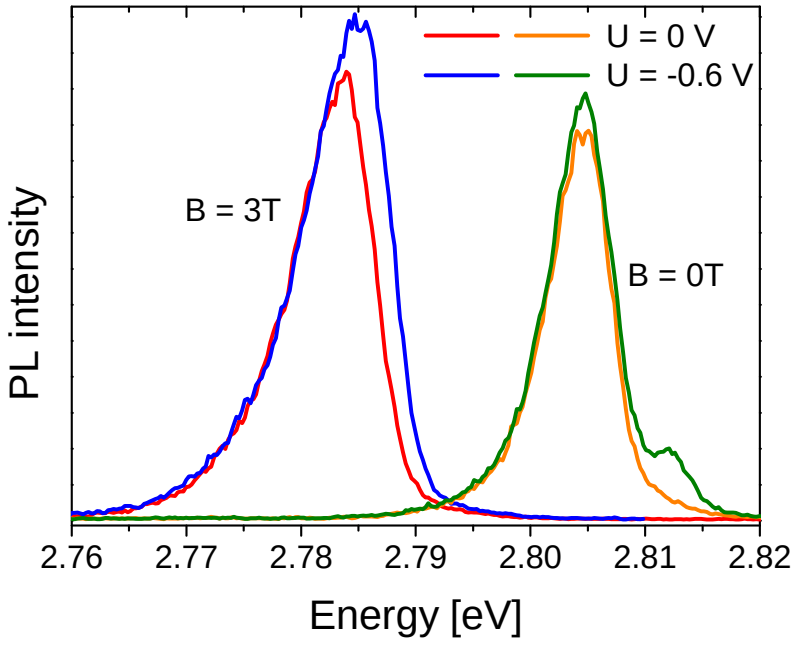

Figure 6.1 – PL spectra at different magnetic fields for two gate voltages of the $Zn_{0.985}Mn_{0.015}Se$/ $Zn_{0.94}Be_{0.06}Se$ sample 1.

Typical PL spectra for one of the $Zn_{0.985}Mn_{0.015}Se/Zn_{0.94}Be_{0.06}Se$ samples (sample 1) measured under cw excitation at magnetic fields of 0 T and 3 T are shown in figure 6.1. The spectra are given for two different gate voltages. The high structural and optical quality of the samples is approved by the narrow linewidth, not exceeding 5 meV. The low energy shift of the PL lines in external magnetic fields is due to the giant Zeeman-splitting of the heavy-hole exciton state. The shift value is equal to the one half of the giant Zeeman-splitting $\Delta E_{giantZeeman}/2$. A gate voltage of -0.6 V causes a small increase of the PL linewidth due to an increase of electron density, and a small decrease of the giant Zeeman shift at $B = 3$ T due to weak heating of the Mn-system by the electrical current through the structure (see figure 6.5 and discussion below). However, the smallness of this current heating does not influence significantly the measurements of the SLR dynamics.

As shown exemplary for $U = 0$ V and -0.6 V in figure 6.2, the giant Zeeman shift for different voltages is rather similar. It amounts to approximately 20 meV at $B = 3$ T and saturates at about 25 meV for higher fields. Measurements made for several other voltages show very similar behavior. This experimental behavior confirms that the static magnetization for the studied samples is independent of the gate voltage and, therefore, is not sensitive to the 2DEG density. This conclusion is in good agreement with the literature data [Kel03]. The solid line in figure 6.2 is a fit of the experimental data for $U = 0$ V by means of equations 3.2 and 3.3.

The measurements for magnetization dynamics have been performed at $B = 3$ T. In the studied structures with relatively low Mn concentration $x = 0.015$, the SLR time exceeds significantly the laser pulse duration of 7 ns and the typical lifetime of nonequilibrium phonons of about 1 µs. Therefore, the SLR time can be extracted from the decay of the dynamical response.

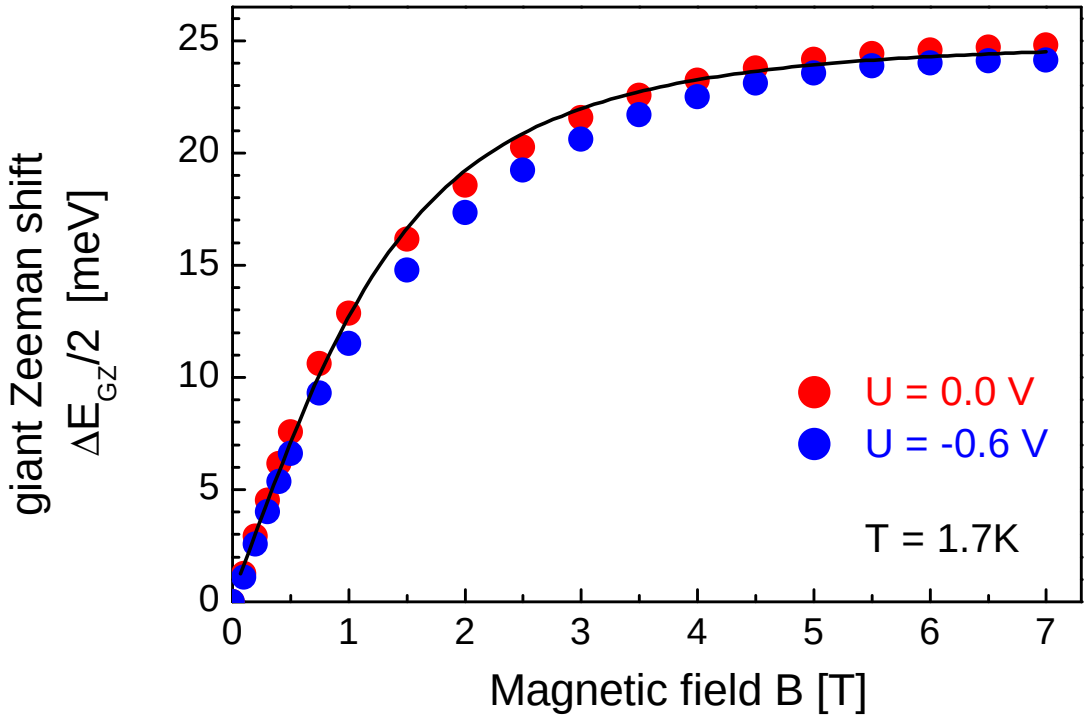

Figure 6.2 – Giant Zeeman shift of PL line (σ^+ polarized) for two different gate voltages ($U = 0$ V and -0.6 V). The line shifts to lower energies. PL is excited by a cw HeCd laser with a power density of 10 mW/cm^2. The solid line shows a fit along equation 3.2 with $x = 0.015$, $S_{eff} = 2.4$ and $T_{eff} = 2.9$ K. The effective values were calculated according to equations 1.55 and 1.56. The measurements were performed with the $Zn_{0.985}Mn_{0.015}Se/Zn_{0.94}Be_{0.06}Se$ sample 1.

The respective experimental data measured for three gate voltages are plotted in figure 6.3. For a suitable comparison, the data sets are normalized to the maximum shift $\Delta E_{PL}^{\max}$ and plotted on a logarithmic scale. Monoexponential fits are shown by solid lines together with the corresponding values of τ_{SLR}. The SLR time decreases from 140 µs for a gate voltage of $U = 0.6$ V down to 1 µs for $U =$ -1.5 V.

Detailed treatment of the SLR time dependence on the voltage applied is depicted in figure 6.4. For voltages between $U = 0.7$ V and -1.5 V the SLR time decreases by more than two orders of magnitude from 160 µs down to 1 µs. It is, therefore, evident that the magnetization dynamics is accelerated by the presence of a 2DEG, whose concentration is tuned by the gate voltage. SLR time as long as 530 µs have been reported for an undoped (Zn,Mn)Se/(Zn,Be)Se QW with a Mn concentration of $x = 0.015$ (sample CB1581 in table A.2). Therefore, the overall tunability range of the SLR time approaches three orders of magnitude.

The applied voltage induces a current flow through the structure with typical values given in figure 6.5 by closed circles. The current may induce heating of the Mn-system. This effects should be taken into account when treating the static and dynamic magnetization by means of the optical spectroscopy. To evaluate it for the studied structures, in the same panel the energy position of PL line maximum is plotted as a function of gate voltages at $B = 3$ T. One can see that the current heating effect is relatively small. In a wide voltage range from 0.7 V

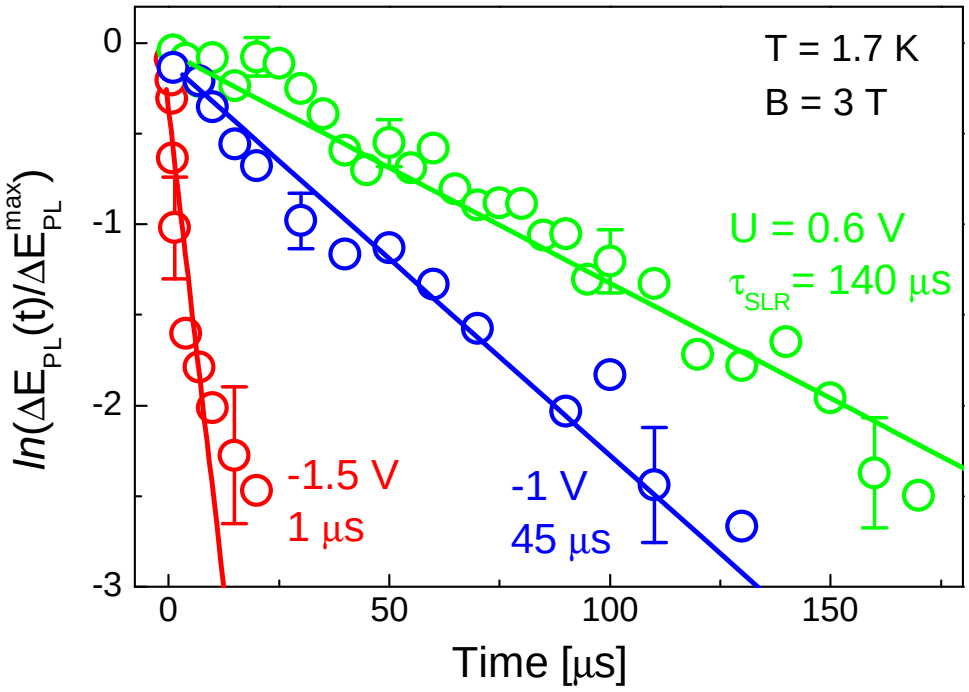

Figure 6.3 – Temporal evolution of PL line shift corresponding to the cooling of the Mn-spin system heated by pulsed laser excitation. The SLR times were evaluated from mono-exponential fits given by solid lines. The measurements were performed with the $Zn_{0.985}Mn_{0.015}Se/Zn_{0.94}Be_{0.06}Se$ sample 1.

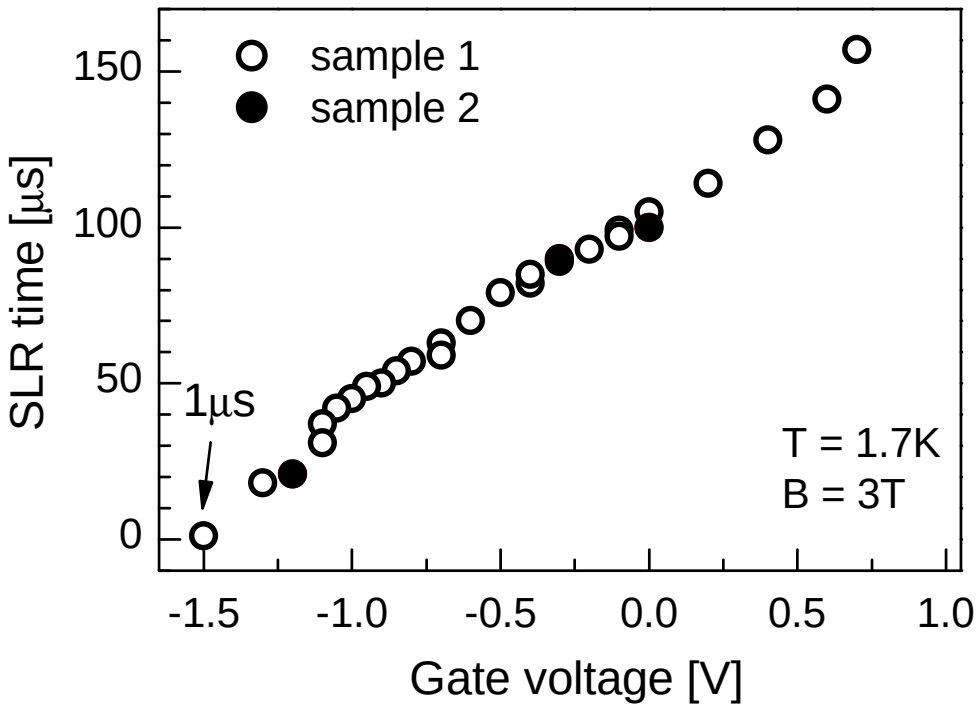

Figure 6.4 – SLR time dependence on gate voltage for n-type modulation-doped $Zn_{0.985}Mn_{0.015}Se/Zn_{0.94}Be_{0.06}Se$ QW. The measurements were performed at $B = 3\,\mathrm{T}$ and $T = 1.7\,\mathrm{K}$.

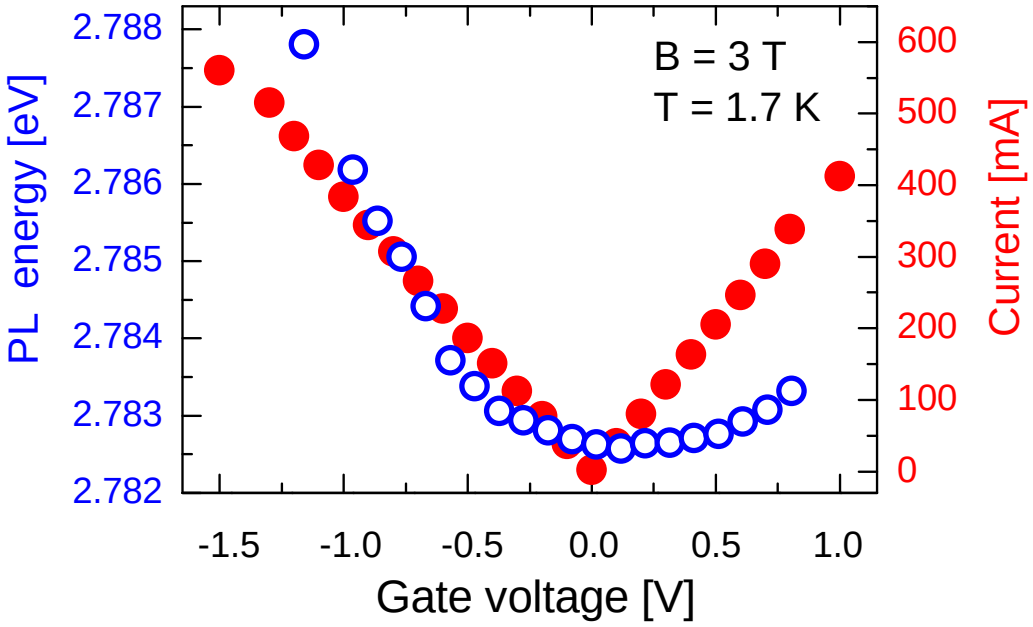

Figure 6.5 – Gate voltage dependence of the PL line maxima energy (open circles) and current (closed circles). The measurements were performed with the $Zn_{0.985}Mn_{0.015}Se/Zn_{0.94}Be_{0.06}Se$ sample 1.

to -0.7 V the energy shift is smaller that 2 meV, which is less than 10 % of the giant Zeeman shift at 3 T. This shift corresponds to a change of the Mn-spin temperature by only 1 K. For U = -1.2 V the energy shift rises to 5 meV corresponding to heating by 2.5 K. It is stressed here that these estimations give the upper boundary for the lattice temperature increase due to current flow, which in practice is considerably smaller than the elevation of T_{Mn}. Therefore, in our experimental conditions the effect of the lattice temperature on the measured SLR time can be neglected.

It is also interesting that independent of the voltage polarity, the PL line shifts to high energies, i.e. the shift is dominated by the Mn heating. The possible contribution of the quantum-confined Stark shift is very small. For the measurements of the Mn-spin dynamics this temporally constant shift is not significant, because only the evolution of the energy shift with time is analyzed. Possible explanation for the more pronounced shift for negative voltages is the asymmetry of the contacts. The voltage was applied between the doped substrate and buffer layers and a 50 nm thick semitransparent gold contact deposited on the top of the sample. In this case the profile of the voltage drop may depend on the polarity.

6.2 Engineering of spin-lattice relaxation by digital growth

So far the common "disordered alloys" with a random distribution of magnetic ions in the cation sublattice were investigated, which have the disadvantage of a strong correlation between the static and dynamic magnetic properties via the Mn concentration. A way to overcome this fun-

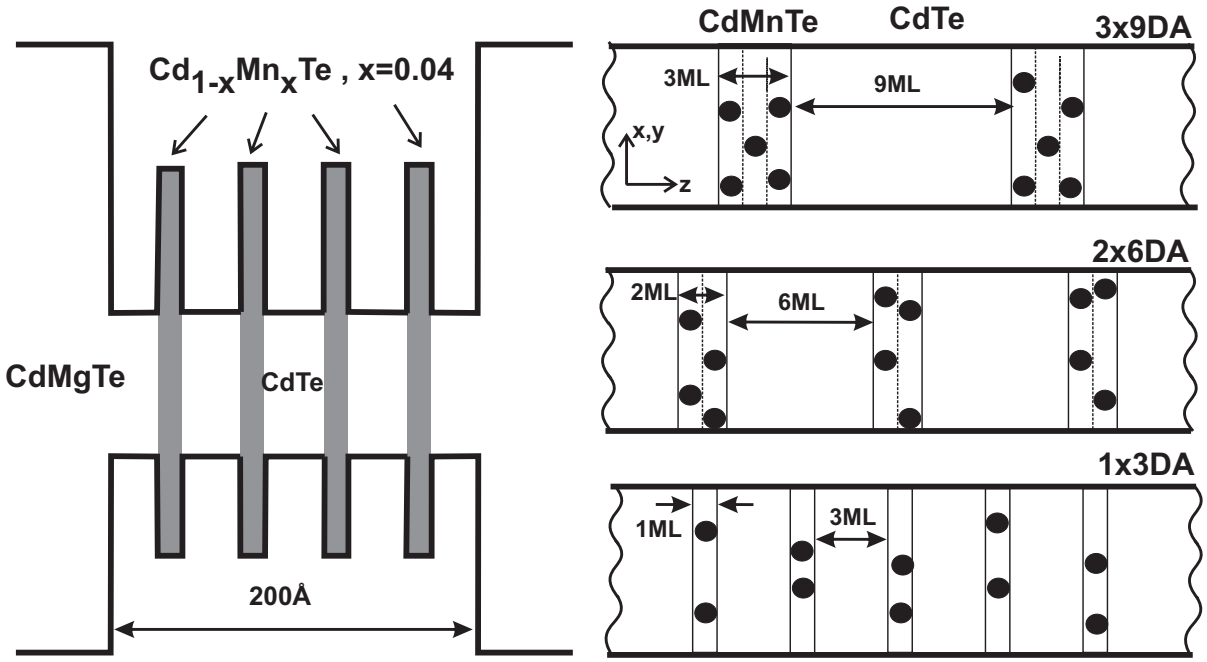

Figure 6.6 – Schematic diagram of the conduction and valence band profile and Mn-ion profile in (Cd,Mn)Te DA structures.

damental limitation is offered by the technological concept of "digital alloying", because static and dynamic properties of DMS are governed by different mechanisms. Paramagnetic Mn-spins give the main contribution to the static magnetization, and their coupling into antiferromagnetic Mn-Mn clusters for increasing Mn content is unfavorable in this respect. On the other hand, the SLR dynamics is controlled by anisotropic exchange interactions of Mn-ions in such clusters.

The concept of growing digital alloys (DA) is described briefly in section A.1.4. In the area of DMS the concept of digital magnetic QWs was introduced in 1995 [Cro95, Woj95]. The possibility of unique spin splitting and spin dynamics engineering was demonstrated for MnSe/(Zn,Cd)Se DAs [Cro95] and for (Cd,Mn)Te/CdTe digitally graded magnetic QW structures [Woj98]. A strong variation of the carrier spin dynamics with the DA parameters has been found. However, no dependence of the Mn-spin dynamics has been established yet. In this section it will be show that the spin dynamics can be engineered to a desired value by a proper choice of DA parameters.

For the studies presented here, three digital alloys (DA), consisting of short-period superlattices $Cd_{0.96}Mn_{0.04}Te$/CdTe with layers of one to ten monolayers, and, additionally, two reference disordered alloy samples with 1-µm-thick layers of $Cd_{0.985}Mn_{0.015}Te$ and $Cd_{0.96}Mn_{0.04}Te$ for comparative studies, were grown. The digital structures are labeled according to the thickness of magnetic and nonmagnetic sheets given in the monolayers (ML): the first sample 1×3DA consists of 18 periods of 1 ML/3 ML, the second sample 2×6DA has nine periods of 2 ML/6 ML and the third sample 3×9DA has six periods of 3 ML/9 ML (see figure 6.6). This choice of layer thicknesses provides the same average Mn concentration $x_{DA} \approx 0.013$ in the

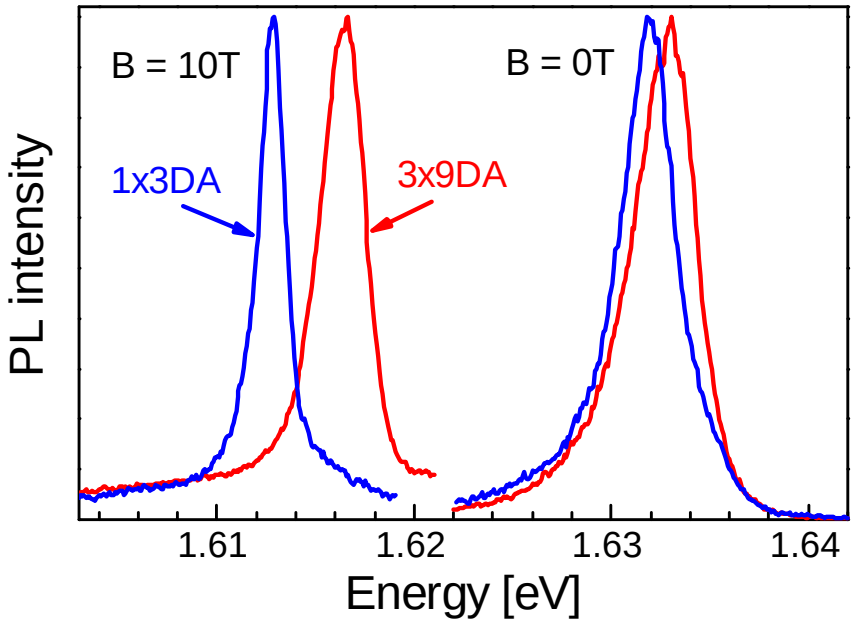

Figure 6.7 – PL spectra for the 1×3 DA (solid line) and the 3×9 DA (dashed line) samples at $B = 0\,\mathrm{T}$ and 10 T. The measurement were performed at $T = 1.7\,\mathrm{K}$.

three DA samples. It is known for DMS heterostructures that the Mn-ions at the interface can diffuse into nonmagnetic layers over a depth of 1 – 2 ML [Oss93]. Therefore, in DA samples the real Mn profile may differ from the nominal technological design.

Typical PL spectra of DA samples measured under cw excitation are given in figure 6.7. Narrow linewidths, not exceeding 4 meV, evidence the high structural and optical quality of the DAs. In external magnetic field the PL lines shift to lower energies as shown in figure 6.8. This shift is equal to one half of the giant Zeeman-splitting of heavy-hole excitons $\Delta E_{giant Zeeman}$.

All three DA samples show very similar giant Zeeman shifts. The Mn contents x''_{DA} extracted from fits of the shifts by equations 3.2 and 3.3 are 0.0147, 0.0130 and 0.0123 for the 1×3DA, 2×6DA and 3×9DA samples, respectively. These values are very close to the average Mn concentration in the DAs $x_{DA} \approx 0.013$, if the distribution of Mn component was assumed to be random. Thus, it is concluded that the static magnetic properties of the studied DAs are weakly affected by the DA growth parameters. Small reduction of the giant Zeeman shift for the DA with thicker $Cd_{0.96}Mn_{0.04}Te$ layers can be explained by binding the paramagnetic Mn-spins into clusters.

The dynamics of SLR of Mn-ions has been measured in a magnetic field of 3 T from the time-resolved energy shift of the PL maxima $\Delta E_{PL}(t)$ induced by the laser pulses. In figure 6.9 these data are given normalized to the maximum shift $\Delta E_{PL}^{\max}$. Closed symbols show data for the three DA samples and open symbols are data for the reference disordered alloys. The SLR times τ_{SLR} of 27 µs and 2.2 µs measured for the disordered alloys with $x = 0.015$ and 0.04, respectively, are in good agreement with literature data (see [Kne06a, Sch00a] and references therein). It is remarkable that τ_{SLR} for all DA samples fall in the 2.5 – 9.5 µs range, i.e., the

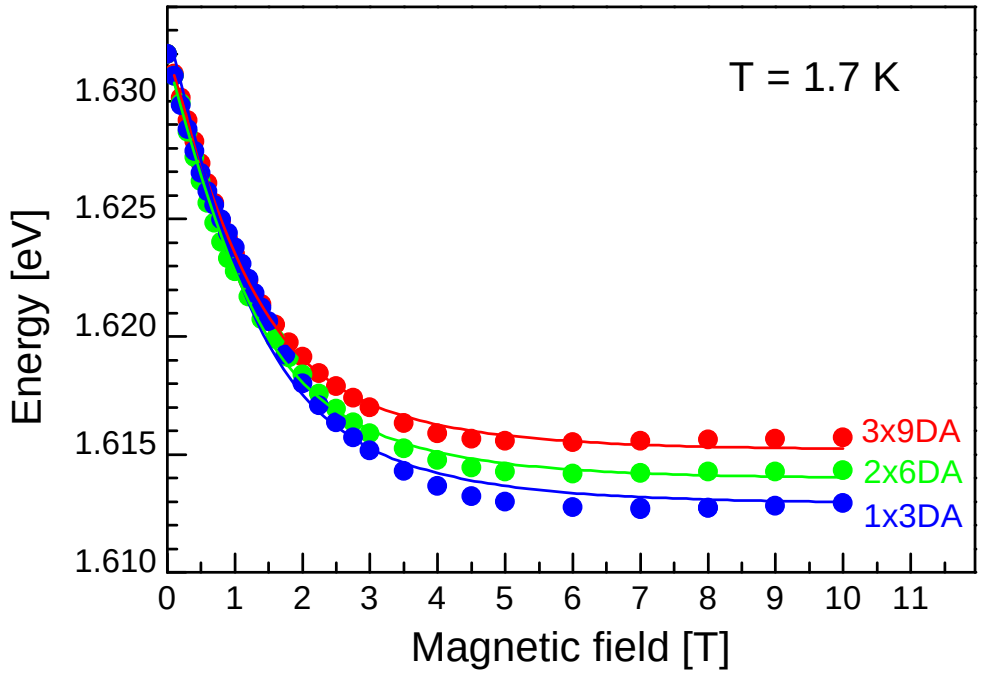

Figure 6.8 – Giant Zeeman-splitting of the PL line (σ^+ polarized) for the three different DA samples. The PL is excited by a cw semiconductor laser with the power density 0.22 W/cm². Lines show best fits to the data using equations 3.2 and 3.3 to determine the average Mn content of the DAs. For the fits $S_{eff} = 1.5$ and $T_0 = 1$ K were used.

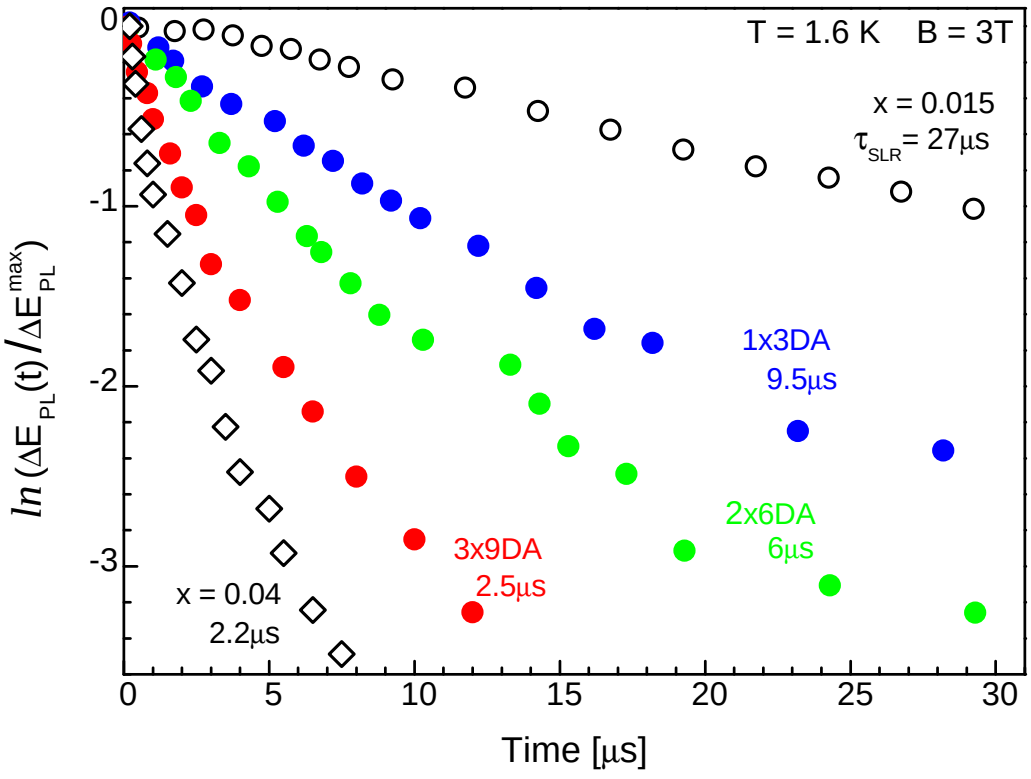

Figure 6.9 – Dynamical shift of the PL lines in DAs showing the cooling of the Mn-spin system heated by pulsed laser excitation. Open symbols correspond to disordered alloys and closed symbols are for the DAs. SLR times were evaluated from mono-exponential fits.

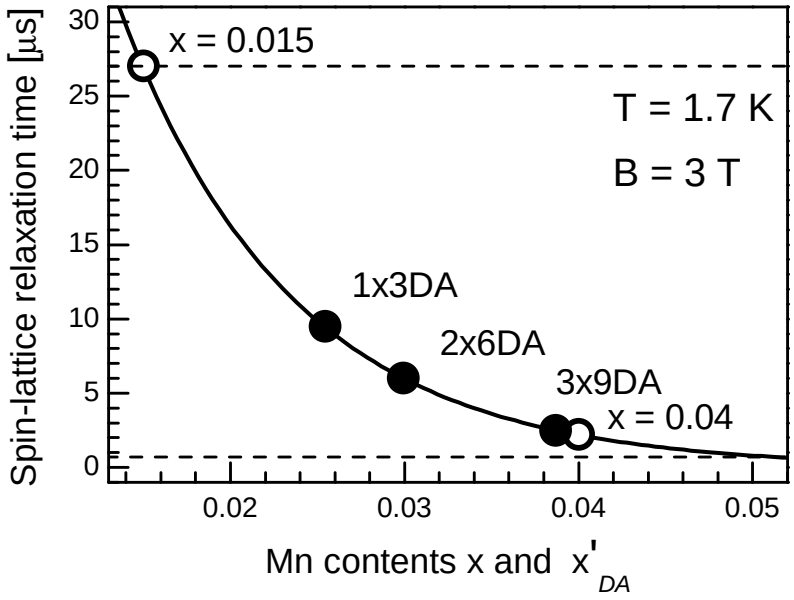

Figure 6.10 – SLR times versus Mn content x in disordered alloys (open circles are the results measured for the DAs, and the solid line is taken from literature data). Closed circles are DA data assigned to the solid line due to their τ_{SLR} values. Their linking to the solid line allows evaluation of the effective Mn content x'_{DA}.

DA SLR times are up to ten times shorter than the 27 µs of the reference $x = 0.015$ sample, whose Mn concentration is very similar to $x_{DA} \approx 0.013$. This demonstrates that the goal to tune independently static and dynamic magnetic properties of DMS materials is achieved by introducing DAs.

In order to give a detailed insight into the capabilities offered by DAs, the DA data points were compared with the $\tau_{SLR}(x)$ dependence known for disordered alloys $Cd_{1-x}Mn_xTe$ [Kne06a, Sch00a]. The latter is shown by the solid line in figure 6.10. The data points for DA samples are positioned on this line according to their τ_{SLR} values, from which an effective Mn concentration x'_{DA} can be assigned to each DA. The x'_{DA} values range from 0.025 up to 0.039 and exceed significantly $x_{DA} \approx 0.013$.

Another instructive way to present the tunability of the DA parameters is given in figure 6.11. Here the correspondence diagram for the effective Mn concentrations determined by the

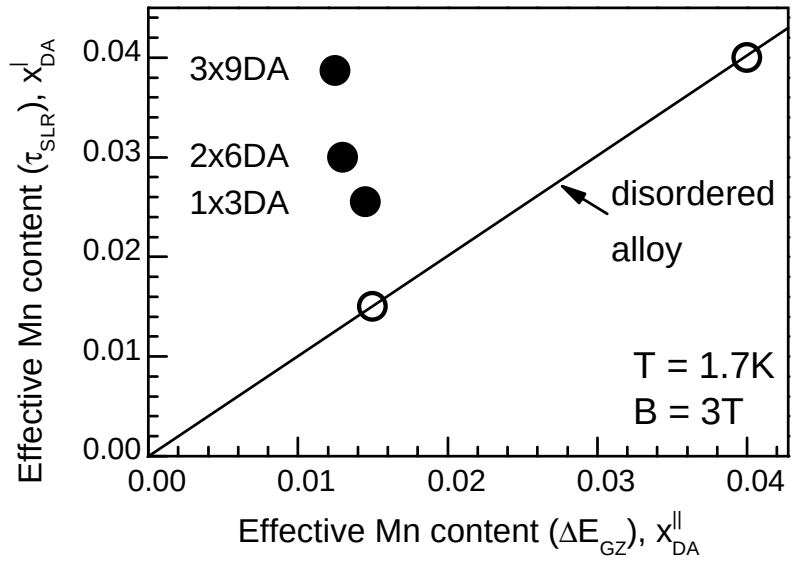

Figure 6.11 – Diagram linking the static (giant Zeeman-splitting) and the dynamic (SLR time) magnetic characteristics of disordered (open circles and solid line) and digital (closed circles) alloys. In disordered alloys applies $x' \equiv x'' \equiv x$.

static (i.e., the giant Zeeman-splitting, the abscissa x''_{DA}) and the dynamic (i.e., the SLR time, ordinate x'_{DA}) magnetic properties in DMS is shown. For disordered alloys these effective concentrations are equal to the "real" Mn content, i.e., $x' \equiv x'' \equiv x$. As a result, the disordered alloys are described in the diagram by the straight solid bisecting line. The open symbols are the experimental data for the two reference disordered alloy samples. The DA data points do not fall onto this line, confirming that the static and dynamic parameters of magnetization in the DMS DAs can be tuned separately.

The origin for the DA flexibility lies in the different mechanisms responsible for the static magnetic properties, i.e., the giant Zeeman-splitting of excitons measured here, and the SLR dynamics. The giant Zeeman-splitting at relatively low Mn concentrations is proportional to the number of Mn-ions and to the overlap of the exciton wave function with a specific Mn-ion. Both these quantities do not vary significantly in wide magnetic QWs with DAs. As demonstrated by figure 6.8, the approach of using the average Mn content for predicting the value of the giant Zeeman-splitting in case of $Cd_{0.95}Mn_{0.05}Te$/CdTe DA works very well.

In contrast, the SLR rate of the Mn-ions is extremely sensitive to the probability of finding another Mn-ion at the nearest-neighbor or next-to-nearest-neighbor position, i.e., it is very sensitive to the Mn-ions clustering. As already mentioned, the reason for that is that the SLR of Mn^{2+}-ions in II-VI semiconductors is controlled by anisotropic Mn-Mn magnetic interactions in clusters [Sch00a]. It is obvious from the scheme of Mn distribution in DAs (see figure 6.6) that the clustering probability is reduced in the 1×3DA structure due to the two-dimensional arrangement of the magnetic ions, but it increases significantly in the 3×9DA sample due to formation of clusters along the growth direction. This is the essential point of this technique. Digital alloying considerably changes the clustering, which modifies the magnetization dynamics, but keeps the number of paramagnetic spins, which control the static magnetization, constant. The reduction of the SLR time in the 3×9DA sample is, therefore, a direct consequence of the stronger clustering probability of Mn-ions in the DA barriers.

This idea is supported by measurements preformed by Scherbakov *et al.* on very thin QWs (6 Å) [Sch04]. Considerable increase of the SLR time by at least 10 times compared with bulk DMS was observed. In thin QWs the situation is similar to the 1×3DA structure. The formation of Mn clusters along growth direction is restricted and the density of clusters is smaller in thin QWs than in in bulk DMS or wide QWs. Hence, the SLR time is longer.

6.3 Spin-lattice relaxation in parabolic and half-parabolic quantum wells

The ability of acceleration of the SLR time by digital alloying has been successfully demonstrated in the previous section. However, the equidistant fragmentation of the active CdTe layer

by the CdMnTe layers results in higher excitation energies, because of the higher absorption in small QWs. This can be overcome by digital sample growth with variation of the respective layer thicknesses and distances. Possible solution is a continuous decrease of the manganese concentration in each layer towards the mid of the QW. Such a variation, which is shown in figure 6.12, results in a parabolic and half-parabolic, respectively, shape of the confining potential. Thus, in these structures several small QWs with corresponding energy levels and wavefunctions do not occur, but one large parabolic well is created with widths exceeding 200 Å. Here respective energy levels and wavefunctions form, as shown in figure 1.23 on page 59. Simultaneously, layers with high Mn content are present, which should be able to accelerate SLR. This is to be proved in this section.

Application of digital growth to fabricate PQWs traces back to [Mil84a, Woj96]. Here, four parabolic and two half-parabolic QWs covering barrier Mn concentrations from $x = 0.13$ to 0.85 are studied. The QW widths are either 190 Å or 254 Å. Survey of the technological sample parameters is given in table A.1 in the appendix.

Measurements of the giant Zeeman shift, exemplarily for some of the parabolic quantum wells (PQW), are given in figure 6.13. The giant Zeeman shift is very similar for all measured PQW samples. Analogue to the previous section, an effective Mn content x''_{PQW} can be calcu-

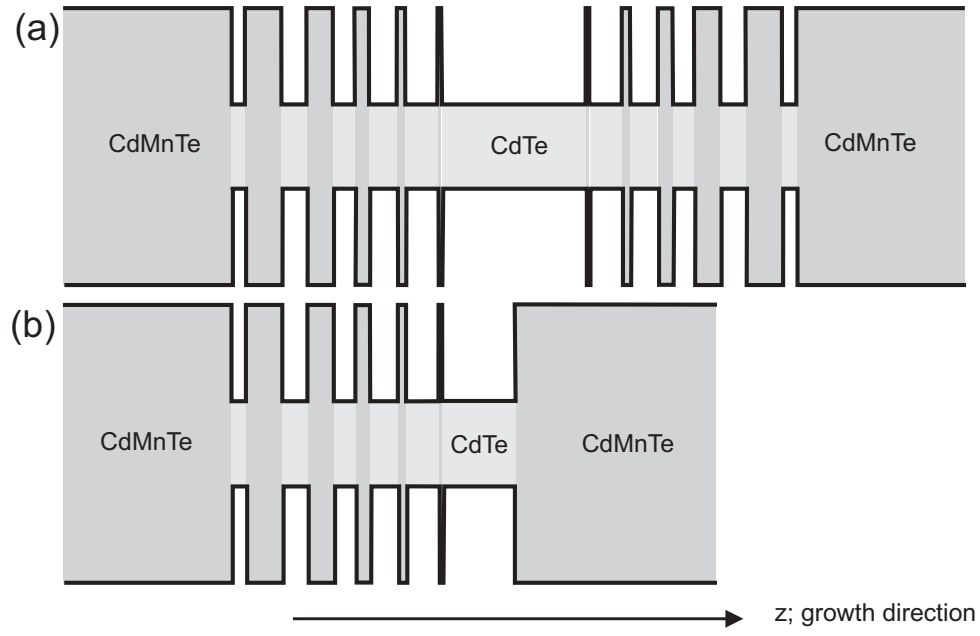

Figure 6.12 – Scheme of digital growth profile for (a) parabolic and (b) half-parabolic QW. For simplification and clarity the parabolic structure can be divided in 11 semi-wide periods, each containing a $Cd_{1-x}Mn_xTe$ layer with the same Mn concentration as the barrier. Only the medial period does not contain such a layer. As described in section A.1.4, the samples rather consist of 40 manganese layers. From the thickness of the $Cd_{1-x}Mn_xTe$ layers results the parabolic devolution of the potential. The half-parabolic structure has on one side a rectangular confining potential. The resulting devolution of the conduction band edge, wavefunctions and energy levels are given in figure 1.23 on page 59.

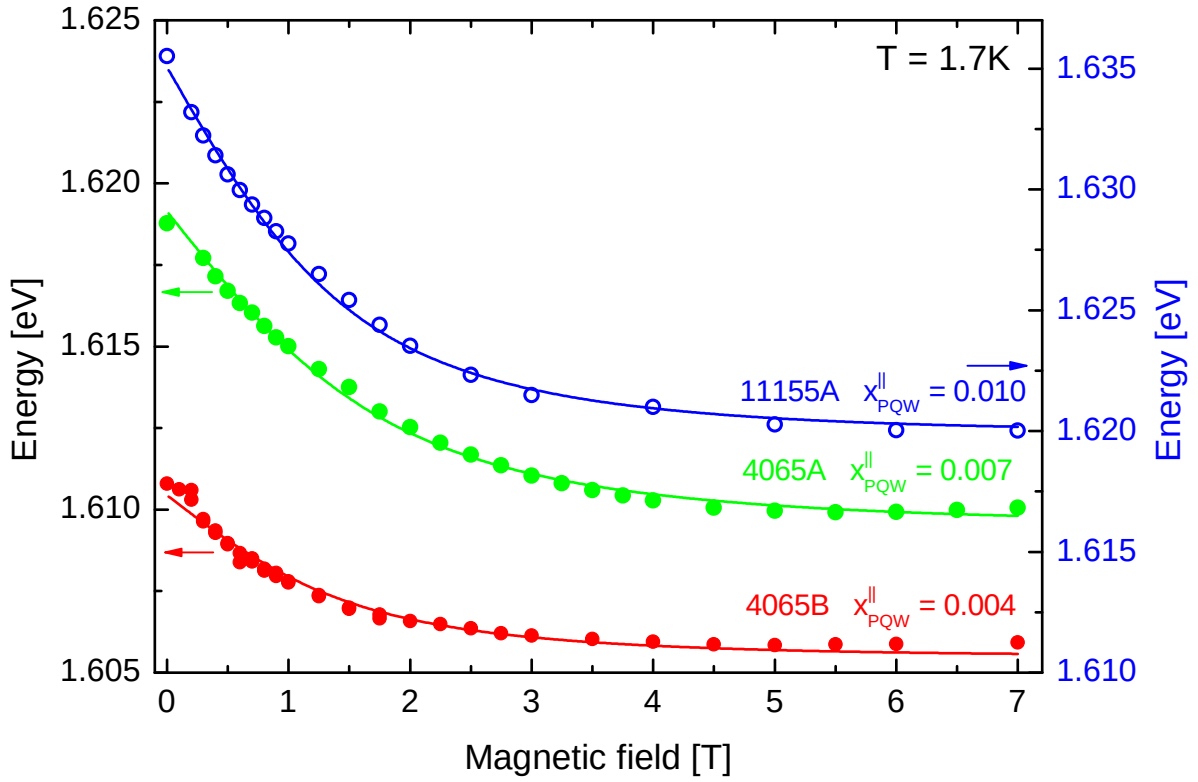

Figure 6.13 – Giant Zeeman shift of the PL line for one HPQW (11155A) and two PQW (4065A/B) samples. The solid lines correspond to Brillouin fits with $S_{eff} = 2.5$ and $T_0 = 0\,\mathrm{K}$, to achieve the effective Mn content related to the giant Zeeman-splitting x''_{PQW}. These effective parameters occur at very low Mn contents $x < 0.01$, which were evaluated for x''_{PQW}. For more perspicuous illustration for the PQW and HPQW samples, different energy axes are used.

lated according to equation 3.3 from the giant Zeeman shift. These calculations were performed with $S_{eff} = 2.5$ and $T_0 = 1\,\mathrm{K}$. The values of all measured samples for x''_{PQW} range from 0.004 up to 0.011, which is for each sample considerably below the manganese barrier content (see table 6.1). It should be mentioned that for measurements at higher magnetic fields $B > 7\,\mathrm{T}$, a considerably diamagnetic shift occurs (see section 1.5.4), which has to be taken into account for calculation of x''_{PQW} [Arl07].

The dynamics of SLR of Mn-ions has been measured in a magnetic field of 4 T from the time-resolved energy shift of the PL maxima $\Delta E_{PL}(t)$ induced by the laser pulses. In figure 6.14 these data are given normalized to the maximum shift $\Delta E_{PL}^{\max}$ for three samples. Analogue to the previous section, these SLR times can be converted into effective Mn contents x'_{PQW}. It is noteworthy that for the half-parabolic quantum well (HPQW) samples two different dynamics can be observed. This is highlighted for both measured HPQW samples in figure 6.15. Both can be separately fitted via mono-exponential function, resulting in two different relaxation times and, hence, two different effective Mn concentrations. Reason for this behavior is devoted to two different possible paths for the spin excitation in regions with low Mn concentration (i.e. slow SLR time) to propagate through the QW towards regions with higher Mn content, where it relaxes to the lattice. The lowest Mn contents are in the region close to the right (Cd,Mn)Te

Table 6.1 – Experimentally determined values for τ_{SLR}, x'_{PQW} and x''_{PQW} for the PQW and HPQW samples. Parabolic structures are labeled by "P" and half-parabolic structures by "HP" in column "type". x barrier is the technological Mn content of the barrier. x'_{PQW} is the effective Mn content linked to the dynamic properties, which was derived from the SLR time τ_{SLR}. In contrast x''_{PQW} is the effective Mn content linked to the static properties, which was derived from the giant Zeeman-splitting.

code	type	x barrier	τ_{SLR} [ns]	x'_{PQW}	x''_{PQW}
4065A	P	0.13	730	0.048	0.007
4065B	P	0.13	700	0.050	0.004
9205B	P	0.68	70	0.082	0.009
9215A	P	0.85	20	0.110	0.011
11155A	HP	0.25	7 (τ_1)	0.150 (τ_1)	0.010
			270 (τ_2)	0.062 (τ_2)	
9265A	HP	0.77	12 (τ_1)	0.140 (τ_1)	0.005
			400 (τ_2)	0.057 (τ_2)	

barrier (compare figure 6.12(b)). Spin excitation can go in direction of the parabolic potential with smoothly rising Mn content as well as in direction of the right barrier with abruptly rising Mn content. As known from the previous sections, the SLR is faster in regions with higher Mn concentration, because of the importance of Mn clustering for the propagation of spin exci-

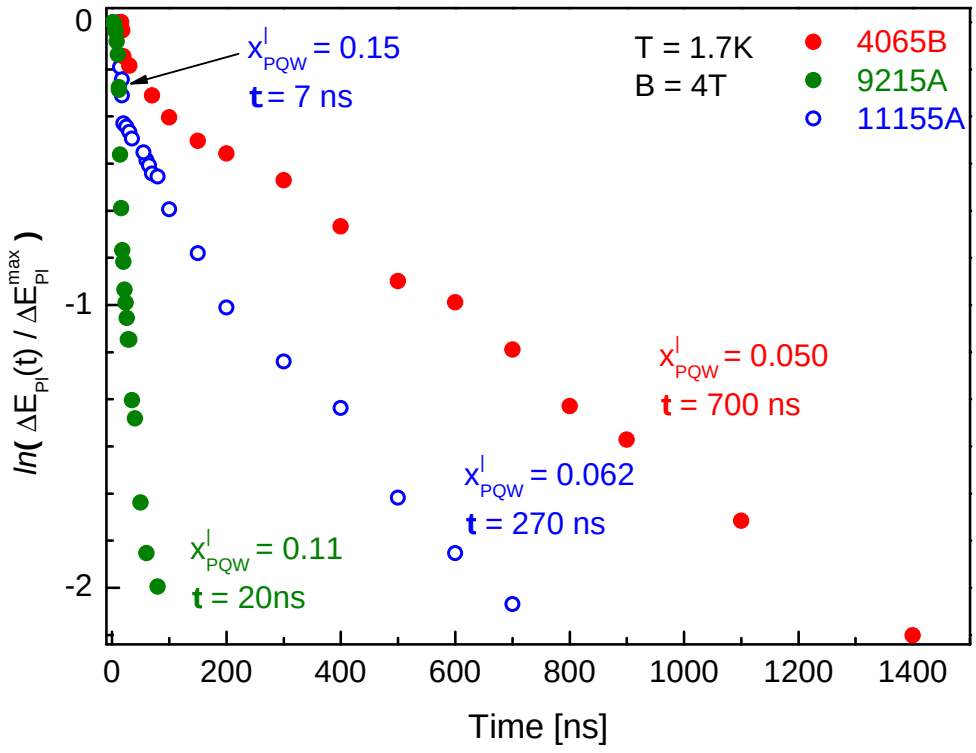

Figure 6.14 – Dynamical shift of the PL lines in (H)PQWs, showing the cooling of the Mn-spin system heated by pulsed laser excitation. Open symbols correspond to a HPQW and closed symbols to PQWs. SLR times were evaluated from mono-exponential fits.

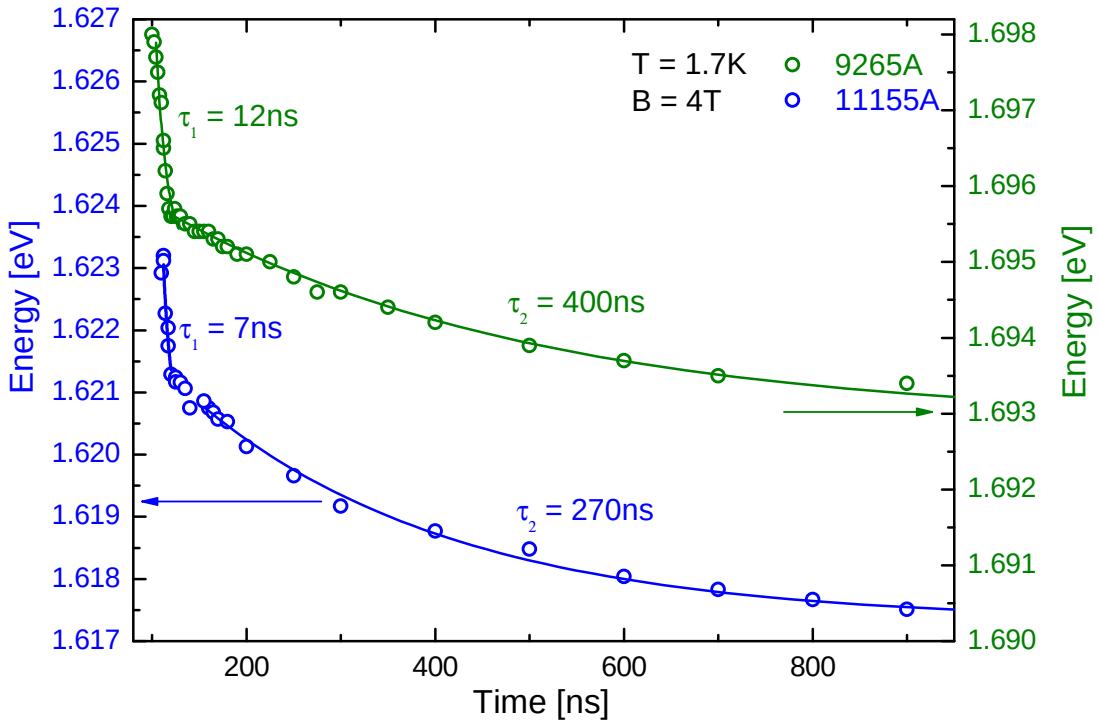

Figure 6.15 – Temporal evolution of the PL line maximum position after laser pulse for the HPQW samples. Remarkable is the existence of two relaxation times, derived from two monoexponential fits.

tation. Therefore, one can conclude that the relaxation through the rectangular confining profile is responsible for the fast part of signal decay. The very high concentration of $x = 0.25$ and $x = 0.77$, respectively, leads to the very short SLR times in the nanosecond range. However, it is not favorable for all spins in regions of the QW with low Mn concentration to diffuse to the barrier. To decide which fraction of spins relaxes via this path, is not an easy task. The diffusion of spins in regions with faster SLR increases the Mn temperature in this region and, therewith, decreases the efficiency of the diffusion. Thus, the relation between the slow SLR time and the diffusion time is important, as well as the fast SLR time, which is important for the cooling of the region in which the spin diffuse. Furthermore, it is also possible that spins diffuse in direction of the parabolic QW with increasing Mn content, as the SLR time increases smoothly in this direction. This path is responsible for the longer SLR time. That spin diffusion is important also for this path can be easily concluded from the fact that the observed times of $\tau_{SLR} = 400\,\text{ns}$ and $\tau_{SLR} = 270\,\text{ns}$, respectively, are considerably shorter than expected for a comparable average DA.

The SLR times and effective Mn contents x'_{PQW} for all measured samples are collected in table 6.1. As expected, the results for x'_{PQW} and x''_{PQW} do not conform to the relation $x'_{PQW} \equiv x''_{PQW} \equiv x$, which holds true for disordered alloys. The effective Mn contents of each sample differ significantly from each other and from the technological Mn content. The effective Mn contents x'_{PQW}, evaluated from the SLR time, are about one order greater than the ef-

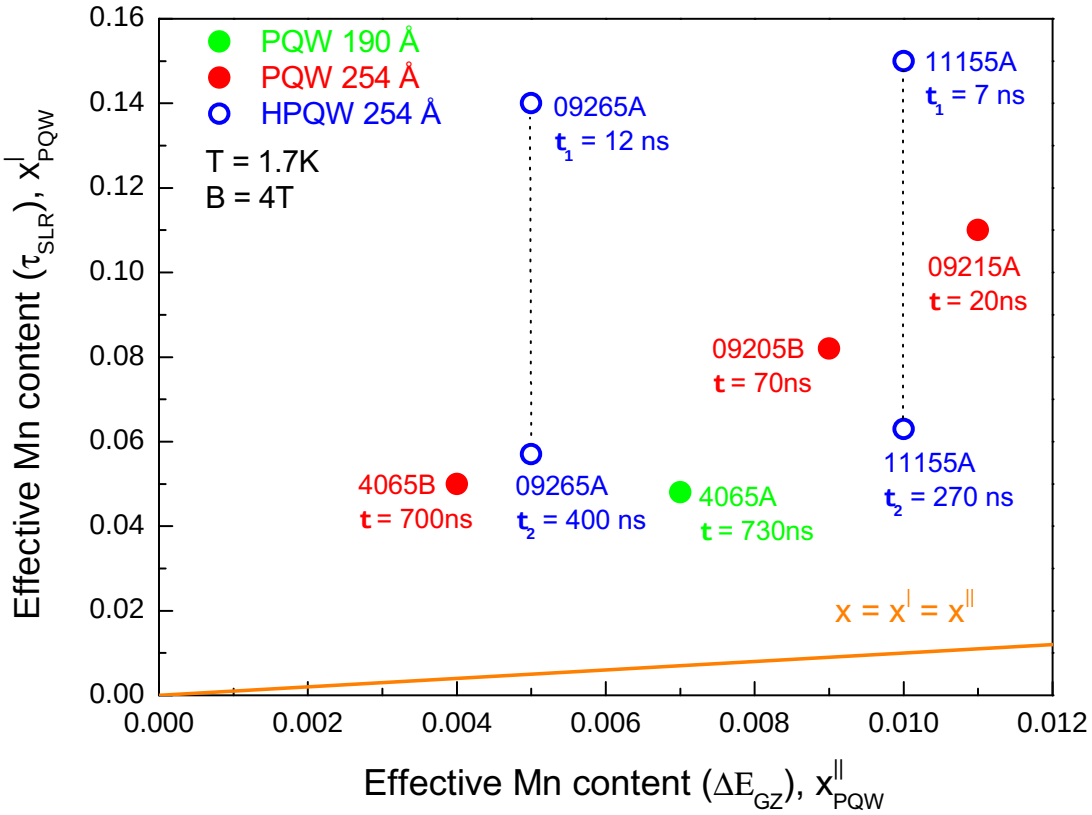

Figure 6.16 – Diagram linking the static (giant Zeeman-splitting) and the dynamic (SLR time) magnetic characteristics of HPQWs (open circles) and PQWs (closed circles). The solid line corresponds to $x' \equiv x'' \equiv x$, which holds true for disordered alloys.

fective Mn contents x''_{PQW}, evaluated from the giant Zeeman-splitting. The barrier Mn contents, in turn, exceed x'_{PQW} by a factor 2 – 14, depending on the respective sample.

In order to give an instructive presentation of the tunability of PQW and HPQW samples, compared with disordered alloys, their effective Mn contents determined by the static (giant Zeeman-splitting) and the dynamic (SLR time) magnetic properties are given in one diagram in figure 6.16. For the HPQWs, two effective Mn contents x'_{PQW} for the two different dynamics are plotted. The dependency of Mn content and SLR time in disordered alloys is represented by the solid line, and agrees with the technological Mn content $x \equiv x' \equiv x''$. The data from the investigated samples do not coincide with this line, confirming that also in PQWs and HPQWs the static and dynamic magnetization can be tuned separately.

As final step of the, in the framework of this thesis, performed investigations on PQWs, the longer SLR time in the HPQW 11155A is examined with respect to possible contribution by phonon dynamics, as this relaxation time is in the typical region of phonon dynamics. Analogue to the investigations in section 4.3 (especially figure 4.8), the power dependence of the SLR time is measured. It is expected that the time constant of the dynamics should decrease in case of SLR dynamics (i.e. faster dynamics) and increase in case of phonon dynamics (i.e. slower dynamics) [Far96, Kaz89, Kne06b, Mak85, Sch00a]. From the measured power dependence in figure 6.17 (especially inset) can be clearly seen that the relaxation time increases with rising

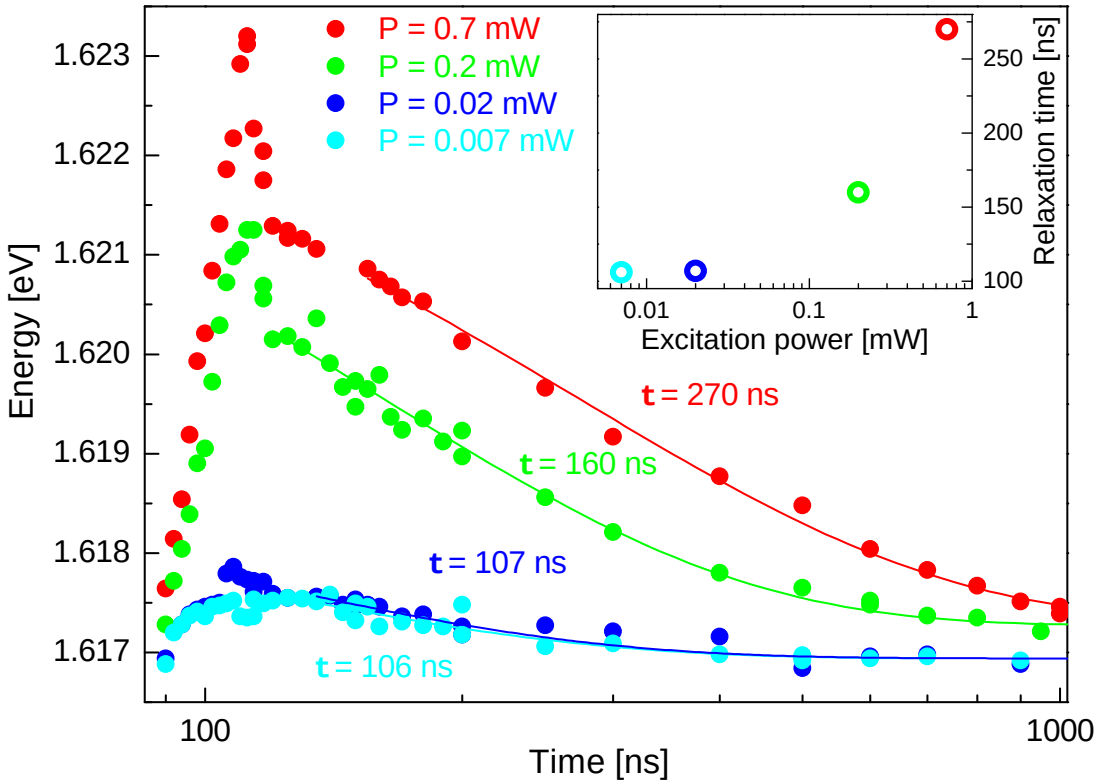

Figure 6.17 – Power dependence of the magnetization dynamics in the HPQW sample 11155A. The pulse laser power was decreased by two orders from $P = 0.7\,\mathrm{mW}$ down to $0.007\,\mathrm{mW}$. The measurements were performed at $B = 4\,\mathrm{T}$ and $T = 1.7\,\mathrm{K}$. Shown is the energetic shift of the PL position in time during heating and cooling of the Mn-spin system. In the inset the achieved time constants for the relaxation are plotted against the excitation power. The increase of the relaxation time with the excitation power is a clear indication for phonon dynamics.

excitation power. This behavior is typical for phonons. Thus, the SLR time for the path in the QW is screened by phonon dynamics. The SLR time is most probably shorter than the measured 270 ns. To measure its value, additional experimental effort is needed.

6.4 Acceleration of spin-lattice relaxation by spin diffusion

Compared with conventional DAs, as those examined in section 6.2, DAs with parabolic growth profile show considerably faster SLR times as expected from the average Mn content, which was estimated from the giant Zeeman-splitting. This reveals especially figure 6.18, where the effective Mn content x', which is related with the SLR time, is plotted versus the average Mn content x'', i.e. the effective Mn content related with the giant Zeeman-splitting. The effective Mn content x'' can be taken as average Mn concentration for the comparison, as the giant Zeeman-splitting at relatively low Mn concentrations is only proportional to the number of Mn-ions and to the overlap of the exciton wave function with a specific Mn-ion. For both quantities the specific design of the QW is irrelevant.

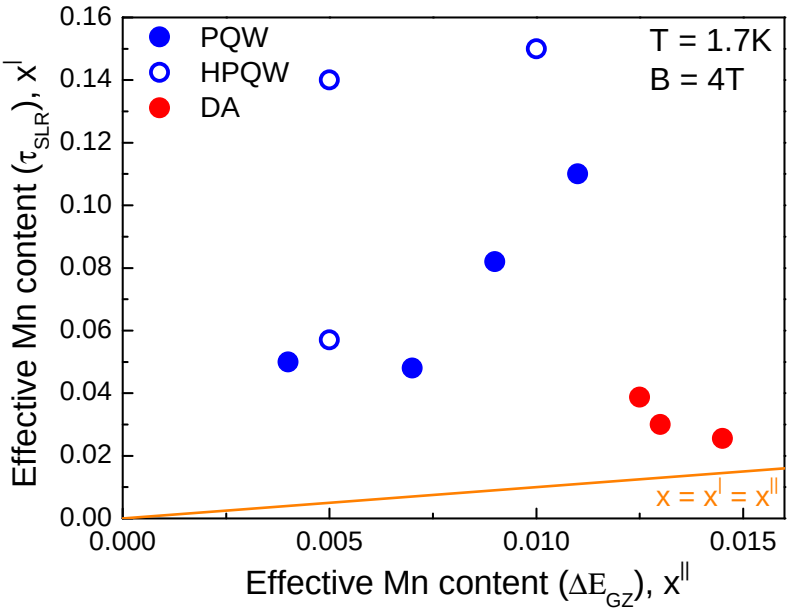

Figure 6.18 – Comparison of the relation between effective Mn contents for static x'' (giant Zeeman-splitting) and dynamic x' (SLR time) magnetic properties for DAs and (H)PQWs. The (H)PQW data points lie farther from the line representing the situation in disordered alloys ($x' \equiv x'' \equiv x$) than the DA data points. This is strong indication of considerable contribution by spin diffusion to spin relaxation, which accelerates the relaxation process.

As seen from figure 6.18, the data points for the PQW and HPQW samples lie farther from the line for disordered alloys ($x' \equiv x'' \equiv x$) than the DA ones. This behavior is related to an additional mechanism, which accelerates the relaxation of the Mn-spin excitation. As already introduced in the previous section for the HPQW samples, the additional contribution to the relaxation arises from spin diffusion. Analogue to the HPQWs, excited spins in the region with low Mn concentrations in the center of the parabolic QW can diffuse also in the PQWs in regions with higher Mn concentrations, and, hence, faster SLR times. Thereby, the time for the path with spin diffusion is lesser than the slow SLR time in the center of the parabolic QW. This leads to the noticeable increase of the relaxation time.

Consequently, spin diffusion plays a crucial role in the dynamics of spin relaxation in PQWs. It contributes to the measured relaxation times, resulting in faster relaxation. As mentioned in section 2.4, also in QDs with magnetic wetting layers and type-II heterostructures, the important influence of spin diffusion was well observed [Sch04, Sch05]. Hence, the simple monoexponential approach, which was used to obtain SLR time so far (see section B.2, especially equations B.2 - B.4), has to be extended by spin diffusion. Thereby, outstanding interest is devoted to determination of the spin-spin diffusion coefficient K_{diff} in DMS, which is yet unknown.

Very suitable to find out the diffusion coefficient is the $Zn_{0.99}Mn_{0.01}Se/Be_{0.93}Mn_{0.07}Te$ heterostructure with type-II band alignment. In this structure the effect of spin diffusion is well established by the measurements by Scherbakov *et al.* [Sch05] (see section 2.4). The advantage of this structure is that it has been grown by conventional MBE and not by modulated-molecular beam epitaxy (MMBE), as the DAs (see section A.1.4 in the appendix). Fitting parameters, which account for the diffusion at the interfaces, complicate the calculation of K_{diff} in DAs. Furthermore, the QW is so wide that overlapping of carrier wave functions with the barriers is negligible. Thus, the giant Zeeman-splitting in this sample depends only on the Mn-spin system in the QW. On basis of the experimental results for the $Zn_{0.99}Mn_{0.01}Se/Be_{0.93}Mn_{0.07}Te$ type-II

structure, it should be possible to evaluate the spin-spin diffusion coefficient K_{diff}. These calculations were performed by Maksimov *et al.* on basis of a model, suggested by Suris [Sur05]. In the framework of the model is being tried to explain fast SLR by spin diffusion from single Mn-ions to Mn clusters, which act as relaxation centers. In the following, the calculations are only briefly described, as they will be published in more detail soon [Mak09]. For the calculations, a sample with nonuniform magnetic ions content is supposed. The kinetics of the spatial distribution of the Mn temperature in such a sample can be described by a one-dimensional partial differential equation. Numerical solution of this equation is taken as initial-boundary value.

The diffusion coefficient K_{diff} was introduced in the framework of equation 2.28 as

$$K_{diff} = \frac{l^2}{3\tau_{ss}}. \tag{6.1}$$

In the case of diffusion of excitations between randomly distributed dipoles, which underlie dipole-dipole interaction, yields for the time for one diffusion step between two Mn-ions: $\tau_{ss} \propto x^{-2}$. Together with $l = r_0 x^{-1/3}$ (compare section 2.4) results for the dependence of K_{diff} on the local Mn content [Bur84]

$$K_{diff} \propto x^{\frac{4}{3}}. \tag{6.2}$$

As elaborately discussed in section 5.1, the Mn content, in turn, determines the SLR time τ_{SLR}. This dependence between τ_{SLR} and Mn concentration can be described analytically by (see figure 6.19)

$$\tau(x) = \frac{1}{800x^{4.5} + 0.05x^2 + 10^{-6}}\,[\text{ns}]. \tag{6.3}$$

The dependence was simply achieved by fitting the experimental data points. It is rather close to the dependence obtained in the theory of spin diffusion controlled SLR processes [Bur84].

The initial excitation of the Mn-spin system is given by the fast exchange interaction between Mn-ions and photoexcited carriers. Thus, usually an uniform distribution of the Mn temperature can be taken to initialize the numerical problem. The solution of such a problem will give spatial and temporal information about the Mn temperature.

To determine K_{diff} the SLR time for different diffusion coefficients was calculated for the $Zn_{0.99}Mn_{0.01}Se/Be_{0.93}Mn_{0.07}Te$ type-II structure. The corresponding results are shown in figure 6.20. The big influence of spin diffusion can be noticeably seen from the figure. In absence of spin diffusion, i.e. the relaxation takes only part via SLR, the relaxation time is about 0.1 ms. In the limit of an infinite spin diffusion coefficient, the SLR time is accelerated by several orders down to 170 ns. The excitation passes over from the $Zn_{0.99}Mn_{0.01}Se$-layer to the $Be_{0.93}Mn_{0.07}Te$-layer very fast.

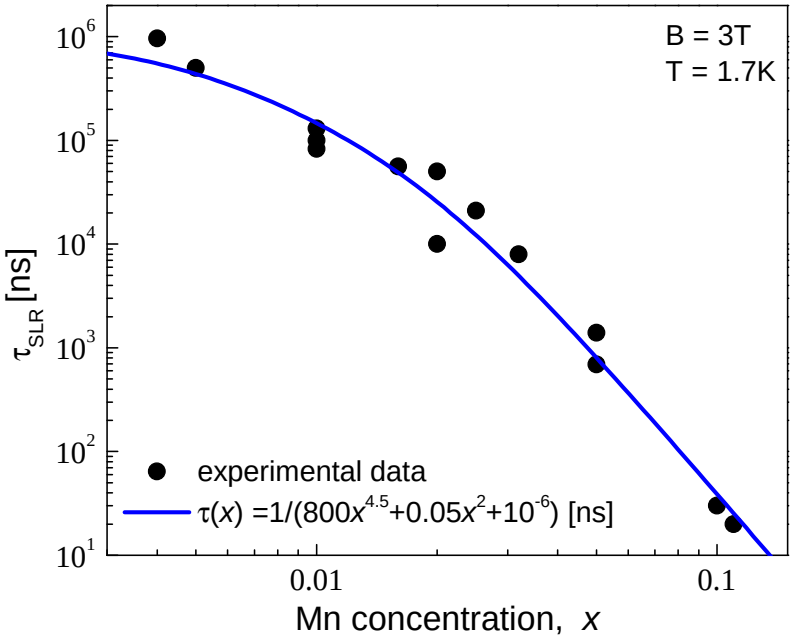

Figure 6.19 – Analytical representation of the dependence of the SLR time on the Mn concentration. Shown is only one possible presentation of analytic form, which fits rather good to the experimental results. Detailed description of the origin of the results was already given in figure 5.2.

Comparison of these calculated results with the experimental data from Scherbakov [Sch05], allows estimation of the spin-spin diffusion coefficient in DMS with rather high accuracy for the first time. As the measured SLR time for the $Zn_{0.99}Mn_{0.01}Se/Be_{0.93}Mn_{0.07}Te$ type-II structure is 6 ns, $K_{diff} = 3.5$ results from the calculations.

Calculation of the kinetics of the Mn temperature based on $K_{diff} = 3.5$ in the center of the QW of the $Zn_{0.99}Mn_{0.01}Se/Be_{0.93}Mn_{0.07}Te$ type-II structure is shown by the red curve in figure 6.21. It corresponds well with the measured dynamics of Mn-spin temperature (black line; see also figure 2.6 on page 83), evidencing the strong dependence of Mn temperature kinetics on K_{diff}. In contrast, calculation with the limit values of no spin diffusion $K_{diff} = 0$ or an infinite

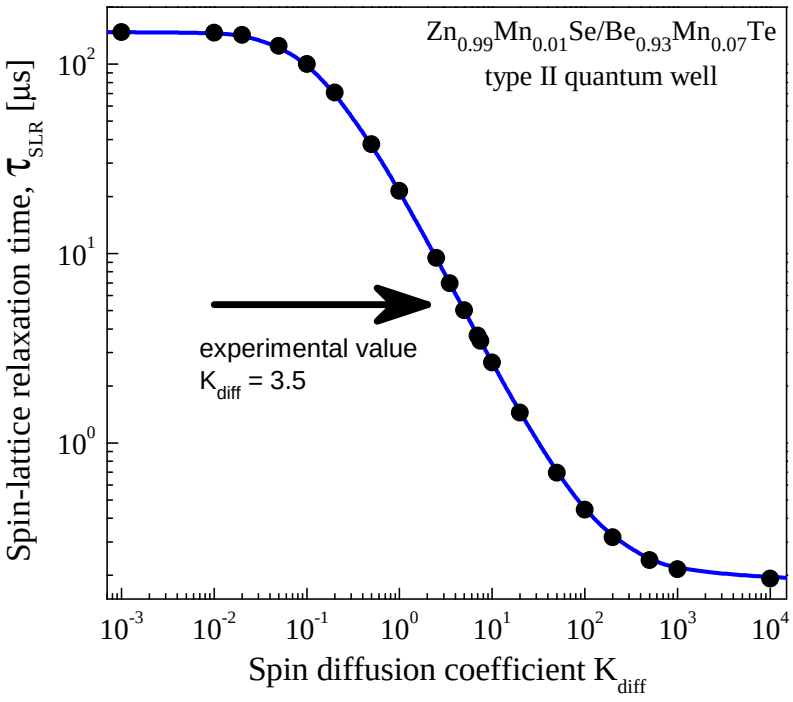

Figure 6.20 – Calculated SLR times for different spin-spin diffusion coefficients for the $Zn_{0.99}Mn_{0.01}Se/Be_{0.93}Mn_{0.07}Te$ type-II QW in the center of the QW. The SLR time $\tau_{SLR} = 6$ ns, which was achieved by Scherbakov *et al.* [Sch05], corresponds to $K_{diff} = 3.5$.

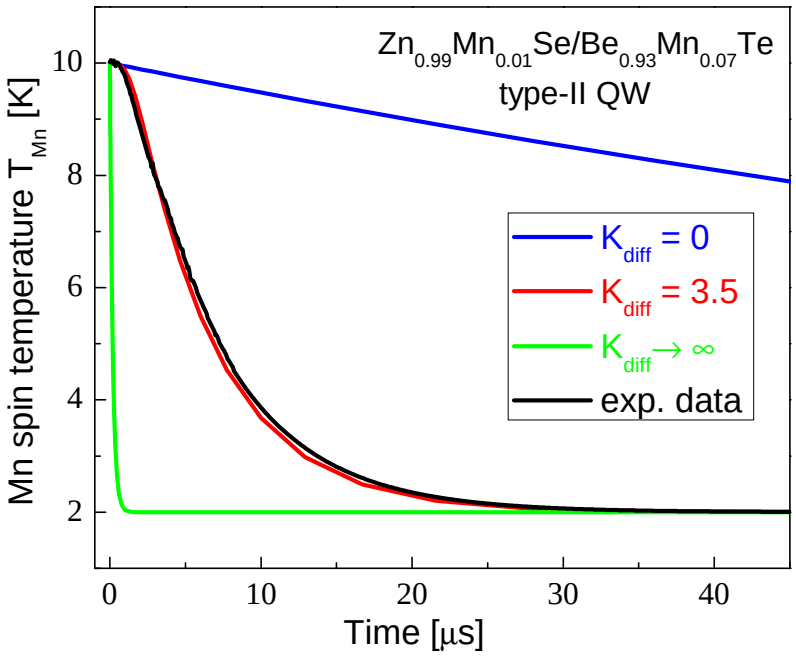

Figure 6.21 – Calculated kinetics of the Mn temperature for different diffusion coefficients in the center of a $Zn_{0.99}Mn_{0.01}Se/Be_{0.93}Mn_{0.07}Te$ type-II QW. The experimental results can be well explained by a diffusion coefficient $K_{diff} = 3.5$.

diffusion coefficient are far away from explaining the experimental results. Compared with the case without spin diffusion, the SLR time is considerably accelerated by spin diffusion.

Based on this successful result, the complete temperature profile during cooling of a heated Mn-spin system can be calculated for the $Zn_{0.99}Mn_{0.01}Se/Be_{0.93}Mn_{0.07}Te$ QW. In absence of spin diffusion ($K_{diff} = 0$), the profile of the Mn-spin temperature is homogeneous. This profile is shown in figure 6.22(a) for four times after heating of the Mn-system. The $Be_{0.93}Mn_{0.07}Te$-layer cools down to bath temperature faster than 1 µs because of the fast SLR time due to the high Mn content. In the $Zn_{0.99}Mn_{0.01}Se$-layer the SLR time is much slower because of the low Mn content. Hence, the Mn temperature in this layer needs much longer time to cool down to bath temperature and is still considerably elevated at 100 µs after the heat impact. This slow cooling corresponds to the situation in the $Zn_{0.99}Mn_{0.01}Se/BeTe$ reference sample in [Sch05] (see figure 2.6 in section 2.4), as in this sample no spin diffusion to the nonmagnetic BeTe-layers can occur.

For the $Zn_{0.99}Mn_{0.01}Se/Be_{0.93}Mn_{0.07}Te$ heterostructure, the temperature profile with the calculated spin diffusion coefficient in DMS, $K_{diff} = 3.5$, is shown in figure 6.22(b). Due to the spin diffusion, the temperature profile gets strongly inhomogeneous. The heated Mn-spin system can cool down much faster. Hence, contrary to the case without spin diffusion, the Mn temperature in the center of the $Zn_{0.99}Mn_{0.01}Se$-layer is only weak elevated at 10 µs and in equilibrium with the bath temperature at 100 µs after the heat impact. The complete cooling process in time and space is shown in figure 6.23 in the case of $K_{diff} = 3.5$.

As particularly known from section 1.4.4, the potential profile of electrons an holes in a DMS QW depends strongly on the Mn temperature. Hence, it is now possible to calculate the exact potential profile for electrons and holes in the QW, on basis of the achieved temperature profile. Therefore, the Schrödinger-equation has to be solved numerically for every moment in time.

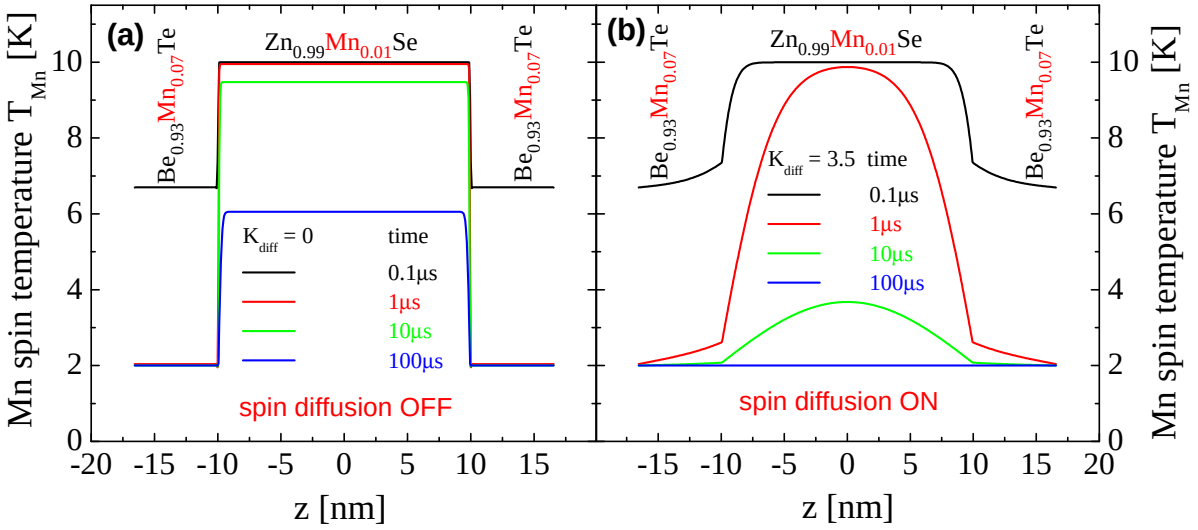

Figure 6.22 – Profiles of Mn spin temperature during spin-lattice relaxation for (a) $K_{diff} = 0$, i.e. without spin diffusion, and (b) $K_{diff} = 3.5$, i.e. with spin diffusion. (a) If spin diffusion is absent, the Mn-spin temperature profile is homogeneous. In this case the Mn-spin temperature in the (Zn,Mn)Se-layer is at 100 µs after the heat impact still considerably elevated with respect to the bath temperature ($T = 2$ K). (b) If spin diffusion is included, the temperature profile gets inhomogeneous. The excitation of the Mn-spin system relaxes much faster, so that the complete structure is in equilibrium with the bath at 100 µs after the heat impact.

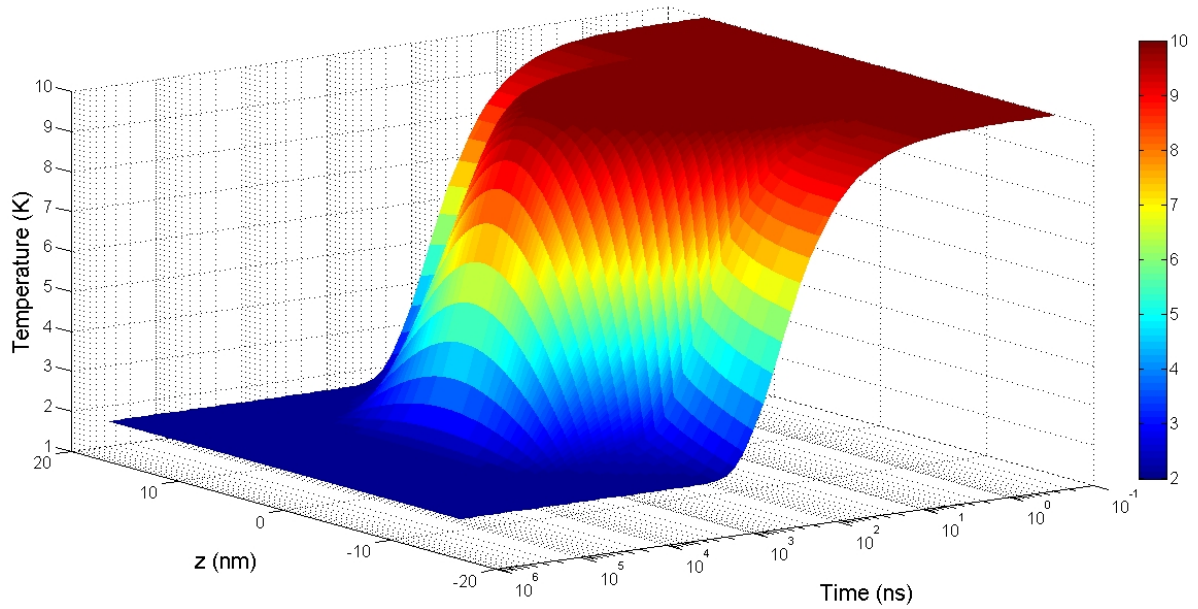

Figure 6.23 – Temporal profile of the Mn temperature in a QW for diffusion coefficient $K_{diff} = 3.5$. The profile gives information about the Mn temperature at each position of the QW during cooling of the Mn-system after heating by laser pulse. The calculations were performed for the $Zn_{0.99}Mn_{0.01}Se/Be_{0.93}Mn_{0.07}Te$ type-II QW. The QW width is 20 nm.

The knowledge of the potential profile allows determination of the giant Zeeman-splitting and the corresponding dynamical changes of the PL peak position.

The utilizability of the achieved model and the evaluated spin diffusion coefficient ($K_{diff} = 3.5$) can be proven, if they were adopted to other DMS structures. In a first step, the model is tested for structures, where no spin diffusion can occur between neighboring layers. This will show whether the model works in general. The $Cd_{0.96}Mn_{0.04}Te$/CdTe DA samples, which were investigated in section 6.2, are particularly suitable for this propose. They are similar structured as the $Zn_{0.99}Mn_{0.01}Se$/$Be_{0.93}Mn_{0.07}Te$ heterostructure, but without manganese in the CdTe-layers, which separate the (Cd,Mn)Te DMS layers.

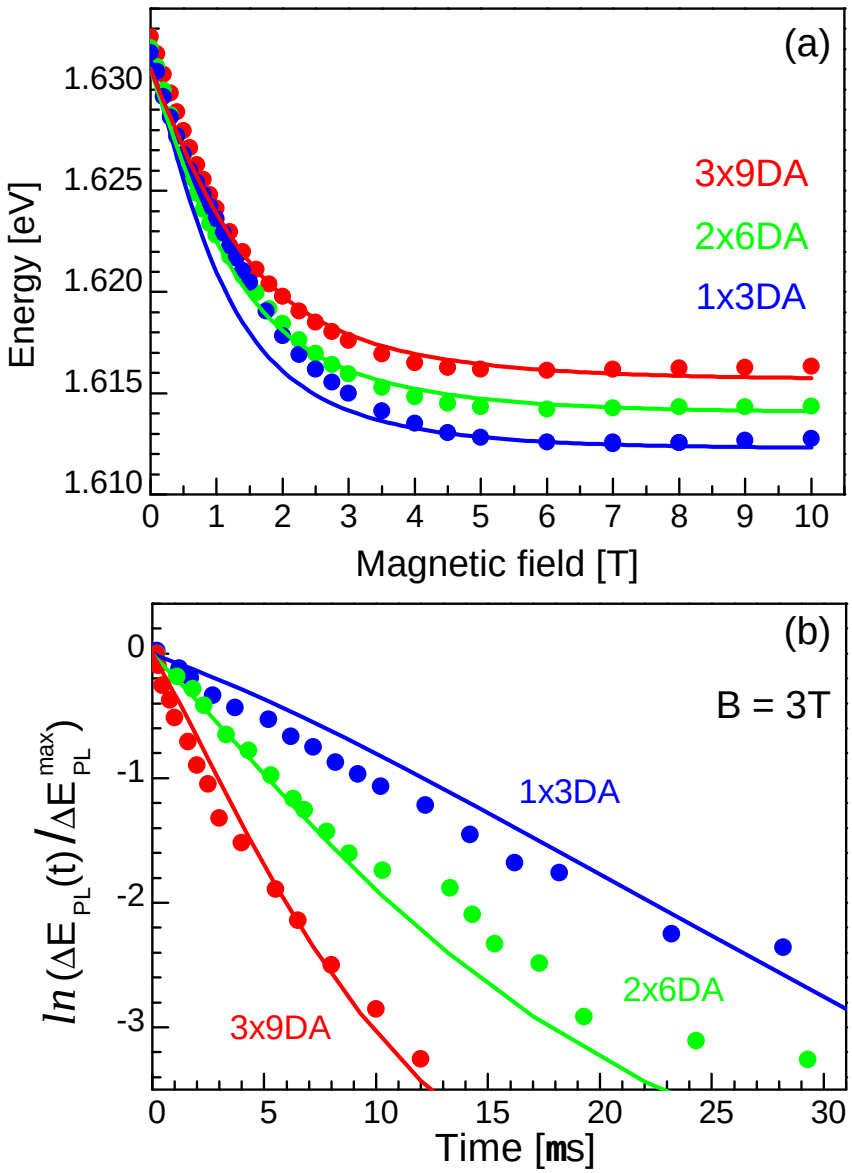

Figure 6.24 – Comparison of model calculations including spin diffusion with experimental results in (Cd,Mn)Te-based digital alloys for (a) the giant Zeeman-splitting and (b) the dynamics of the PL energy. Both experimental results corresponds very well with the calculations for all three DA samples. The model is even able to reproduce the small deviations between the different designed DAs. Bath temperature for experiment and calculations was $T = 1.6$ K.

The calculations were performed for the static and the dynamic magnetic properties of the three DA samples. The calculated results and the experimentally measured results are given for the giant Zeeman-splitting and the dynamics of the PL energy maximum in figure 6.24. As one can see from the figures, the calculated results (lines) correspond very well with the experimental results (dots). The model is even able to predict the special features of both properties. These are on the one hand the minor variations of the giant Zeeman-splitting value of the three DA structures, which were tentatively yet explained by influence of the DA growth parameters on the static magnetization (compare section 6.2). On the other hand also the non-exponential decay of the SLR dynamics, which can be clearly seen for the 2×6DA and the 3×9DA samples, is reproduced by the calculations. Likewise the different behavior of the static and dynamic properties in the DAs, which is related to Mn-ions clustering, can be predicted, i.e. the similar giant Zeeman-splitting as well as the considerable differences in the SLR dynamics (compare section 6.2).

After determination of K_{diff} and the successful application of the model on conventional DAs, now it should be possible to explain the dynamics of the magnetization in the more complicated structures, like e.g. the DAs with parabolic band profile. Comparison of calculations with $K_{diff} = 3.5$ and experimental results is shown in figure 6.25 for the three PQWs with

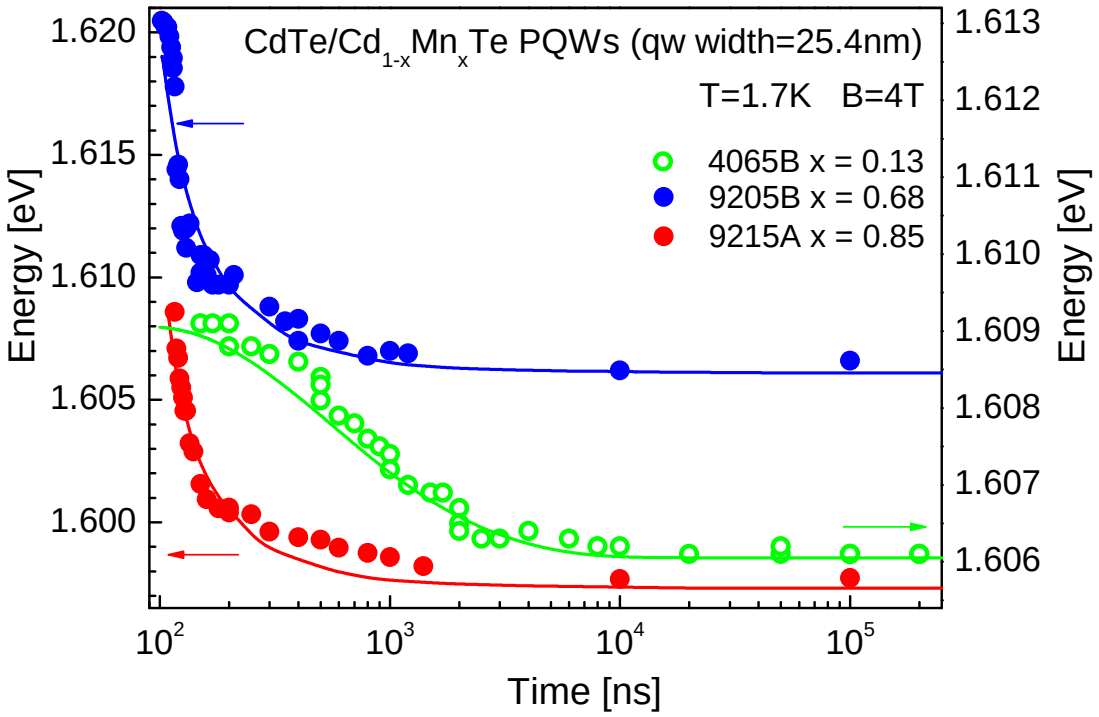

Figure 6.25 – Comparison of model calculations including spin diffusion ($K_{diff} = 3.5$) with experimental results for PQWs. The comparison is performed for the three CdTe/$Cd_{1-x}Mn_xTe$ PQWs with QW width of 25.4 nm. Whose Mn concentrations are $x = 0.13$, 0.68 and 0.85. It can be clearly seen that the calculations and experimental data match very well. This confirms the big influence of spin diffusion on spin dynamics in these structures. For the sake of clear arrangement, the energy scale of the 9205B and 9215A samples is given on the left side and of the 4065B sample on the right side.

QW width of 25.4 nm. Also for these structures the calculations including spin diffusion cover very close the experimental results. This affirms, on the one hand, that the model accounts well for all key features determining the relaxation in DMS QWs. On the other hand, the assumption that spin diffusion from single ions to relaxation centers (clusters) is responsible for the strong acceleration of the SLR dynamics in DMS with a nonuniform distribution of Mn-ions was successfully approved. This makes the influence of the Mn concentration on the relaxation dynamics even stronger, as the very effect due to clustering, pointed out in section 5.1.

Summary

Magnetization dynamics in DMS heterostructures is controlled by the interacting systems of magnetic ions, free carriers and lattice (phonon system). In this thesis spin and energy transfer from hot carriers to the Mn-spin system, and the cooling of the Mn-spin system by SLR to bath temperature in DMS heterostructures was experimentally addressed. Spin-flip exchange scattering is responsible for energy and spin transfer between carrier and magnetic ions, which can be influenced by nonequilibrium carrier polarization generated by different spin temperatures between the systems. The SLR of the Mn-ions is controlled by interactions between the magnetic ions.

The systems of DMS were heated by hot photocarriers generated by laser pulses, whose duration of 7 ns is considerably shorter than the typical lifetime of nonequilibrium acoustical phonons of about 1 µs. Access to the static magnetization was received from PL spectra measured under steady-state conditions, e.g. under cw excitation, which follows directly from equations 3.2 and 3.3. Following the evolution of the Mn-spin temperature in time domain, the contribution of the direct energy transfer from the indirect one, mediated by the phonon system, could be distinguished clearly. It has been shown that over a wide range of Mn concentrations and excitation densities the direct energy transfer dominates in (Zn,Mn)Se heterostructures.

The physical reasons for the different contributions of direct and indirect paths of energy transfer in (Zn,Mn)Se and (Cd,Mn)Te require further clarification. Especially, detailed study of (Cd,Mn)Te with different Mn concentrations is needed. Exchange scattering times of carriers on magnetic ions should not differ strongly in these materials as the exchange constants $N_0\alpha$ and $N_0\beta$ do not differ considerably. It can be supposed that the stronger indirect path in (Cd,Mn)Te is related to stronger nonradiative recombination known for this material in comparison with (Zn,Mn)Se. As a result a larger part of photocarrier energy is converted to the phonon system and then reaches the Mn-spin system via the indirect path.

For the sake of simplicity, only the energy transfer from hot free carriers to the Mn-system is discussed. This is correct for the indirect transfer involving nonequilibrium phonons. The direct transfer via carrier-Mn spin exchange scattering is based on the flip-flop process and, therefore, combines energy and spin transfer (see, e.g., [Kre89, Kön00b]. Further experiments with spin oriented photocarriers generated by circular polarized light in the vicinity of the band gap are planned to address this problem.

The dynamics of SLR in $Zn_{1-x}Mn_xSe$ QWs has been studied in detail by time-resolved PL. Until now, only very recently experimental studies have been extended toward (Zn,Mn)Se heterostructures [Sch05, Yak04]. Implementation of pulsed laser excitation allows to extend the dynamical range for measurements of the SLR times to cover magnetic ion concentrations from $x = 0.004$ up to $x = 0.11$ in (Zn,Mn)Se-based heterostructures. In prior studies, only concentrations below $x \sim 0.06$ could be addressed [Far96, Sca96a, Sch00a]. At liquid helium temperature the SLR times of Mn-ions vary by five orders of magnitude from milliseconds to nanoseconds with increasing Mn content. The relaxation times and their dependence on the Mn content are very similar in (Zn,Mn)Se and (Cd,Mn)Te DMS materials. This confirms that the SLR dynamics is controlled by interactions within the system of Mn-ions, but is only weakly sensitive to the II-VI semiconductor host material, into which the Mn-ions are embedded. As a result, the static and dynamic magnetization in bulk DMS becomes strongly related with each other.

Two different approaches to control the magnetization dynamics of the Mn-spin system, independent of the static magnetic properties, were demonstrated in this thesis. One is enabled by a 2DEG, which acts as an efficient bypass channel for the energy transfer from the Mn-ion system to the lattice. In modulation doped samples with high concentration of carriers, the SLR dynamics was accelerated the by more than one order of magnitude. This is due to the strong coupling of free carriers with both magnetic ions and phonons. Controlling the density of the 2DEG by means of an external electric field, generated by a gate voltage, results in tuning of the SLR time in n-type modulation-doped (Zn,Mn)Se/(Be,Mg)Se heterostructure QWs by more than two orders of magnitude. The static magnetization, responsible for the giant Zeeman-spin splitting of excitons, is not influenced by the 2DEG density. The acceleration of the SLR process via doping seems favorable for spintronics, because the shorter the SLR time, the faster is addressing of the the magnetization, and the higher are possible frequencies.

The second demonstrated approach uses the digital growth technique to create DMS heterostructures with inhomogeneous profile of Mn-ions. Here opens the strong sensitivity of the magnetization dynamics to clustering of the Mn-ions a degree of freedom for spin engineering. It has been shown that digital alloying of DMS provides considerable enhancing changes in clustering, which modify the magnetization dynamics, while keeping about constant the number of paramagnetic spins, which control the static magnetization. Also for parabolic and half-parabolic growth profiles of the Mn-ions, strong acceleration of the SLR time was observed. In this case spin diffusion in the system of Mn-ions serves as bypass channel for slow SLR and plays a key role for very fast SLR. The nonequilibrium spins from regions with low relaxation rates (i.e. low Mn concentration) moves to regions with high relaxation rates (i.e. high Mn concentration). Hence, spin diffusion is only present in DMS heterostructures with nonuniform concentration of magnetic ions. The important role of spin diffusion for acceleration of the SLR time could be successfully approved by a theoretical model. From the theoretical calculations

based on the experimental results, the spin-spin diffusion coefficient in DMS, $K_{diff} = 3.5$, was determined for the first time.

Because both methods to control magnetization dynamics (2DEG and DA) are based on different mechanism, a combination of both possibilities to address magnetization dynamics is possible. Alternatively, the electric field control can also be combined with the recently reported spin control in heteromagnetic nanostructures [Sch05].

Summing up, by implementation of free carriers via modulation doping and control of these carriers by means of gate voltage, and by digital growth, several powerful possibilities could be realized to control spin dynamics in DMS nanostructures, which lead to independent tuning of static and dynamic properties of DMS.

Appendix A

Samples

A.1 Preparation of the samples

Epitaxial techniques, like molecular beam epitaxy (MBE), enable the production of samples, consisting of layers of different materials with atomic precession. By means of lithography or etching, low-dimensional structures of nearly arbitrary size and design can be made.

All samples measured in this thesis were grown by MBE. This technique and the design of those samples, which were measured in the framework of this thesis, are consecutively described. Thereby, principle design of all samples is the same: On the substrate, a buffer layer is grown, to improve the surface quality and the lattice constant matching between substrate and successional barrier material. On the barrier, the QW layers are grown and the structure is terminated by a topping, consisting of the barrier material, to hold off nonradiative surface recombination centers from the QW.

A.1.1 Molecular beam epitaxy

The big advantage of MBE, compared with other epitaxial growth techniques, like liquid phase epitaxy (LPE) and vapor phase epitaxy (VPE), is the possibility to control the material deposition with monolayer precession (0.3 nm). Epitaxy means that the crystal structures of the grown up layer conforms to the crystal structure of the substrate. This is only possible, if the physical properties of the two materials do not differ significantly. If lattice constants are different, strain and lattice defects occur.

To achieve the high precession, MBE takes place in ultra high vacuum (10^{-8} Pa). The deposition rate is very slow (typically less than 1000 nm per minute), to allow the epitaxial growth. The growth materials are located in separate effusion cells as ultra-pure elements. It is also possible to grow organic semiconductors by this technique. In this case, effusion cells with molecules are used rather than atoms. The cells are heated during the growth process, so that

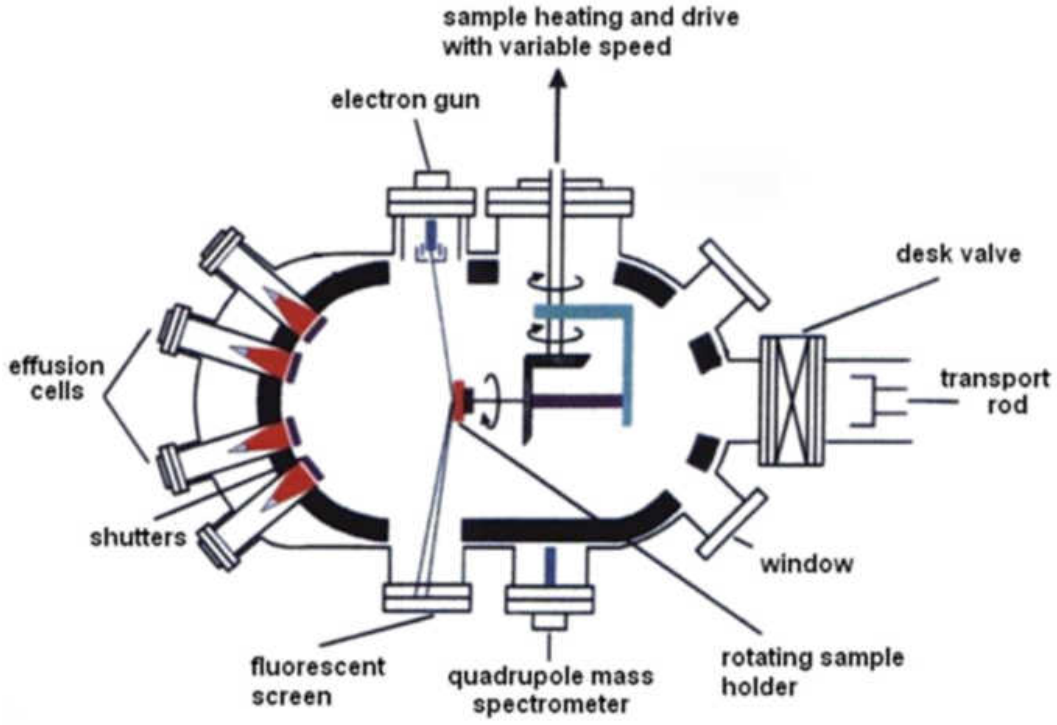

Figure A.1 – Schematical picture of MBE chamber. The atomic beams generated in the effusion cells can be controlled by the shutters to allow structure growth with high precession on the substrate mounted on the sample holder. The electron gun and the screen are used to monitor the growth via RHEED.

the elements can sublimate and form a collimated atomic beam. Because of the long mean free path of the atoms, they do not interact with other atoms until they reach the wafer with the substrate. This beam impinges on the heated surface of the wafer[1], where the atoms form the lattice. To increase the uniformity of the grown structure, the wafer can be rotated.

Exact control of the layer materials is given by computer controlled shutters in front of the effusion cell orifices, which can start and stop the atomic beam. To monitor the growth process during operation, the so-called reflection high energy electron diffraction (RHEED) technique is used. This technique is sensitive to surface morphology and informs about smoothness, orientation, and monocrystallinity of the topmost surface layer during its growth.

Schematical picture of a MBE chamber, equipped with effusion cells, rotatable and heatable sample holder, and electron gun and fluorescent screen for RHEED, is given in figure A.1.

A.1.2 Quantum well heterostructures

The $Zn_{1-x}Mn_xSe/Zn_{1-y}Be_ySe$ heterostructures with QWs were grown on (100)-oriented GaAs substrates. Typical thickness of substrates is 0.3 – 0.4 mm. The substrates were covered by

[1]The heating temperatures amount ∼850 K for “classical” semiconductors and ∼500 K for ferromagnetic semiconductors.

a buffer consisting of 10-Å-thick BeTe, 20-Å-thick ZnSe, and 4000-Å-thick $Zn_{0.97}Be_{0.03}Se$ layers. Subsequently, the QW structures were grown. The Mn content in the $Zn_{1-x}Mn_xSe$ QW layers was varied from $x = 0.004$ up to 0.11 and the Be content in the barrier layers was $y = 0.06$ or 0.11 to provide efficient confinement of both, electrons and holes, in the DMS QW layers. The structural parameters for the studied (Zn,Mn)Se-based samples are collected in table A.2. Information about the optical characterization of the (Zn,Mn)Se-based structures can be found in [Kel01, Kön99].

The $Cd_{1-x}Mn_xTe/Cd_{1-z}Mg_zTe$ heterostructures with QWs were grown on (100)-oriented CdTe substrates. Structure parameters for the (Cd,Mn)Te-based structures are given in table A.2.

Most of the samples were nominally undoped, so that the background electron density in the wells does not exceed 10^{10} cm^{-2}. Also a set of modulation doped $Zn_{1-x}Mn_xSe/Zn_{1-y}Be_ySe$ samples with two-dimensional electron gas concentrations up to 5.5×10^{11} cm^{-2} was grown, which were used in this thesis to study the effect of free carriers on the SLR dynamics.

Some of the samples are multiple QW structures with up to 50 periods.

A.1.3 Structure with electric contacts

The structure was grown on (001)-oriented n-doped GaAs substrate overgrown by n-doped GaAs buffer. The II-VI layers were nominally undoped, except a 2 nm thick part of $Zn_{0.94}Be_{0.06}Se$ barrier, doped with Iodine donors, and separated by a 20 nm thick spacer from $Zn_{0.985}Mn_{0.015}Se$ QW. The structures consists of following layers: 30 nm $Zn_{0.92}Be_{0.08}Se$, 55 nm of $Zn_{0.94}Be_{0.06}Se$ (it includes the modulation doped layer), 2 nm $Zn_{0.985}Mn_{0.015}Se$ QW, 15 nm of $Zn_{0.94}Be_{0.06}Se$ and 30 nm $Zn_{0.92}Be_{0.08}Se$. A semitransparent gold contact was deposited on the top, so that a gate voltage can be applied along the structure growth axis, to tune the 2DEG density in the $Zn_{0.985}Mn_{0.015}Se$ QW.

A.1.4 Digital growth technique

The concept of digital growth technique has been brought about by the great sub-monolayer atomic precision of MBE. During the growth, some constituent of the structure, say MnTe, with a certain thickness (frequently submonolayer), is introduced into a base material, say CdTe, at strictly predefined positions [Kaw83, Mil84a]. Therefore, this technique allows for engineering arbitrary shape of the confining potential in quantum structures in a digital fashion. If the constituents are built in periodically with a very small period of the order of a single monolayer, the result is a short-period superlattice, which is referred to as DA [Gos94, Gos82, Mou00]. This is to be contrasted with the disordered alloys, in which both constituents are introduced

simultaneously to form mixed crystals (e.g., $Cd_{1-x}Mn_xTe$). In contrast to conventional MBE, this modification is called modulated-molecular beam epitaxy (MMBE) [Gér91, Zha94, Zha95].

The (Cd,Mn)Te-based DA samples were grown on (100)-oriented GaAs substrates after depositing a 4.2-µm-thick $Cd_{0.8}Mg_{0.2}Te$ buffer layer. They contain 23-nm-thick layers (corresponding to about 70 ML) of a $Cd_{0.95}Mn_{0.05}Te$/CdTe digital magnetic quantum well (DMQW), confined from both sides by $Cd_{0.8}Mg_{0.2}Te$ barriers, to form digital magnetic QWs [Woj95]. Characteristic for the DMQW is the period of the superlattice, i.e. the relation between well width and barrier width.

The parabolic and half-parabolic DA samples were grown on (100)-oriented GaAs substrate with a 4 µm thick CdTe buffer and a 0.4 µm $Cd_{1-x}Mn_xTe$ barrier layer. Growth of the (half-)parabolic QW, containing CdTe and $Cd_{1-x}Mn_xTe$, was divided into 41 steps, controlled by pulsed operation of the shutter of the Mn cell. The respective growth profiles are shown in figure 6.12 on page 140. During each step, the Mn-shutter was opened as long as it takes to grow a Mn concentration, which is needed to create a parabolic profile. Thereby, the Mn concentration in the barrier and in the QW layers, containing manganese are the same. Several PQW samples with different Mn contents and QW widths were grown. Their concrete values are given in table A.1. As the nominal Mn concentration in the middle of the QW is zero for all structures, complete description of the potential devolution is possible by the QW width and the Mn concentration in the barrier. Further details on the growth procedure contains [Fie97].

A.2 Tables of samples

Table A.1 – Technological parameters of PQW and HPQW samples. Parabolic structures are labeled by "P" and half-parabolic structures by "HP" in column "type". Given are the nominal well width, the barrier Mn content x, which was determined experimentally by x-ray diffractometry (XDR), the full width at half maximum (FWHM) of the excitonic PL, and the subband distance C of the heavy-hole exciton transitions[a] according to [Fie97]. The small FWHM suggest good structural quality of the samples. The energetic position of the PL increases with falling well width and rising barrier Mn content, respectively [Fie97].

code	type	QW width [Å]	x barrier	FWHM [meV]	C [meV]
4065A	P	190	0.13	1	220
4065B	P	254	0.13	0.8	53
9205B	P	254	0.68	10	147
9215A	P	254	0.85	17	117
11155A	HP	190	0.25	5	76
9265A	HP	254	0.77	10	106

[a] The equidistant subband distance C is the energy difference between two subbands $C = (E_{n+1}^{CB} - E_n^{CB}) + (E_{n+1}^{VB} - E_n^{VB}) = \frac{2\hbar}{l_z}\sqrt{\frac{2\Delta E_g}{m_0}}\left(\sqrt{\frac{1-Q_{VB}}{m_{eff}}} + \sqrt{\frac{Q_{VB}}{m_{eff,hh}}}\right)$ for an optical transition (compare equations 1.96 and 1.97 for the conduction band and valence band in PQWs on page 58).

Table A.2 – Technological parameters and experimentally measured values for τ_{SLR} for the (Zn,Mn)Se/(Zn,Be)Se samples, and after the double line for the (Cd,Mn)Te/(Cd,Mg)Te samples.

code	Mn content, x	electron concentration $\times 10^{10}$ [cm^{-2}]	SLR time [μs]	QW width [Å]	barrier width [Å]	Be content, y	number of periods	PL linewidth FWHM [meV]
CB1542	0.004	undoped	960	100	200	0.06	5	2.0
CB2033	0.004	3	550	100	—	0.06	1	2.0
CB2034	0.004	32	100	100	—	0.06	1	4.2
CB2037	0.004	55	70	100	—	0.06	1	6.9
CB1651	0.012	undoped	600	150	200	0.06	1	2.2
CB1541	0.013	undoped	580	100	200	0.06	5	2.2
CB1581	0.015	undoped	530	150	—	0.04	1	2.1
CB2422	0.02	undoped	100	100	—	0.06	1	2.6
CB1649	0.03	undoped	45	100	200	0.06	5	1.9
CB2169	0.035	undoped	11	100	—	0.06	1	2.3
CB2165	0.035	30	4.7	100	—	0.06	1	4.8
CB868	0.05	undoped	0.7	10,30,100	250	[a]	1 per QW width	5.2
CB1433	0.06	undoped	1.8	200	100	0.05	10	2.7
CB1340	0.1	undoped	0.03	3000	—	—	epilayer	8.5
CB886	0.11	undoped	0.02-0.07	100	95	0.11	10	6.5
code	**Mn content, x**	**electron concentration $\times 10^{10}$ [cm^{-2}]**	**SLR time [μs]**	**QW width [Å]**	**barrier width [Å]**	**Mg content, y**	**number of periods**	**PL linewidth FWHM [meV]**
CT965	0.004	undoped	2.2	—	—	—	—	4.1
CT969	0.015	undoped	27	75	—	0.4	50	3.8

[a] Barrier consists of BeMgZnSe.

A.3 Lattice and electronic properties

Table A.3 – Structure (stable at room temperature (RT)), lattice constants and energy gap (for zincblende semiconductors: Γ_{8vb} - Γ_{6cb} transition) of binary II-VI semiconductors. For more detailed data see [Mad99].

material	structure (RT)	lattice constants [Å]	E_g [eV] (RT)	E_g [eV] (1.6 K)
BeSe	zincblende [a,b]	$a_0 = 5.15$ [c,d]	5.6 [e]	
CdTe	zincblende [f]	$a_0 = 6.487$ [g]	1.5 [h,i]	1.606 [j,k,l]
MgTe	wurtzite [m,n,o,p]	$a = 4.5$; $c = 7.4$ [m,q,r] ($a_0 = 6.4454$ for zincblende structure [r])	3.49 [s]	3.2 (10 K) [t]
ZnSe	zincblende [f]	$a_0 = 5.667$ [u,v,w,x]	2.72 [y]	2.82 [z,aa,ab,ac,ad]

[a] [Wyc63] [b] [Mad99] [c] [Gal97] [d] [Yim72] [e] [Wil99] [f] [Yeh92] [g] [Bot81] [h] [Han82]
[i] [Sob81] [j] [Ave67] [k] [Naw79] [l] [Neu88] [m] [Kle51] [n] [Kuh71] [o] [Par71] [p] [Zac27]
[q] [Li95] [r] [Cam97] [s] [Lit96] [t] [Oh93] [u] [Kar96] [v] [McI80] [w] [Nas90] [x] [Smi65]
[y] [Tou96] [z] [Cam75] [aa] [Dea69] [ab] [Man95] [ac] [Soo79] [ad] [Ven79]

Table A.4 – Electronic properties of CdTe and ZnSe. For more detailed data see [Mad99]. It should be mentioned that in literature exist partly drastically different valence band parameters (see e.g. [Fri94]).

material	CdTe	ZnSe
bare Kohn-Luttinger parameters of valence band[2]	$\gamma_1 = 5.35$ $\gamma_2 = 1.73$ $\gamma_3 = 2.03$ ($T = 1.8$ K) [r]	$\gamma_1 = 2.45$ $\gamma_2 = 0.61$ $\gamma_3 = 1.11$ ($T = 4.2$ K) [p,q]
effective electron mass (m^*_{eff}/m_0)	0.099 ($T = 4.2$ K) [d]	0.147 ($T = 4.2$ K) [p,q]
spin-orbit splitting energies Δ_{SO}	0.95 eV [a,n,o]	0.43 eV [f,g,h]
exciton energy E_X(1S)	1.596 eV [b,c]	2.803 eV ($T = 1.6$ K) [i,j,k] 2.804 eV ($T = 6$ K) [l]
E_{bind} free exciton (1S)	10 meV (T =1.6 K) [c,d,e]	20 meV ($T = 1.6$ K) [m] 18.7 meV ($T = 6$ K) [l]
diamagnetic susceptibility χ_d	-3.1 $4\pi Am^2/kg$ [s]	-3.2 $4\pi Am^2/kg$ [t]

[a] [Nil91] [b] [Fen85] [c] [Naw79] [d] [Neu88] [e] [Rös81] [f] [Qte92] [g] [Sto91] [h] [Wör97]
[i] [Kud92] [j] [Kud93] [k] [Poh94] [l] [Man95] [m] [Son77a] [n] [Poo95] [o] [Al-03] [p] [Höl83]
[q] [Höl85] [r] [Dan82] [s] [Can78] [t] [Sin80]

[2] If the interaction of holes and electrons with the polarization field of the optical phonons is neglected, bare electron mass m_{eff} and bare valence band parameters γ_i characterize a (polar) semiconductor. To remain the conduction and valence band structure identical (apart from a constant self-energy), if this interaction is taken into

Table A.5 – Structure (stable at room temperature (RT)) and lattice constants of MnSe and MnTe. For more detailed data see [Mad99].

material	structure (RT)	lattice constants [Å]
MnSe	rocksalt (NaCl)[a,b]	a_0 = 5.46 [d,e] ($a_0 = 5.46$ for metastable zincblende [h])
MnTe	hexagonal NiAs[c,f]	$a = 4.17$; $c = 6.78$ [g] ($a_0 =$ 6.34 for zincblende [i,j])

[a] [Dur89] [b] [Sch98a] [c] [Sch98b] [d] [Dec71] [e] [Jac70] [f] [Oft27] [g] [Grø72] [h] [Bar38] [i] [Bus94] [j] [Jan95]

Table A.6 – Band gap of ternary II-VI semiconductors at liquid helium temperature ($T = 4.2$ K).

material	band gap ($\Gamma_{8v} - \Gamma_{6c}$) [eV]	
CdMgTe	1.606 + 1.755z ($z < 0.6$)	[Oss94]
CdMnTe	1.606 + 1.592x ($x < 0.77$)	[Bot81, Hei86, Yod85]
ZnBeSe	2.82 + 2.3y ($y < 0.6$)	[Fur88a, Slo06]
ZnMnSe	2.82 + 0.48 x	[Fur88a]

Table A.7 – Valence band offset (VBO) of ternary II-VI semiconductors.

material	VBO Q_{VB}
CdTe/CdMgTe	0.3 [Kuh94]
CdTe/CdMnTe	0.3 [Kuh93]
ZnSe/ZnBeSe	0.4 [Kim00]
ZnSe/ZnMnSe	0.2 [Kla98]

Table A.8 – Mn 3d-electron exchange constants of (Cd,Mn)Te and (Zn,Mn)Se.

material	exchange constants
CdMnTe	$\alpha = 0.22$; $\beta = -0.88$ [Gaj79]
ZnMnSe	$\alpha = 0.26$ [Twa84] ; $\beta = -1.32$ [Hei84]

account by second order perturbation theory, the bare parameters are replaced by the renormalized parameters m^*_{eff} and γ_{i^*}. Information about the conversion from bare parameters to renormalized parameters is given in [Tre75].

Appendix B

Measurement and treatment of the experimental data

In this thesis access to the static and dynamic magnetization of DMS via the Mn-spin system temperature was obtained via PL of the excitonic line. The physical background is based on the dependency of the giant Zeeman-splitting on the Mn-spin temperature, as explained in section 3.1 (especially equations 3.2 and 3.3). So far unexplained is, how the information about giant Zeeman-splitting or SLR time was explicit measured, and how the measured PL data were treated.

B.1 Giant Zeeman shift

To measure the giant Zeeman shift, no time resolution is needed. Therefore, it is sufficient to illuminate the sample only by the cw probe laser. To measure the integrated PL signal, either usual CCD camera or GCCD camera in cw mode was used.

The course of experimental measurement of the giant Zeeman-splitting of a excitonic line is as follows. First of all, the PL of the excitonic line is measured without magnetic field. This measurement is repeated in magnetic field for several different field strengths. The interval between two steps determines the resolution of the giant Zeeman shift measurement. The two branches of the giant Zeeman-splitting can be distinguished via analysis of the circular polarization of the PL (σ^+ or σ^-), which differs for spin-up and spin-down states.[1] With regard to the Pauli principle, the spin-down state is filled in magnetic field at first. The energetically higher spin-up state is filled, once no free spin-down states exist any longer. Thus, the PL intensity of the spin-up branch is weaker than that of the spin-down branch.

[1] Possible mixing of the states may result in occurrence of both branches in both polarization. In this case only the intensity of the respective branches depends on the polarization.

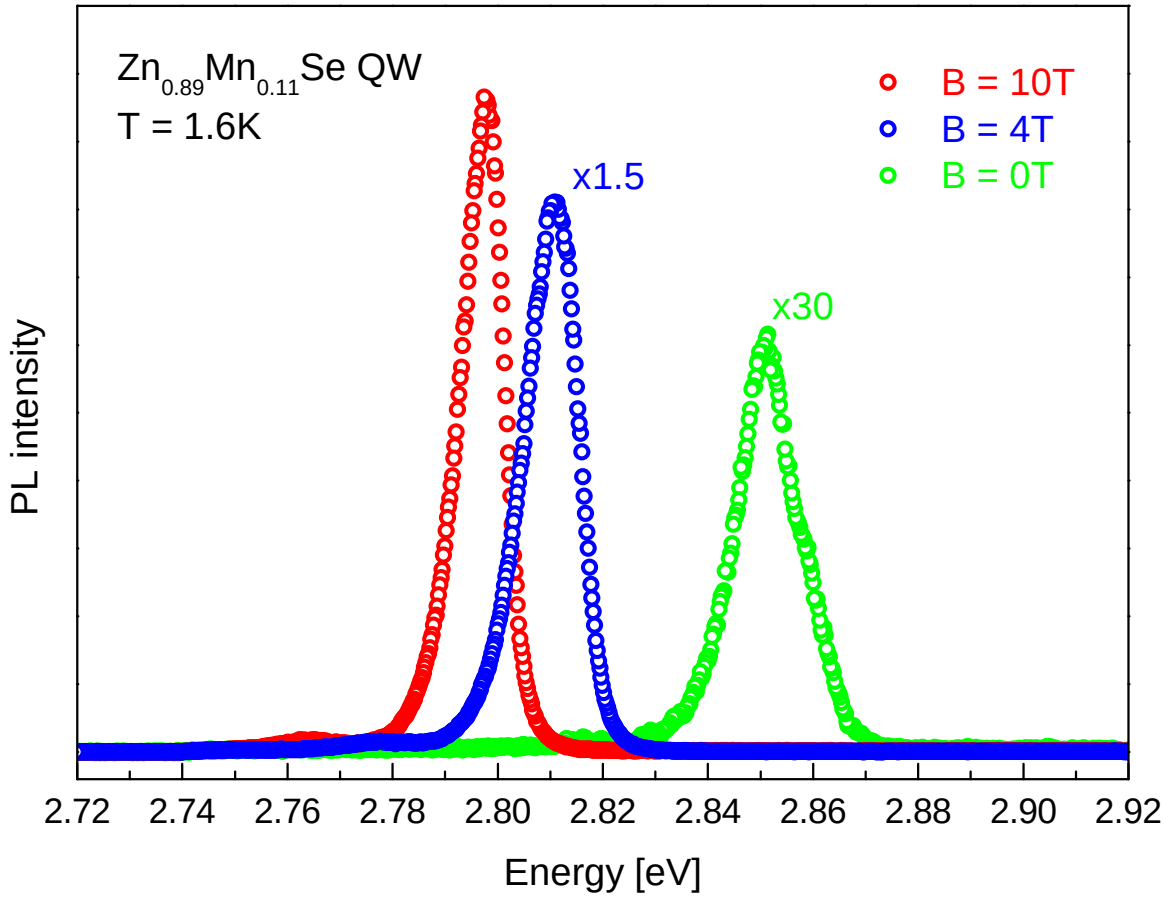

Figure B.1 – Spectrally resolved PL line of a $Zn_{0.89}Mn_{0.11}Se$ QW for different magnetic field strengths. For better comparison the weak measured signals for $B = 4\,\mathrm{T}$ and especially $B = 0\,\mathrm{T}$ were multiplied by a factor 1.5 and 30, respectively.

Via calibration of the spectrometer with the employed CCD camera, the intensity of the PL was measured spectrally resolved. Typical spectra for different magnetic field strengths are given in figure B.1. The signal was recorded via the software Winspec and stored in the Winspec file-format *spe*. These files can be converted using Winspec into comma-separated binary ASCII data files containing spectroscopic position in nm and PL intensity in units, which depend on the particular CCD chip. The set of ASCII data files, generated during giant Zeeman shift measurement, can be imported into Origin via *Multiple ASCII import*. During this procedure, the spectroscopic position in nm was converted into eV, which is more convenient for analyzing energy shifts, via a simple worksheet script (see listing B.1). This script was stored in a worksheet template, named *peakpos.otw*, which consists of three columns *A*, *B* and *C*. The

```
for (i=1;i<=wks.maxRows;i++){
    col(b)[i]=1240.66472634/col(a)[i];
};
```

Listing B.1 – Origin worksheet script for nm to eV conversion.

gained Origin worksheet contains the spectroscopic position in nanometers in column *A*, the spectroscopic position in electronvolt in column *B* and the corresponding signal intensity in column *C*.

To trace the energy shift of the PL, the position of the energy maximum has to be determined from the spectroscopic data files. Therefore, each spectra has to be fitted by means of a Gauss function. As this is very hard work for a sizeable amount of data files, the Origin C function *gfit* was programmed for this purpose (see listing B.2). This function can be started via the OriginPro *Script Window*. The syntax of the command is: gfit("name of the worksheet, where the results should be stored","name of the first data file to be fitted","body of the name of the Origin data files to be fitted"). To improve the quality of the fit, it is possible to use user-defined parameters to initialize the Gauss function. These are set via the parameters *peakint*, *peakarea*, *peakoffset* and *peakw*. To activate the user-defined parameters, the boolean variable *peak* has to be set on *true*.

For proper working of the function, the template *peakpos.otw* must exists and the data files must have the same name, except an incrementing number. The latter is automatically fulfilled for sets of files generated via Winspec.

If a spectra contains more than one spectral line (e.g. exciton and trion), the automatic analysis may fail. If these lines lie so far away from each other that they do not interfere, it is sufficient to analyze only part of the data file, containing the line to be investigated. This can be accomplished by the parameters *anf* and *en*, which correspond to the first and last, respectively, data point regarded for the Gauss fit.

```
void gfit(string winName, string strCurveUeber, int anfang, int ende)
 {
   using NLSF = LabTalk.NLSF;              // Pointer to the NLSF object
   Worksheet wks;                  // create worksheet
   wks.Create("peakpos.otw", CREATE_VISIBLE_SAME);
   wks.GetPage().Rename(winName);

   Column col;
   col = wks.Columns("A"); col.SetName("peakpos");
   col = wks.Columns("B"); col.SetName("peakarea");
   col = wks.Columns("C"); col.SetName("peakoffset");
   int colNum4 = wks.AddCol ("peakwidth");
   int colNum5 = wks.AddCol ("peakheigth");

   UINT rows = ende - anfang + 1;  //create data set for worksheet
   Dataset dd1(winName + "_peakpos");
   Dataset dd2(winName + "_peakarea");
   Dataset dd3(winName + "_peakoffset");
   Dataset dd4(winName + "_peakwidth");
```

```
    Dataset dd5(winName + "_peakheigth");
    dd1.SetSize(rows);dd2.SetSize(rows);
    dd3.SetSize(rows);dd4.SetSize(rows);dd5.SetSize(rows);

    int ii=0;

    int anf = 200;                          //user set parameters
    int en = 800;

    bool peak = false;    //user set initialization parameters
    int peakint = 2.78;     //example parameters
    int peakarea = 300;
    int peakoffset = 600;
    int peakw = 0.007;

    for (int i=anfang;i<=ende;i++)          //loop over all data fiels
     {
        string k = i;
        string strCurve = strCurveUeber + k + "1_c";    //get data file
        NLSF.Init();                // Initialize the fitter
        NLSF.dataBegin = anf;
        NLSF.dataEnd = en;

        if (peak = true)    //true = given parameters, false =
           automatic parameters
          {
              NLSF.P1 = peakoffset;
              NLSF.P2 = peakint;
              NLSF.P3 = peakw;
              NLSF.P4 = peakarea;
          }

        NLSF.Func$ = "Gauss";               // assign fitting function
        NLSF.FitData$ = strCurve;           // assign dataset name
        NLSF.Execute("parainit");           // perform automatic
           parameter initialization
        NLSF.Fit(100);    // perform fit up to 100 iterations

        dd1[ii]=NLSF.P2;                // assign results to worksheet
        dd2[ii]=NLSF.P4;
        dd3[ii]=NLSF.P1;
        dd4[ii]=NLSF.P3;
        dd5[ii]=NLSF.P1+NLSF.P4/(NLSF.P3*sqrt(pi/2));

        ii++;
    }
}
```

Listing B.2 – OriginPro C function *gfit*.

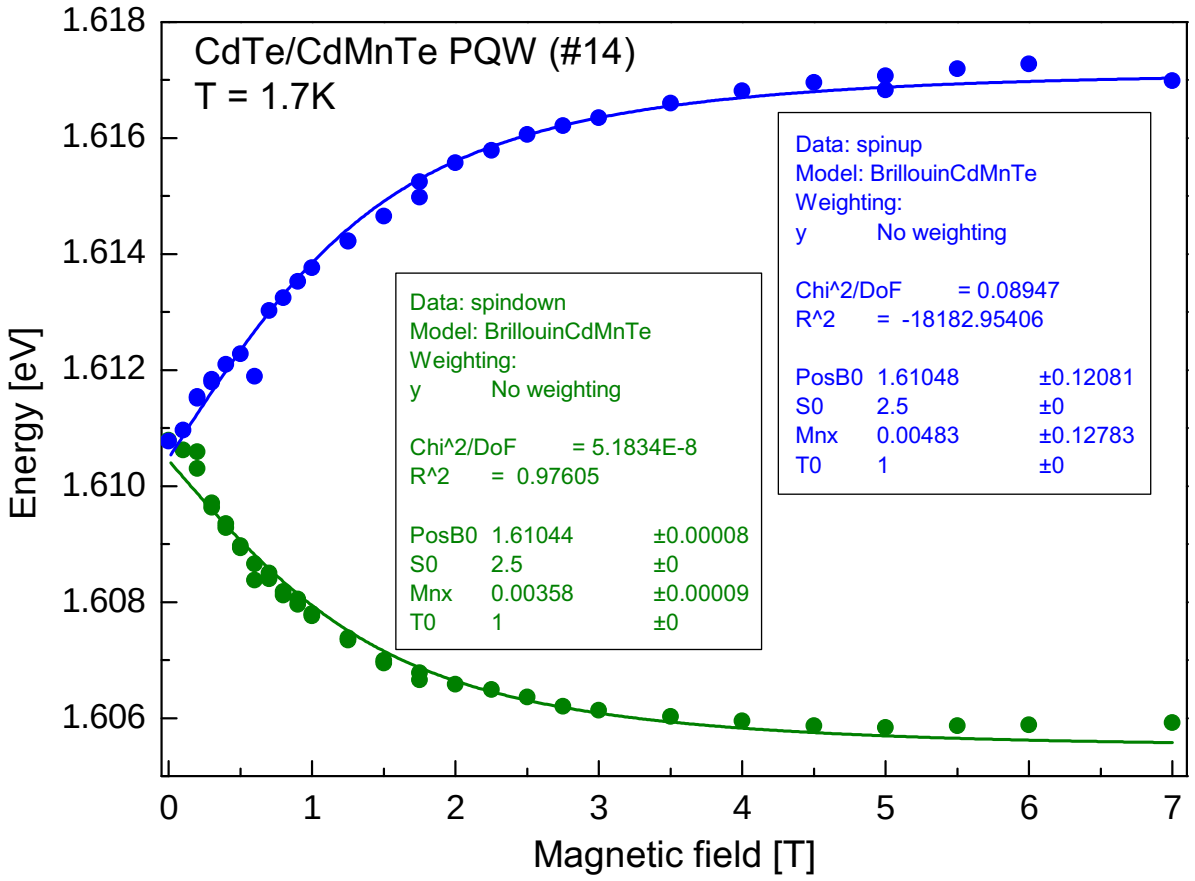

Figure B.2 – Giant Zeeman-splitting of the PL line in magnetic field for a (Cd,Mn)Te-based PQW. Both, spin-up and spin-down, states are occupied. The solid lines show fits of the data by means of equations 3.3 and 3.2 with $S_{eff} = 2.5$ and $T_0 = 1\,\mathrm{K}$. The achieved fitting parameters for the respective branches are given in the two boxes.

Despite the flexible adjustment and the big advantage of this function in fitting huge amount of data files, one has to take care in analyzing the results. Unexpected features and additional signals, which were not taken into account for initialization of the fit function, can corrupt the results. Therefore, it is important to proof manually the accuracy of the results by regarding some of the measured PL spectra, especially in case of curious results.

The worksheet, created by the function *gfit*, contains information about the position of the maximum of the PL line for each measured spectra in electronvolts. Now, this information has to be combined with the corresponding magnetic field strength in tesla in a new worksheet. Graphical representation of this worksheet shows the wanted giant Zeeman shift of the PL energy in magnetic field. Exemplary, this is shown for a CdMnTe-based sample in figure B.2.

These data can be fitted via the equations for the giant Zeeman-splitting given in 3.3 and 3.2 on page 88. This relation between energy shift and magnetic field is not included in the Origin standard functions, so that a new function has to be defined. The definition file of the new function is given in listing B.3. This function file can be added to the Origin functions via the *Advanced Fitting Tool* (menu *Analysis - Non-linear Curve Fit*). By the very same menu

```
[GENERAL INFORMATION]
Function Name=Brillouin
Brief Description=
Function Source=N/A
Function Type=User-Defined
Function Form=Y-Script
Number Of Parameters=4
Number Of Independent Variables=1
Number Of Dependent Variables=1
Analytical Derivatives for User-Defined=Off

[FITTING PARAMETERS]
Naming Method=User-Defined
Names=PosB0,S0,Mnx,T0
Meanings=?
Initial Values=--(V)
Lower Bounds=--(X,OFF)
Upper Bounds=--(X,OFF)
Number Of Significant Digits=

[FORMULA]
Temperature=1.7;
alpha=220; beta=-880;

j=5/2;
gMn=2;
kB = 1.38062*10^(-23);
muB = 9.274078*10^(-24);

k=(2*j+1)/(2*j);
h=1/(2*j);

temp = j*gMn*B*muB/((T0+Temperature)*kB);

tempa = (exp(k*temp)+exp(-k*temp))/(exp(k*temp)-exp(-k*temp));

tempb = (exp(h*temp)+exp(-h*temp))/(exp(h*temp)-exp(-h*temp));

y=PosB0-1/2*Mnx*(alpha-beta)/10^3*S0*(k*tempa-h*tempb)

[CONSTRAINTS]

[CONSTANTS]

[Parameters Initialization]

[INITIALIZATIONS]

[AFTER FITTING]
```

```
[ON PARAM CHANGE]

[INDEPENDENT VARIABLES]
B=

[DEPENDENT VARIABLES]
y=

[CONTROLS]
General Linear Constraints=Off
Initialization Scripts=Off
Scripts After Fitting=Off
Number Of Duplicates=N/A
Duplicate Offset=N/A
Duplicate Unit=N/A
Generate Curves After Fitting=Yes
Curve Point Spacing=Uniform on X-Axis Scale
Generate Peaks After Fitting=Yes
Generate Peaks During Fitting=Yes
Generate Peaks with Baseline=Yes
Paste Parameters to Plot After Fitting=Yes
Paste Parameters to Notes Window After Fitting=Yes
Generate Residuals After Fitting=No
Keep Parameters=No
Enable Parameters Initialization=0
Compile On Param Change Script=0

[COMPILE FUNCTION]
Compile=0
Compile Parameters Initialization=1
On Param Change Scripts Enabled=0

[ORIGIN C FUNCTION HEADER]

[ORIGIN C PARAMETER INITIALIZATION HEADER]
```

Listing B.3 – Origin function definition file *Brillouin.fdf*.

this function can be started to fit a dataset. The function has four parameters, which can be varied during fitting: *PosB0*, *S0*, *xMn* and *T0*. The first parameter *PosB0* is the PL energy in zero magnetic field. *S0* and *T0* are the phenomenological parameters S_{eff} and T_0 in equation 3.3. The last parameter *xMn* corresponds to the Mn content. Reasonable starting values for the effective spin S_{eff} and for the antiferromagnetic temperature T_0 can be calculated according to section 1.4.1. Starting value for *PosB0* can be taken from a PL measurement at $B = 0\,\mathrm{T}$ and *xMn* is either known or should be estimated from the giant Zeeman shift (see sections 6.2 and 6.3).

Further fixed parameters and constants are set via the edit-dialog of the *Advanced Fitting Tool*. These are the bath temperature (*Temperature*), at which the measurements were performed; the band exchange constants α and β, which are given for CdMnTe and ZnMnSe in table A.8; the total angular momentum $J = 5/2$ of the Mn^{2+}-ion; the Landé g-factor of the manganese electrons $g_{Mn} = 2$; the Boltzmann constant $k_B = 1.38062 \cdot 10^{-23}$ JK^{-1} and the Bohr magneton $\mu_B = \frac{e\hbar}{2m_0} = 9.274078 \cdot 10^{-24}$ Am^2($\hat{=}$ J/T) $= 5.78838174 \cdot 10^{-5}$ eV/T.

For calculation of the Brillouin-function, the formulation according to equation 1.27 was used. As Origin does not provide a predefined $\coth$-function, the hyperbolic cotangent was converted, using a well-known mathematical relation with the exponential function [Bro05]

$$\coth x = \frac{e^x + e^{-x}}{e^x - e^{-x}}. \tag{B.1}$$

The independent fitting-variable is the magnetic field *B* and, thus, the abscissa in figure B.2. The dependent fitting-variable y corresponds to the energy shift in eV (ordinate in figure B.2). The results of the fitting is given as fitting curve as well as list of the used variable parameters including their errors. This is exemplarily shown in figure B.2 for a (Cd,Mn)Te-based PQW.

Concerning files recorded with the older OSMA-GCCD-system, one further aspect has to be regarded. These files contain very large pixel numbers at the borders of the chip, which exceed significantly tiny signal intensities. Without removal of these noise-related signals, automatic analysis with the *gfit*-function would try to fit one of the borders, instead of a small real PL signal in another region of the spectra. To get rid of theses noise-signals, the Origin-C function *partdata* was coded, which extracts a predefined region from one Origin worksheet into a new worksheet (see listing B.4). After import of the complete data files into Origin, the function *partdata* has to be started via the OriginPro *Script Window*. The syntax of the command is: partdata(“body of the name of the Origin data files to be imported”,“name of the first data file to be imported”,“name of the last data file to be imported”,“number of first data point to be imported”,“number of last data point to be imported”). The worksheets containing the respective part of the data have the same name with added “part”. For proper working of the function the same conditions as for the function *gfit* have to be fulfilled. The function is even able to handle input of multiple data files in one sweep.

```
void partdata(string fileName, int anfang, int ende, int anf, int en)
{
   UINT rows = (en-anf+1);
   int ii;

   for (int i=anfang;i<=ende;i++)   //loop for all data files
      {
            Worksheet wks;      //create worksheet for part of data
            wks.Create("peakpos.otw", CREATE_VISIBLE_SAME);
            string winName = fileName + i + "1part";
            wks.GetPage().Rename(winName);

            Column col;
            col = wks.Columns("A");
            col.SetName("wavelength");
            col = wks.Columns("B");
            col.SetName("energy");
            col = wks.Columns("C");
            col.SetName("signal");

                //create dataset from new worksheet
            Dataset dd1(winName + "_wavelength");
            Dataset dd2(winName + "_energy");
            Dataset dd3(winName + "_signal");
            dd1.SetSize(rows);
            dd2.SetSize(rows);
            dd3.SetSize(rows);

                //create dataset containing data file i
            string valA = fileName + i + "1_a";
            string valB = fileName + i + "1_b";
            string valC = fileName + i + "1_c";

            Dataset vA(valA); vA.SetSize(en);
            Dataset vB(valB); vB.SetSize(en);
            Dataset vC(valC); vC.SetSize(en);

                //loop to fill part of data in new dataset
            ii=0;
            for (int j=anf;j<=en;j++)
                  {
                        dd1[ii] = vA[j-1];
                        dd2[ii] = vB[j-1];
                        dd3[ii] = vC[j-1];
                        ii++;
                  }
      }
}
```

Listing B.4 – OriginPro C function *partdata*

B.2 Spin-lattice relaxation time

The principle experimental method to measure the SLR time was already described in section 3.3. Additionally to the cw laser, used for the giant Zeeman-splitting measurements, a second pulsed laser is utilized to generate the heat impact for the Mn-spin system. Analogue to the measurements of the giant Zeeman-splitting, the PL excited by the cw laser is recorded, i.e. pump-probe technique is utilized. The crucial modification is that the PL spectra are measured after a certain time Δt after the heat pulse with a time resolution of 2 ns, provided by a GCCD camera.

For a time-resolved measurement, several temporal parameters have to be set, to get feasible results. These parameters are defined for the duration T between two laser pulses, which is determined by the repetition rate with the frequency ν: $T = \frac{1}{\nu}$. Thereby, T has to be considerably longer than the dynamics, which is to be measured.

For better understanding of the meanings of the subsequently introduced temporal parameters, the time scheme of a GCCD camera measurement is shown in figure B.3.

The gate delay t_{gd} is the time between a time t_{ppg} and the time, where the gate camera starts to measure PL signal. The time t_{ppg} is provided by means of a PPG (see section 3.4), which acts as timing reference of the setup. Thus, all other times are defined in respect of t_{ppg}. For simplification, this time is assumed as 0 ns. The GCCD camera and the pulse laser are such synchronized, that the maximum of the PL intensity, generated during the heat pulse, occurs around $t_{gd} = 50\,\mathrm{ns}$. I.e., the GCCD camera measures exactly at that time, the maximum of the PL strikes the GCCD camera chip. The synchronization is rather tricky because of the considerably different transit times for the signal, which is sent from the PPG to start GCCD camera measurement and the PL signal, respectively. The latter transit time consists e.g. of the transit time of the electronic signal between PPG and pulse laser, the transit time of the the

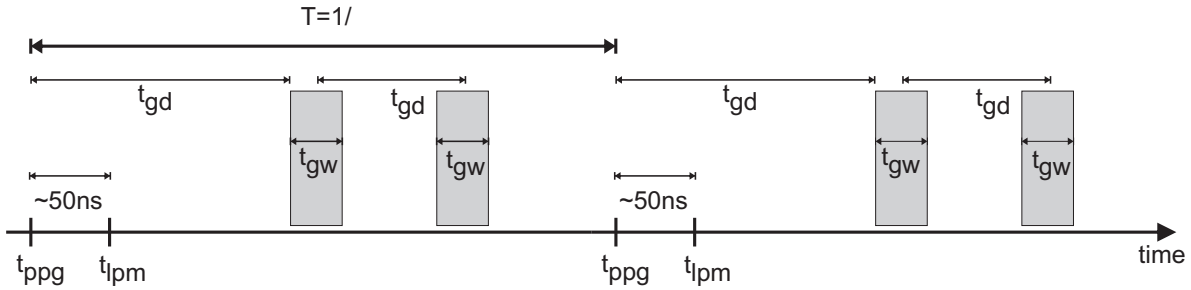

Figure B.3 – Time scheme of GCCD camera measurement: The time $t_{ppg} = 0\,\mathrm{ns}$ is determined by the PPG so that the laser pulse maximum can be observed by the GCCD camera at $t_{lpm} \sim 50\,\mathrm{ns}$. The GCCD camera starts integration of a signal at t_{gd} for a duration of t_{gw}. The distance between two gates, for measuring PL at different times after the laser pulse, is given by Δt_{gd}. This time should not be confused with the time T between two gates, if gates of several laser pulses are recorded during one measurement, to improve integrated PL intensity. This interval is determined by the repetition frequency of the PPG ν.

laser light to the sample, and the transit times of the PL to the GCCD camera. To perform the synchronization, an oscilloscope was used, to monitor camera gate and laser pulses. That t_{gd} was not adjusted to 0 ns just accounts for the desideratum to measure also heating of the Mn-spin system from the very beginning, i.e. before the PL maximum occurs. Otherwise this would be impossible, as the soft- and hardware for adjusting t_{gd} allows only setting-up positive times. For the improved measurements with a pulsed probe laser, also this laser has to be synchronized with GCCD camera and pump laser, which is described more detailed in [Deb08].

The gate delay was changed between two measured PL spectra by the gate delay step width Δt_{gd}. As this accounts for 1 ns at small $t_{gd} < 100$ ns, it increases up to 1 µs and more for gate delays exceeding 10 µs. Further very important temporal parameter is the gate width t_{gw}. This is the duration, which the GCCD camera measures the PL signal, i.e. which the camera integrates the signal between $t_{gd} < t < t_{gd} + t_{gw}$. Especially to get reasonable signal from the cw laser for times exceeding the laser pulse duration, the gate width has to be increased up to 1 µs and more. Thereby, one has to take account of a reasonable relation between t_{gd}, Δt_{gd} and t_{gw}, to get good temporal resolution, i.e. it makes no sense to measure at $t_{gd} = 100$ ns with $\Delta t_{gd} = 50$ ns or $t_{gw} = 50$ ns. From these three parameters ensue the time resolution of a measurement.

One challenging problem of time-resolved measurement is that no integrated signals, but only short temporal parts, depending on the gate width, are measured. Thus, the resulting measured PL intensity is rather short, especially for times around 50 ns after the laser pulse, when only PL from the weak cw laser is measured, but the gate widths have to be still small (1 – 5 ns). Therefore, enhancement of the PL signal is crucial for conclusive results and several steps were taken to procure this.

On the hand, actions to improve the PL intensity are circumspect alignment of the optical setup between the sample and the GCCD camera and the usage of low-loss components, like e.g. quartz lenses. Also careful setting up of the laser power is important. Thereby, a balance between sufficient PL intensity and slight heating impact on the Mn-spin system has to be found. Big improvement in this respect was yielded by the usage of a pulsed probe laser (see section 3.4).

On the other hand, the measured signal was electronically improved by variable signal gain of the PI-Max GCCD camera and by the integration of several gates. The latter was effected by the OSMA system by means of an exposure time (i.e. integration time) and, more precise, by the PI-Max system by means of indication of the number of gates, which shall be integrated.

If adequate intensity was obtained, the PL spectra were measured via Winspec. While with the OSMA system the temporal parameters t_{gd} and t_{gw} have to be set manually for each measurements, provides the newer PI-Max the possibility to measure sweeps with predefined t_{gd}, Δt_{gd}, t_{gw} and Δt_{gw}. The latter enables considerably faster and comfortable measurements.

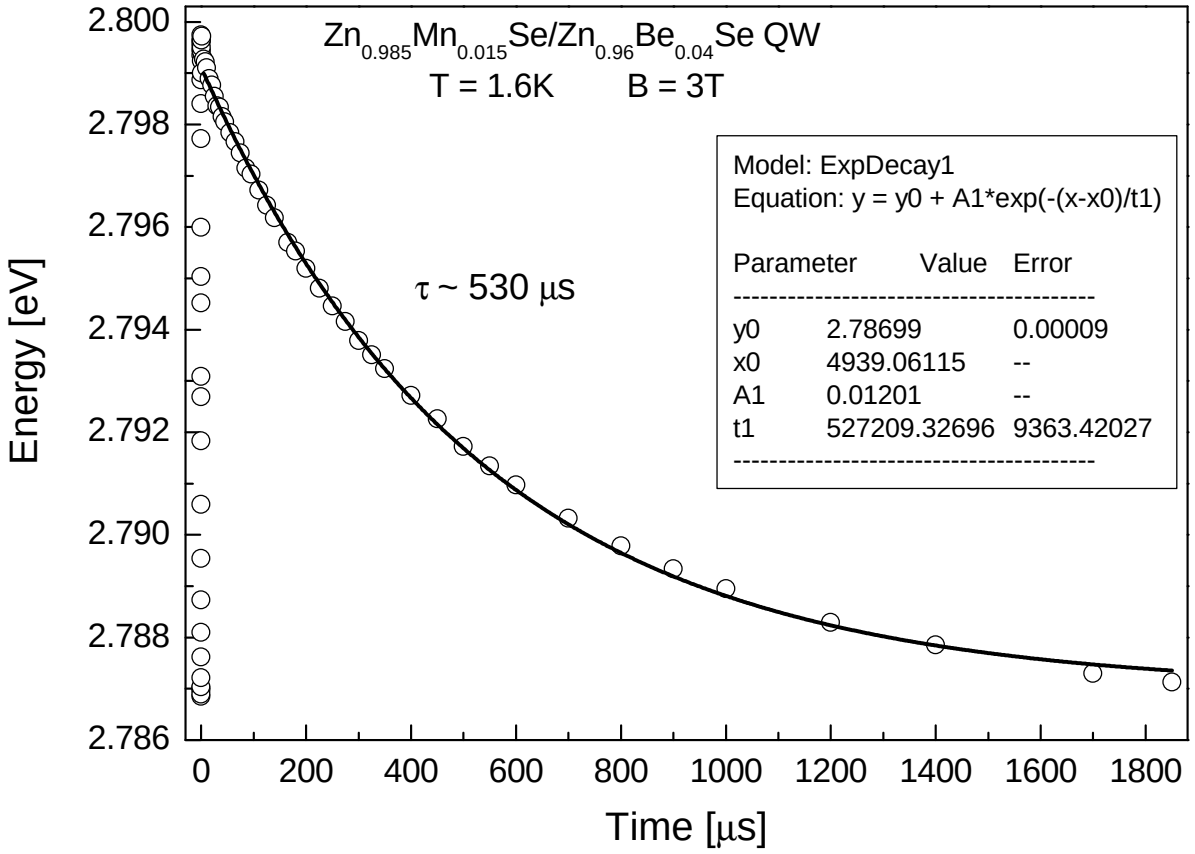

Figure B.4 – Dynamics of PL line for a $Zn_{0.985}Mn_{0.015}Se/Zn_{0.96}Be_{0.04}Se$ QW. The measurements were preformed at $T = 1.6\,\mathrm{K}$ and $B = 3\,\mathrm{T}$. The solid line shows fit of the data by means of an exponential decay with time constant $t \sim 530\,\mu\mathrm{s}$.

Analysis of the measured spectra proceeds as described in section B.1 via import to Origin and fitting of the PL spectra via the function *gfit*. The achieved worksheet, containing the position of the maximum of the PL line, has to be extended by the corresponding gate delay times. Graphical representation of such a worksheet is given in figure B.4.

According to chapter 2, the manganese temperature is determined by heating from the photoelectrons to the Mn-system and by energy relaxation with the lattice. In static equilibrium the total energy of the Mn-system is constant with respect to time:

$$\frac{dE}{dt} = \left.\frac{\partial E}{\partial t}\right|_{e-Mn} + \left.\frac{\partial E}{\partial t}\right|_{Mn-L} = 0. \tag{B.2}$$

The second term corresponds to the SLR, i.e. the decrease of the excitonic PL line in time, and is given phenomenologically by [Kön00a]

$$\left.\frac{\partial E}{\partial t}\right|_{Mn-L} \approx -\frac{E(B, \Delta\beta_{Mn})}{\tau_{SLR}}, \tag{B.3}$$

with the difference of the inverted temperatures $\Delta\beta_{Mn} = \beta_{Mn} - \beta_L$. Such a differential equation can be solved by a monoexponential approach:

$$E(t) \propto \exp\left(-\frac{t}{\tau_{SLR}}\right). \tag{B.4}$$

Hence, the SLR time can be obtained by fitting the data in figure B.4 with a simple exponential decay function. For some samples monoexponential fits do not lead to satisfying results, but two monoexponential fits. This problem is related to different cluster-types (pairs or triads) with different dynamics and is further addressed in [Deb08].

Bibliography

[Abr65] M. Abramowitz and I. A. Stegun. *Handbook of mathematical functions with formulas, graphs, and mathematical table* (Dover Publications Inc., New York, 1965). ISBN 0486612724 58

[Abr70] A. Abragam and B. Bleaney. *Electronic paramagnetic resonance of transition ions* (Clarendon, Oxford, 1970). ISBN 0198512503 4, 23, 24, 70, 80, 81, 82, 117

[Abr85] S. C. Abrahams, P. Marsh and P. M. Bridenbaugh. *Atomic substitution in $Cd_{1-x}Mn_xTe$ for 0.1 $< x <$ 0.4*. Acta Crystallographica Section C **45** (4), 545– (1985). ISSN 0108-2701. DOI http://dx.doi.org/10.1107/S010827018801296X 14

[Agg85] R. L. Aggarwal, S. N. Jasperson, P. Becla and R. R. Gałązka. *Optical determination of the antiferromagnetic exchange constant between nearest-neighbor Mn^{2+} ions in $Cd_{0.95}Mn_{0.05}Te$*. Physical Review B **32** (8), 5132–5137 (1985). ISSN 0163-1829. DOI http://dx.doi.org/10.1103/PhysRevB.32.5132 37, 38

[Agg87] R. L. Aggarwal, J. K. Furdyna and S. von Molnar (Editors). *Diluted Magnetic (Semimagnetic) Semiconductors*, volume 89 of *Materials Research Society Symposia Proceedings* (Materials Research Society, Pittsburgh, 1987). ISBN 0931837545 19, 187, 202, 219

[Agu96] V. F. Aguekian, D. E. Ashenford, B. Lunn, A. V. Koudinov, Yu. G. Kusrayev and B. P. Zakharchenya. *Photoluminescence spectra of CdTe/CdMnTe quantum well structures in an external magnetic field*. Physica Status Solidi (B) - Basic Research **195** (2), 647–652 (1996). ISSN 0370-1972. DOI http://dx.doi.org/10.1002/pssb.222195023171

[Aha73] A. Aharony and M. Fisher. *Critical behavior of magnets with dipolar interactions. I. Renormalization group near four dimensions*. Physical Review B **8** (7), 3323–3341 (1973). ISSN 0163-1829. DOI http://dx.doi.org/10.1103/PhysRevB.8.3323 27

[Aki93] H. Akinaga, T. Abe, K. Ando, S. Yoshida, K. Uchida, S. Sasaki and N. Miura. *High-field magnetoabsorption study of heterointerface effects in CdTe/$Cd_{0.6}Mn_{0.4}Te$ multi-*

ple quantum wells. Physical Review B **47** (23), 15954–15957 (1993). ISSN 0163-1829. DOI http://dx.doi.org/10.1103/PhysRevB.47.15954 51

[Aki97] A. V. Akimov, A. V. Scherbakov, A. L. Zhmodikov, V. P. Kochereshko, D. R. Yakovlev, W. Ossau, G. Landwehr, T. Wojtowicz, G. Karczewski and J. Kossut. *Luminescence detection of nonequilibrium phonons in CdTe/$Cd_{0.6}Mn_{0.4}$Te semimagnetic quantum wells*. Physical Review B **56**, 12100–12103 (1997). ISSN 0163-1829. DOI http://dx.doi.org/10.1103/PhysRevB.56.12100 95

[Aki02] H. Akinaga and H. Ohno. *Semiconductor spintronics*. IEEE Transactions on Nanotechnology **1** (1), 19–31 (2002). ISSN 1236-125X. DOI http://dx.doi.org/10.1109/TNANO.2002.1005423 2, 3

[Aki06a] A. V. Akimov, A. V. Scherbakov and D. R. Yakovlev. *Spin-lattice relaxation in magnetic semiconductor nanostructures*. In *Spintronics and Nanoelectronics*, edited by A. A. Balandin and K. L. Wang, volume 3 of *Handbook of semiconductor nanostructures and nanodevices*, chapter 2, 45–93 (American Scientific Publishers, Los Angeles, 2006). ISBN 1-58883-076-4 3, 5, 6, 32, 42, 43, 69, 81, 82, 95, 120

[Aki06b] A. V. Akimov, A. V. Scherbakov, D. R. Yakovlev, I. A. Merkulov, M. Bayer, A. Waag and L. W. Molenkamp. *Multiple transfer of angular momentum quanta from a spin-polarized hole to magnetic ions in $Zn_{1-x}Mn_xSe/Zn_{1-y}Be_ySe$ quantum wells*. Physical Review B **73** (16), 165328 (5pp.) (2006). ISSN 0163-1829. DOI http://dx.doi.org/10.1103/PhysRevB.73.165328 68, 93

[Al-03] Y. Al-Douri, R. Khenata, Z. Chelahi-Chikr, M. Driz and H. Aourag. *Effect of spin orbit on the electronic properties of zinc-blende compounds*. Journal of Applied Physics **94** (7), 4502–4506 (2003). ISSN 0021-8979. DOI http://dx.doi.org/10.1063/1.1607516 16, 164

[Alt83a] M. Altarelli. *Electronic structure and semiconductor-semimetal transition in InAs-GaSb superlattices*. Physical Review B **28** (2), 842–845 (1983). ISSN 0163-1829. DOI http://dx.doi.org/10.1103/PhysRevB.28.842 10

[Alt83b] M. Altarelli. *Electronic structure of semiconductor supperlattices*. Lecture Notes in Physics **177**, 174 (1983). ISSN 1616-6361 49

[And50a] P. W. Anderson. *Antiferromagnetism. Theory of superexchange interaction*. Physical Review **79** (2), 350–356 (1950). ISSN 0031-899X. DOI http://dx.doi.org/10.1103/PhysRev.79.350 37

[And50b] P. W. Anderson. *Generalizations of the Weiss molecular field theory of antiferromagnetism*. Physical Review **79** (4), 705–710 (1950). ISSN 0031-899X. DOI http://dx.doi.org/10.1103/PhysRev.79.705 39

[And58] V. V. Andreev and V. I. Gerasimenko. *On the theory of paramagnetic*. Pis'ma v Zhurnal Eksperimental'noy i Teoreticheskoy Fizika **35**, 1209–1215 (1958). ISSN 0370-274X 70

[And59] P. W. Anderson. *New approach to the theory of superexchange interactions*. Physical Review **115** (1), 2–13 (1959). ISSN 0031-899X. DOI http://dx.doi.org/10.1103/PhysRev.115.2 37

[And74] T. Ando and Y. Uemura. *Theory of quantum transport in a two-dimensional electron system under magnetic fields. I. characteristics of level broadening and transport under strong fields*. Journal of the Physical Society of Japan (JPSJ) **36** (4), 959–967 (1974). ISSN 0031-9015. DOI http://dx.doi.org/10.1143/JPSJ.36.959 54

[And82] T. Ando, A. B. Fowler and F. Stern. *Electronic properties of two-dimensional systems*. Reviews of Modern Physics **54** (2), 437–672 (1982). ISSN 0034-6861. DOI http://dx.doi.org/10.1103/RevModPhys.54.437 52

[And95] L. C. Andreani. *Optical transitions, excitons and polaritons in bulk and low-dimensional semiconductor structures*. In *Confined electrons and photons: New physics and applications*, edited by E. Burstein and C. Weisbuch, volume 340 of *NATO ASI Series B*, 1. edition, 57–112 (Plenum Press, New York, 1995). ISBN 0306449900 64

[Arl07] M. Arlt. *Magnetolumineszenz und Spin-Flip Raman Streuung in Halbleiter-Nanostrukturen*. master thesis, Universität Dortmund, Dortmund (2007) 141

[Ash76] N. W. Ashcroft and N. D. Mermin. *Solid state physics* (Holt, Rinehart and Winston, New York, 1976). ISBN 0030839939 14, 26, 27, 30, 31

[Ash07] N. W. Ashcroft and N. D. Mermin. *Festkörperphysik*. 3. edition (Oldenbourg, München, 2007). ISBN 3486582739 26, 27, 30, 31

[Ast02] G. V. Astakhov, D. R. Yakovlev, V. P. Kochereshko, W. Ossau, W. Faschinger, J. Puls, F. Henneberger, S. A. Crooker, Q. McCulloch, D. Wolverson, N. A. Gippius and A. Waag. *Binding energy of charged excitons in ZnSe-based quantum wells*. Physical Review B **65** (16), 165335 (17pp.) (2002). ISSN 0163-1829. DOI http://dx.doi.org/10.1103/PhysRevB.65.165335 64, 65, 66

[Ave67] M. Aven and J. S. Prewer (Editors). *Physics and chemistry of II-VI compounds* (North Holland Publishing Company, Amsterdam, 1967). ISBN 0720401127 11, 12, 13, 164

[Aws87a] D. D. Awschalom, J. M. Hong, L. L. Chang and G. Grinstein. *Dimensional-crossover studies of magnetic susceptibility in diluted-magnetic-semiconductor superlattices*.

Physical Review Letters **59** (15), 1733–1736 (1987). ISSN 0031-9007. DOI http://dx.doi.org/10.1103/PhysRevLett.59.1733 40

[Aws87b] D. D. Awschalom, J. Warnock and S. von Molnár. *Low-temperature magnetic spectroscopy of a dilute magnetic semiconductor*. Physical Review Letters **58**, 812–815 (1987). ISSN 0031-9007. DOI http://dx.doi.org/10.1103/PhysRevLett.58.812 72

[Aws87c] D. D. Awschalom, J. Warnock, J. R. Rozen and M. B. Ketchen. *Integrated magnetic spectroscopy of dilute magnetic semiconductors (invited)*. Journal of Applied Physics **61** (8), 3532–3536 (1987). ISSN 0021-8979. DOI http://dx.doi.org/10.1063/1.338715 67

[Aws91] D. D. Awschalom, M. R. Freeman, N. Samarth, H. Luo and J. K. Furdyna. *Observation of polaron dynamics in magnetic quantum wells*. Physical Review Letters **66** (9), 11212–1215 (1991). ISSN 0031-9007. DOI http://dx.doi.org/10.1103/PhysRevLett.66.1212 67

[Aws02] D. D. Awschalom, D. Loss and N. Samarth (Editors). *Semiconductor spintronics and quantum computation* (Springer, Heidelberg, 2002). ISBN 3540421769 2, 4

[Bai88] M. N. Baibich, J. M. Broto, A. Fert, F. Nguyen van Dau, F. Petroff, P. Etienne, G. Creuzet, A. Friederich and J. Chazelas. *Giant magnetoresistance of (001)Fe/(001)Cr magnetic superlattices*. Physical Review Letters **61**, 2472–2475 (1988). ISSN 0031-9007. DOI http://dx.doi.org/10.1103/PhysRevLett.61.2472 2

[Bal85] J. J. Balmer. *Notizen über die Spektrallinien des Wasserstoffs*. Annalen der Physik **25**, 80–87 (1885). 3rd series 1

[Bal62] C. J. Ballhausen. *Introduction to ligand field theory* (McGraw-Hill Education, New York, 1962). ISBN 0070035806 24

[Bal84] A. Balzarotti, M. Czyzyk, A. Kisiel, N. Motta, M. Podgòrny and M. Zimnal-Starnawska. *Local structure of ternary semiconducting random solid solutions: Extended x-ray-absorption fine structure of $Cd_{1-x}Mn_xTe$*. Physical Review B **30** (4), 2295–2298 (1984). ISSN 0163-1829. DOI http://dx.doi.org/10.1103/PhysRevB.30.2295 14

[Bar19] H. Barkhausen. *Zwei mit Hilfe der neuen Verstärker entdeckte Erscheinungen*. Zeitschrift für Physik **20** (17), 401–403 (1919). ISSN 0044-3328 28

[Bar38] A. Baroni. *The polymorphism of manganese selenide*. Zeitschrift für Kristallographie **99**, 336–339 (1938). ISSN 0044-2968. In Italian 165

[Bar81] S. E. Barnes. *Theory of electron spin resonance of magnetic ions in metals*. Advances in Physics **30** (6), 801–938 (1981). ISSN 0001-8732. DOI http://dx.doi.org/10.1080/00018738100101447 121

[Bar87] D. U. Bartholomew, E.-K. Suh, A. K. Redriguez, A. K. Ramdas and R. L. Aggarwal. *Raman scattering from antiferromagnetically coupled Mn^{2+} ion pairs in $Cd_{1-x}Mn_xS$ and $Cd_{1-x}Mn_xSe$*. Solid State Communications **62** (4), 235–238 (1987). ISSN 0038-1098. DOI http://dx.doi.org/10.1016/0038-1098(87)90802-7 39

[Bas81] G. Bastard. *Superlattice band structure in the envelope-function approximation*. Physical Review B **24**, 5693–5697 (1981). ISSN 0163-1829. DOI http://dx.doi.org/10.1103/PhysRevB.24.5693 49

[Bas82] G. Bastard. *Theoretical investigations of superlattice band structure in the envelope-function approximation*. Physical Review B **25**, 7584–7597 (1982). ISSN 0163-1829. DOI http://dx.doi.org/10.1103/PhysRevB.25.7584 49

[Bas90] G. Bastard. *Wave mechanics applied to semiconductor heterostructures* (Editions de Physique, France, 1990). ISBN 2868830927 49

[Bau94] J. J. Baumberg, S. A. Crooker, D. D. Awschalom, N. Samarth, H. Luo and J. K. Furdyna. *Ultrafast Faraday spectroscopy in magnetic semiconductor quantum structures*. Physical Review B **50**, 7689–7700 (1994). ISSN 0163-1829. DOI http://dx.doi.org/10.1103/PhysRevB.50.7689 71

[Bay95] B. Baylac, T. Amand, X. Marie, B. Dareys, M. Brousseau, G. Bacquet and V. Thierry-Mieg. *Hole spin relaxation in n-modulation doped quantum wells*. Solid State Communications **93** (1), 57–60 (1995). ISSN 0038-1098. DOI http://dx.doi.org/10.1016/0038-1098(94)00721-7 55

[Bec88] W. M. Becker. *Band structure and optical properties of wide-gap $A^{II}_{1-x}Mn_xB^{VI}$ alloys at zero magnetic fields*. In Furdyna and Kossut [Fur88b], chapter 2, 35–72. ISBN 0127521259 19, 22

[Ben78] G. Beni and T. M. Rice. *Theory of electron-hole liquid in semiconductors*. Physical Review B **18** (2), 768–785 (1978). ISSN 0163-1829. DOI http://dx.doi.org/10.1103/PhysRevB.18.768 17

[Bha83] A. K. Bhattacharjee, G. Fishman and B. Coqblin. *Virtual bound state model for the exchange interaction in semimagnetic semiconductors such as $Cd_{1-x}Mn_xTe$*. Physica B+C **117-118** (1), 449–451 (1983). ISSN 0378-4363. DOI http://dx.doi.org/10.1016/0378-4363(83)90555-7 23, 35

[Bic84] R. N. Bicknell, R. W. Yanka, N. C. Giles-Taylor, D. K. Blanks, E. L. Buckland and J. F. Schetzina. *$Cd_{1-x}Mn_xTe$-CdTe multilayers grown by molecular beam epitaxy*. Applied Physics Letters **45** (1), 92–94 (1984). ISSN 0003-6951. DOI http://dx.doi.org/10.1063/1.94981 3, 46

[Bin89] G. Binasch, P. Grünberg, F. Saurenbach and W. Zinn. *Enhanced magnetoresistance in layered magnetic structures with antiferromagnetic interlayer exchange*. Physical Review B **39** (7), 4828–4830 (1989). ISSN 0163-1829. DOI http://dx.doi.org/10.1103/PhysRevB.39.4828 2

[Bin91] V. Bindilatti, T. Q. Vu and Y. Shapira. *Phonon bottleneck in the spin relaxation of dilute magnetic semiconductors: New model for the narrowing of the magnetization steps in pulsed fields*. Solid State Communications **77** (6), 423–426 (1991). ISSN 0038-1098. DOI http://dx.doi.org/10.1016/0038-1098(91)90229-O 6, 82, 116

[Bir75] G. L. Bir, A. G. Aronov and G. E. Pikus. *Spin relaxation of electrons due to scattering by holes*. Journal of Experimental and Theoretical Physics (JETP) **42**, 705–712 (1975). ISSN 1063-7761 78

[Blo46] F. Bloch. *Nuclear induction*. Physical Review **70**, 460–474 (1946). ISSN 0031-899X. DOI http://dx.doi.org/10.1103/PhysRev.70.460 70

[Blo55] N. Bloembergen and T. J. Rowland. *Nuclear spin exchange in solids: Tl^{203} and Tl^{205} magnetic resonance in thallium and thallic oxide*. Physical Review **97** (6), 1679–1698 (1955). ISSN 0031-899X. DOI http://dx.doi.org/10.1103/PhysRev.97.1679 37

[Blu62] M. Blume and R. Orbach. *Spin-lattice relaxation of s-state ions: Mn^{2+} in a cubic environment*. Physical Review **127**, 1587–1592 (1962). ISSN 0031-899X. DOI http://dx.doi.org/10.1103/PhysRev.127.1587 5, 118

[Boh13] N. Bohr. *On the constitution of atoms and molecules*. Philosophical Magazine **26**, 1–25 (1913). Series 6 1

[Bot81] N. Bottka, J. Stankiewicz and W. Giriat. *Electroreflectance studies in $Cd_{1-x}Mn_xTe$ solid solutions*. Journal of Applied Physics **52** (6), 4189–4193 (1981). ISSN 0021-8979. DOI http://dx.doi.org/10.1063/1.329233 12, 13, 19, 164, 165

[Bou36] L. P. Bouckaert, R. Smoluchowski and E. Wigner. *Theory of brillouin zones and symmetry properties of wave functions in crystals*. Physical Review **50** (1), 58–67 (1936). ISSN 0031-899X. DOI http://dx.doi.org/10.1103/PhysRev.50.58 13

[Bra84] N. B. Brandt and V. V. Moshchalkov. *Semimagnetic semiconductors*. Advances in Physics **33** (3), 193–256 (1984). ISSN 0001-8732. DOI http://dx.doi.org/10.1080/00018738400101661 40

[Bre33] G. Breit. *Quantum theory of dispersion*. Reviews of Modern Physics **4** (3), 504–576 (1933). ISSN 0034-6861. DOI http://dx.doi.org/10.1103/RevModPhys.4.504 87

[Bro85] W. Bron. *Nonequilibrium Phonon Dynamics*, volume 124 of *Nato Advanced Study Institute Series B: Physics*. 1. edition (Springer, New York, 1985). ISBN 0306420082 95

[Bro93] P. J. Brown. *Magnetic structure studied with zero-field neutron polarimetry*. Physica B: Condensed Matter **192** (1-2), 14–24 (1993). ISSN 0921-4526. DOI http://dx.doi.org/10.1016/0921-4526(93)90104-E 29

[Bro05] I. N. Bronstein, K. A. Semendjajew, G. Musiol and H. Mühlig. *Taschenbuch der Mathematik*. 6. edition (Verlag Harri Deutsch, Frankfurt, 2005). ISBN 3817120060 174

[Bru84] J. A. Brum, G. Bastard and C. Guillemot. *Screened Coulombic impurity bound states in semiconductor quantum wells*. Physical Review B **30**, 905–908 (1984). ISSN 0163-1829. DOI http://dx.doi.org/10.1103/PhysRevB.30.905 122

[Bun87a] B. A. Bunker. *Extended x-ray absorption fine-structure studies of semiconductor structure*. Journal of Vacuum Science and Technology A **5** (5), 3003–3008/ (1987). ISSN 0734-2101. DOI http://dx.doi.org/10.1116/1.574247 14

[Bun87b] B. A. Bunker, W.-F. Pong, V. Debska, D. R. Yoder-Short and J. K. Furdyna. *EXAFS determination of bond lengths in $Zn_{1-x}Mn_xSe$*. In Aggarwal *et al.* [Agg87], 231–260. ISBN 0931837545 14

[Bur84] A. I. Burshtein. *Concentration quenching of noncoherent exciation in solutions*. Soviet Physics - Uspekhi **27** (8), 579–606 (1984). ISSN 0038-5670. Translation of: Usp. Fiz. Nauk, USSR **143**, 553-600 (August 1984) 147

[Bus94] J. R. Buschert, F. C. Peiris, N. Samarth, H. Luo and J. K. Furdyna. *Unusual elastic constants of cubic MnTe in strained-layer superlattices measured by X-ray diffraction*. Physical Review B **49** (7), 4619–4622 (1994). ISSN 0163-1829. DOI http://dx.doi.org/10.1103/PhysRevB.49.4619 165

[Byc84a] Y. A. Bychkov and E. I. Rashba. *Oscillatory effects and the magnetic susceptibility of carriers in inversion layers*. Journal of Physics C: Solid State Physics **17** (33), 6039–6045 (1984). ISSN 0022-3719. DOI http://dx.doi.org/10.1088/0022-3719/17/33/015 50

[Byc84b] Y. A. Bychkov and E. I. Rashba. *Properties of a 2D electron gas with lifted spectral degeneracy*. Journal of Experimental and Theoretical Physics Letters (JETP) **39** (2),

78–81 (1984). ISSN 0021-3640. URL http://www.jetpletters.ac.ru/ps/1264/article_19121.shtml 50

[Byl86] R. B. Bylsma, W. M. Becker, J. Kossut, U. Debska and D. Yoder-Short. *Dependence of energy gap on x and T in $Zn_{1-x}Mn_xSe$: The role of exchange interaction*. Physical Review B **33** (12), 8207–8215 (1986). ISSN 0163-1829. DOI http://dx.doi.org/10.1103/PhysRevB.33.8207 20

[Byl87] R. B. Bylsma, J. Kossut, W. M. Becker, L. A. Kolodziejski, R. L. Gunshor and R. Frohne. *Photoluminescence and excitation spectra of $Zn_{1-x}Mn_xSe$ films and superlattices grown by molecular-beam epitaxy*. Journal of Applied Physics **61** (8), 3011–3019 (1987). ISSN 0021-8979. DOI http://dx.doi.org/10.1063/1.337851 20, 52

[Cai86] W. Cai and C. S. Ting. *Screening effect on the Landau-level broadening for electrons in GaAs-$Ga_{1-x}Al_xAs$ heterojunctions*. Physical Review B **33**, 3967–3972 (1986). ISSN 0163-1829. DOI http://dx.doi.org/10.1103/PhysRevB.33.3967 54

[Cam75] J. Camassel and D. Auvergne. *Temperature dependence of the fundamental edge of germanium and zinc-blende-type semiconductors*. Physical Review B **12** (8), 3258–3267 (1975). ISSN 0163-1829. DOI http://dx.doi.org/10.1103/PhysRevB.12.3258 164

[Cam97] P. E. van Camp, V. E. van Doren and J. L. Martins. *High-pressure phases of magnesium selenide and magnesium telluride*. Physical Review B **55** (2), 775–779 (1997). ISSN 0163-1829. DOI http://dx.doi.org/10.1103/PhysRevB.55.775 13, 164

[Cam01] C. Camilleri, F. Teppe, D. Scalbert, Y. G. Semenov, M. Nawrocki, M. D'yakonov, J. Cibert, S. Tatarenko and T. Wojtowicz. *Electron and hole spin relaxation in modulation-doped CdMnTe quantum wells*. Physical Review B **64** (8), 085331 (7pp.) (2001). ISSN 0163-1829. DOI http://dx.doi.org/10.1103/PhysRevB.64.085331 6, 76

[Can78] R. M. Candea, S. J. Hudgens and M. Kastner. *Ionicity trends in the diamagnetism and its temperature dependence in average-valence-four semiconductors*. Physical Review B **18** (6), 2733–2738 (1978). ISSN 0163-1829. DOI http://dx.doi.org/10.1103/PhysRevB.18.2733 164

[Cha88] S.-K. Chang, A. V. Nurmikko, J.-W. Wu, L. A. Kolodziejski and R. L. Gunshor. *Band offsets and excitons in CdTe/(Cd,Mn)Te quantum wells*. Physical Review B **37** (3), 1191–1198 (1988). ISSN 0163-1829. DOI http://dx.doi.org/10.1103/PhysRevB.37.1191 17, 52

[Cha89] L. L. Chang. *CdTe—CdMnTe superlattices*. Superlattices and Microstructures **6** (1), 39–45 (1989). ISSN 0749-6036. DOI http://dx.doi.org/10.1016/0749-6036(89)90091-8 48

[Cha00] E. Chauvet, C. nd Tournié and J.-P. Faurie. *Nature of the band gap in $Zn_{1-x}Be_xSe$ alloys*. Physical Review B **61** (8), 5332–5336 (2000). ISSN 0163-1829. DOI http://dx.doi.org/10.1103/PhysRevB.61.5332 19

[Che76] J. R. Chelikowsky and M. L. Cohen. *Nonlocal pseudopotential calculations for the electronic structure of eleven diamond and zinc-blende semiconductors*. Physical Review B **14** (2), 556–582 (1976). ISSN 0163-1829. DOI http://dx.doi.org/10.1103/PhysRevB.14.556 18

[Che93] D. S. Chemla. *Special issue: Optics of nanostructures*. Physics Today **46** (6), 22–23 (1993). ISBN 0031-9228. DOI http://dx.doi.org/10.1063/1.881351 46

[Cho70] A. Y. Cho, M. B. Panish and I. Hayashi. *Molecular beam epitaxy of GaAs, $Al_xGa_{1-x}As$ and GaP*. In *Proceedings Third Int. Symp. on Gallium Arsenide and Related Compounds*, edited by K. Paulus, 18–29 (Aachen, 1970) 46

[Coh77] C. Cohen-Tannoudji, B. Diu and F. Laloë (Editors). *Quantum mechanics*, volume 1. 2. edition (John Wiley & Sons, Paris, 1977). ISBN 0471164321 48

[Cor86] L. M. Corliss, J. M. Hastings, S. M. Shapiro, Y. Shapira and P. Becla. *Magnetic exchange constant in $Zn_{1-x}Mn_xTe$*. Physical Review B **33** (1), 608–609 (1986). ISSN 0163-1829. DOI http://dx.doi.org/10.1103/PhysRevB.33.608 39

[Cro95] S. A. Crooker, D. A. Tulchinsky, J. Levy, D. D. Awschalom, R. Garcia and N. Samarth. *Enhanced spin interactions in digital magnetic heterostructures*. Physical Review Letters **75**, 505–508 (1995). ISSN 0031-9007. DOI http://dx.doi.org/10.1103/PhysRevLett.75.505 135

[Cro97] S. A. Crooker, D. D. Awschalom, J. J. Baumberg, F. Flack and N. Samarth. *Optical spin resonance and transverse spin relaxation in magnetic semiconductor quantum wells*. Physical Review B **56**, 7574–7588 (1997). ISSN 0163-1829. DOI http://dx.doi.org/10.1103/PhysRevB.56.7574 6, 76

[Dam91] T. C. Damen, L. Via, J. E. Cunningham, J. Shah and L. J. Sham. *Subpicosecond spin relaxation dynamics of excitons and free carriers in GaAs quantum wells*. Physical Review Letters **67** (24), 3432–3435 (1991). ISSN 0031-9007. DOI http://dx.doi.org/10.1103/PhysRevLett.67.3432 55

[Dan82] L. S. Dang, G. Neu and R. Romestain. *Optical detection of cyclotron resonance of electron and holes in CdTe*. Solid State Communications **44** (8), 1187–1190 (1982). ISSN 0038-1098. DOI http://dx.doi.org/10.1016/0038-1098(82)91082-1 164

[Dat85] S. Datta, J. K. Furdyna and R. L. Gunshor. *Diluted magnetic semiconductor superlattices and heterostructures*. Superlattices and Microstructures **1** (4), 327–334 (1985). ISSN 0749-6036. DOI http://dx.doi.org/10.1016/0749-6036(85)90094-1 11, 43, 46, 51, 52

[Dau94] J. Daughton, J. Brown, E. Chen, R. Beech, A. Pohm and W. Kude. *Magnetic field sensors using GMR multilayer*. IEEE Transactions on Magnetics **30** (6 (1-2)), 4608–4610 (1994). ISSN 0018-9464. DOI http://dx.doi.org/10.1109/20.334164 2

[Dau99] J. M. Daughton, A. V. Pohm, R. T. Fayfield and C. H. Smith. *TOPICAL REVIEW: Applications of spin dependent transport materials*. Journal of Physics D: Applied Physics **32**, R169–R177 (1999). ISSN 0022-3727. DOI http://dx.doi.org/10.1088/0022-3727/32/22/201 2

[Dea69] P. J. Dean and J. L. Merz. *Pair spectra and "Edge Emission" in zinc selenide*. Physical Review **178** (3), 1310–1318 (1969). ISSN 0031-899X. DOI http://dx.doi.org/10.1103/PhysRev.178.1310 164

[Deb81] U. Debeska, M. Dietl, G. Grabecki, E. Janik, E. Kierzek-Pecold and M. Klimeiewicz. *Energy band gaps of $Hg_xCd_yMn_zTe$ (x + y + z = 1) epitaxial layers*. Physica Status Solidi (A) - Applied Research **64** (2), 707–713 (1981). ISSN 0031-8965. DOI http://dx.doi.org/10.1002/pssa.2210640236 3

[Deb08] J. Debus. *Spin-Gitter-Relaxationsdynamik in (Zn,Mn)Se/(Zn,Be)Se Quantentrögen und Magneto-Photolumineszenz von Fe*$13+$*-Verunreinigungszentren in ZnO*. master thesis, Universität Dortmund, Dortmund (2008) 82, 177, 179

[Dec71] D. L. Decker and R. L. Wild. *Optical properties of* α*-MnSe*. Physical Review B **4** (10), 3425–3437 (1971). ISSN 0163-1829. DOI http://dx.doi.org/10.1103/PhysRevB.4.3425 165

[Del90] E. Deleporte, J. M. Berroir, G. Bastard, C. Delalande, J. M. Hong and L. L. Chang. *Magnetic-field-induced type-I→ type-II transition in a semimagnetic $CdTe/Cd_{0.93}Mn_{0.07}Te$ superlattice*. Physical Review B **42** (9), 5891–5894 (1990). ISSN 0163-1829. DOI http://dx.doi.org/10.1103/PhysRevB.42.5891 64

[Den91] A. R. Denton and N. W. Ashcroft. *Vegard's law*. Physical Review A **43** (6), 3161–3164 (1991). ISSN 1050-2947. DOI http://dx.doi.org/10.1103/PhysRevA.43.3161 12

[Die81] T. Dietl. *Semimagnetic semiconductors in magnetic fields*. In *Physics in High Magnetic Fields*, edited by S. Chikazumi and N. Miura, volume 24 of *Springer series in solid-state sciences*, 344 (Springer, Berlin, Heidelberg, New-York, 1981). ISBN 3540105875. Proceedings of the Oji International Seminar [on the Application of High Magnetic Fields in the Physics of Semiconductors and Magnetic Materials], Hakone, Japan, Sept. 10 - 13, 1980 35

[Die83] T. Dietl and J. Spałek. *Effect of thermodynamic fluctuations of magnetization on the bound magnetic polaron in dilute magnetic semiconductors*. Physical Review B **28** (3), 1548–1563 (1983). ISSN 0163-1829. DOI http://dx.doi.org/10.1103/PhysRevB.28.1548 4

[Die94] T. Dietl. *(Diluted) magnetic semiconductors*. In *Materials, properties, and preparation*, edited by S. Mahajan and T. S. Moss, volume 3b of *Handbook of semiconductors*, 2. edition, chapter 17, 1251–1342 (North-Holland Publishing Company, Amsterdam, 1994). ISBN 0444888357 3, 4, 120

[Die95] T. Dietl, P. Peyla, W. Grieshaber and Y. Merle d'Aubigné. *Dynamics of spin organization in diluted magnetic semiconductors*. Physical Review Letters **74**, 474–477 (1995). ISSN 0031-9007. DOI http://dx.doi.org/10.1103/PhysRevLett.74.474 67, 70, 71, 92, 130

[Dio85] J. Diouri, J. P. Lascaray and M. El Amrani. *Effect of the magnetic order on the optical-absorption edge in $Cd_{1-x}Mn_xTe$*. Physical Review B **31** (12), 7995–7999 (1985). ISSN 0163-1829. DOI http://dx.doi.org/10.1103/PhysRevB.31.7995 20

[DiV95] D. P. DiVincenzo . *Quantum computation*. Science **270** (5234), 255–261 (1995). ISSN 0036-8075. DOI http://dx.doi.org/10.1126/science.270.5234.255 3

[Döh04] S. Döhrmann, D. Hägele, J. Rudolph, M. Bichler, D. Schuh and M. Oestreich. *Anomalous spin dephasing in (110) GaAs quantum wells: Anisotropy and intersubband effects*. Physical Review Letters **93** (14), 147405 (4pp.) (2004). ISSN 0031-9007. DOI http://dx.doi.org/10.1103/PhysRevLett.93.147405 76, 78

[Dol82] G. Dolling, T. M. Holden, V. F. Sears, J. K. Furdyna and W. Giriat. *Neutron diffraction studies of diluted magnetic semiconductors (invited)*. Journal of Applied Physics **53**, 7644–7648 (1982). ISSN 0021-8979. DOI http://dx.doi.org/10.1063/1.330174 40

[Dre55] G. Dresselhaus. *Spin-orbit coupling effects in zinc blende structures*. Physical Review **100** (2), 580–586 (1955). ISSN 0031-899X. DOI http://dx.doi.org/10.1103/PhysRev.100.580 17

[Dre04] J. Dreßen and A. Hoffknecht. *Nichtflüchtige Datenspeicher*. Physik Journal **1**, 39–43 (2004). ISSN 1617-9439 2

[Dur89] S. M. Durbin, J. Han, Sungki O, M. Kobayashi, D. R. Menke, R. L. Gunshor, Q. Fu, N. Pelekanos, A. V. Nurmikko, D. Li, J. Gonsalves and N. Otsuka. *Zinc-blende MnTe: Epilayers and quantum well structures*. Applied Physics Letters **55** (20), 2087–2089 (1989). ISSN 0003-6951. DOI http://dx.doi.org/10.1063/1.102091 3, 11, 165

[D'y71] M. I. D'yakonov and V. I. Perel. *Spin orientation of electrons associated with the interband absorption of light in semiconductors*. Journal of Experimental and Theoretical Physics (JETP) **33** (5), 1053–1059 (1971). ISSN 1063-7761 13

[D'y72] M. I. D'yakonov and V. I. Perel. *Spin relaxation of conduction electrons in noncentrosymmetric semiconductors*. Soviet Physics - Solid State **13**, 3023–3026 (1972). ISSN 0038-5654 77

[D'y74] M. I. D'yakonov and V. I. Perel. *Optical orientation in a system of electrons and lattice nuclei in semiconductors theory*. Journal of Experimental and Theoretical Physics (JETP) **38**, 177–183 (1974). ISSN 1063-7761 79

[D'y84] M. I. D'yakonov and V. I. Perel. *Optical orientation*. In Meier and Zakharchenya [Mei84], 11–71. ISBN 0444867414 17, 55

[D'y86] M. I. D'yakonov and V. Yu. Kachorovskii. *Spin relaxation of conduction electrons in noncentrosymmetric semiconductors*. Soviet Physics - Semiconductors **20** (1), 110–112 (1986). ISSN 0038-5700 50, 78

[Dzy57] I. E. Dzyaloshinskii. *Thermodynamic theory of "weak" ferromagnetism in antiferromagnetic substances*. Journal of Experimental and Theoretical Physics (JETP) **5**, 6 (1957). ISSN 1063-7761 36

[Dzy58] I. Dzyaloshinsky. *A thermodynamic theory of "weak" ferromagnetism of antiferromagnetics*. Journal of Physics and Chemistry of Solids **4** (4), 241–255 (1958). ISSN 0022-3697. DOI http://dx.doi.org/10.1016/0022-3697%2858%2990076-3 36, 119

[Dzy00] A. B. Dzyubenko and A. Y. Sivachenko. *Charged magnetoexcitons in two-dimensions: magnetic translations and families of dark states*. Physical Review Letters **84**, 4429–4432 (2000). ISSN 0031-9007. DOI http://dx.doi.org/10.1103/PhysRevLett.84.4429 66

[Ein15] A. Einstein and W. J. de Haas. *Experimenteller Nachweis der Ampèreschen Molekularströme*. Deutsche Physikalische Gesellschaft, Verhandlungen **17**, 152–170 (1915) 1

[Eis86] W. Eisenmenger and A. A. Kaplyanskii (Editors). *Nonequilibrium phonons in nonmetallic crystals*, volume 16 of *Modern problems in condensed matter sciences* (Elsevier Science, North Holland, Amsterdam, 1986). ISBN 0444869891 95

[Ell54a] R. J. Elliott. *Spin-orbit coupling in band theory-character tables for some "double" space groups*. Physical Review **96** (2), 280–287 (1954). ISSN 0031-899X. DOI http://dx.doi.org/10.1103/PhysRev.96.280 13

[Ell54b] R. J. Elliott. *Theory of the effect of spin-orbit coupling on magnetic resonance in some semiconductors*. Physical Review **96** (2), 266–279 (1954). ISSN 0031-899X. DOI http://dx.doi.org/10.1103/PhysRev.96.266 13, 78

[Ell57] R. J. Elliott. *Intensity of optical absorption by excitons*. Physical Review **108**, 1384–1389 (1957). ISSN 0031-899X. DOI http://dx.doi.org/10.1103/PhysRev.108.1384 60, 62

[Esc82] M. Escorne and A. Mauger. *Spin-glass versus antiferromagnetic clustering in $Cd_{1-x}Mn_xTe$*. Physical Review B **25** (7), 4674–4678 (1982). ISSN 0163-1829. DOI http://dx.doi.org/10.1103/PhysRevB.25.4674 40

[Fab99] J. Fabian and S. Das Sarma. *Spin relaxation of conduction electrons*. Journal of Vacuum Science and Technology B: Microelectronics and Nanometer Structures **17** (4), 1708–1715 (1999). ISSN 1071-1023. DOI http://dx.doi.org/10.1116/1.590813 76, 78, 79

[Fal03] H. Falk, J. Hübner, P. J. Klar and W. Heimbrodt. *Intralayer and interlayer energy transfer from excitonic states into the Mn $3d^5$ shell in diluted magnetic semiconductor structures*. Physical Review B **68** (16), 165203 (12pp.) (2003). ISSN 0163-1829. DOI http://dx.doi.org/10.1103/PhysRevB.68.165203 92, 120

[Far96] W. Farah, D. Scalbert and M. Nawrocki. *Magnetic relaxation studied by transient reflectivity in $Cd_{1-x}Mn_xTe$*. Physical Review B **53**, 10461–10464 (1996). ISSN 0163-1829. DOI http://dx.doi.org/10.1103/PhysRevB.53.R10461 6, 71, 82, 92, 93, 108, 112, 114, 116, 117, 119, 144, 156

[Feh55] G. Feher and A. F. Kip. *Electron spin resonance absorption in metals. I. Experimental*. Physical Review **98** (2), 337–348 (1955). ISSN 0031-899X. DOI http://dx.doi.org/10.1103/PhysRev.98.337 87

[Fen85] Z. C. Feng, A. Mascarenhas, W. J. Choyke, R. F. C. Farrow, F. A. Shirland and W. J. Takei. *A photoluminescence study of molecular beam epitaxy grown CdTe films on (001)InSb substrates*. Applied Physics Letters **47** (1), 24–25 (1985). ISSN 0003-6951. DOI http://dx.doi.org/10.1063/1.96420 164

[Fie97] R. Fiederling. *Magnetooptik an parabolischen und halbparabolischen CdTe/CdMnTe Quantentrögen - Magnetische Lokalisation in digitalen magnetischen Heterostrukturen*. master thesis, Universität Würzburg, Würzburg (1997) 48, 51, 57, 58, 59, 60, 162

[Fie99] R. Fiederling, M. Keim, G. Reuscher, W. Ossau, G. Schmidt, A. Waag and L. W. Molenkamp. *Injection and detection of a spin-polarized current in a light-emitting diode*. Nature **402** (6763), 787–791 (1999). ISSN 0028-0836. DOI http://dx.doi.org/10.1038/45502 3

[Fin61] C. B. P. Finn, R. Orbach and W. P. Wolf. *Spin-lattice relaxation in cerium magnesium nitrate at liquid helium temperature: A new process*. Proceedings of the Physical Society **77** (2), 261–268 (1961). ISSN 0368-3516. DOI http://dx.doi.org/10.1088/0370-1328/77/2/305 81

[Fin95] G. Finkelstein, H. Shtrikman and I. Bar-Joseph. *Optical spectroscopy of a two-dimensional electron gas near the metal-insulator transition*. Physical Review Letters **74**, 976–979 (1995). ISSN 0031-9007. DOI http://dx.doi.org/10.1103/PhysRevLett.74.976 66

[Fou22] J. B. J. Fourier. *Théorie analytique de la chaleur* (1822) 71

[Fra85] A. Franciosi, S. Chang, R. Reifenberger, U. Debska and R. Riedel. *Resonant photoemission from $Cd_{1-x}Mn_xSe$: A probe of Mn 3d character and hybridization*. Physical Review B **32** (10), 6682–6687 (1985). ISSN 0163-1829. DOI http://dx.doi.org/10.1103/PhysRevB.32.6682 20

[Fre92] J. Frey, R. Frey and C. Flytzanis. *Magnetic-field and temperature dependence of the photoinduced Faraday effect in diluted magnetic semiconductors*. Physical Review B **45**, 4056–4064 (1992). ISSN 0163-1829. DOI http://dx.doi.org/10.1103/PhysRevB.45.4056 71

[Fre99] A. J. Freeman and S. D. Bader (Editors). *Magnetism beyond 2000* (Elsevier Science, North Holland, Amsterdam, 1999). ISBN 0444503374 4

[Fri94] T. Friedrich, J. Kraus, M. Meininger, G. Schaack and W. O. G. Schmitt. *Zeeman levels of the shallow lithium acceptor and band parameters in cadmium telluride*. Journal of Physics: Condensed Matter **6** (23), 4307–4316 (1994). ISSN 0953-8984. DOI http://dx.doi.org/10.1088/0953-8984/6/23/010 xi, 164

[Fur82] J. K. Furdyna. *Diluted magnetic semiconductors: An interface of semiconductor physics and magnetism (invited)*. Journal of Applied Physics **53** (11), 7637–7643 (1982). ISSN 0021-8979. DOI http://dx.doi.org/10.1063/1.330137 4

[Fur83] J. K. Furdyna, W. Giriat, D. F. Mitchell and G. I. Sproule. *The dependence of the lattice parameter and density of $Zn_{1-x}Mn_xTe$ on composition*. Journal of Solid State Chemistry **46** (3), 349–352 (1983). ISSN 0022-4596. DOI http://dx.doi.org/10.1016/0022-4596(83)90160-3 12

[Fur86] J. K. Furdyna. *Diluted magnetic semiconductors: Issues and opportunities*. Journal of Vacuum Science and Technology A **4**, 2002–2009 (1986). ISSN 0734-2101 4

[Fur87a] J. K. Furdyna, J. Kossut and A. K. Ramdas. *Quantum wells and superlattices of diluted magnetic semiconductors*. In *Optical properties of narrow-gap low dimensional structures*, edited by C. M. Sotomayor Torres and J. C. Portal, volume 152 of *NATO Science Series B*, 1. edition, 135–147 (Plenum Press, New York, 1987). ISBN 0306425661. Proceedings of NATO Advanced Research Workshop, St. Andrews, Scotland 1986 48, 52

[Fur87b] J. K. Furdyna and N. Samarth. *Magnetic properties of diluted magnetic semiconductors: A review (invited)*. Journal of Applied Physics **61** (8), 3526–3531 (1987). ISSN 0021-8979. DOI http://dx.doi.org/10.1063/1.338714 38

[Fur88a] J. K. Furdyna. *Diluted magnetic semiconductors*. Journal of Applied Physics **64**, R29–R64 (1988). ISSN 0021-8979. DOI http://dx.doi.org/10.1063/1.341700 3, 4, 11, 12, 13, 19, 37, 39, 42, 43, 46, 48, 67, 119, 165

[Fur88b] J. K. Furdyna and J. Kossut (Editors). *Diluted magnetic semiconductors*, volume 25 of *Semiconductors and Semimetals* (Academic Press, Boston, 1988). ISBN 0127521259 3, 4, 21, 22, 33, 185, 195, 197, 218

[Fur96] J. K. Furdyna, M. Dobrowolska and H. Luo. *Semiconductors, Diluted Magnetic*. In *Scientific Computing by Numerical Methods to Separation Processes*, edited by G. L. Trigg, volume 17 of *Encyclopedia of Applied Physics*, chapter 13-B, 373–402 (Wiley-VCH, Weinheim, 1996). ISBN 3527281398 3, 4, 12, 13, 19, 20, 23, 24, 33, 34, 37, 43

[Gaj78] J. A. Gaj, R. R. Gałązka and M. Nawrocki. *Giant exciton Faraday rotation in $Cd_{1-x}Mn_xTe$ mixed crystals*. Solid State Communications **25** (3), 193–195 (1978). ISSN 0038-1098. DOI http://dx.doi.org/10.1016/0038-1098(78)91477-1 4, 43

[Gaj79] J. A. Gaj, R. Planel and G. Fishman. *Relation of magneto-optical properties of free excitons to spin alignment of Mn^{2+} ions in $Cd_{1-x}Mn_xTe$*. Solid State Communications **29** (5), 435–438 (1979). ISSN 0038-1098. DOI http://dx.doi.org/10.1016/0038-1098(79)91211-0 34, 40, 41, 165

[Gaj87] J. A. Gaj and A. Golnik. *Influence of magnetic fluctuations on energy gap in CdMnTe*. Acta Physica Polonica A **71** (2), 197–203 (1987). ISSN 0587-4246 20

[Gaj88] J. A. Gaj. *Magnetooptical properties*. In Furdyna and Kossut [Fur88b], chapter 7, 279–309. ISBN 0127521259 45

[Gaj93] J. A. Gaj, C. Bodin-Deshayes, P. Peyla, J. Cibert, G. Feuillet, Y. Merle d'Aubigné, R. Romestain and A. Wasila. In *21st International Conference on the Physics of Semiconductors: Proceedings of the 21st International Conference*, edited by P. Jiang and H.-Z. Zheng, International Conference on the Physics of Semiconductors/Proceedings, 1939 (World Scientific Publishing Co Pte Ltd, Singapore, 1993). ISBN 9810211562 51

[Gał80a] R. R. Gałązka and J. Kossut. *Narrow-gap semimagnetic semiconductors*. In *Narrow gap semiconductors physics and applications*, edited by W. Zawadzki, volume 133 of *Lecture Notes in Physics*, 245–265 (Springer, Berlin, 1980). ISBN 9783540102618. Proceedings of the International Summer School Held in Nimes, France, September 3 - 15, 1979 34

[Gał80b] R. R. Gałązka, S. Nagata and P. H. Keesom. *Paramagnetic-spin-glass-antiferromagnetic phase transitions in $Cd_{1-x}Mn_xTe$ from specific heat and magnetic susceptibility measurements*. Physical Review B **22** (7), 3344–3355 (1980). ISSN 0163-1829. DOI http://dx.doi.org/10.1103/PhysRevB.22.3344 40

[Gal97] A. Gall. master thesis, Universität Würzburg, Würzburg (1997) 13, 164

[Gar99] S. Gardelis, C. G. Smith, C. H. W. Barnes, E. H. Linfield and D. A. Ritchie. *Spin-valve effects in a semiconductor field-effect transistor: A spintronic device*. Physical Review B **60** (11), 7764–7767 (1999). ISSN 0163-1829. DOI http://dx.doi.org/10.1103/PhysRevB.60.7764 3

[Ger22a] W. Gerlach and O. Stern. *Das magnetische Moment des Silberatoms*. Zeitschrift für Physik A: Hadrons and Nuclei **9** (1), 353–355 (1922). ISSN 0939-7922. DOI http://dx.doi.org/10.1007/BF01326984 1

[Ger22b] W. Gerlach and O. Stern. *Der experimentelle Nachweis der Richtungsquantelung im Magnetfeld*. Zeitschrift für Physik A: Hadrons and Nuclei **9** (1), 349–352 (1922). ISSN 0939-7922. DOI http://dx.doi.org/10.1007/BF01326983 1

[Ger22c] W. Gerlach and O. Stern. *Der experimentelle Nachweis des magnetischen Moments des Silberatoms*. Zeitschrift für Physik A: Hadrons and Nuclei **8** (1), 110–111 (1922). ISSN 0939-7922. DOI http://dx.doi.org/10.1007/BF01329580 1

[Gér91] J. M. Gérard, J. Y. Marzin and B. Jusserand. *Modulated molecular beam epitaxy: a successful route toward high quality highly strained heterostructures*. Journal of Crystal Growth **111** (1-4), 205–209 (1991). ISSN 0022-0248. DOI http://dx.doi.org/10.1016/0022-0248(91)90972-8 162

[Ger08] M. Gerbracht, G. Bartsch, P. Wojnar, D. R. Yakovlev, U. Woggon, J. Kossut and M. Bayer. *Optically detected resonance study of CdMnTe quantum dots* (2008). To be published in Physical Review B 92

[Gie82] T. M. Giebułtowicz, W. Minor, H. Kepa, J. Ginter and R. R. Gałązka. *A phenomenological description of the paramagnet-antiferromagnet transition in $Cd_{1-x}Mn_xTe$*. Journal of Magnetism and Magnetic Materials **30** (2), 215–222 (1982). ISSN 0304-8853. DOI http://dx.doi.org/10.1016/0304-8853(82)90200-1 40

[Gie84] T. M. Giebułtowicz, B. Lebech, B. Buras, W. Minor, H. Kepa and R. R. Gałązka. *Neutron scattering studies of $Cd_{1-x}Mn_xTe$ (invited)*. Journal of Applied Physics **55** (6), 2305–2309 (1984). ISSN 0021-8979. DOI http://dx.doi.org/10.1063/1.333643 39

[Gie87] T. M. Giebułtowicz, J. J. Rhyne and J. K. Furdyna. *Mn-Mn exchange constants in zinc-manganese chalcogenides*. Journal of Applied Physics **61** (8), 3537–3539 (1987). ISSN 0021-8979. DOI http://dx.doi.org/10.1063/1.338716 39

[Gie88] T. Giebultowicz and T. M. Holden. *Neutron scattering studies of the magnetic structure and synamics of diluted magnetic semiconductors*. In Furdyna and Kossut [Fur88b], chapter 4, 125–181. ISBN 0127521259 39

[Gie90] T. M. Giebułtowicz, J. J. Rhyne, J. K. Furdyna and P. Klosowski. *Inelastic neutron scattering studies of II-VI diluted magnetic semiconductors (invited)*. Journal of Applied Physics **67** (9), 5096–5101 (1990). ISSN 0021-8979. DOI http://dx.doi.org/10.1063/1.344683 39

[Gil75] J. C. Gill. *The establishment of thermal equilibrium in paramagnetic crystals*. Reports on Progress in Physics **38** (1), 91–150 (1975). ISSN 0034-4885. DOI http://dx.doi.org/10.1088/0034-4885/38/1/002 80, 82, 118

[Gis93] S. J. C. H. M. van Gisbergen, M. Godlewski, R. R. Gałązka, T. Gregorkiewicz, C. A. J. Ammerlaan and Nguyen The Khoi. *Optically detected magnetic resonance of $Cd_{0.905}Mn_{0.095}Te$*. Physical Review B **48** (16), 11767–11771 (4pp.) (1993). ISSN 0163-1829. DOI http://dx.doi.org/10.1103/PhysRevB.48.11767 92

[Goe88] O. Goede and W. Heimbrodt. *Optical properties of (Zn, Mn) and (Cd, Mn) chalcogenide mixed crystals and superlattices*. Physica Status Solidi (B) - Basic Research **146** (1), 11–62 (1988). ISSN 0370-1972. DOI http://dx.doi.org/10.1002/pssb.2221460102 4

[Gon85] C. E. T. Gonçalves da Silva. *Bound magnetic polarons in semimagnetic quantum wells*. Physical Review B **32** (10), 6962–6964 (1985). ISSN 0163-1829. DOI http://dx.doi.org/10.1103/PhysRevB.32.6962 51

[Gon86] C. E. T. Gonçalves da Silva. *Magnetic polaron effects for excitons in narrow CdTe-(Cd,Mn)Te quantum wells*. Physical Review B **33** (4), 2923–2925 (1986). ISSN 0163-1829. DOI http://dx.doi.org/10.1103/PhysRevB.33.2923 51

[Gor85] E. Gornik, R. Lassnig, G. Strasser, H. L. Stormer, A. C. Gossard and W. Wiegmann. *Specific heat of two-dimensional electrons in GaAs-GaAlAs multilayers*. Physical Review Letters **54**, 1820–1823 (1985). ISSN 0031-9007. DOI http://dx.doi.org/10.1103/PhysRevLett.54.1820 54

[Gos82] A. C. Gossard, W. Brown, C. L. Allyn and W. Wiegmann. *Molecular beam epitaxial growth and electrical transport of graded barriers for nonlinear current conduction*. Journal of Vacuum Science and Technology **20**, 694–700 (1982). ISSN 0022-5355. DOI http://dx.doi.org/10.1116/1.571633 161

[Gos94] A. C. Gossard, M. Sundaram and P. F. Hopkins. *Wide graded potential wells*. In *Epitaxial microstructures*, edited by A. C. Gossard, volume 40 of *Semiconductors and semimetals*, chapter 2, 153–218 (Academic Press, Boston, 1994). ISBN 0127521402 161

[Gra80] E. M. Gray. *The alternating susceptibility of spin glasses*. Journal of Magnetism and Magnetic Materials **15-18** (1), 177–178 (1980). ISSN 0304-8853. DOI http://dx.doi.org/10.1016/0304-8853(80)91005-7 40

[Gri61] J. S. Griffith. *The theory of transition-metal ions*. 1 edition (Cambridge University Press, Cambridge, 1961). ISBN 0521051509 23, 24

[Grø72] F. Grønvold, N. J. Kveseth, F. dos Santos Marques and J. Tichy. *Thermophysical properties of manganese monotelluride from 298 to 700 K. Lattice constants, magnetic susceptibility, and antiferromagnetic transition*. Journal of Chemical Thermodynamics **4** (6), 795–806 (1972). ISSN 0021-9614 165

[Grü86] P. Grünberg, R. Schreiber, Y. Pang, M. B. Brodsky and H. Sowers. *Layered magnetic structures: Evidence for antiferromagnetic coupling of Fe layers across Cr interlayers*. Physical Review Letters **57**, 2442–2445 (1986). ISSN 0031-9007. DOI http://dx.doi.org/10.1103/PhysRevLett.57.2442 2

[Gui04] Y. S. Gui, C. R. Becker, J. Liu, M. König, V. Daumer, M. N. Kiselev, H. Buhmann and L. W. Molenkamp. *Current heating of a magnetic two-dimensional electron gas in $Hg_{1-x}Mn_xTe/Hg_{0.3}Cd_{0.7}Te$ quantum wells*. Physical Review B **70** (19), 195328 (4pp.) (2004). ISSN 0163-1829. DOI http://dx.doi.org/10.1103/PhysRevB.70.195328 71

[Gun85] R. L. Gunshor, N. Otsuka, M. Yamanishi, L. A. Kolodziejski, T. C. Bonsett, R. B. Bylsma, S. Datta, W. M. Becker and J. K. Furdyna. *Diluted magnetic semiconductor*

superlattices. Journal of Crystal Growth **72** (1-2), 294–298 (1985). ISSN 0022-0248. DOI http://dx.doi.org/10.1016/0022-0248(85)90161-7 34, 46

[Gun89] O. Gunnarsson, O. K. Andersen, O. Jepsen and J. Zaanen. *Density-functional calculation of the parameters in the Anderson model: Application to Mn in CdTe*. Physical Review B **39** (3), 1708–1722 (1989). ISSN 0163-1829. DOI http://dx.doi.org/10.1103/PhysRevB.39.1708 19

[Häg98] D. Hägele, M. Oestreich, W. W. Rühle, N. Nestle and K. Eberl. *Spin transport in GaAs*. Applied Physics Letters **73** (11), 1580–1582 (1998). ISSN 0003-6951. DOI http://dx.doi.org/10.1063/1.122210 3

[Hal03] K. C. Hall, K. Gündoğdu, E. Altunkaya, W. H. Lau, M. E. Flatté, T. F. Boggess, J. J. Zinck, W. B. Barvosa-Carter and S. L. Skeith. *Spin relaxation in (110) and (001) InAs/GaSb superlattices*. Physical Review B **68** (11), 115311 (5pp.) (2003). ISSN 0163-1829. DOI http://dx.doi.org/10.1103/PhysRevB.68.115311 77

[Ham99] P. R. Hammar, B. R. Bennett, M. J. Yang and M. Johnson. *Observation of spin injection at a ferromagnet-semiconductor interface*. Physical Review Letters **83** (1), 203–206 (1999). ISSN 0031-9007. DOI http://dx.doi.org/10.1103/PhysRevLett.83.203 3

[Ham00] P. R. Hammar and M. Johnson. *Potentiometric measurements of the spin-split subbands in a two-dimensional electron gas*. Physical Review B **61** (11), 7207–7210 (2000). ISSN 0163-1829. DOI http://dx.doi.org/10.1103/PhysRevB.61.7207 3

[Han24] W. Hanle. *Über magnetische Beeinflussung der Polarisation der Resonanzfluoreszenz*. Zeitschrift für Physik **30**, 93–105 (1924). ISSN 0044-3328 87

[Han82] G. L. Hansen, J. L. Schmit and T. N. Casselman. *Energy gap versus alloy composition and temperature in $Hg_{1-x}Cd_xTe$*. Journal of Applied Physics **53** (10), 7099–7101 (1982). ISSN 0021-8979. DOI http://dx.doi.org/10.1063/1.330018 164

[Har89] R. L. Harper, Jr., R. N. Bicknell, D. K. Blanks, N. C. Giles, J. F. Schetzina, Y. R. Lee and A. K. Ramdas. *Excited confined quantum states in CdMnTe-CdTe superlattices*. Journal of Applied Physics **65** (2), 624–628 (1989). ISSN 0021-8979. DOI http://dx.doi.org/10.1063/1.343094 17

[Har00] U. Hartmann (Editor). *Magnetic Multilayers and Giant Magnetoresistance*, volume 37 of *Springer Series in Surface Sciences*. 1. edition (Springer, Berlin, 2000). ISBN 3540655689 2

[Has83] K. C. Hass and H. Ehrenreich. *Empirical tight binding description of $Hg_{1-x}Mn_xTe$ and $Hg_{1-x}Cd_xTe$*. Journal of Vacuum Science and Technology A **1** (3), 1678–1682 (1983). ISSN 0734-2101. DOI http://dx.doi.org/10.1116/1.572256 19

[Has86] K. C. Hass, B. E. Larson, H. Ehrenreich and A. E. Carlson. *Magnetic interactions in diluted magnetic semiconductors*. Journal of Magnetism and Magnetic Materials **54-57** (3), 1283–1284 (1986). ISSN 0304-8853. DOI http://dx.doi.org/10.1016/0304-8853(86)90819-X 23

[Has88] K. C. Hass and H. Ehrenreich. *Band structures of semimagnetic compounds*. Acta Physica Polonica A **73** (6), 933–941 (1988). ISSN 0587-4246 19

[Has90] K. C. Hass and H. Ehrenreich. *Electronic and magnetic properties of II-VI diluted magnetic semiconductors*. Journal of Crystal Growth **86** (1-4), 8–14 (1990). ISSN 0022-0248. DOI http://dx.doi.org/10.1016/0022-0248(90)90691-D 19, 23, 35

[Hei28] W. Heisenberg. *Zur Theorie des Ferromagnetismus*. Zeitschrift für Physik A: Hadrons and Nuclei **49** (9-10), 619–636 (1928). ISSN 0939-7922. DOI http://dx.doi.org/10.1007/BF01328601 24, 27

[Hei36] W. Heitler and E. Teller. *Time effects in the magnetic cooling method. I*. Proceedings of the Royal Society of London - Series A: Mathematical and Physical Sciences **155** (886), 629–639 (1936). ISSN 0080-4630. DOI http://dx.doi.org/10.1098/rspa.1936.0124 117

[Hei84] D. Heiman, Y. Shapira and S. Foner. *Exchange energy for conduction electrons in (ZnMn)Se derived from spin-flip Raman scattering and magnetization*. Solid State Communications **51** (8), 603–606 (1984). ISSN 0038-1098. DOI http://dx.doi.org/10.1016/0038-1098(84)91068-8 165

[Hei86] D. Heiman, P. Becla, R. Kershaw, D. Ridgley, K. Dwight, A. Wold and R. R. Gałązka. *Field-induced exchange effects in (Cd,Mn)Te and (Cd,Mn)Se from photoluminescence measurements*. Physical Review B **34** (6), 3961–3969 (1986). ISSN 0163-1829. DOI http://dx.doi.org/10.1103/PhysRevB.34.3961 19, 165

[Hei87] D. Heiman, E. D. Isaacs, P. Becla and S. Foner. *High-field magnetization of (Cd,Mn)Te*. Physical Review B **35**, 3307–3310 (1987). ISSN 0163-1829. DOI http://dx.doi.org/10.1103/PhysRevB.35.3307 42

[Her84] M. A. Herman, O. Jylhä and M. Pessa. *Atomic layer epitaxy of $Cd_{1-x}Mn_xTe$ grown on CdTe (111)B substrates*. Journal of Crystal Growth **66** (2), 480–483 (1984). ISSN 0022-0248. DOI http://dx.doi.org/10.1016/0022-0248(84)90236-7 46

[Hir02] E. Hirota, H. Sakakima and K. Inomata (Editors). *Giant magneto-resistance devices*, volume 40 of *Springer series in surface sciences* (Springer, Berlin, 2002). ISBN 3540418199 2, 202

[Höl83] H. W. Hölscher and A. Nöthe. *Investigation of bandmasses and g-values by two-photon-magneto-absorption (TPMA) in ZnSe*. Physica B+C **117-118** (1), 395–397 (1983). ISSN 0378-4363. DOI http://dx.doi.org/10.1016/0378-4363(83)90540-5 164

[Höl85] H. W. Hölscher, A. Nöthe and C. Uihlein. *Investigation of band masses and g values of ZnSe by two-photon magnetoabsorption*. Physical Review B **31**, 2379–2387 (1985). ISSN 0163-1829. DOI http://dx.doi.org/10.1103/PhysRevB.31.2379 164

[Hu98] C. Y. Hu, W. Ossau, D. R. Yakovlev, G. Landwehr, T. Wojtowicz, G. Karczewski and J. Kossut. *Optically detected magnetic resonance of excess electrons in type-I quantum wells with a low-density electron gas*. Physical Review B **58** (4), R1766–R1769 (1998). ISSN 0163-1829. DOI http://dx.doi.org/10.1103/PhysRevB.58.R1766 92

[Hui89] P. M. Hui, H. Ehrenreich and K. C. Hass. *Effects of d bands on semiconductor sp Hamiltonians*. Physical Review B **40** (18), 12346–12352 (1989). ISSN 0163-1829. DOI http://dx.doi.org/10.1103/PhysRevB.40.12346 19

[Hun05a] A. Hundt, J. Puls, A. V. Akimov, Y. H. Fan and F. Henneberger. *Photocarrier-induced spin heating and spin-lattice relaxation in diluted magnetic Stranski-Krastanov quantum dots*. Physical Review B **72** (3), 033304 (4pp.) (2005). ISSN 0163-1829. DOI http://dx.doi.org/10.1103/PhysRevB.72.033304 71, 93, 112, 114

[Hun05b] A. Hundt, J. Puls, A. V. Akimov and F. Henneberger. *Spin-lattice relaxation in diluted magnetic (Cd,Mn)Se quantum dots*. Physica Status Solidi (C) - Current Topics on Solid State Physics **2**, 867–870 (2005). ISSN 1610-1634. DOI http://dx.doi.org/10.1002/pssc.200460335 71, 93, 112

[Ike68] M. Ikeda, K. Itoh and H. Sato. *Electrical and Optical Properties of CdS-MnS Single Crystals*. Journal of the Physical Society of Japan (JPSJ) **25** (2), 455–460 (1968). ISSN 0031-9015. URL http://www.journalarchive.jst.go.jp/english/jnlabstract_en.php?cdjournal=jpsj1946&cdvol=25&noissue=2&startpage=455 20

[Ima99] A. Imamoglu, D. D. Awschalom, G. Burkard, D. P. DiVincenzo, D. Loss, M. Sherwin and A. Small. *Quantum information processing using quantum dot spins and cavity QED*. Physical Review Letters **83** (20), 4204–4207 (1999). ISSN 0031-9007. DOI http://dx.doi.org/10.1103/PhysRevLett.83.4204 3

[Ino02] K. Inomata. *Magnetic random access memory (MRAM)*. In Hirota *et al.* [Hir02], chapter 6, 135–157. ISBN 3540418199 2

[Iva07] V. Y. Ivanov, M. Godlewski, D. R. Yakovlev, S. M. Ryabchenko, G. Karczewski and A. Waag. *Time-resolved optically-detected magnetic resonance of II-VI diluted-magnetic-semiconductor heterostructures*. Physica Status Solidi (A) - Applied Research **204** (1), 174–178 (2007). ISSN 0031-8965. DOI http://dx.doi.org/10.1002/pssa.200673023 92

[Iva08] V. Y. Ivanov, M. Godlewski, D. R. Yakovlev, S. M. Ryabchenko, M. K. Kneip, M. Bayer and A. Waag. *Optically detected magnetic resonance in ZnMnSe/ZnBeSe quantum wells* (2008). To be published in Physical Review B 92

[Jac70] A. J. Jacobson and B. E. F. Fender. *Covalency parameters in MnSe and $MnSe_2$*. Journal of Chemical Physics **52** (9), 4563–4566 (1970). ISSN 0021-9606. DOI http://dx.doi.org/10.1063/1.1673685 165

[Jai92] M. Jain (Editor). *Diluted magnetic semiconductors* (Word Scientific, Singapore, 1992). ISBN 9810201761 3, 4

[Jan95] E. Janik, E. Dynowska, J. Bąk-Misiuk, M. Leszczyński, W. Szuszkiewicz, T. Wojtowicz, G. Karczewski, A. K. Zakrzewski and J. Kossut. *Structural properties of cubic MnTe layers grown by MBE*. Thin Solid Films **267** (1-2), 74–78 (1995). ISSN 0040-6090. DOI http://dx.doi.org/10.1016/0040-6090(95)06632-2 165

[Joh85] M. Johnson and R. H. Silsbee. *Interfacial charge-spin coupling: Injection and detection of spin magnetization in metals*. Physical Review Letters **55** (17), 1790–1793 (1985). ISSN 0031-9007. DOI http://dx.doi.org/10.1103/PhysRevLett.55.1790 87

[Joh98] M. Johnson. *Theory of spin-dependent transport in ferromagnet-semiconductor heterostructures*. Physical Review B **58** (15), 9635–9638 (1998). ISSN 0163-1829. DOI http://dx.doi.org/10.1103/PhysRevB.58.9635 3

[Jon87] W. J. M. de Jonge, A. Twardowski and C. J. M. Denissen. *The relevance of long range interactions in diluted magnetic semiconductors*. In Aggarwal *et al.* [Agg87], 153–158. ISBN 0931837545 40

[Jon00] B. T. Jonker, Y. D. Park, B. R. Bennett, H. D. Cheong, G. Kioseoglou and A. Petrou. *Robust electrical spin injection into a semiconductor heterostructure*. Physical Review B **62**, 8180–8183 (2000). ISSN 0163-1829. DOI http://dx.doi.org/10.1103/PhysRevB.62.8180 3

[Jul75] M. Julliere. *Tunneling between ferromagnetic films*. Physics Letters A **54** (3), 225–226 (1975). ISSN 0375-9601. DOI http://dx.doi.org/10.1016/0375-9601(75)90174-7 2

[Juz56] R. Juza, A. Rabenau and G. Pascher. *Über feste Lösungen in den Systemen ZnS/MnS, ZnSe/MnSe und ZnTe/MnTe*. Zeitschrift für Anorganische und Allgemeine Chemie **285** (1-2), 60–61 (1956). ISSN 0044-2313. DOI http://dx.doi.org/10.1002/zaac.19562850107 12

[Kac01] P. Kacman. *Spin interactions in diluted magnetic semiconductors and magnetic semiconductor structures*. Semiconductor Science and Technology **16** (4), R25–R39 (2001). ISSN 0268-1242. DOI http://dx.doi.org/10.1088/0268-1242/16/4/201 36, 37

[Kai03] J. Kainz, U. Rössler and R. Winkler. *Anisotropic spin-splitting and spin-relaxation in asymmetric zinc blende semiconductor quantum structures*. Physical Review B **68** (7), 075322 (6pp.) (2003). ISSN 0163-1829. DOI http://dx.doi.org/10.1103/PhysRevB.68.075322 17, 50

[Kai04] J. Kainz, U. Rössler and R. Winkler. *Temperature dependence of Dyakonov-Perel spin relaxation in zinc-blende semiconductor quantum structures*. Physical Review B **70**, 195322 (2004). ISSN 0163-1829. DOI http://dx.doi.org/10.1103/PhysRevB.70.195322 50

[Kap59] J. I. Kaplan. *Application of the diffusion-modified bloch equation to electron spin resonance in ordinary and ferromagnetic metals*. Physical Review **115**, 575–577 (1959). ISSN 0031-899X. DOI http://dx.doi.org/10.1103/PhysRev.115.575 70

[Kar96] H. Karzel, W. Potzel, M. Köfferlein, W. Schiessl, M. Steiner, U. Hiller, G. M. Kalvius, D. W. Mitchell, T. P. Das, P. Blaha, K. Schwarz and M. P. Pasternak. *Lattice dynamics and hyperfine interactions in ZnO and ZnSe at high external pressures*. Physical Review B **53** (17), 11425–11438 (1996). ISSN 0163-1829. DOI http://dx.doi.org/10.1103/PhysRevB.53.11425 164

[Kat00] R. R. Katti and Kaakani H. *GMRAM: giant magneto-resistance random-access memory*. In *Aerospace Conference Proceedings, 2000 IEEE*, volume 5, 371–376 (Big Sky, MT, USA, 2000). ISBN 0-7803-5846-5. DOI http://dx.doi.org/10.1109/AERO.2000.878510 2

[Kaw83] M. Kawabe, M. Kondo, N. Matsuura and K. Yamamoto. *Photoluminescence of $Al_xGa_{1-x}As/Al_yGa_{1-y}As$ multiquantum wells grown by pulsed molecular beam epitaxy*. Japanese Journal of Applied Physics (JJAP) **22**, L64–L66 (1983). ISSN 0021-4922. DOI http://dx.doi.org/10.1143/JJAP.22.L64 161

[Kaz89] D. V. Kazakovtsev, A. A. Maksimov, D. A. Pronin and I. I. Tartakovskiĭ. *Relaxation of rf acoustic phonons*. Journal of Experimental and Theoretical Physics Letters (JETP) **49**, 61–64 (1989). ISSN 0021-3640. URL http://www.jetpletters.ac.ru/ps/1439/article_21891.shtml. Translation of: Pis'ma v Zhurnal Eksperimental'noy i Teoreticheskoy Fizika, USSR **49**(1), 52-55 (1989) 108, 144

[Kel99] A. Keller. *Elektronische Spinflip-Ramanspektroskopie an magnetischen und nichtmagnetischen II-VI Halbleiter Heterostrukturen*. PhD thesis, Universität Würzburg, Würzburg (1999) 66

[Kel01] D. Keller, D. R. Yakovlev, B. König, W. Ossau, T. Gruber, A. Waag, L. W. Molenkamp and A. V. Scherbakov. *Heating of the magnetic ion system in (Zn,Mn)Se/(Zn,Be)Se semimagnetic quantum wells by means of photoexcitation*. Physical Review B **65** (3), 035313 (9pp.) (2001). ISSN 0163-1829. DOI http://dx.doi.org/10.1103/PhysRevB.65.035313 6, 41, 42, 66, 71, 90, 91, 93, 94, 106, 112, 120, 161

[Kel02] D. Keller, D. R. Yakovlev, Th. Gruber, W. Waag, A. Ossau, L. W. Molenkamp, F. Pulizzi, P. C. M. Christianen and J. C. Maan. *Diffusion of carriers induced by exchange interaction with magnetic-ion system in (Zn,Mn)Se/(Zn,Be)Se quantum wells*. Physica Status Solidi (B) - Basic Research **229** (2), 797–801 (2002). ISSN 0370-1972. DOI http://dx.doi.org/10.1002/1521-3951(200201)229:2⟨797::AID-PSSB797⟩3.0.CO;2-G 71

[Kel03] D. Keller, G. V. Astakhov, D. R. Yakovlev, L. Hansen, W. Ossau and S. A. Crooker. *Optical studies of spin polarized 2DEG in modulation-doped (Zn,Mn)Se/(Zn,Be)Se qunatum wells in high magnetic fields*. In *Optical Properties of 2D Systems with Interacting Electrons*, edited by W. J. Ossau and R. Suris, volume 119 of *NATA Science Series II. Mathematics, Physics amd Chemistry*, 1. edition, 217–232 (Kluwer Academic Publishers, Dordrecht, The Netherlands, 2003). ISBN 1402015498. Proceedings of the NATO Advanced Research Workshop on Optical Properties of 2D Systems with Interacting Electrons, St. Petersburg, Russia, 13-16 June (2002) 131

[Kel04] D. Keller. *Optische Eigenschaften ZnSe-basierter zweidimensionaler Elektronengase und ihre Wechselwirkungen mit magnetischen Ionen*. PhD thesis, Universität Würzburg, Würzburg (2004) 6, 24, 45, 47, 53, 55, 64, 65, 118, 119, 127

[Ket81] H. Kett, W. Gebhardt, U. Krey and J. K. Furdyna. *Magnetic phases of a Heisenberg spin glass in strong magnetic fields: High field faraday rotation in $Cd_{1-x}Mn_xTe$*. Journal of Magnetism and Magnetic Materials **25** (2), 215–220 (1981). ISSN 0304-8853. DOI http://dx.doi.org/10.1016/0304-8853(81)90122-0 40

[Kha81] G. D. Khattak, C. D. Amarasekara, S. Nagata, R. R. Gałązka and P. H. Keesom. *Specific heat, magnetic susceptibility, and the spin-glass transition in $Hg_{1-x}Mn_xSe$.*

Physical Review B **23** (7), 3553–3554 (1981). ISSN 0163-1829. DOI http://dx.doi.org/10.1103/PhysRevB.23.3553 40

[Khe93] K. Kheng, R. T. Cox, M. Y. D' Aubigné, F. Bassani, K. Saminadayar and S. Tatarenko. *Observation of negatively charged excitons X^- in semiconductor quantum wells*. Physical Review Letters **71**, 1752–1755 (1993). ISSN 0031-9007. DOI http://dx.doi.org/10.1103/PhysRevLett.71.1752 66

[Kie84] E. Kierzek-Pecold, W. Szymańska and R. R. Gałązka. *Dynamical behavior of spin-glass $Cd_{1-x}Mn_xTe$ from low field faraday rotation measurements*. Solid State Communications **50** (7), 685–687 (1984). ISSN 0038-1098. DOI http://dx.doi.org/10.1016/0038-1098(84)90159-5 40

[Kik99] J. M. Kikkawa and D. D. Awschalom. *Lateral drag of spin coherence in gallium arsenide*. Nature **397**, 139–141 (1999). ISSN 0028-0836. DOI http://dx.doi.org/10.1038/16420 3

[Kim00] M. Kim, C. S. Kim, S. Lee, J. K. Furdyna and M. Dobrowolska. *Band offset determination in ZnSe-based heterostructures involving ZnBeSe*. Journal of Crystal Growth **214-215**, 325–329 (2000). ISSN 0022-0248. DOI http://dx.doi.org/10.1016/S0022-0248(00)00102-0 165

[Kit05] C. Kittel. *Introduction to solid state physics*. 8. edition (Wiley, New York, 2005). ISBN 0471680575 14, 25, 27, 29, 31

[Kla98] P. J. Klar, D. Wolverson, J. J. Davies, W. Heimbrodt and M. Happ. *Determination of the chemical valence-band offset for $Zn_{1-x}Mn_xSe/ZnSe$ multiple-quantum-well structures of high x*. Physical Review B **57** (12), 7103–7113 (1998). ISSN 0163-1829. DOI http://dx.doi.org/10.1103/PhysRevB.57.7103 47, 165

[Kle51] W. Klemm and K. Wahl. *Notiz über das Magnesiumtellurid*. Zeitschrift für Anorganische und Allgemeine Chemie **266** (6), 289–292 (1951). ISSN 0044-2313. DOI http://dx.doi.org/10.1002/zaac.19512660603 11, 164

[Kli06] C. F. Klingshirn. *Semiconductor optics*. 3. edition (Springer, Berlin, 2006). ISBN 354038345X 62, 66

[Kna96] W. Knap, C. Skierbiszewski, A. Zduniak, E. Litwin-Staszewska, D. Bertho, F. Kobbi, J. L. Robert, G. E. Pikus, F. G. Pikus, S. V. Iordanskii, V. Mosser, K. Zekentes and Yu. B. Lyanda-Geller. *Weak antilocalization and spin precession in quantum wells*. Physical Review B **53** (7), 3912–3924 (1996). ISSN 0163-1829. DOI http://dx.doi.org/10.1103/PhysRevB.53.3912 18

[Kne06a] M. K. Kneip, D. R. Yakovlev, M. Bayer, A. A. Maksimov, I. I. Tartakovskiĭ, D. Keller, W. Ossau, L. W. Molenkamp and A. Waag. *Direct energy transfer from photocarriers to Mn-ion system in II-VI diluted-magnetic-semiconductor quantum wells*. Physical Review B **73**, 035306 (8pp.) (2006). ISSN 0163-1829. DOI http://dx.doi.org/10.1103/PhysRevB.73.035306 93, 136, 138

[Kne06b] M. K. Kneip, D. R. Yakovlev, M. Bayer, A. A. Maksimov, I. I. Tartakovskiĭ, D. Keller, W. Ossau, L. W. Molenkamp and A. Waag. *Spin-lattice relaxation of Mn-ions in ZnMnSe/ZnBeSe quantum wells measured under pulsed photoexcitation*. Physical Review B **73**, 045305 (8pp.) (2006). ISSN 0163-1829. DOI http://dx.doi.org/10.1103/PhysRevB.73.045305 144

[Kno63] R. S. Knox. *Theory of excitons*, volume 5 of *Solid state physics: Supplement* (Academic Press, New York, 1963). ISBN 0126077657 61

[Koh65] W. Kohn and L. J. Sham. *Self-consistent equations including exchange and correlation effects*. Physical Review **140**, 1133–1138 (1965). ISSN 0031-899X. DOI http://dx.doi.org/10.1103/PhysRev.140.A1133 121

[Kol84a] L. A. Kolodziejski, T. C. Bonsett, R. L. Gunshor, S. Datta, R. B. Bylsma, W. M. Becker and N. Otsuka. *Molecular beam epitaxy of diluted magnetic semiconductor ($Cd_{1-x}Mn_xTe$) superlattices*. Applied Physics Letters **45** (4), 440–442 (1984). ISSN 0003-6951. DOI http://dx.doi.org/10.1063/1.95223 3, 46

[Kol84b] L. A. Kolodziejski, T. Sakamoto, R. L. Gunshor and S. Datta. *Molecular beam epitaxy of $Cd_{1-x}Mn_xTe$*. Applied Physics Letters **44** (8), 799–801 (1984). ISSN 0003-6951. DOI http://dx.doi.org/10.1063/1.94890 3

[Kol85] L. A. Kolodziejski, R. L. Gunshor, T. C. Bonsett, R. Venkatasubramanian, S. Datta, R. B. Bylsma, W. M. Becker and N. Otsuka. *Wide gap II-VI superlattices of ZnSe-$Zn_{1-x}Mn_xSe$*. Applied Physics Letters **47** (2), 169–171 (1985). ISSN 0003-6951. DOI http://dx.doi.org/10.1063/1.96251 46

[Kol86a] L. A. Kolodziejski, R. L. Gunshor, N. Otsuka, S. Datta, W. Becker and A. Nurmikko. *Wide-gap II-VI superlattices*. IEEE Journal of Quantum Electronics **22** (9), 1666–1676 (1986). ISSN 0018-9197 48

[Kol86b] L. A. Kolodziejski, R. L. Gunshor, N. Otsuka, B. P. Gu, Y. Hefetz and A. V. Nurmikko. *Two-dimensional metastable magnetic semiconductor structures*. Applied Physics Letters **48** (21), 1482–1484 (1986). ISSN 0003-6951. DOI http://dx.doi.org/10.1063/1.96896 3, 11

[Kol86c] L. A. Kolodziejski, R. L. Gunshor, R. Vebkatasubramanian, T. C. Bonsett, Frohne R., S. Datta, N. Otsuka, R. B. Bylsma, W. M. Becker and A. V. Nurmikko. *Summary Abstract: (100)-oriented wide gap II-VI superlattices*. Journal of Vacuum Science and Technology B: Microelectronics and Nanometer Structures **4** (2), 583–584 (1986). ISSN 1071-1023. DOI http://dx.doi.org/10.1116/1.583380 20, 22

[Kom77] A. V. Komarov, S. M. Riabchenko, O. V. Terletskii, I. I. Zheru and R. D. Ivanchuk. *Magneto-optical studies and the double opticomagnetic resonance of the exciton band in Mn^{2+}-doped CdTe*. Pis'ma v Zhurnal Eksperimental'noy i Teoreticheskoy Fizika **73**, 608–618 (1977). ISSN 0370-274X 92

[Kön99] B. König, U. Zehnder, D. R. Yakovlev, W. Ossau, T. Gerhard, M. Keim, A. Waag and G. Landwehr. *Magneto-optical properties of $Zn_{0.95}Mn_{0.05}Se/Zn_{0.76}Be_{0.08}Mg_{0.16}Se$ quantum wells and $Zn_{0.91}Mn_{0.09}Se/Zn_{0.972}Be_{0.028}Se$ spin superlattices*. Physical Review B **60**, 2653–2660 (1999). ISSN 0163-1829. DOI http://dx.doi.org/10.1103/PhysRevB.60.2653 161

[Kön00a] B. König. *Wechselwirkung zwischen Ladungsträgern und magnetischen Ionen in semimagnetischen Halbleiter-Heterostrukturen*. PhD thesis, Universität Würzburg, Würzburg (2000) 67, 71, 72, 74, 75, 90, 94, 127, 178

[Kön00b] B. König, I. A. Merkulov, D. R. Yakovlev, W. Ossau, S. M. Ryabchenko, M. Kutrowski, T. Wojtowicz, G. Karczewski and J. Kossut. *Energy transfer from photocarriers into the magnetic ion system mediated by a two-dimensional electron gas in (Cd,Mn)Te/(Cd,Mg)Te quantum wells*. Physical Review B **61**, 16870–16882 (2000). ISSN 0163-1829. DOI http://dx.doi.org/10.1103/PhysRevB.61.16870 67, 71, 74, 75, 92, 93, 112, 124, 125, 155

[Kos69] G. F. Koster, J. O. Dimmock, R. C. Wheeler and H. Statz. *Properties of the thirty-two point groups*. 3. edition (MIT Press, Cambridge, 1969) 15

[Kos93] J. Kossut and W. Dobrowolski. *Diluted magnetic semiconductors*. In *Handbook of magnetic materials*, edited by K. H. J. Buschow, volume 7, 232–305 (North-Holland, Amsterdam, London, New York, Tokyo, 1993). ISBN 0444898530 14, 19, 20, 33, 37, 39, 43, 52

[Kos09] J. Kossut and J. A. Gaj. *Introduction to physics of diluted magnetic semiconductors* (Springer, Heidelberg, 2009). Planned release date 213, 234

[Kou03] A. V. Koudinov, Y. G. Kusrayev and I. G. Aksyanov. *Light-induced heating effects in semimagnetic quantum wells*. Physical Review B **68** (8), 085315 (4pp.) (2003). ISSN 0163-1829. DOI http://dx.doi.org/10.1103/PhysRevB.68.085315 71, 93, 112

[Kre65] M. M. Kreitman and D. L. Barnett. *Probability tables for clusters of foreign atoms in simple lattices assuming next-nearest-neighbor interactions*. Journal of Chemical Physics **43** (2), 364–371 (1965). ISSN 0021-9606. DOI http://dx.doi.org/10.1063/1.1696753 39, 118

[Kre66] M. M. Kreitman, F. J. Milford, R. P. Kenan and J. G. Daunt. *Magnetic susceptibility of Mn^{2+} in CdS and effects of antiferromagnetic exchange*. Physical Review **144** (2), 367–372 (1966). ISSN 0031-899X. DOI http://dx.doi.org/10.1103/PhysRev.144.367 119

[Kre85a] R. E. Kremer and J. K. Furdyna. *Investigation of EPR in $Cd_{1-x}Mn_xTe$ by microwave Faraday effect*. Physical Review B **32** (9), 5591–5599 (1985). ISSN 0163-1829. DOI http://dx.doi.org/10.1103/PhysRevB.32.5591 83

[Kre85b] H. Krenn, W. Zawadzki and G. Bauer. *Optically induced magnetization in a dilute magnetic semiconductor - $Hg_{1-x}Mn_xTe$*. Physical Review Letters **55**, 1510–1513 (1985). ISSN 0031-9007. DOI http://dx.doi.org/10.1103/PhysRevLett.55.1510 71, 72

[Kre89] H. Krenn, K. Kaltenegger, T. Dietl, J. Spałek and G. Bauer. *Photoinduced magnetization in dilute magnetic (semimagnetic) semiconductors*. Physical Review B **39**, 10918–10934 (1989). ISSN 0163-1829. DOI http://dx.doi.org/10.1103/PhysRevB.39.10918 71, 72, 155

[Kro39] R. de L. Kronig. *On the mechanism of paramagnetic relaxation*. Physica **6** (1), 33–43 (1939). ISSN 0031-8914. DOI http://dx.doi.org/10.1016/S0031-8914(39)90282-X 117

[Kru68] S. Krupička and J. Sternberk. *Elements of theoretical magnetism* (Iliffe Books, London, 1968). ISBN 0592050378 27

[Kud92] G. Kudlek, N. Presser, U. W. Pohl, J. Gutowski, J. Lilja, E. Kuusisto, K. Imai, M. Pessa, K. Hingerl and H. Sitter. *Exciton complexes in ZnSe layers: a tool for probing the strain distribution*. Journal of Chemical Physics **117** (1-4), 309–315 (1992). ISSN 0022-0248. DOI http://dx.doi.org/10.1016/0022-0248(92)90765-B 164

[Kud93] G. H. Kudlek, U. W. Pohl, C. Fricke, R. Heitz, A. Hoffmann, J. Gutowski and I. Broser. *Electronic structure and dynamical behaviour of different bound-exciton complexes in ZnSe bulk crystals*. Physica B: Condensed Matter **185** (1-4), 325–331 (1993). ISSN 0921-4526. DOI http://dx.doi.org/10.1016/0921-4526(93)90255-5 164

[Kuh71] A. Kuhn, A. Chevy and M.-J. Naud. *Preparation and some physical properties of magnesium telluride single crystals*. Journal of Crystal Growth **9**, 263–265 (1971). ISSN 0022-0248. DOI http://dx.doi.org/10.1016/0022-0248(71)90239-9 11, 164

[Kuh93] B. Kuhn-Heinrich, W. Ossau, H. Heinke, F. Fischer, T. Litz, A. Waag and G. Landwehr. *Optical investigation of confinement and strain effects in CdTe/(CdMg)Te quantum wells*. Applied Physics Letters **63** (21), 2932–2934 (1993). ISSN 0003-6951. DOI http://dx.doi.org/10.1063/1.110277 165

[Kuh94] B. Kuhn-Heinrich, W. Ossau, T. Litz, A. Waag and G. Landwehr. *Determination of the band offset in semimagnetic CdTe/$Cd_{1-x}Mn_xTe$ quantum wells: A comparison of two methods*. Journal of Applied Physics **75** (12), 8046–8052 (1994). ISSN 0021-8979. DOI http://dx.doi.org/10.1063/1.356545 165

[Kuh95] B. Kuhn-Heinrich. *Magneto-optische Untersuchungen semimagnetischer Schichtstrukturen auf der Basis von $Cd_{1-x}Mn_xTe$*. PhD thesis, Universität Würzburg, Würzburg (1995) 16, 49, 54, 64, 65

[Kul96] V. D. Kulakovskii, M. G. Tyazhlov, A. I. Filin, D. R. Yakovlev, A. Waag and G. Landwehr. *Hierarchy of relaxation times in the system of Mn-ion spins in photoexcited semimagnetic quantum wells*. Physical Review B **54**, R8333–R8336 (1996). ISSN 0163-1829. DOI http://dx.doi.org/10.1103/PhysRevB.54.R8333 71, 93, 114

[Kur02] T. Kuroda, F. Minami and S. Seto. *Strong excitation effect of excitonic magnetic polarons in $Cd_{1-x}Mn_xTe$*. Physica Status Solidi (B) - Basic Research **229** (2), 757–760 (2002). ISSN 0370-1972. DOI http://dx.doi.org/10.1002/1521-3951(200201)229:2⟨757::AID-PSSB757⟩3.0.CO;2-W 71

[Lam58] M. A. Lampert. *Mobile and immobile effective-mass-particle complexes in nonmetallic solids*. Physical Review Letters **1**, 450–453 (1958). ISSN 0031-9007. DOI http://dx.doi.org/10.1103/PhysRevLett.1.450 66

[Lam60] J. Lambe and C. Kikuchi. *Paramagnetic resonance of CdTe: Mn and CdS: Mn*. Physical Review **119**, 1256–1260 (1960). ISSN 0031-899X. DOI http://dx.doi.org/10.1103/PhysRev.119.1256 5

[Lan30] L. Landau. *Diamagnetismus der Metalle*. Zeitschrift für Physik **64** (9-10), 629–637 (1930). ISSN 0044-3328. DOI http://dx.doi.org/10.1007/BF01397213 31

[Lan65] D. Langer and S. Ibuki. *Zero-phonon lines and phonon coupling in ZnS:Mn*. Physical Review **138** (3A), A809–A815 (1965). ISSN 0031-899X. DOI http://dx.doi.org/10.1103/PhysRev.138.A809 23

[Lan80] L. D. Landau and E. M. Lifschitz. *Statistical Physics*, volume 5 of *Course of theoretical physics*. 3. edition (Pergamon Press, 1980). ISBN 0080230385 74

[Lar85] B. E. Larson, K. C. Hass, H. Ehrenreich and A. E. Carlson. *Exchange mechanisms in diluted magnetic semiconductors*. Solid State Communications **56** (4), 347–350 (1985). ISSN 0038-1098. DOI http://dx.doi.org/10.1016/0038-1098(85)90399-0 19, 23, 37

[Lar86] B. E. Larson, K. C. Hass and R. L. Aggarwal. *Effects of internal exchange fields on magnetization steps in diluted magnetic semiconductors*. Physical Review B **33**, 1789–1796 (1986). ISSN 0163-1829. DOI http://dx.doi.org/10.1103/PhysRevB.33.1789 37, 38, 41, 119, 130

[Lar88a] B. E. Larson, K. C. Hass, H. Ehrenreich and A. E. Carlsson. *Erratum: Theory of exchange interactions and chemical trends in diluted magnetic semiconductors [Phys. Rev. B 37, 4137 (1988)]*. Physical Review B **38**, 7842 (1988). ISSN 0163-1829. DOI http://dx.doi.org/10.1103/PhysRevB.38.7842 23, 37

[Lar88b] B. E. Larson, K. C. Hass, H. Ehrenreich and A. E. Carlsson. *Theory of exchange interactions and chemical trends in diluted magnetic semiconductors*. Physical Review B **37**, 4137–4154 (1988). ISSN 0163-1829. DOI http://dx.doi.org/10.1103/PhysRevB.37.4137 14, 19, 23, 35, 36, 37

[Lar89] B. E. Larson and H. Ehrenreich. *Anisotropic superexchange and spin-resonance linewidth in diluted magnetic semiconductors*. Physical Review B **39**, 1747–1759 (1989). ISSN 0163-1829. DOI http://dx.doi.org/10.1103/PhysRevB.39.1747 35, 36

[Law71] P. Lawaetz. *Valence-band parameters in cubic semiconductors*. Physical Review B **4** (10), 3460–3467 (1971). ISSN 0163-1829. DOI http://dx.doi.org/10.1103/PhysRevB.4.3460 17

[Lee84] Y: R. Lee and A. K. Ramdas. *A piezomodulation study of the absorption edge and Mn^{++} internal transition in $Cd_{1-x}Mn_xTe$, a prototype of diluted magnetic semiconductors*. Solid State Communications **51** (11), 861–863 (1984). ISSN 0038-1098. DOI http://dx.doi.org/10.1016/0038-1098(84)91088-3 20, 21

[Lee86] Y. R. Lee, A. K. Ramdas and R. L. Aggarwal. *Origin of the Mn^{2+} optical transition in Mn-based II-VI diluted magnetic semiconductors*. Physical Review B **33** (10), 7383–7385 (1986). ISSN 0163-1829. DOI http://dx.doi.org/10.1103/PhysRevB.33.7383 20

[Lei97] D. Leinen. *Excitonic energy transfer to the 3d electrons of Mn^{2+}sin Cd_{1-x} Mn_x Te*. Physical Review B **55**, 6975–6980 (1997). ISSN 0163-1829. DOI http://dx.doi.org/10.1103/PhysRevB.55.6975 92, 120

[Lew88] A. Lewicki, J. Spałek, J. K. Furdyna and R. R. Gałązka. *Magnetic susceptibility of diluted magnetic (semimagnetic) semiconductors: Further evidence for superexchange*. Physical Review B **37**, 1860–1863 (1988). ISSN 0163-1829. DOI http://dx.doi.org/10.1103/PhysRevB.37.1860 39

[Li95] Ting Li, Huan Luo, Raymond G. Greene, Arthur L. Ruoff, Steven S. Trail and Francis J. DiSalvo, Jr. *High pressure phase of MgTe: Stable structure at STP?*. Physical Review Letters **74** (26), 5232–5235 (1995). ISSN 0031-9007. DOI http://dx.doi.org/10.1103/PhysRevLett.74.5232 164

[Lip98] A. A. Lipovskii, E. V. Kolobkova and V. D. Petrikov. *Effect of spin-orbit splitting on electron-hole transitions in microscopic CdS and CdTe crystals*. Physics of the Solid State **40** (5), 794–795 (1998). ISSN 1063-7834. DOI http://dx.doi.org/10.1134/1.1130398 16

[Lit96] M. T. Litz, K. Watanabe, M. Korn, H. Ress, U. Lunz, W. Ossau, A. Waag, G. Landwehr, T. Walter, B. Neubauer, D. Gerthsen and U. Schüssler. *Epitaxy of $Zn_{1-x}Mg_xSe_yTe_{1-y}$ on (100)InAs*. Journal of Crystal Growth **159** (1-4), 54–57 (1996). ISSN 0022-0248. DOI http://dx.doi.org/10.1016/0022-0248(95)00881-0. Proceedings of the seventh international conference on II-VI compouds and devices 164

[Liu61] S. H. Liu. *Exchange interaction between conduction electrons and magnetic shell electrons in rare-earth metals*. Physical Review **121**, 451–455 (1961). ISSN 0031-899X. DOI http://dx.doi.org/10.1103/PhysRev.121.451 34

[Liu04] X. Liu and J. K. Furdyna. *Optical dispersion of ternary II-VI semiconductor alloys*. Journal of Applied Physics **95** (12), 7754–7764 (2004). ISSN 0021-8979. DOI http://dx.doi.org/10.1063/1.1739291 19

[Los98] D. Loss and D. P. Divincenzo. *Quantum computation with quantum dots*. Physical Review A **57**, 120–126 (1998). ISSN 1050-2947. DOI http://dx.doi.org/10.1103/PhysRevA.57.120 3

[Lut55] J. M. Luttinger and W. Kohn. *Motion of electrons and holes in perturbed periodic fields*. Physical Review **97** (4), 869–883 (1955). ISSN 0031-899X. DOI http://dx.doi.org/10.1103/PhysRev.97.869 16

[Lut56] J. M. Luttinger. *Quantum theory of cyclotron resonance in semiconductors: general theory*. Physical Review **102**, 1030–1041 (1956). ISSN 0031-899X. DOI http://dx.doi.org/10.1103/PhysRev.102.1030 10, 16

[Lym06] T. Lyman. *The spectrum of hydrogen in the region of extremely short wave-lengths*. Astrophysical Journal, The **23**, 181 (1906). DOI http://dx.doi.org/10.1086/141330 1

[LYV96] L. C. Lew Yan Voon, M. Willatzen, M. Cardona and N. E. Christensen. *Terms linear in k in the band structure of wurtzite-type semiconductors*. Physical Review B **53** (16), 10703–10714 (1996). ISSN 0163-1829. DOI http://dx.doi.org/10.1103/PhysRevB.53.10703 13

[Mac94] G. Mackh, W. Ossau, D. R. Yakovlev, A. Waag, G. Landwehr, R. Hellmann and E. O. Göbel. *Localized exciton magnetic polarons in $Cd_{1-x}Mn_xTe$*. Physical Review B **49**, 10248–10258 (1994). ISSN 0163-1829. DOI http://dx.doi.org/10.1103/PhysRevB.49.10248 91

[Mac96] G. Mackh. *Magnetische Lokalisation und Dynamik von Exzitonen in semimagnetischen Halbleitern*. PhD thesis, Universität Würzburg, Würzburg (1996) 20, 63

[Mad99] O. Madelung, U. Rössler and M. Schulz (Editors). *II-VI and I-VII compounds; semimagnetic compounds*, volume Group III - Condensed Matter, Vol.41 - Semiconductors, Subvol. B of *Landolt-Börnstein - Numerical data and functional relationships in science and technology* (Springer, Berlin, Heidelberg, New York, 1999). ISBN 3540649646. Suppl. zu: Zahlenwerte und Funktionen aus Naturwissenschaften und Technik ; Gruppe 3, Bd. 17, Teilbd. b und Bd. 22, Teilbd. a xi, 13, 164, 165

[Mai93] M. Z. Maialle, E. A. de Andrada E Silva and L. J. Sham. *Exciton spin dynamics in quantum wells*. Physical Review B **47** (23), 15776–15788 (1993). ISSN 0163-1829. DOI http://dx.doi.org/10.1103/PhysRevB.47.15776 80

[Mak85] A. A. Maksimov and I. I. Tartakovskiĭ. *Propagation and relaxation of rf acoustic phonons in thin crystal plates*. Journal of Experimental and Theoretical Physics Letters (JETP) **42**, 568–572 (1985). ISSN 0021-3640. Translation of: Pis'ma v Zhurnal Eksperimental'noy i Teoreticheskoy Fizika, USSR **42** (11), 458-461 (1985) 108, 144

[Mak09] A. A. Maksimov, D. R. Yakovlev, M. K. Kneip, M. Arlt, M. Bayer, T. Wojtowicz, G. Karczewski and J. Kossut. *Spin diffusion in (Cd,Mn)Te diluted magnetic semiconductors* (2009). In preparation for Physical Review B 147

[Mal83] A. V. Malyavkin. *Optically detected magnetic resonance in $Zn_{1-x}Mn_xTe$*. Physica Status Solidi (B) - Basic Research **115** (2), 353–358 (1983). ISSN 0370-1972. DOI http://dx.doi.org/10.1002/pssb.2221150204 92

[Mal85] A. V. Malyavkin and A. A. Dremin. *ESR saturation and exciton luminescence in $Cd_{1-x}Mn_xSe$*. Journal of Experimental and Theoretical Physics Letters (JETP) **42**, 114–117 (1985). ISSN 0021-3640. Translation of: Pis'ma v Zhurnal Eksperimental'noy i Teoreticheskoy Fizika, USSR, **42** (3), 95-97 (1985) 92

[Man95] A. Mang, K. Reimann and S. Rübenacke. *Two-photon spectroscopy in ZnSe under hydrostatic pressure*. In *Proceedings of the 22nd International Conference on the Physics of Semiconductors, Vancouver 1994*, edited by D. J. Lockwood, 317–320 (World Scientific, Singapore, 1995) 164

[Man00] C. Mann. *Vierwellen-Mischen an II-VI-Halbleiter-Nanostrukturen*. master thesis, Universität Dortmund, Dortmund (2000) 49, 63

[Maš87] J. Mašek and B. Velický. *Mn 3d states in photoelectron spectra from $Cd_{1-x}Mn_xTe$*. Physica Status Solidi (B) - Basic Research **140** (1), 135–140 (1987). ISSN 0370-1972. DOI http://dx.doi.org/10.1002/pssb.2221400114 19

[Mau90] A. Mauger, J. Villain, Y. Zhou, C. Rigaux, N. Bontemps and J. Férré. *Spin-glass ordering in three-dimensional Heisenberg systems*. Physical Review B **41** (7), 4587–4592 (1990). ISSN 0163-1829. DOI http://dx.doi.org/10.1103/PhysRevB.41.4587 40

[McI80] G. J. McIntyre, G. Moss and Z. Barnea. *Anharmonic temperature factors of zinc selenide determined by X-ray diffraction from an extended-face crystal*. Acta Crystallographica Section A **36** (3), 482–490 (1980). ISSN 1600-5724. DOI http://dx.doi.org/10.1107/S0567739480001003 164

[Mei84] F. Meier and B. P. Zakharchenya (Editors). *Optical orientation*, volume 8 of *Modern Problems in Condensed Matter Sciences* (North-Holland Publishing Company, Amsterdam, 1984). ISBN 0444867414 3, 4, 74, 87, 192, 219

[Mer99] I. A. Merkulov, D. R. Yakovlev, A. Keller, W. Ossau, J. Geurts, A. Waag, G. Landwehr, G. Karczewski, T. Wojtowicz and J. Kossut. *Kinetic exchange between the conduction band electrons and magnetic ions in quantum-confined structures*. Physical Review Letters **83** (7), 1431–1434 (1999). ISSN 0031-9007. DOI http://dx.doi.org/10.1103/PhysRevLett.83.1431 48

[Mer09] I. A. Merkulov and A. V. Rodina. *Exchange interaction between carriers and magnetic ions in quantum size heterostructures*. In Kossut and Gaj [Kos09], chapter 3. (Planned for 2009) 68

[Mil84a] R. C. Miller, A. C. Gossard, D. A. Kleinman and O. Munteanu. *Parabolic quantum wells with the GaAs-$Al_xGa_{1-x}As$ system*. Physical Review B **29**, 3740–3743 (1984). ISSN 0163-1829. DOI http://dx.doi.org/10.1103/PhysRevB.29.3740 57, 140, 161

[Mil84b] R. C. Miller, D. A. Kleinman and A. C. Gossard. *Energy-gap discontinuities and effective masses for GaAs-$Al_xGa_{1-x}As$ quantum wells*. Physical Review B **29**, 7085–7087 (1984). ISSN 0163-1829. DOI http://dx.doi.org/10.1103/PhysRevB.29.7085 57

[Mil85] R. C. Miller, A. C. Gossard and D. A. Kleinman. *Band offsets from two special GaAs-$Al_xGa_{1-x}As$ quantum-well structures*. Physical Review B **32** (8), 5443–5446 (1985). ISSN 0163-1829. DOI http://dx.doi.org/10.1103/PhysRevB.32.5443 58

[Mis69] P. K. Misra and L. M. Roth. *Theory of diamagnetic susceptibility of metals*. Physical Review **177** (3), 1089–1102 (1969). ISSN 0031-899X. DOI http://dx.doi.org/10.1103/PhysRev.177.1089 31

[Miy95] T. Miyazaki and N. Tezuka. *Giant magnetic tunneling effect in Fe/Al_2O_3/Fe junction*. Journal of Magnetism and Magnetic Materials **139** (3), L231–L234 (1995). ISSN 0304-8853. DOI http://dx.doi.org/10.1016/0304-8853(95)90001-2 2

[Moo95] Moodera, J. S. and Kinder, L. R. and Wong, T. M. and Meservey, R. *Large magnetoresistance at room temperature in ferromagnetic thin film tunnel junctions*. Physical Review Letters **74** (16), 3273–3276 (1995). ISSN 0031-9007. DOI http://dx.doi.org/10.1103/PhysRevLett.74.3273 2

[Moo96] J. S. Moodera and L. R. Kinder. *Ferromagnetic-insulator-ferromagnetic tunneling: Spin-dependent tunneling and large magnetoresistance in trilayer junctions (invited)*. Journal of Applied Physics **79** (8), 4724–4729 (1996). ISSN 0021-8979. DOI http://dx.doi.org/10.1063/1.361653 2

[Mor60] T. Moriya. *Anisotropic superexchange interaction and weak ferromagnetism*. Physical Review **120**, 91–98 (1960). ISSN 0031-899X. DOI http://dx.doi.org/10.1103/PhysRev.120.91 36, 119

[Mor82] M. M. Moriwaki, W. M. Becker, W. Gebhardt and R. R. Gałązka. *Study of the 2.0-eV photoluminescence band in $Cd_{1-x}Mn_xTe$ semiconductor alloys*. Physical Review B **26** (6), 3165–3171 (1982). ISSN 0163-1829. DOI http://dx.doi.org/10.1103/PhysRevB.26.3165 20, 23

[Mor84] J. E. Morales Toro, W. M. Becker, B. I. Wang, U. Debska and J. W. Richardson. *Identification of new absorption bands in $Zn_{1-x}Mn_xTe$*. Solid State Communications **52** (1), 41–43 (1984). ISSN 0038-1098. DOI http://dx.doi.org/10.1016/0038-1098(84)90714-2 23

[Mou00] C. Mourad, D. Gianardi, K. J. Malloy and R. Kaspi. *2 μm GaInAsSb/AlGaAsSb midinfrared laser grown digitally on GaSb by modulated-molecular beam epitaxy*. Journal of Applied Physics **88** (10), 5543 (4pp.) (2000). ISSN 0021-8979. DOI http://dx.doi.org/10.1063/1.1319967 161

[Myc81] J. Mycielski. *Semimagnetic semiconductors*. In *Recent developments in condensed matter physics*, edited by J. T. DeVreese, volume 1, 725 (Plenum Press, New York,

1981). ISBN 0306406462. Invited papers presented at the First General Conference of the Condensed Matter Division of the European Physical Society, held April 9 - 11, 1980, at the University of Antwerp (RUCA and UIA), Antwerp, Belgium 34

[Nag80] S. Nagata, R. R. Gałązka, D. P. Mullin, H. Akbarzadeh, G. D. Khattak, J. K. Furdyna and P. H. Keesom. *Magnetic susceptibility, specific heat, and the spin-glass transition in $Hg_{1-x}Mn_xTe$*. Physical Review B **22**, 3331–3343 (1980). ISSN 0163-1829. DOI http://dx.doi.org/10.1103/PhysRevB.22.3331 37, 39, 40

[Nas90] A. Nasar and M. Shamsuddin. *Thermodynamic properties of zinc selenide and zinc telluride*. Zeitschrift für Metallkunde **81**, 244 (1990). ISSN 0179-4841 164

[Naw79] M. Nawrocki and A. Twardowski. *Oscillatory magnetoabsorption in CdTe*. Physica Status Solidi (B) - Basic Research **97** (1), K61–K64 (1979). ISSN 0370-1972. DOI http://dx.doi.org/10.1002/pssb.2220970157 164

[Naw81] M. Nawrocki, R. Planel, G. Fishman and R. R. Gałązka. *Exchange-induced spin-flip raman scattering in a semimagnetic semiconductor*. Physical Review Letters **46** (11), 735–738 (1981). ISSN 0031-9007. DOI http://dx.doi.org/10.1103/PhysRevLett.46.735 4

[Ned65] G. M. Nedlin. *Possible ordered magnetic structures of $YMnO_3$-Type crystals*. Soviet Physics - Solid State **6**, 2156 (1965). ISSN 0038-5654 29

[Neu88] C. Neumann, A. Nöthe and N. O. Lipari. *Two-photon magnetoabsorption of ZnTe, CdTe, and GaAs*. Physical Review B **37**, 922–932 (1988). ISSN 0163-1829. DOI http://dx.doi.org/10.1103/PhysRevB.37.922 164

[Ngu83] Nguyen The Khoi and J. A. Gaj. *Fundamental absorption edge of $Cd_{1-x}Mn_xTe$ mixed crystals*. Physica Status Solidi (B) - Basic Research **83** (2), K133–K135 (1983). ISSN 0370-1972. DOI http://dx.doi.org/10.1002/pssb.2220830244 20

[Nic95] R. J. Nicholas, M. J. Lawless, H. H. Cheng, D. E. Ashenford and B. Lunn. *A modified phenomenological description of the exchange interactions in dilute magnetic semiconductors*. Semiconductor Science and Technology **10** (6), 791–796 (1995). ISSN 0268-1242. DOI http://dx.doi.org/10.1088/0268-1242/10/6/008 42

[Nil91] D. W. Niles and H. Höchst. *Critical test of CdTe(100) angle-resolved photoemission spectra with band-structure calculations*. Physical Review B **43** (2), 1492–1499 (1991). ISSN 0163-1829. DOI http://dx.doi.org/10.1103/PhysRevB.43.1492 164

[Nol96] W. Nolting. *Statistische Physik*, volume 6 of *Vieweg-Lehrbuch : Grundkurs theoretische Physik*. 2. edition (Vieweg, Braunschweig, Wiesbaden, 1996). ISBN 3528069368 28

[Nov81] M. A. Novak, S. Oseroff and O. G. Symko. *Transition from spin-glass to single impurity behavior in Cd—Mn—Te*. Physica B+C **107** (1-3), 313–314 (1981). ISSN 0378-4363. DOI http://dx.doi.org/10.1016/0378-4363(81)90462-9 40

[Nov84] M. A. Novak, O. G. Symko, D. J. Zheng and S. Oseroff. *Magnetic phase diagram of $Cd_{1-x}Mn_xSe$ below the nearest neighbor percolation limit*. Physica B+C **126** (1-3), 469–470 (1984). ISSN 0378-4363. DOI http://dx.doi.org/10.1016/0378-4363(84)90209-2 40

[Nov85] M. A. Novak, O. G. Symko, D. J. Zheng and S. Oseroff. *Spin glass behavior of $Cd_{1-x}Mn_xTe$ below the nearest-neighbor percolation limit*. Journal of Applied Physics **57** (8), 3418–3420 (1985). ISSN 0021-8979. DOI http://dx.doi.org/10.1063/1.335062 40

[Nov86] M. A. Novak, O. G. Symko, D. J. Zheng and S. Oseroff. *Spin freezing below the nearest-neighbor percolation concentration in $Cd_{1-x}Mn_xTe$ and $Cd_{1-x}Mn_xSe$*. Physical Review B **33**, 6391–6394 (1986). ISSN 0163-1829. DOI http://dx.doi.org/10.1103/PhysRevB.33.6391 40

[Nur85] A. V. Nurmikko, X.-C. Zhang, S.-K. Chang, L. A. Kolodziejski, R. L. Gunshor and S. Datta. *Excitons in CdTe/$Cd_{1-x}Mn_xTe$ multiquantum wells*. Journal of Luminescence **34** (1-2), 89–97 (1985). ISSN 0022-2313. DOI http://dx.doi.org/10.1016/0022-2313(85)90098-5 51, 52

[Nur86] A. V. Nurmikko, R. L. Gunshor and L. A. Kolodziejski. *Optical properties of CdTe/(Cd, Mn)Te multiple quantum wells*. IEEE Journal of Quantum Electronics **22** (9), 1785–1792 (1986). ISSN 0018-9197 48

[Nur89] A. V. Nurmikko, Q. Fu, D. Lee, L. A. Kolodziejski and R. L. Gunshor. 1523–1534 (Institute of Physics, Polish Academy of Science, 1989). Proceedings of the 19th International Conference on the Physics of Semiconductors, Warsaw 1988 48

[Oel82] P. Oelhafen, M. P. Vecchi, J. L. Freeouf and V. L. Moruzzi. *The delocalized d-electrons in the semimagnetic alloy $Cd_{1-x}Mn_xTe$*. Solid State Communications **44** (12), 1547–1550 (1982). ISSN 0038-1098. DOI http://dx.doi.org/10.1016/0038-1098(82)90675-5 20

[Oes99] M. Oestreich, J. Hübner, D. Hägele, P. J. Klar, W. Heimbrodt, W. W. Rühle, D. E. Ashenford and B. Lunn. *Spin injection into semiconductors*. Physical Review Letters **74**, 1251–1253 (1999). ISSN 0003-6951. DOI http://dx.doi.org/10.1063/1.123515 3

[Oes02] M. Oestreich, M. Bender, J. Hübner, D. Hägele, W. W. Rühle, T. Hartmann, P. J. Klar, W. Heimbrodt, M. Lampalzer, K. Volz and W. Stolz. *Spin injection, spin transport*

and spin coherence. Semiconductor Science and Technology **17** (4), 285–297 (2002). ISSN 0268-1242. DOI http://dx.doi.org/10.1088/0268-1242/17/4/302 3, 6

[Oft27] I. Oftedal. Zeitschrift für Physikalische Chemie **128**, 135–158 (1927). ISSN 0942-9352 11, 165

[Oh93] E. Oh, C. Parks, I. Miotkowski, M. D. Sciacca, A. J. Mayur and A. K. Ramdas. *Optical properties of Mg-based II-VI ternaries and quaternaries:* $Cd_{1-x}Mg_xTe$ *and* $Cd_{1-x-y}Mg_xMn_yTe$. Physical Review B **48** (20), 15040–15046 (1993). ISSN 0163-1829. DOI http://dx.doi.org/10.1103/PhysRevB.48.15040 164

[Ohn98] H. Ohno. *Making Nonmagnetic Semiconductors Ferromagnetic*. Science **281** (5379), 951–956 (1998). ISSN 0036-8075. DOI http://dx.doi.org/10.1126/science.281.5379.951 2

[Ohn99a] Y. Ohno, R. Terauchi, T. Adachi, F. Matsukura and H. Ohno. *Spin relaxation in GaAs(110) quantum wells*. Physical Review Letters **83** (20), 4196–4199 (1999). ISSN 0031-9007. DOI http://dx.doi.org/10.1103/PhysRevLett.83.4196 78

[Ohn99b] Y. Ohno, D. K. Young, B. Beschoten, F. Matsukura, H. Ohno and D. D. Awschalom. *Electrical spin injection in a ferromagnetic semiconductor heterostructure*. Nature **402**, 790–792 (1999). ISSN 0028-0836. DOI http://dx.doi.org/10.1038/45509 3

[Ole01] J. T. Olesberg, W. H. Lau, M. E. Flatté, C. Yu, E. Altunkaya, E. M. Shaw, T. C. Hasenberg and T. F. Boggess. *Interface contributions to spin relaxation in a short-period InAs/GaSb superlattice*. Physical Review B **64** (20), 201301 (4pp.) (2001). ISSN 0163-1829. DOI http://dx.doi.org/10.1103/PhysRevB.64.201301 77

[Orb61] R. Orbach. *Spin-Lattice Relaxation in Rare-Earth Salts*. Proceedings of the Royal Society of London - Series A: Mathematical and Physical Sciences **264** (1319), 458–484 (1961). ISSN 0080-4630. DOI http://dx.doi.org/10.1098/rspa.1961.0211 80

[Ort82] M. von Ortenberg. *Spin superlattice with tunable minigap*. Physical Review Letters **49**, 1041–1043 (1982). ISSN 0031-9007. DOI http://dx.doi.org/10.1103/PhysRevLett.49.1041 52

[Ose80] S. B. Oseroff, R. Calvo and W. Giriat. *Magnetic properties of* $Cd_{1-x}Mn_xTe$. Solid State Communications **35** (7), 539–542 (1980). ISSN 0038-1098. DOI http://dx.doi.org/10.1016/0038-1098(80)90892-3 33, 40

[Ose81] S. B. Oseroff and F. Acker. *Magnetic susceptibility on semimagnetic semiconductors*. Solid State Communications **37** (1), 19–23 (1981). ISSN 0038-1098. DOI http://dx.doi.org/10.1016/0038-1098(81)90880-2 40

[Ose82] S. B. Oseroff. *Magnetic susceptibility and EPR measurements in concentrated spin-glasses: $Cd_{1-x}Mn_xTe$ and $Cd_{1-x}Mn_xSe$.* Physical Review B **25** (11), 6584–6594 (1982). ISSN 0163-1829. DOI http://dx.doi.org/10.1103/PhysRevB.25.6584 39, 40

[Ose85] S. B. Oseroff and F. G. Gandra. *Time, temperature, and field dependence of the remanent magnetization in $Cd_{1-x}Mn_xTe$.* Journal of Applied Physics **57** (8), 3421 (1985). ISSN 0021-8979. DOI http://dx.doi.org/10.1063/1.335063 40

[Ose88] S. Oseroff and P. H. Keesom. *Magnetic properties: Macroscopic studies*. In Furdyna and Kossut [Fur88b], chapter 3, 73–123. ISBN 0127521259 33

[Oss93] W. J. Ossau and B. Kuhn-Heinrich. *Dimensional dependence of antiferromagnetism in diluted magnetic semiconductor heterostructures*. Physica B: Condensed Matter **184**, 422–431 (1993). ISSN 0921-4526. DOI http://dx.doi.org/10.1016/0921-4526(93)90392-J 41, 59, 64, 136

[Oss94] W. Ossau, U. Zehnder, B. Kuhn-Heinrich, A. Waag, T. Litz, G. Landwehr, R. Hellmann and E. O. Göbel. *$Cd_{1-x}Mg_xTe$: A new promising barrier material to CdTe based heterostructures*. Superlattices and Microstructures **16** (1), 5–10 (1994). ISSN 0749-6036. DOI http://dx.doi.org/10.1006/spmi.1994.1099 165

[Ove53] A. W. Overhauser. *Paramagnetic relaxation in metals*. Physical Review **89** (4), 689–700 (1953). ISSN 0031-899X. DOI http://dx.doi.org/10.1103/PhysRev.89.689 79

[Paj78] A. Pajaczkowska. *Physicochemical properties and crystal growth of $A^{II}B^{VI}$ - MnB^{VI} systems*. Progress in Crystal Growth and Characterization **1** (3), 289–326 (1978). ISSN 0146-3535. DOI http://dx.doi.org/10.1016/0146-3535(78)90004-7 12

[Par71] S. G. Parker, A. R. Reinberg, J. E. Pinnell and W. C. Holton. *Preparation and properties of $Mg_xZn_{1-x}Te$*. Journal of the Electrochemical Society **118** (6), 979–983 (1971). ISSN 0013-4651. DOI http://dx.doi.org/10.1149/1.2408236 11, 164

[Par99] S. S. P. Parkin, K. P. Roche, M. G. Samant, P. M. Rice, R. B. Beyers, R. E. Scheuerlein, E. J. O'Sullivan, S. L. Brown, J. Bucchigano, D. W. Abraham, Y. Lu, M. Rooks, P. L. Trouilloud, R. A. Wanner and W. J. Gallagher. *Exchange-biased magnetic tunnel junctions and application to nonvolatile magnetic random access memory (invited)*. Journal of Applied Physics **85**, 5828–5833 (1999). ISSN 0021-8979. DOI http://dx.doi.org/10.1063/1.369932 2

[Pas08] F. Paschen. *Zur Kenntnis ultraroter Linienspektra. I. (Normalwellenlängen bis 27000 Å.-E.)*. Annalen der Physik **332** (13), 537–570 (1908). ISSN 0003-3804. DOI http://dx.doi.org/10.1002/andp.19083321303 1

[Pas95] Y. G. Pashkevich, V. L. Sobolev, S. A. Fedorov and A. V. Eremenko. *Theory of raman light scattering in the many-sublattice exchange-noncollinear magnets UO_2, $RMnO_3$, and Nd_2CuO_4 (R=rare-earth ion).* Physical Review B **51** (22), 15898–15919 (1995). ISSN 0163-1829. DOI http://dx.doi.org/10.1103/PhysRevB.51.15898 29

[Pat07] B. Patrick. *Die Entdeckung des Riesen-Magnetowiderstandes. Physik-Nobelpreis 2007*. Physik in unserer Zeit **38** (6), 272–273 (2007). ISSN 0031-9252. DOI http://dx.doi.org/10.1002/piuz.200790087 2

[Pau25] W. Pauli. *Über den Zusammenhang des Abschlusses der Elektronengruppen im Atom mit der Komplexstruktur der Spektren*. Zeitschrift für Physik **31**, 765–783 (1925). ISSN 0044-3328 1

[Pau27] W. Pauli, Jr. *Über Gasentartung und Paramagnetismus*. Zeitschrift für Physik **41** (6-7), 81–102 (1927). ISSN 0044-3328. DOI http://dx.doi.org/10.1007/BF01391920 29

[Pei55] R. E. Peierls. *Quantum theory of solids*. Oxford Classic Texts in the Physical Sciences (Oxford Press, New York, 1955). ISBN 019850781X 31

[Pes87] M. Pessa. *Diluted Magnetic (Semimagnetic) Semiconductors*. In Aggarwal *et al.* [Agg87], 303. ISBN 0931837545 46

[Pet85] A. Petrou, J. Warnock, R. N. Bicknell, N. C. Giles-Taylor and J. F. Schetzina. *Photoluminescence of a $Cd_{0.55}Mn_{0.45}Te$-CdTe multiple quantum well structure in a magnetic field*. Applied Physics Letters **46** (7), 692–694 (1985). ISSN 0003-6951. DOI http://dx.doi.org/10.1063/1.95477 51

[Pie95] J. Pietruczanis, W. Mac, A. Twardowski, G. Karczewski, A. J. Zakrzewski, E. Janik, T. Wojtowicz and J. Kossut. *Magnetic phase diagram of highly concentrated $Cd_{1-x}Mn_xTe$ (0.4$< x <$1.0).* Materials Science Forum **182-184**, 687–690 (1995). ISBN 0-87849-689-0. Joint Proceedings of the 3rd European Workshop on II-VI Compounds and the 4^{th} International Workshop on Semimagnetic (Diluted Magnetic) Semiconductors, both held in Linz, Austria, September 1994 40

[Pik71] G. E. Pikus and G. L. Bir. *Exchange interaction in excitons in semiconductors*. Journal of Experimental and Theoretical Physics (JETP) **33**, 108–114 (1971). ISSN 1063-7761 80

[Pik84] G. Pikus and A. N. Titkov. *Spin relaxation and optical orientation*. In Meier and Zakharchenya [Mei84], chapter 3, 73–131. ISBN 0444867414 77

[Pik95] F. G. Pikus and G. E. Pikus. *Conduction-band spin splitting and negative magnetoresistance in A_3B_5 heterostructures*. Physical Review B **51** (23), 16928–16935 (1995). ISSN 0163-1829. DOI http://dx.doi.org/10.1103/PhysRevB.51.16928 50

[Pin55] D. Pines and C. P. Slichter. *Relaxation times in magnetic resonance*. Physical Review **100**, 1014–1020 (1955). ISSN 0031-899X. DOI http://dx.doi.org/10.1103/PhysRev.100.1014 70

[Plo83] K. Ploog and G. H. Döhler. *Compositional and doping superlattices in III-V semiconductors*. Advances in Physics **32** (3), 285–359 (1983). ISSN 0001-8732. DOI http://dx.doi.org/10.1080/00018738300101561 121

[Poh94] U. W. Pohl, G. H. Kudlek, A. Klimakow and A. Hoffmann. *Shallow impurity- and defect-related complexes in undoped ZnSe crystals*. Journal of Crystal Growth **138** (1-4), 385–390 (1994). ISSN 0022-0248. DOI http://dx.doi.org/10.1016/0022-0248(94)90838-9 164

[Pon90] W.-F. Pong, R. A. Mayanovic, B. A. Bunker, J. K. Furdyna and U. Debska. *Extended x-ray-absorption fine-structure studies of $Zn_{1-x}Mn_xSe$ alloy structure*. Physical Review B **41** (12), 8440–8448 (1990). ISSN 0163-1829. DOI http://dx.doi.org/10.1103/PhysRevB.41.8440 14

[Poo95] H. C. Poon, Z. C. Feng, Y. P. Feng and M. F. Li. *Relativistic band structure of ternary II-VI semiconductor alloys containing Cd, Zn, Se and Te*. Journal of Physics: Condensed Matter **7** (14), 2783–2799 (1995). ISSN 0953-8984. DOI http://dx.doi.org/10.1088/0953-8984/7/14/017 164

[Pri98] G. A. Prinz. *Magnetoelectronics*. Science **282** (5394), 1660–1663 (1998). ISSN 0036-8075. DOI http://dx.doi.org/10.1126/science.282.5394.1660 2

[Pri08] Princeton Instruments Acton. *Selecting the Right ICCD Camera!*. Roper webpage (2008). URL http://www.roperscientific.de/datasheets/select%20iccd%20camera%20tech%20note%20revised2.pdf 100

[Pul03] V. I. Puller, L. G. Mourokh, N. J. M. Horing and A. Y. Smirnov. *Electron spin relaxation in a semiconductor quantum well*. Physical Review B **67** (15), 155309 (9pp.) (2003). ISSN 0163-1829. DOI http://dx.doi.org/10.1103/PhysRevB.67.155309 76

[Qaz95] M. Qazzaz, G. Yang, S. H. Xin, L. Montes, H. Luo and J. K. Furdyna. *Electron paramagnetic resonance of Mn^{2+} in strained-layer semiconductor superlattices*. Solid State Communications **96** (6), 405–409 (1995). ISSN 0038-1098. DOI http://dx.doi.org/10.1016/0038-1098(95)00373-8 69

[Qte92] A. Qteish and R. J. Needs. *Improved model-solid-theory calculations for valence-band offsets at semiconductor-semiconductor interfaces*. Physical Review B **45** (3), 1317–1326 (1992). ISSN 0163-1828. DOI http://dx.doi.org/10.1103/PhysRevB.45.1317 164

[Rad63] G. T. Rado and H. Suhl. *Magnetism*, volume 1 (Academic Press Inc., New York, 1963). ISBN 0125753012 28

[Ram92] M. T. Ramsbey, S. Tamura and J. P. Wolfe. *Mode-selective scattering of phonons in a semi-insulating GaAs crystal: A case study using phonon imaging*. Physical Review B **46** (3), 1358–1364 (1992). ISSN 0163-1829. DOI http://dx.doi.org/10.1103/PhysRevB.46.1358 95

[Riv01] C. Riva, F. M. Peeters and K. Varga. *Magnetic field dependence of the energy of negatively charged excitons in semiconductor quantum wells*. Physical Review B **63** (11), 115302 (9pp.) (2001). ISSN 0163-1829. DOI http://dx.doi.org/10.1103/PhysRevB.63.115302 66

[Rös81] U. Rössler and H.-R. Trebin. *Exchange and polaron corrections for excitons in the degenerate-band case*. Physical Review B **23** (4), 1961–1970 (1981). ISSN 0163-1829. DOI http://dx.doi.org/10.1103/PhysRevB.23.1961 164

[Rot60] W. L. Roth. *Neutron and optical studies in NiO*. Journal of Applied Physics **31** (11), 2000–2011 (1960). ISSN 0021-8979. DOI http://dx.doi.org/10.1063/1.1735486 29

[Rud05] J. Rudolph. *Spinelektronik in Quantenfilmen*. PhD thesis, Universität Hannover, Hannover (2005) 16, 18, 50, 55, 77, 78

[Rut11] E. Rutherford. *The scattering of α and β particles by matter and the structure of the atom*. Philosophical Magazine **21**, 669–668 (1911). Series 6 1

[Rya81] S. M. Ryabchenko, O. V. Terletskii, I. B. Mizetskaya and G. S. Olenik. Soviet Physics - Semiconductors **15**, 1345 (1981). ISSN 0038-5700. Translation of: Fizika i Tekhnika Poluprovodnikov, **15**, 2314 (1981) 64

[Rya82] S. M. Ryabchenko, Y. G. Semenov and O. V. Terletskii. Journal of Experimental and Theoretical Physics (JETP) **55**, 557 (1982). ISSN 1063-7761. Translation of: Pis'ma v Zhurnal Eksperimental'noy i Teoreticheskoy Fizika, USSR **82**, 951 (1982) 71, 92

[Sa00] D. Sa, R. Valentí and C. Gros. *A generalized Ginzberg-Landau approach to second harmonic generation*. European Physical Journal B (EPJ B), The - Condensed Matter **14** (2), 301–305 (2000). ISSN 1434-6028. DOI http://dx.doi.org/10.1007/s100510050133 29

[Sad03] M. L. Sadowski, M. Byszewski, M. Potemski, A. Sachrajda and G. Karczewski. *Optical detection of electron paramagnetic resonance in CdMnTe single quantum wells*. Applied Physics Letters **82** (21), 3719–3721 (2003). ISSN 0003-6951. DOI http://dx.doi.org/10.1063/1.1578511 92

[Sän06] I. Sänger. *Magnetic-field-induced second harmonic generation in semiconductors and insulators*. PhD thesis, Universität Dortmund, Dortmund (2006) 30, 44

[Sas01] H. Sasakura, S. Muto and T. Ohshima. *Quantum gates using spin states of triple quantum dot*. Physica E: Low-dimensional Systems and Nanostructures **10** (1-3), 458–462 (2001). ISSN 1386-9477. DOI http://dx.doi.org/10.1016/S1386-9477(01)00137-0 3

[Saw94] M. Sawicki, M. A. Brummell, P. A. J. de Groot, G. J. Tomka, D. E. Ashenford and B. Lunn. *Magnetic properties of $Cd_{1-x}Mn_xTe$ grown by molecular beam epitaxy*. Journal of Crystal Growth **138** (1-4), 900–904 (1994). ISSN 0022-0248. DOI http://dx.doi.org/10.1016/0022-0248(94)90928-8 40

[Say85] H. A. Sayad and S. M. Bhagat. *Dynamic random fields in diluted magnetic semiconductors: $Cd_{1-x}Mn_xTe$*. Physical Review B **31** (1), 591–593 (1985). ISSN 0163-1829. DOI http://dx.doi.org/10.1103/PhysRevB.31.591 83

[Sca88] D. Scalbert, J. Cernogora and C. Benoit a la Guillaume. *Spin-lattice relaxation in paramagnetic CdMnTe*. Solid State Communications **66** (6), 571–574 (1988). ISSN 0038-1098. DOI http://dx.doi.org/10.1016/0038-1098(88)90210-4 6, 82, 116

[Sca95] D. Scalbert. *Contribution of spins clusters to magnetization relaxation in $Cd_{1-x}Mn_xTe$*. Materials Science Forum **182-184**, 451–454 (1995). ISBN 0-87849-689-0. Joint Proceedings of the 3rd European Workshop on II-VI Compounds and the 4^{th} International Workshop on Semimagnetic (Diluted Magnetic) Semiconductors, both held in Linz, Austria, September 1994 119

[Sca96a] D. Scalbert. *Spin-lattice relaxation in diluted magnetic semiconductors*. Physica Status Solidi (B) - Basic Research **193** (1), 189–204 (1996). ISSN 0370-1972. DOI http://dx.doi.org/10.1002/pssb.2221930121 6, 36, 81, 82, 93, 115, 117, 118, 119, 156

[Sca96b] D. Scalbert, W. Farah and M. Nawrocki. *Transient photoreflectance as a probe of magnetic relaxation in semimagnetic semiconductors*. In *Proceedings of 23^{rd} International Conference on the Physics of Semiconductors*, edited by M. Scheffler and R. Zimmermann, volume 1, 433–436 (World Scientific, Singapore, 1996). ISBN 981-02-2777-9. Proc. of 23^{rd} International Conference on the Physics of Semiconductors, Berlin, Germany 1996 112, 114

[Sch66] J. R. Schrieffer and P. A. Wolff. *Relation between the Anderson and Kondo Hamiltonians*. Physical Review **149** (2), 491–492 (1966). ISSN 0031-899X. DOI http://dx.doi.org/10.1103/PhysRev.149.491 35

[Sch67] J. R. Schrieffer. *The Kondo effect - The link between magnetic and nonmagnetic impurities in metals?*. Journal of Applied Physics **38** (3), 1143–1150 (1967). ISSN 0021-8979. DOI http://dx.doi.org/10.1063/1.1709517 35

[Sch85] S. Schmitt-Rink, D. S. Chemla and D. A. B. Miller. *Theory of transient excitonic optical nonlinearities in semiconductor quantum-well structures*. Physical Review B **32**, 6601–6609 (1985). ISSN 0163-1829. DOI http://dx.doi.org/10.1103/PhysRevB.32.6601 122

[Sch89] S. Schmitt-Rink, D. S. Chemla and D. A. B. Miller. *Linear and nonlinear optical properties of semiconductor quantum wells*. Advances in Physics **38** (2), 89–188 (1989). ISSN 0001-8732. DOI http://dx.doi.org/10.1080/00018738900101102 121

[Sch93] M. Schubert and G. Weber. *Quantentheorie: Grundlagen und Anwendungen* (Spektrum Akademischer Verlag, Heidelberg-Berlin-Oxford, 1993). ISBN 3860253301 58

[Sch98a] M. E. Schlesinger. *The Mn-Se (manganese-selenium) system*. Journal of Phase Equilibria and Diffusion **19** (6), 588–590 (1998). ISSN 1547-7037. URL http://www.springerlink.com/content/lu3j13412p8p6j63 165

[Sch98b] M. E. Schlesinger. *The Mn-Te (manganese-tellurium) system*. Journal of Phase Equilibria and Diffusion **19** (6), 591–596 (1998). ISSN 1547-7037. URL http://www.springerlink.com/content/v3q51q801n844477 165

[Sch99] A. V. Scherbakov, A. V. Akimov, D. R. Yakovlev, W. Ossau, A. Waag, G. Landwehr, T. Wojtowicz, G. Karczewski and J. Kossut. *Heating of the spin system by nonequilibrium phonons in semimagnetic (Cd,Mn,Mg)Te quantum wells*. Physical Review B **60**, 5609–5616 (1999). ISSN 0163-1829. DOI http://dx.doi.org/10.1103/PhysRevB.60.5609 95, 102, 110

[Sch00a] A. V. Scherbakov, A. V. Akimov, D. R. Yakovlev, W. Ossau, G. Landwehr, T. Wojtowicz, G. Karczewski and J. Kossut. *Spin-lattice relaxation in semimagnetic CdMnTe/ CdMgTe quantum wells*. Physical Review B **62**, R10641 – R10644 (2000). ISSN 0163-1829. DOI http://dx.doi.org/10.1103/PhysRevB.62.R10641 6, 81, 82, 95, 103, 108, 115, 117, 118, 120, 136, 138, 139, 144, 156

[Sch00b] G. Schmidt, D. Ferrand, L. W. Molenkamp, A. T. Filip and B. J. van Wees. *Fundamental obstacle for electrical spin injection from a ferromagnetic metal into a diffu-*

sive semiconductor. Physical Review B **62**, R4790–R4793 (2000). ISSN 0163-1829. DOI http://dx.doi.org/10.1103/PhysRevB.62.R4790 3

[Sch01a] A. V. Scherbakov, A. V. Akimov, D. R. Yakovlev, W. Ossau, L. W. Molenkamp, S. Tatarenko and J. Cibert. *Spin-lattice relaxation in semimagnetic CdMnTe/ CdMgZnTe quantum wells with a two-dimensonal hole gas tuned by optical excitation*. Solid State Communications **120** (1), 17–20 (2001). ISSN 0038-1098. DOI http://dx.doi.org/10.1016/S0038-1098(01)00314-3 6, 121, 123, 130

[Sch01b] A. V. Scherbakov, D. R. Yakovlev, A. V. Akimov, I. A. Merkulov, B. König, W. Ossau, L. W. Molenkamp, T. Wojtowicz, G. Karczewski, G. Cywinski and J. Kossut. *Acceleration of the spin-lattice relaxation in diluted magnetic quantum wells in the presence of a two-dimensional electron gas*. Physical Review B **64** (15), 155205 (6pp.) (2001). ISSN 0163-1829. DOI http://dx.doi.org/10.1103/PhysRevB.64.155205 6, 121, 122, 123, 124, 125, 126, 130

[Sch04] A. V. Scherbakov, D. R. Yakovlev, A. V. Akimov, W. Ossau, L. W. Molenkamp, Y. Terai, S. Kuroda, K. Takita, I. Souma and Y. Oka. *Dynamics of localized Mn spins in diluted-magnetic-semiconductor nanostructures with quantum dots*. Physica Status Solidi (B) - Basic Research **241** (2), 361–369 (2004). ISSN 0370-1972. DOI http://dx.doi.org/10.1002/pssb.200301916 82, 83, 84, 139, 146

[Sch05] A. V. Scherbakov, A. V. Akimov, D. R. Yakovlev, W. Ossau, L. Hansen, A. Waag and L. W. Molenkamp. *Spin control in heteromagnetic nanostructures*. Applied Physics Letters **86**, 162104 (3pp.) (2005). ISSN 0003-6951. DOI http://dx.doi.org/10.1063/1.1906322 46, 82, 83, 84, 85, 120, 146, 148, 149, 156, 157

[Sha74] J. Shah, R. F. Leheny and W. F. Brinkman. *I_1 line shape as a temperature probe: The thermal relaxation of highly excited CdS*. Physical Review B **10**, 659–664 (1974). ISSN 0163-1829. DOI http://dx.doi.org/10.1103/PhysRevB.10.659 72, 92, 102, 108, 110

[Sha84] Y. Shapira, S. Foner, D. H. Ridgley, K. Dwight and A. Wold. *Technical saturation and magnetization steps in diluted magnetic semiconductors: Predictions and observations*. Physical Review B **30** (7), 4021–4023 (1984). ISSN 0163-1829. DOI http://dx.doi.org/10.1103/PhysRevB.30.4021 37

[Sha86] Y. Shapira, S. Foner, P. Becla, D. N. Domingues, M. J. Naughton and J. S. Brooks. *Nearest-neighbor exchange constant and Mn distribution in $Zn_{1-x}Mn_xTe$ from high-field magnetization step and low-field susceptibility*. Physical Review B **33** (1), 356–365 (1986). ISSN 0163-1829. DOI http://dx.doi.org/10.1103/PhysRevB.33.356 37

[Sha87] Y. Shapira and N. F. Oliveira. *High-field magnetization steps and the nearest-neighbor exchange constant in $Cd_{1-x}Mn_xS$, $Cd_{1-x}Mn_xTe$, and $Zn_{1-x}Mn_xSe$*. Physical Review B **35** (13), 688–6893 (1987). ISSN 0163-1829. DOI http://dx.doi.org/10.1103/PhysRevB.35.6888 37, 38

[Sha90] Y. Shapira. *Magnetization steps in dilute magnetic semiconductors (invited)*. Journal of Applied Physics **67** (9), 5090–5095 (1990). ISSN 0021-8979. DOI http://dx.doi.org/10.1063/1.344682 41

[Sha93] L. J. Sham. *Spin relaxation in semiconductor quantum wells*. Journal of Physics: Condensed Matter **5**, A51–A60 (1993). ISSN 0953-8984. DOI http://dx.doi.org/10.1088/0953-8984/5/33A/005 76

[Shi66] M. Shinada and S. Sugano. *Interband optical transitions in extremely anisotropic semiconductors. I. bound and unbound exciton absorption*. Journal of the Physical Society of Japan (JPSJ) **21** (10), 1936–1946 (1966). ISSN 0031-9015. DOI http://dx.doi.org/10.1143/JPSJ.21.1936 63, 66

[Sin80] S. Singh and P. Singh. *The role of some physical parameters on the magnetic susceptibility of group II-VI semiconducting compounds*. Journal of Physics and Chemistry of Solids **41** (2), 135–140 (1980). ISSN 0022-3697. DOI http://dx.doi.org/10.1016/0022-3697(80)90044-X 164

[Sla60] G. A. Slack. *Crystallography and domain walls in antiferromagnetic NiO crystals*. Journal of Applied Physics **31** (9), 1571–1582 (1960). ISSN 0021-8979. DOI http://dx.doi.org/10.1063/1.1735895 29

[Sli89] C. P. Slichter. *Principles of magnetic resonance*, volume 1 of *Solid-state sciences*. 3. edition (Springer, Berlin, Heidelberg, New York, 1989). ISBN 3540501576 79

[Slo06] T. Slobodskyy. *Semimagnetic heterostructures for spintronics*. PhD thesis, Universität Würzburg, Würzburg (2006) 19, 165

[Smi65] P. L. Smith and J. E. Martin. *The high-pressure structures of zinc sulphide and zinc selenide*. Physical Review Letters **19** (7), 541–543 (1965). ISSN 0031-9007. DOI http://dx.doi.org/10.1016/0031-9163(65)90766-3 164

[Sob81] V. V. Sobolev, O. G. Maksimova and S. G. Kroitoru. *Reflectivity spectra and band structure of the ZnTe-CdTe system*. Physica Status Solidi (B) - Basic Research **103** (2), 499–509 (1981). ISSN 0370-1972. DOI http://dx.doi.org/10.1002/pssb.2221030206 164

[Som93] D. Some and A. V. Nurmikko. *Hot-exciton luminescence and energy transfer into d-electron states in $Zn_{1-x}Mn_xSe$*. Physical Review B **48** (7), 4418–4422 (1993). ISSN 0163-1829. DOI http://dx.doi.org/10.1103/PhysRevB.48.4418 92, 120

[Son76] U. Sondermann. *Magnetic investigations on solid solutions of the quasi binary alloy systems (Cd Te)$_{1-x}$ (Mn Te)$_x$ and (Sn Te)$_{1-x}$ (Mn Te)$_x$*. Journal of Magnetism and Magnetic Materials **2** (1-3), 216–222 (1976). ISSN 0304-8853. DOI http://dx.doi.org/10.1016/0304-8853(75)90125-0 40

[Son77a] M. Sondergeld. *Two-photon absorption by envelope-hole coupled exciton states in cubic ZnSe. I. Energy spectrum of the hd term and valence-band parameters*. Physica Status Solidi (B) - Basic Research **81** (1), 253–262 (1977). ISSN 0370-1972. DOI http://dx.doi.org/10.1002/pssb.2220810127 164

[Son77b] U. Sondermann and E. Vogt. *Magnetic behaviour of magnese in tellurides of BII and BIV elements*. Journal of Magnetism and Magnetic Materials **6**, 223–225 (1977). ISSN 0304-8853. DOI http://dx.doi.org/10.1016/0304-8853(77)90115-9 40

[Soo79] L. Soonckindt, D. Etienne, J. P. Marchand and L. Lassabatere. *The composition and temperature dependences of the fundamental band gap in ZnS_xSe_{1-x} alloys*. Surface Science **86**, 378–383 (1979). ISSN 0039-6028. DOI http://dx.doi.org/10.1016/0039-6028(79)90416-3 164

[Spa85] J. Spałek. *Kinetics of the bound magnetic polaron and the decay rate of thermodynamic fluctuation*. Physical Review B **32** (6), 3900–3903 (1985). ISSN 0163-1829. DOI http://dx.doi.org/10.1103/PhysRevB.32.3900 67

[Spa86] J. Spałek, A. Lewicki, Z. Tarnawski, J. K. Furdyna, R. R. Gałązka and Z. Obuszko. *Magnetic susceptibility of semimagnetic semiconductors: The high-temperature regime and the role of superexchange*. Physical Review B **33** (5), 3407–3418 (1986). ISSN 0163-1829. DOI http://dx.doi.org/10.1103/PhysRevB.33.3407 39, 40

[Ste53] K. W. H. Stevens. *A note on exchange interactions*. Reviews of Modern Physics **25** (1), 166 (1953). ISSN 0034-6861. DOI http://dx.doi.org/10.1103/RevModPhys.25.166 36

[Ste88] O. Stern. *Ein Weg zur experimentellen Prüfung der Richtungsquantelung im Magnetfeld*. Zeitschrift für Physik D: Atoms, Molecules and Clusters **10** (2-3), 111–113 (1988). ISSN 0178-7683. DOI http://dx.doi.org/10.1007/BF01384841. Aus: Zeitschrift für Physik, Bd. VII, S. 249-253 (1921) 1

[Ste98] A. Steane. *Quantum computing*. Reports on Progress in Physics **61** (2), 117–173 (1998). ISSN 0034-4885. DOI http://dx.doi.org/10.1088/0034-4885/61/2/002 3

[Sto94] G. J. Stoney. *Of the "Electron", or Atom of Electricity*. Philosophical Magazine **38**, 418–420 (1894). Series 5 1

[Sto95] G. J. Stoney. Philosophical Magazine **40**, 372 (1895). Series 5 1

[Sto91] M. Stoehr, F. Hamdani, J. P. Lascaray and M. Maurin. *Reflectivity studies of the strain dependence on E_0 and $E_0+\Delta_0$ excitonic transitions in ZnSe/GaAs*. Physical Review B **44** (16), 8912–8917 (1991). ISSN 0163-1829. DOI http://dx.doi.org/10.1103/PhysRevB.44.8912 164

[Sto96] T. Story, C. H. W. Swüste, P. J. T. Eggenkamp, H. J. M. Swagten and W. J. M. de Jonge. *Electron paramagnetic resonance knight shift in semimagnetic (diluted magnetic) semiconductors*. Physical Review Letters **77** (13), 2802–2805 (1996). ISSN 0031-9007. DOI http://dx.doi.org/10.1103/PhysRevLett.77.2802 121

[Stö04] H. Stöcker. *Taschenbuch der Physik*. 5. edition (Harri Deutsch, Frankfurt, 2004). ISBN 3817117205 26

[Str90] T. Strutz, A. M. Witowski, R. E. M. de Bekker and P. Wyder. *Pick-up coil as a tool of measuring spin-lattice relaxation under electron spin resonance condition at high magnetic fields*. Applied Physics Letters **57** (8), 831–833 (1990). ISSN 0003-6951. DOI http://dx.doi.org/10.1063/1.103404 6, 92, 95, 116

[Str92] T. Strutz, A. M. Witowski and P. Wyder. *Spin-lattice relaxation at high magnetic fields*. Physical Review Letters **68**, 3912–3915 (1992). ISSN 0031-9007. DOI http://dx.doi.org/10.1103/PhysRevLett.68.3912 6, 82, 92, 95, 115, 116, 119, 124

[Sug70] S. Sugano. *Multiplets of transition-metal ions in crystals* (Academic Press, New York, 1970). ISBN 0126760500 23, 24

[Sun85] T. Suntola and J. Hyvarinen. *Atomic layer epitaxy*. Annual Review of Materials Science **15**, 177–195 (1985). ISSN 0084-6600 46

[Sur05] R. A. Suris (2005). Private communication with D. R. Yakovlev and A. A. Maksimov 147

[Tan54] Y. Tanabe and S. Sugano. *On the absorption spectra of complex ions. I*. Journal of the Physical Society of Japan (JPSJ) **9** (5), 753–766 (1954). ISSN 0031-9015. URL http://www.journalarchive.jst.go.jp/english/jnlabstract_en.php?cdjournal=jpsj1946&cdvol=9&noissue=5&startpage=753 23

[Tan86] M. Taniguchi, L. Ley, R. L. Johnson, J. Ghijsen and M. Cardona. *Synchrotron radiation study of $Cd_{1-x}Mn_xTe$ ($0 \leq x \leq 0.65$)*. Physical Review B **33** (2), 1206–1212 (1986). ISSN 0163-1829. DOI http://dx.doi.org/10.1103/PhysRevB.33.1206 20

[Tao82] R. Y. Tao, M. M. Moriwaki, W. M. Becker and R. R. Gałązka. *Comparison of excitation spectra of 1.2- and 2.0-eV photoluminescence bands in $Cd_{1-x}Mn_xTe$ for* $0.4 < x \leq 0.7$. Journal of Applied Physics **53** (5), 3772–3776 (1982). ISSN 0021-8979. DOI http://dx.doi.org/10.1063/1.331117 20, 23

[Teh00] S. Tehrani, B. Engel, J. M. Slaughter, E. Chen, M. DeHerrera, M. Durlam, P. Naji, R. Whig, J. Janesky and J. Calder. *Recent developments in magnetic tunnel junction MRAM*. IEEE Transactions on Magnetics **36** (5 (1)), 2752–2757 (2000). ISSN 0018-9464. DOI http://dx.doi.org/10.1109/20.908581 2

[Ter99] R. Terauchi, Y. Ohno, T. Adachi, A. Sato, F. Matsukura, A. Tackeuchi and H. Ohno. *Carrier mobility dependence of electron spin relaxation in GaAs quantum wells*. Japanese Journal of Applied Physics (JJAP) **38**, 2549–2551 (1999). ISSN 0021-4922. DOI http://dx.doi.org/10.1143/JJAP.38.2549 78

[Ter01] F. J. Teran Garcinuño. *Spin dependent phenomena in n-type modulation doped CdMnTe quantum well structures*. PhD thesis, Grenoble High Magnetic Field Laboratory, Grenoble (2001) 48, 53

[Tho97] J. J. Thomson. Philosophical Magazine **44**, 293 (1897). Series 5 1

[Tho04] J. J. Thomson. *On the structure of the atom: An investigation of the stability and periods of oscillation of a number of corpuscles arranged at equal intervals around the circumference of a circle; with application of the results to the theory of atomic structure*. Philosophical Magazine **7** (39), 237–265 (1904). Series 6 1

[Tho67] A. G. Thompson and J. C. Woolley. *Energy-gap variation in mixed III-V alloys*. Canadian Journal of Physics **45** (2), 255–261 (1967). ISSN 0008-4204. URL http://pubs.nrc-cnrc.gc.ca/cgi-bin/rp/rp2_abst_e?cjp_p67-026_45_ns_nf_cjp 19

[Ton98] M. Tondra, J. M. Daughton, D. Wang, R. S. Beech, A. Fink and J. A. Taylor. *Picotesla field sensor design using spin-dependent tunneling devices*. Journal of Applied Physics **83**, 6688–6690 (1998). ISSN 0021-8979. DOI http://dx.doi.org/10.1063/1.367861 2

[Tor56] H. C. Torrey. *Bloch equations with diffusion terms*. Physical Review **104**, 563–565 (1956). ISSN 0031-899X. DOI http://dx.doi.org/10.1103/PhysRev.104.563 70

[Tou96] E. Tournié, C. Morhain, G. Neu, M. Laügt, C. Ongaretto, J.-P. Faurie, R. Triboulet and J. O. Ndap. *Structural and optical characterization of ZnSe single crystals grown by solid-phase recrystallization*. Journal of Applied Physics **80** (5), 2983–2989 (1996). ISSN 0021-8979. DOI http://dx.doi.org/10.1063/1.363155 164

[Tre75] H.-R. Trebin and U. Rössler. *Polarons in the degenerate-band case*. Physica Status Solidi (B) - Basic Research **70** (2), 717–726 (1975). ISSN 0370-1972. DOI http://dx.doi.org/10.1002/pssb.2220700232 165

[Tsa94] C. Tsang, R. E. Fontana, T. Lin, D. E. Heim, V. S. Speriosu, B. A. Gurney and M. L. Williams. *Design, fabrication and testing of spin-valve read heads for highdensity recording*. IEEE Transactions on Magnetics **30** (6 (1-2)), 3801–3806 (1994). ISSN 0018-9464. DOI http://dx.doi.org/10.1109/20.333909 2

[Twa83] A. Twardowski, T. Dietl and M. Demianiuk. *The study of the s-d type exchange interaction in ZnMnSe mixed-crystals*. Solid State Communications **48** (10), 845–848 (1983). ISSN 0038-1098. DOI http://dx.doi.org/10.1016/0038-1098(83)90130-8 22

[Twa84] A. Twardowski, M. von Ortenberg, M. Demianiuk and R. Pauthenet. *Magnetization and exchange constants in $Zn_{1-x}Mn_xSe$*. Solid State Communications **51** (11), 849–852 (1984). ISSN 0038-1098. DOI http://dx.doi.org/10.1016/0038-1098(84)91085-8 165

[Twa86] A. Twardowski, C. J. M. Denissen, W. J. M. de Jonge, A. T. A. M. de Waele, M. Demianiuk and R. Triboulet. *Spinglass behaviour of $Zn_{1-x}Mn_xSe$ and $Zn_{1-x}Mn_xTe$ semimagnetic semiconductors*. Solid State Communications **59** (4), 199–203 (1986). ISSN 0038-1098. DOI http://dx.doi.org/10.1016/0038-1098(86)90579-X 40

[Tya97] M. G. Tyazhlov, A. I. Filin, A. V. Larionov, V. D. Kulakovskii, D. R. Yakovlev, A. Waag and G. Landwehr. *Spin relaxation of Mn ions in (CdMn)Te/(CdMg)Te quantum wells under picosecond optical pumping*. Journal of Experimental and Theoretical Physics (JETP) **85** (4), 784–796 (1997). ISSN 1063-7761. DOI http://dx.doi.org/10.1134/1.558366. Translation of: Pis'ma v Zhurnal Eksperimental'noy i Teoreticheskoy Fizika, USSR **112**(4), 1440-1463 (1997) 71, 93, 114

[Tya99] M. G. Tyazhlov, V. D. Kulakovskii, A. I. Filin, D. R. Yakovlev, A. Waag and G. Landwehr. *Mn spin domains in highly photoexcited (Cd,Mn)Te/(Cd,Mg)Te quantum wells*. Physical Review B **59**, 2050–2056 (1999). ISSN 0163-1829. DOI http://dx.doi.org/10.1103/PhysRevB.59.2050 93, 114

[Uhl25] G. E. Uhlenbeck and S. Goudsmit. *Ersetzung der Hypothese vom unmechanischen Zwang durch eine Forderung bezüglich des inneren Verhaltens jedes einzelnen Elektrons*. Naturwissenschaften **47**, 953–954 (1925). ISSN 0028-1042 1

[Uhl26] G. E. Uhlenbeck and S. Goudsmit. *Spinning electrons and the structure of spectra*. Nature **177**, 264–265 (1926) 1

[Veg21] L. Vegard. *Die Konstitution der Mischkristalle und die Raumfüllung der Atome*. Zeitschrift für Physik A: Hadrons and Nuclei **5** (1), 17–26 (1921). ISSN 0939-7922. DOI http://dx.doi.org/10.1007/BF01349680 12

[Ven79] H. Venghaus. *Valence-band parameters and g factors of cubic zinc selenide derived from free-exciton magnetoreflectance*. Physical Review B **19**, 3071–3082 (1979). ISSN 0163-1829. DOI http://dx.doi.org/10.1103/PhysRevB.19.3071 164

[Vle40] J. H. van Vleck. *Paramagnetic relaxation times for titanium and chrome alum*. Physical Review **57**, 426–447 (1940). ISSN 0031-899X. DOI http://dx.doi.org/10.1103/PhysRev.57.426 117

[Wal32] I. Waller. *Über die Magnetisierung von paramagnetischen Kristallen in Wechselfeldern*. Zeitschrift für Physik A: Hadrons and Nuclei **79** (5-6), 370–388 (1932). ISSN 0939-7922. DOI http://dx.doi.org/10.1007/BF01349398 116

[Wal89] A. Wall, A. Franciosi, Y. Gao, J. H. Weaver, M.-H. Tsai, J. D. Dow and R. V. Kasowski. *Inverse photoemission and resonant photoemission characterization of semimagnetic semiconductors*. Journal of Vacuum Science and Technology A **7** (3), 656–662 (1989). ISSN 0734-2101. DOI http://dx.doi.org/10.1116/1.575861 20

[Wan53] R. K. Wangsness and F. Bloch. *The dynamical theory of nuclear induction*. Physical Review **89**, 728–739 (1953). ISSN 0031-899X. DOI http://dx.doi.org/10.1103/PhysRev.89.728 70

[Wan90] X. Wang, D. Heiman, S. Foner and P. Becla. *Magnetic-ion triplet clusters and nonnearest-neighbor exchange effect in (Cd,Mn)Te*. Physical Review B **41** (2), 1135–1139 (1990). ISSN 0163-1829. DOI http://dx.doi.org/10.1103/PhysRevB.41.1135 39

[Wan92] X. Wang, M. Dahl, D. Heiman, P. A. Wolff and P. Becla. *Spin-lattice relaxation of spin pairs in CdSe:Mn by the Dzyaloshinski-Moriya exchange interaction*. Physical Review B **46**, 11216–11219 (1992). ISSN 0163-1829. DOI http://dx.doi.org/10.1103/PhysRevB.46.11216 118, 119

[War85] J. Warnock, A. Petrou, R. N. Bicknell, N. C. Giles-Taylor, D. K. Blanks and J. F. Schetzina. *Photoluminescence of $Cd_{1-x}Mn_x$Te-CdTe multiple-quantum-well structures and superlattices in a magnetic field*. Physical Review B **32** (12), 8116–8125 (1985). ISSN 0163-1829. DOI http://dx.doi.org/10.1103/PhysRevB.32.8116 59, 64

[Web81] C. Webb, M. Kaminska, M. Lichtensteiger and J. Lagowski. *Valence band states of semi-magnetic semiconductors: $Cd_{1-x}Mn_x$Te*. Solid State Communications **40** (5), 609–611 (1981). ISSN 0038-1098. DOI http://dx.doi.org/10.1016/0038-1098(81)90586-X 20

[Wei07] P. Weiss. *L'hypothèse du champ moléculaire et la propriété ferromagnétique*. Journal de Physique Théorique and Appliquée **6** (1), 661–690 (1907). URL http://jphystap.journaldephysique.org/index.php?option=toc&url=/articles/jphystap/abs/1907/01/contents/contents.html 24, 28

[Wei86] S.-H. Wei and A. Zunger. *Alloy-stabilized semiconducting and magnetic zinc-blende phase of MnTe*. Physical Review Letters **56** (22), 2391–2394 (1986). ISSN 0031-9007. DOI http://dx.doi.org/10.1103/PhysRevLett.56.2391 19

[Wei87] S.-H. Wei and A. Zunger. *Total-energy and band-structure calculations for the semimagnetic $Cd_{1-x}Mn_xTe$ semiconductor alloy and its binary constituents*. Physical Review B **35** (5), 2340–2365 (1987). ISSN 0163-1829. DOI http://dx.doi.org/10.1103/PhysRevB.35.2340 19

[Wei91] C. Weisbuch and B. Vinter. *Quantum semiconductor structures: Fundamentals and applications* (Academic Press, San Diego, 1991). ISBN 0127426809 49, 64

[Wie97] E. Wiechert. Schriften der Königsberger Gesellschaft **38** (1897) 1

[Wil99] K. Wilmers, T. Wethkamp, N. Esser, C. Cobet, W. Richter, M. Cardona, V. Wagner, H. Lugauer, F. Fischer, T. Gerhard and M. Keim. *Ellipsometric studies of $Be_xZn_{1-x}Se$ between 3 eV and 25 eV*. Physical Review B **59**, 10071–10075 (1999). ISSN 0163-1829. DOI http://dx.doi.org/10.1103/PhysRevB.59.10071 164

[Win03] R. Winkler. *Spin orbit coupling effects in two-dimensional electron and hole systems*, volume 191 of *Springer tracts in modern physics* (Springer, Berlin, 2003). ISBN 3540011870 15, 50

[Win04] R. Winkler and M. Oestreich. *Spinelektronik - Das Potenzial des Elektronenspins in der Halbleiterelektronik*. Physik Journal **11**, 39–44 (2004). ISSN 1617-9439 2, 5

[Wit95] A. M. Witowski, T. Strutz, Ch. Kutter and P. Wyder. *Magnetization and spin-lattice relaxation in semimagnetic semiconductors at high magnetic fields*. Physica B: Condensed Matter **211**, 372–377 (1995). ISSN 0921-4526. DOI http://dx.doi.org/10.1016/0921-4526(94)01067-B 118, 119

[Woj79] R. Wojtal, A. Golnik and J. A. Gaj. *Acceptor photoionization and light-to-heavy hole absorption in $Cd_{1-x}Mn_xTe$*. Physica Status Solidi (B) - Basic Research **92** (1), 241–247 (1979). ISSN 0370-1972. DOI http://dx.doi.org/10.1002/pssb.2220920127 17

[Woj95] T. Wojtowicz, G. Karczewski, A. Zakrzewski, M. Kutrowski, E. Janik, E. Dynowska, K. Kopalko, S. Kret, J. Kossut and J. Y. Laval. *Digital magnetic quantum wells for*

the study of interface sharpness of molecular beam epitaxy grown structures. Acta Physica Polonica A **87**, 165–168 (1995). ISSN 0587-4246 135, 162

[Woj96] T. Wojtowicz, M. Kutrowski, G. Cywinski, E. Dynowska, G. Karczewski, J. Kossut, R. Fiederling, G. Mackh, U. Zehnder and W. Ossau. *$Cd_{1-x}Mn_xTe$ parabolic quantum wells*. Acta Physica Polonica A **90** (6), 997 (1996). ISSN 0587-4246 140

[Woj98] T. Wojtowicz, M. Kutrowski, G. Cywinski, G. Karczewski, E. Janik, E. Dynowska, J. Kossut, R. Fiederling, A. Pfeuffer-Jeschke and W. Ossau. *Excitons in $Cd_{1-x}Mn_xTe$ quantum wells with a parabolic confining potential*. Journal of Crystal Growth **184**, 936–941 (1998). ISSN 0022-0248. DOI http://dx.doi.org/10.1016/S0022-0248(98)80195-4 135

[Wój00] A. Wójs, J. J. Quinn and P. Hawrylak. *Charged excitons in a dilute two-dimensional electron gas in a high magnetic field*. Physical Review B **62**, 4630–4637 (2000). ISSN 0163-1829. DOI http://dx.doi.org/10.1103/PhysRevB.62.4630 66

[Wol95] D. Wolverson, S. V. Railson, M. P. Halsall, J. J. Davies, D. E. Ashenford and B. Lunn. *Selective excitation of spin-flip Raman scattering from electrons bound to donors in semiconductor quantum well structures*. Semiconductor Science and Technology **10**, 1475–1483 (1995). ISSN 0268-1242. DOI http://dx.doi.org/10.1088/0268-1242/10/11/008 71

[Wol01] S. A. Wolf, D. D. Awschalom, R. A. Buhrman, J. M. Daughton, S. von Molnár, M. L. Roukes, A. Y. Chtchelkanova and D. M. Treger. *Spintronics: a spin-based electronics vision for the future*. Science **294**, 1488–1495 (2001). ISSN 0036-8075. DOI http://dx.doi.org/10.1126/science.1065389 2, 3, 6

[Wör97] M. Wörz, E. Griebl, T. Reisinger, R. Flierl, B. Haserer, T. Semmler, T. Frey and W. Gebhardt. *Gap energies, exciton binding energies and band offsets in ternary ZnMgSe compounds and ZnSe/ZnMgSe heterostructures*. Physica Status Solidi (B) - Basic Research **202**, 805–816 (1997). ISSN 0370-1972. DOI http://dx.doi.org/10.1002/1521-3951(199708)202:2⟨805::AID-PSSB805⟩3.0.CO;2-O 16, 164

[Wu86] J.-W. Wu, A. V. Nurmikko and J. J. Quinn. *Magnetic polaron effects in $CdTe/Cd_{1-x}Mn_xTe$ quantum well systems*. Solid State Communications **57** (11), 853–856 (1986). ISSN 0038-1098. DOI http://dx.doi.org/10.1016/0038-1098(86)90165-151

[Wyc63] R. W. G. Wyckoff. *Crystal structures*. 2. edition (Interscience Publ., New York, 1963). ISBN 0470968605 11, 164

[Yaf63] Y. Yafet. *g factors and spin-lattice relaxation of conduction electrons*. In *Advances in research and applications*, edited by F. Seitz and D. Turnbull, volume 14 of *Solid state physics*, 1. edition, 2 (Academic Press, 1963). ISBN 0126077142 78

[Yak95] D. R. Yakovlev, G. Mackh, B. Kuhn-Heinrich, W. Ossau, A. Waag, G. Landwehr, R. Hellmann and E. O. Göbel. *Exciton magnetic polarons in short-period CdTe/ $Cd_{1-x}Mn_xTe$ superlattices*. Physical Review B **52**, 12033–12038 (1995). ISSN 0163-1829. DOI http://dx.doi.org/10.1103/PhysRevB.52.12033 41

[Yak96] D. R. Yakovlev and K. V. Kavokin. *Exciton magnetic polarons in semimagnetic quantum wells and superlattices*. Comments Condensed Matter Physics **18**, 51–81 (1996). ISSN 0885-4483 91

[Yak97] D. R. Yakovlev, K. V. Kavokin, I. A. Merkulov, G. Mackh, W. Ossau, R. Hellmann, E. O. Göbel, A. Waag and G. Landwehr. *Picosecond dynamics of magnetic polarons governed by energy transfer to the Zeeman reservoir*. Physical Review B **56**, 9782–9788 (1997). ISSN 0163-1829. DOI http://dx.doi.org/10.1103/PhysRevB.56.9782 91

[Yak98] D. R. Yakovlev. *Exciton magnetic polarons in diluted magnetic semiconductor heterostructures*. habilthesis, A.F. Ioffe Physico-Technical Initute, St. Petersburg, Russia (1998). In Russian 40

[Yak00] D. R. Yakovlev, J. Puls, G. V. Mikhailov, G. V. Astakhov, V. P. Kochereshko, W. Ossau, J. Nürnberger, W. Faschinger, F. Henneberger and G. Landwehr. *Charged exciton dynamics in ZnSe/ZnMgSSe QWs*. Physica Status Solidi (A) - Applied Research **178**, 501–505 (2000). ISSN 0031-8965. DOI http://dx.doi.org/10.1002/1521-396X(200003)178:1⟨501::AID-PSSA501⟩3.0.CO;2-D 97

[Yak01] D. R. Yakovlev, C. Sas, B. König, L. Hansen, W. Ossau, G. Landwehr, L. W. Molenkamp and A. Waag. *Magnetoluminescence of Zn(Mn)Se/Be(Mn)Te semimagnetic heterostructures with a type-II band alignment*. Applied Physics Letters **78** (13), 1870–1872 (2001). ISSN 0003-6951. DOI http://dx.doi.org/10.1063/1.1357446 84

[Yak02] D. R. Yakovlev, A. V. Platonov, E. L. Ivchenko, V. P. Kochereshko, C. Sas, W. Ossau, L. Hansen, A. Waag, G. Landwehr and L. W. Molenkamp. *Hidden in-plane anisotropy of interfaces in Zn(Mn)Se/BeTe quantum wells with a type-II band alignment*. Physical Review Letters **88** (25), 257401 (4pp.) (2002). ISSN 0031-9007. DOI http://dx.doi.org/10.1103/PhysRevLett.88.257401 84

[Yak04] D. R. Yakovlev, M. Kneip, A. A. Maksimov, I. I. Tartakovskiĭ, M. Bayer, D. Keller, W. Ossau, L. W. Molenkamp, A. V. Scherbakov, A. V. Akimov and A. Waag. *Spin and*

energy transfer between magnetic ions and free carriers in diluted-magnetic semiconductor heterostructures. Physica Status Solidi (C) - Current Topics on Solid State Physics **1**, 989–882 (2004). ISSN 1610-1634. DOI http://dx.doi.org/10.1002/pssc.200304288 71, 82, 93, 121, 156

[Yak05] D. R. Yakovlev, M. Kneip, M. Bayer, A. A. Maksimov, I. I. Tartakovskiĭ, A. V. Scherbakov, A. V. Akimov, D. Keller, W. Ossau, L. W. Molenkamp and A. Waag. *Spin dynamics of Mn-ion system in diluted-magnetic-semiconductor heterostructures based on ZnMnSe*. In *American Institute of Physics Conference Proceedings 772: Physics of Semiconductors*, edited by J. Menendez and C. G. Van de Walle, 1301–1302 (American Institute of Physics, 2005). ISSN 0094-243X. DOI http://dx.doi.org/10.1063/1.1994589. 27^{th} International Conference on the Physics of Semiconductors - ICPS-27, Flagstaff, USA 2004 93

[Yak07] D. R. Yakovlev. *Dynamics of spin interactions in diluted magnetic semiconductor heterostructures*. Physica Status Solidi (A) - Applied Research **1**, 179–185 (2007). ISSN 0031-8965. DOI http://dx.doi.org/10.1002/pssa.200673024 73

[Yak09] D. R. Yakovlev and I. A. Merkulov. *Spin and energy transfer between carriers, magnetic ions and lattice*. In Kossut and Gaj [Kos09], chapter 9. (Planned for 2009) 5, 67, 68, 69, 72, 73, 74, 90, 94, 120

[Yeh92] C.-Y. Yeh, Z. W. Lu, S. Froyen and A. Zunger. *Zinc-blende-wurtzite polytypism in semiconductors*. Physical Review B **46** (16), 10086–10097 (1992). ISSN 0163-1829. DOI http://dx.doi.org/10.1103/PhysRevB.46.10086 11, 164

[Yim72] W. M. Yim, J. P. Dismukes, E. J. Stofko and R. J. Paff. *Synthesis and some properties of BeTe, BeSe and BeS*. Journal of Physics and Chemistry of Solids **33** (2), 501–505 (1972). ISSN 0022-3697. DOI http://dx.doi.org/10.1016/0022-3697(72)90032-7 164

[Yod85] D. R. Yoder-Short, U. Debska and J. K. Furdyna. *Lattice parameters of $Zn_{1-x}Mn_xSe$ and tetrahedral bond lengths in $A^{II}_{1-x}Mn_xB^{VI}$ alloys*. Journal of Applied Physics **58** (11), 4056–4060 (1985). ISSN 0021-8979. DOI http://dx.doi.org/10.1063/1.335585 13, 19, 165

[Yos57] K. Yosida. *Magnetic properties of Cu-Mn alloys*. Physical Review **106** (5), 893–898 (1957). ISSN 0031-899X. DOI http://dx.doi.org/10.1103/PhysRev.106.893 37

[Yu92] S.-S. Yu and V.-C. Lee. *Indirect exchange interaction in diluted magnetic semiconductors*. Journal of Physics: Condensed Matter **4** (11), 2961–2975 (1992). ISSN 0953-8984. DOI http://dx.doi.org/10.1088/0953-8984/4/11/021 39

[Yu95] W. Y. Yu, A. Twardowski, L. P. Fu, A. Petrou and B. T. Jonker. *Magnetoanisotropy in $Zn_{1-x}Mn_xSe$ strained epilayers*. Physical Review B **51**, 9722–9727 (1995). ISSN 0163-1829. DOI http://dx.doi.org/10.1103/PhysRevB.51.9722 41, 42

[Yu05] P. Y. Yu and M. Cardona. *Fundamentals of semiconductors - Physics and materials properties*. 3. edition (Springer, Berlin, 2005). ISBN 3540254706 49

[Yue93] W.-P. Yuen. *Exact analytic analysis of finite parabolic quantum wells with and without a static electric field*. Physical Review B **48**, 17316–17320 (1993). ISSN 0163-1829. DOI http://dx.doi.org/10.1103/PhysRevB.48.17316 58

[Zac27] W. Zachariasen. Zeitschrift für Physikalische Chemie **128**, 417 (1927). ISSN 0942-9352 11, 164

[Zak95] A. K. Zakrewski, E. Janik, E. Dynowska, M. Leszczynski, M. Kutrowski, T. Wojtowicz, G. Karczewski, J. Bak-Misiuk, J. Domagala and J. Kossut. Acta Physica Polonica A **87**, 443 (1995). ISSN 0587-4246 11

[Zay87] J. J. Zayhowski, R. N. Kershaw, D. Ridgley, K. Dwight, A. Wold, R. R. Gałązka and W. Giriat. *Dynamics of magnetic-polaron formation in $Cd_{1-x}Mn_xSe$ and $Cd_{1-x}Mn_xTe$*. Physical Review B **35** (13), 6950–6955 (1987). ISSN 0163-1829. DOI http://dx.doi.org/10.1103/PhysRevB.35.6950 67

[Zee97] P. Zeeman. *The effect of magnetisation on the nature of light emitted by a substance*. Nature **55**, 347 (1897). ISSN 0028-0836. URL http://www.nature.com/nature/journal/v55/n1424/pdf/055347a0.pdf 30

[Zeh98] U. Zehnder. *Magnetooptische Untersuchungen an neuartigen und semimagnetischen II-VI-Halbleiter-Heterostrukturen*. PhD thesis, Universität Würzburg, Würzburg (1998) 41, 56

[Zen51] C. Zener. *Interaction between the d-shells in the transition metals. II. Ferromagnetic compounds of manganese with perovskite structure*. Physical Review **82** (3), 403–405 (1951). ISSN 0031-899X. DOI http://dx.doi.org/10.1103/PhysRev.82.403 37

[Zha85a] X.-C. Zhang, S.-K. Chang, A. V. Nurmikko, D. Heiman, L. A. Kolodziejski, R. L. Gunshor and S. Datta. *Influence of high magnetic fields on exciton luminescence of $Cd_{1-x}Mn_xTe$ multiquantum wells*. Solid State Communications **56** (3), 255–259 (1985). ISSN 0038-1098. DOI http://dx.doi.org/10.1016/0038-1098(85)91006-3 51

[Zha85b] X.-C. Zhang, S.-K. Chang, A. V. Nurmikko, L. A. Kolodziejski, R. L. Gunshor and S. Datta. *Interface localization of excitons in CdTe/$Cd_{1-x}Mn_x$Te multiple quantum wells*. Physical Review B **31** (6), 4056–4059 (1985). ISSN 0163-1829. DOI http://dx.doi.org/10.1103/PhysRevB.31.4056 51, 52

[Zha85c] X.-C. Zhang, S.-K. Chang, A. V. Nurmikko, L. A. Kolodziejski, R. L. Gunshor and S. Datta. *Time-resolved exciton recombination in CdTe/$Cd_{1-x}Mn_xTe$ multiple quantum wells*. Applied Physics Letters **47** (1), 59–61 (1985). ISSN 0003-6951. DOI http://dx.doi.org/10.1063/1.96404 51

[Zha86] X.-C. Zhang, Y. Hefetz, S.-K. Chang, J. Nakahara, A. V. Nurmikko, L. A. Kolodziejski, R. L. Gunshor and S. Datta. *Excitons and their kinetics in CdTe/(Cd, Mn)Te and ZnSe/(Zn, Mn)Se quantum wells*. Surface Science **174** (1-3), 292–292 (1986). ISSN 0039-6028. DOI http://dx.doi.org/10.1016/0039-6028(86)90424-3 52

[Zha94] Y.-H. Zhang and D. H. Chow. *Improved crystalline quality of $AlAs_xSb_{1-x}$ grown on InAs by modulated molecular-beam epitaxy*. Applied Physics Letters **65** (25), 3239–3241 (1994). ISSN 0003-6951. DOI http://dx.doi.org/10.1063/1.112424 162

[Zha95] Y.-H. Zhang. *Accurate control of As and Sb incorporation ratio during solid-source molecular-beam epitaxy*. Journal of Crystal Growth **150** (2), 838–843 (1995). ISSN 0022-0248. DOI http://dx.doi.org/10.1016/0022-0248(95)80057-J 162

[Zhu06] E. A. Zhukov, D. R. Yakovlev, M. Bayer, G. Karczewski, T. Wojtowicz and J. Kossut. *Spin coherence of two-dimensional electron gas in CdTe/(Cd,Mg)Te quantum wells*. Physica Status Solidi (B) - Basic Research **243**, 878–881 (2006). ISSN 0370-1972. DOI http://dx.doi.org/10.1002/pssb.200564604 73

[Žut04] I. Žutić, J. Fabian and S. Das Sarma. *Spintronics: fundamentals and applications*. Reviews of Modern Physics **76** (2), 323–410 (2004). ISSN 0034-6861. DOI http://dx.doi.org/10.1103/RevModPhys.76.323 2, 3, 5, 70, 71, 76, 78, 79, 87

Index

Symbols and Abbreviations

General

CB	conduction band
e	electron
h	hole
hh	heavy-hole
lh	light-hole
RT	room temperature
so	spin-off
UV	ultraviolet
VB	valence band
Δ	difference
δ_{ij}	Kronecker delta

Elements

Ar	Argon
As	Arsenic
Be	Beryllium
Cd	Cadmium
Cl	Chlorine
Cr	Chromium
Fe	Iron

Ga	Gallium
He	Helium
Hg	Mercury
In	Indium
Mg	Magnesium
Mn	Manganese
Na	Sodium
Ni	Nickel
N	Nitrogen
Nd	Neodymium
O	Oxygen
Se	Selenium
S	Sulfur
Te	Tellurium
V	Vanadium
Zn	Zinc

Constants

c	speed of light in vacuum (299,792,458 m/s)
e	unit charge ($1.602176 \cdot 10^{-19}$ C)
g_{Mn}	g-factor of d-shell electrons of Mn^{2+}-ions ($g_{Mn} = 2$)
h	Planck constant ($6.62606896(33) \cdot 10^{-34}$ J·s $= 4.13566733(10) \cdot 10^{-15}$ eV·s)
$\hbar$	Dirac constant ($h/2\pi = 1.054571628(53) \cdot 10^{-34}$ J·s $= 6.58211899(16) \cdot 10^{-16}$ eV·s)
k_B	Boltzmann constant ($1.38062 \cdot 10^{-23}$ J/K)
m_0	free electron mass ($9.109381 \cdot 10^{-31}$ kg)
ε_0	dielectric constant in vacuum

ε_r	dielectric constant in mater
μ_0	magnetic permeability ($4\pi \cdot 10^{-7}$ Vs/Am)
μ_B	Bohr magneton ($\frac{e\hbar}{2m_e} = 9.274078 \cdot 10^{-24}$ Am^2 (= J/T))

Units

A	Ampere
Å	Angstrom
C	Coulomb
eV	electron volt (1 eV $= 1.602176 \cdot 10^{-19}$ J)
g	gram
Hz	Hertz
J	Joule
K	Kelvin
ML	monolayer
m	meter
Pa	Pascal
s	second
T	Tesla
V	Volt
W	Watt
k	kilo- (10^3)
c	centi- (10^{-2})
m	milli- (10^{-3})
µ	micro- (10^{-6})
n	nano- (10^{-9})
p	pico- (10^{-12})

Variables and Parameters

$\downarrow$	spin-down
$\uparrow$	spin-up
a_B	Bohr-radius
a_0	lattice constant
$\vec{A}$	vector potential
$\vec{B}$, B	magnetic field (magnetic flux density)
$\mathcal{B}$	Brillouin-function
C, C_0	Curie constant
C_i	specific heat, heat capacity
D	diffusion coefficient
d	mean cation distance
$D\left(E\right)$	density of states
E	energy
$e_d^{+\sigma}$, $e_d^{-\sigma}$	ground and excited state of the d-electrons in zincblende $A^{II}_{1-x}\mathrm{Mn}_x B^{VI}$ semiconductor
E_e	electron kinetic energy, energy of electron system
E_F	Fermi-energy
E_g	band gap energy
E_{Mn}	energy of Mn-spin system
E_{PL}	energy of PL line
F	free energy
f	focal length
g	g-factor
g^{eff}	effective g-factor
G_i	energy flux from external sources into DMS subsystem

$\vec{H}$, H	magnetic field strength
$H_n(z)$	Hermite polynomial
$\hat{H}$	Hamilton operator
I	photoluminescence intensity
$I_c(t)$	carrier impact
$I_L(t)$	laser pulse impact
$I_{ph}(t)$	phonon impact
$\vec{J}$,J	total angular momentum
J_n	exchange constant
$\hat{J}$	exchange tensor
K	restoring force constant
K_{diff}	spin-spin diffusion coefficient
$\vec{k}$, k	wave vector
$\vec{L}$, L	orbital angular momentum
l_B	magnetic length
l	free electron orbital angular momentum, Landau-level quantization index
l_z	QW width (in z-direction)
$\vec{M}$,M	magnetization
m	mass, magnetic quantum number
m_{eff}	bare effective electron mass
m^*_{eff}	renormalized effective electron mass
m_j	z-component of hole spin
m_s	z-component of electron spin
n	subband index, number of magnetic moments per unit cell volume
n_e	electron concentration

n_{Mn}	concentration of Mn-ions
N_0	inverse unit-cell volume
$N_0\alpha$	exchange constant for conduction band
$N_0\beta$	exchange constant for valence band
P	excitation density, polarization
$\vec{p}$	electron momentum operator
q	boundary thermal conductivity
$\tilde{q}$	renormalized boundary thermal conductivity
Q_{cb}	conduction band offset
Q_{vb}	valence band offset
$\vec{r}$, $\vec{R}$, $\vec{R}_i$	lattice vectors
S_{eff}	effective spin
S, $\vec{S}$	(Mn) electron spin (operator, vector)
$\langle \vec{s}_{NE} \rangle$	nonequilibrium electron spin
$\langle S_z \rangle$	mean value of the z-component of the Mn-spin
T	temperature, trion
T_e	electron temperature
T_{eff}	effective temperature
T_g	critical temperature
T_L	lattice temperature
T_{Mn}	Mn-spin temperature
T_{Neel}	Neél temperature
T_0	antiferromagnetic temperature
t	time
t_{gd}	gate delay

t_{gw}	gate width
t_{ppg}	reference time, provided by a programmable pulse generator (PPG)
t_1	energy relaxation time
t_2	dephasing time
U	voltage
V, u	potential
V_{pd}	hybridization parameter
X	exciton
x	Manganese content, x-axis, x-component
x'	effective Manganese content determined by SLR time
x''	effective Manganese content determined by giant Zeeman-splitting
x_{DA}	average Manganese content in DAs
x'_{DA}	effective Manganese content determined by SLR time in DAs
x''_{DA}	effective Manganese content determined by giant Zeeman-splitting in DAs
x'_{PQW}	effective Manganese content determined by SLR time in (H)PQWs
x''_{PQW}	effective Manganese content determined by giant Zeeman-splitting in (H)PQWs
y	Beryllium content, y-axis, y-component
z	Magnesium content, z-axis, z-component
α	exchange integral for s-like Γ_6 electrons
β	exchange integral for p-like Γ_8 electrons
β_i	inverted temperature
$\hat{\chi}_m$, χ	magnetic susceptibility
δ_e	parameter for heterostructures, which takes leaking of electron wave function into nonmagnetic layer into account
$\delta_{(h)h}$	parameter for heterostructures, which takes leaking of (heavy-)hole wave function into nonmagnetic layer into account

$\Delta E_{e_d^\sigma}$	energy difference between ground and excited state of the d-electrons in zincblende $A^{II}_{1-x}\mathrm{Mn}_x B^{VI}$ semiconductor
$\Delta E_{giantZeeman}$	energy of giant Zeeman-splitting
ΔE_{Zeeman}	energy of Zeeman-splitting (Zeeman energy)
Δt_c	duration of carrier impact
Δt_{gd}	gate delay step width
Δt_{gw}	gate width step width
Δt_{ph}	duration of phonon impact
γ	spin-orbit coefficient
γ_i	bare Kohn-Luttinger parameters of valence band
γ_{i^*}	renormalized Kohn-Luttinger parameters of valence band
κ	conductivity
λ	wavelength
λ_{JS}	rate of electron spin relaxation on magnetic ions
μ	reduced mass, magnetic moment
μ_r	relative permeability of a material
ν	filling factor, frequency
ω	angular frequency
ω_c	cyclotron frequency
$\vec{\Omega}$	effective magnetic field
Φ, Ψ	wave function
π	linear polarization degree of light
$\vec{\sigma}$, σ	spin (operator, vector)
ς	Rashba parameter
σ^+, σ^-	circular polarization degree of light (right- and left-hand, respectively)
τ	life time, relaxation time

$\hat{\tau}$	operator for time reversal
τ_{c-Mn},τ_{Mn-c}	typical time for carrier exchange scattering on localized Mn-spins
τ_D	spin diffusion time
τ_{e-L}	time for energy relaxation between electron system and lattice
τ_{e-Mn},τ_{Mn-e}	typical time for electron exchange scattering on localized Mn-spins
$\tau_{e-phonon}$	electron-phonon interaction time
τ_{in}	characteristic time for heating of the Mn-system via photogeneration
τ_{Mn-L}	time for energy relaxation between Mn-spin system and lattice
τ_{nes}	nonequilibrium carrier spin relaxation time
τ_{PL}	time for photoluminescence decay
τ_{spin}	spin relaxation time
τ_{SLR}	SLR time
τ_{SLR}^{Mn-L}	SLR time caused by direct coupling of Mn-ions with lattice
τ_{ss}	spin-spin interaction time
τ_{2DEG}	characteristic time for Mn-ion interaction with 2DEG
Θ, Θ_0	Curie-Weiss temperature
Θ_c	Mn-system maximum temperature resulted from carrier impact
Θ_{ph}	Mn-system maximum temperature resulted from phonon impact
Υ	envelope-function

List of Acronyms

bulk inversion asymmetry (BIA) , 17, 49, 77

charge-couple-device (CCD) , 100, 167

conduction-electron spin resonance (CESR) , 87

continuous wave (cw) , 96–98, 104, 112, 130, 131, 136, 155, 167, 176, 177

digital alloy (DA) , 46, 130, 135, 136, 138, 139, 141, 145, 146, 149, 151, 152, 157, 161, 162, 245

digital magnetic quantum well (DMQW) , 162

diluted magnetic semiconductors (DMS) , 3–6, 10, 11, 19, 33, 36, 39, 42, 46, 48, 50, 51, 63, 64, 66–68, 71, 75, 80, 82, 87–89, 92–95, 107, 113, 115, 118, 120–122, 127, 129, 134–136, 138, 139, 146, 147, 149, 151, 152, 155–157, 160, 167, 242, 255

dynamic random access memory (DRAM) , 2

electron paramagnetic resonance (EPR) , 82

electron spin resonance (ESR) , 82, 92

face-centered-cubic (fcc) , 12

field-effect transistor (FET) , 2

far-infrared (FIR) , 92

full width at half maximum (FWHM) , 162, 163

gated charge-couple-device (GCCD) , 96, 100, 167, 174, 176, 177

giant magnetoresistance (GMR) , 2

half-parabolic quantum well (HPQW) , 58, 140, 141, 143–145, 162

intensified charge-couple-device (ICCD) , 100

light emitting diode (LED) , 2

liquid phase epitaxy (LPE) , 46, 159

molecular beam epitaxy (MBE) , 11, 46, 130, 146, 159–161

microchannel plate (MCP) , 100

molecular field approximation (MFA) , 34

modulated-molecular beam epitaxy (MMBE) , 146, 161

metal organic chemical vapor deposition (MOCVD) , 46

metal organic vapor phase epitaxy (MOVPE) , 46

multiple quantum well (MQW) , 51, 108

magnetoresistive random access memory (MRAM) , 2

magnetic tunnel junction (MTJ) , 2

microwave (MW) , 92

nuclear magnetic resonance (NMR) , 70

pseudo-dipolar (PD) , 36

photoluminescence (PL) , 4, 55, 87–90, 96–98, 100, 102, 103, 108, 115, 122, 130–132, 134, 136, 140, 141, 144, 149, 151, 155, 162, 163, 167, 169, 171, 174, 176–178

photoluminescence excitation (PLE) , 88–90

programmable pulse generator (PPG) , 100, 176, 244

parabolic quantum well (PQW) , 58, 59, 140, 141, 143–146, 152, 162, 171, 174, 245

programmable timing generator (PTG) , 100

quantum dot (QD) , 79, 82, 93, 112, 146

quantum well (QW) , 6, 10, 11, 46–59, 63–66, 71, 72, 76–79, 88–90, 93–97, 102–104, 106, 108, 110, 112, 114, 115, 121, 122, 124, 125, 129, 130, 132, 135, 139–141, 144–149, 152, 155, 156, 159–163, 167, 177, 243

random access memory (RAM) , 2

reflection high energy electron diffraction (RHEED) , 160

Ruderman-Kittel-Kasuya-Yosida (RKKY) , 36

resonant tunneling device (RTD) , 2

structure inversion asymmetry (SIA) , 50, 77

spin-lattice relaxation (SLR) , 6, 36, 67–70, 80–82, 84, 92, 93, 95, 96, 102, 103, 106–108, 110, 112, 115, 116, 118–127, 129–132, 134, 136, 138, 139, 141, 143–149, 151, 152, 155, 156, 161, 163, 167, 176, 178, 179, 245, 247

static random access memory (SRAM) , 2

tunneling magnetoresistance (TMR) , 2

two-dimensional electron gas (2DEG) , 54, 72, 94, 115, 121–124, 126, 127, 129–132, 156, 157, 161, 247

two-dimensional hole gas (2DHG) , 122

valence band offset (VBO) , 47, 48

virtual crystal approximation (VCA) , 19, 34

vertical cavity surface emitting laser (VCSEL) , 2

vapor phase epitaxy (VPE) , 46, 159

x-ray diffractometry (XDR) , 162

yttrium aluminum garnet (YAG) , 97, 102, 103

List of Publications

1. A. A. Maksimov, D. R. Yakovlev, M. K. Kneip, M. Arlt, M. Bayer, T. Wojtowicz, G. Karczewski, and J. Kossut *Spin diffusion in (Cd,Mn)Te diluted magnetic semiconductors* In preparation for Phys. Rev. B (2009).

2. V. Y. Ivanov, M. Godlewski, D. R. Yakovlev, S. M. Ryabchenko, M. K. Kneip, M. Bayer and A. Waag *Optically detected magnetic resonance in ZnMnSe/ZnBeSe quantum wells* Accepted for publication in Phys. Rev. B **78**, (2008).

3. M. K. Kneip *Migration eines Mittelverwaltungssystems in eine Multiuserumgebung* Grin Publishing , Fernuniversität Hagen, ISBN 3638929733 (2007).

4. M. K. Kneip, D. R. Yakovlev, M. Bayer, G. Karczewski, T. Wojtowicz, and J. Kossut *Engineering of the spin-lattice relaxation dynamics by digital growth of diluted magnetic semiconductor (Cd,Mn)Te* Applied Physics Letters **88**, 152105 (2006).

5. M. K. Kneip, D. R. Yakovlev, M. Bayer, T. Slobodskyy, G. Schmidt and L. W. Molenkamp *Electric field control of magnetization dynamics in ZnMnSe/ZnBeSe diluted-magnetic-semiconductor heterostructures* Applied Physics Letters **88**, 212105 (2006).

6. M. K. Kneip, D. R. Yakovlev, M. Bayer, A. A. Maksimov, I. I. Tartakovskii, D. Keller, W. Ossau, L. W. Molenkamp, and A. Waag *Direct energy transfer from photocarriers to Mn-ion system in II-VI diluted-magnetic-semiconductor quantum wells* Phys. Rev. B **73**, 035306 (2006).

7. M. K. Kneip, D. R. Yakovlev, M. Bayer, A. A. Maksimov, I. I. Tartakovskii, D. Keller, W. Ossau, L. W. Molenkamp, and A. Waag *Spin-lattice relaxation of Mn-ions in ZnMnSe/ZnBeSe quantum wells measured under pulsed photoexcitation* Phys. Rev. B **73**, 045305 (2006).

8. M. Fiebig, T. Lottermoser, M. K. Kneip and M. Bayer *Correlations between magnetic and electrical ordering in multiferroic manganites* J. Appl. Phys. **99**, Issue 8, 08E302-1 - 08E302-5 (2006).

9. M. K. Kneip *Data Mining* Grin Publishing , Fernuniversität Hagen, ISBN 3638927840 (2005).

10. L. Bryja, M. Kubisa, K. Ryczko, J. Misiewicz, M. K. Kneip, M. Bayer, R. Stępniewski, M. Byszewski, M. Potemski, D. Reuter, and A. Wieck *Investigations of interface excitons at p-type GaAlAs/GaAs single heterojunctions in continues wave and time resolved magneto photoluminescence experiments* In *AIP Conf. Proc. 772: Physics of Semiconductors*, edited by J. Menendez and C. G. Van de Walle, 1158–1159 (American Institute of Physics, 2005) Proc. 27^{th} Int. Conf. on the Physics of Semiconductors, Flagstaff, USA 2004.

11. D. R. Yakovlev, M. K. Kneip, M. Bayer, A. A. Maksimov, I. I. Tartakovskii, A. V. Scherbakov, A. V. Akimov, D. Keller, W. Ossau, L. W. Molenkamp, and A. Waag *Spin dynamics of Mn-ion system in diluted-magnetic-semiconductor heterostructures based on ZnMnSe* In *AIP Conf. Proc. 772: Physics of Semiconductors*, edited by J. Menendez and C. G. Van de Walle, 1301–1302 (American Institute of Physics, 2005) Proc. 27^{th} Int. Conf. on the Physics of Semiconductors, Flagstaff, USA 2004.

12. D. R. Yakovlev, M. K. Kneip, A. A. Maksimov, I. I. Tartakovskii, M. Bayer, D. Keller, W. Ossau, L. W. Molenkamp, A. V. Scherbakov, A. V. Akimov, and A. Waag *Spin and energy transfer between magnetic ions and free carriers in diluted-magnetic semiconductor heterostructures* Phys. Stat. Sol. (c) **1**, 989 (2004).

13. M. K. Kneip *Magnetische Phasendiagramme und Spinrotationsprozesse in hexagonalen Manganiten* Grin Publishing , Universität Dortmund, ISBN 3638927444 (2003).

Acknowledgments

Many people have made their contribution to success of this work. Those I would like to express my gratitude subsequently.

First of all I would like to cordially thank Priv.-Doz. Dr. Dmitri R. Yakovlev for familiarizing me with the interesting topic of DMS. His excellent supervision and guidance of this work and his continuous willingness to answer all encountered questions were the irreplaceable preconditions for the achieved results.

Sincere thank is acknowledged to Prof. Dr. Manfred Bayer for the opportunity to perform these studies at his department. His steady assistance with any problems added a great deal to the successful completion of this work.

I am much obliged to Prof. Dr. Metin Tolan for refereeing this thesis. In addition I thank Dr. Bärbel Siegmann, Prof. Dr. Bernhard Spaan and Prof. Dr. Werner Weber for their willingness to participate in the examination board.

For the fruitful collaboration and excellent teamwork during the whole project, I appreciate Dr. Andrei Maksimov. In several discussions I have strongly profited from his extensive knowledge. Special thanks goes to Prof. Dr. Ilja I. Tartakovskii, who helped me in building up the experimental setup and introduced me to the technique of time-resolved spectroscopy. I have learned a lot from his high experience.

Thanks to Prof. Dr. Andrei V. Akimov, Dr. Dirk Keller, Dr. Leszek Bryja, Dr. Gerhard Ortner, Dr. Alexey V. Scherbakov, and Marcel Arlt for the successful measurements and the nice lab-time we had together.

Furthermore, I highly cherish the technical support of Klaus Wiegers and Frank Plückebaum. They have solved any mechanical (and other) problems by their great know-how within next to no time. Thanks to Thomas Stöhr and the team of the electronic workshop for the assistance with electrotechnical troubles. For optimal supply with liquid gases, I am beholden to Eberhard Gall, Klaus Widynski and Klaus Wiegers. I am thankful as well to the mechanical workshop under the direction of Susanne Kralemann for constructions and the team of the preparation lab - Dirk Schemionek, Gisela Pike and Najeeba Lenser - for sample preparations. Definitely not to forgotten should be the fast and easy administrative support, provided by Michaela Wäscher. Therefor sincere thanks.

As no spectroscopy is possible without samples of high quality, I appreciate Prof. Dr. Laurens W. Molenkamp, Prof. Dr. Wolfgang Ossau, Priv.-Doz. Dr. Georg Schmidt, and Dr. Taras Slobodskyy, from the university of Würzburg, Prof. Dr. Andreas Waag from the technical university of Braunschweig and Prof. Dr. Grzegorz Karczewski, Prof. Dr. Jacek Kossut, and Prof. Dr. Tomasz Wojtowicz from the Institute of Physics, Polish Academy of Sciences in Warsaw for handover of samples.

For the harmonious collaboration and nice time during the past years, I thank all current and prior members and guests of the Experimentelle Physik II group. To prevent forgetting someone inadvertently, I am not going to try to list everyone in person. However, I want to highlight merely the unique office atmosphere together with Thomas Stöhr, Dr. Ingo Sänger and, for the last years, also with Benjamin Kaminski. I am indebted especially to Ingo, as our good teamwork and friendship, during the many years of studying physics, played a decisive role in finishing my academic studies with this work.

For their financial and moral support during my academic studies, I am heartily grateful to my parents Konrad and Maria Kneip. This aid provided the basis for me to perform this thesis. Finally, I am deeply indebted to my well beloved wife Christiane and my cute daughter Sophie, who encouraged me with their love, although I had often only very sparse time for them.